



<https://theses.gla.ac.uk/>

Theses Digitisation:

<https://www.gla.ac.uk/myglasgow/research/enlighten/theses/digitisation/>

This is a digitised version of the original print thesis.

Copyright and moral rights for this work are retained by the author

A copy can be downloaded for personal non-commercial research or study,
without prior permission or charge

This work cannot be reproduced or quoted extensively from without first
obtaining permission in writing from the author

The content must not be changed in any way or sold commercially in any
format or medium without the formal permission of the author

When referring to this work, full bibliographic details including the author,
title, awarding institution and date of the thesis must be given

Enlighten: Theses

<https://theses.gla.ac.uk/>
research-enlighten@glasgow.ac.uk

MODELLING AND CONTROL OF AIRCRAFT
GAS TURBINE ENGINES

A DISSERTATION
SUBMITTED TO THE FACULTY OF ENGINEERING
OF GLASGOW UNIVERSITY
IN PARTIAL FULFILLMENT OF THE REQUIREMENTS
FOR THE DEGREE OF
DOCTOR OF PHILOSOPHY

By
Oliver Feng Qi
April 1992

© Copyright 1992 by Oliver Feng Qi
All Rights Reserved

ProQuest Number: 10987101

All rights reserved

INFORMATION TO ALL USERS

The quality of this reproduction is dependent upon the quality of the copy submitted.

In the unlikely event that the author did not send a complete manuscript and there are missing pages, these will be noted. Also, if material had to be removed, a note will indicate the deletion.



ProQuest 10987101

Published by ProQuest LLC (2018). Copyright of the Dissertation is held by the Author.

All rights reserved.

This work is protected against unauthorized copying under Title 17, United States Code
Microform Edition © ProQuest LLC.

ProQuest LLC.
789 East Eisenhower Parkway
P.O. Box 1346
Ann Arbor, MI 48106 – 1346

Abstract

In this thesis the main theme is to demonstrate the potential performance improvements of gas turbine engines that are brought about by using multivariable control systems. Particular emphasis is on designing such control systems using the well-established engine thermodynamic models since these models are considered as the true representations of engine thermodynamic process and enable engine variable geometry features to be easily incorporated and their effects studied.

The approach taken is to recognise that good control builds on the reliability of the models. Towards this end, a refined modelling approach using Intercomponent Volumes (ICV) method has been adopted to increase the reliabilities of the engine models (at the component level) and the simulation efficiency. This is especially important when the models are directly used to synthesise nonlinear controllers. The model validations are also carried out to ensure that the developed models are primarily in line with the available base models. A procedure for the design of open-loop fuel schedule (using pressure ratio as independent variable) using optimisation techniques has been devised. This is to ensure safe operations of the engines during transients.

Model-based control system design methodologies are increasingly being looked upon as a possible replacement to the traditional control used on aircraft gas turbine engines. Most designs in the past were carried out based upon linear models which are generated in one way or another (e.g. using identification techniques or nonlinear simulations). Although various control design techniques such as

classical Multivariable Frequency Domain (MFD) and the Linear Quadratic Regulator (LQG) approaches have been used, it seems that research into the following aspects may be still necessary to attain successful engine control systems:

- Setpoint design. this includes the design of desired responses for the main engine performance variables (e.g. engine shaft speed) and their steady-state schedule. These are related to the engine steady-state and transient performance requirements.
- Design using the engine nonlinear models (e.g. thermodynamic models). Control systems designed using the linear models can, sometime in the case of mild nonlinearities, provide good control, however design using the nonlinear models directly can offer great improvements, especially in the case of large variations in engine dynamics and performance parameters.

Another concern in the present study is to ensure the safety of the engines during transients, particularly the compressor surge and turbine over-temperature during accelerations. This is achieved by formulating the appropriate transient tracking schedule on the compressor characteristic for engines to track during accelerations.

The difficulties in designing nonlinear controllers for gas turbine engines arise from the two aspects: large variations in engine dynamics and performance variables over their operating range; and the main performance variables such as engine thrust cannot be directly measured.

Two control strategies are used to cope with these two inherent difficulties in control system design. The use of gain scheduling is to derive nonlinear controllers to cope with engine dynamics variations over the entire operating range. The use of model-based control technique is to achieve the direct control on the unmeasured engine thrust. This can be considered as an alternative to avoid the complex procedure of engine control mode analysis.

Acknowledgements

I wish to express my deepest gratitude to my two supervisors Professor P.J. Gawthrop and Professor N.R.L. Maccallum for their valuable guidance, encouragement and inspiration conveyed to me during the course of this study.

Deep appreciation is also expressed to Dr. R.W. Jones who spent his valuable time in discussing relevant issues in using model-based control.

I wish to thank all the members of the Control Group, especially Dr. D. Ballance, Dr. J. Howell, Dr. H. Mirab, Mrs. Y. Mather, Mr. G. Worship, Mr. N. Marrison and Mr. D. Sbarbaro. Their continuous support and encouragement served to lighten the burden of this work.

I also wish to thank The British Council and Chinese Ministry of Education for providing financial support, which made this thesis possible.

I am also indebted to my parents and my wife, Kallen, for their continuous support and encouragement throughout my education.

Contents

Abstract	ii
Acknowledgements	iv
1 Modelling and Control of Gas Turbine Engines	1
1.1 Introduction	1
1.1.1 Modelling Gas Turbine Engines	2
1.1.2 Control Objectives	3
1.2 An Overview of Engine Modelling	4
1.2.1 Linear Empirical Modelling	4
1.2.2 Identifying Dynamic Models	8
1.2.3 Nonlinear Aerothermodynamic Models	9
1.2.4 Nonlinear Thermodynamic Models	10
1.2.5 The Lumped Continuity Model	11
1.2.6 The Stage-Stacked Momentum Continuity Model	13
1.2.7 Bond Graph Models	14
1.2.8 Remarks on Modelling	14
1.3 An Overview of Engine Control	15
1.3.1 Linear Design Model	15
1.3.2 Model Reduction	15
1.3.3 Control Mode and Structure Analysis	16
1.3.4 Control Design Methods	17

1.3.5	Proposed Engine Control Problem	18
1.3.6	Multivariable Frequency Domain Methods	19
1.3.7	Control Using Linear Quadratic Methods	23
1.3.8	Control Using Alternative Methods	28
1.4	Modelling Approach and Control Strategy	30
1.5	Contribution of This Thesis	31
2	Thermodynamic Models for Gas Turbine Engines	33
2.1	Introduction	33
2.2	System Description	34
2.2.1	Single-Spool Engine	34
2.2.2	Typical Modern Turbofan Engine	35
2.3	Gas Turbine Modelling	36
2.3.1	Inlet	36
2.3.2	Fan and Compressors	36
2.3.3	Combustion Chamber Model	37
2.3.4	Turbines	39
2.3.5	Propulsion Nozzle Model	39
2.4	Dynamic Equations	39
2.4.1	State Selections	39
2.4.2	Lumped Volume Dynamics	40
2.4.3	Shaft Inertia	41
2.5	Effects of Variable Geometry	41
2.5.1	Compressor Characteristic with Variable Geometry	42
2.5.2	A Simple Model for Considering Variable Geometry	42
2.6	Thermodynamic Modelling of Engines	43
2.6.1	The Single-spool Engine	43
2.6.2	The Two-spool Turbofan	46
2.7	Transient Thermal Characteristics	53

2.8	Handling of the Fan and Turbine Characteristics	54
3	A Method for Approximating Compressor and Turbine Characteristics	55
3.1	Introduction	55
3.2	Compressor Models and their Problems	57
3.2.1	Compressor Models	57
3.2.2	Problems Associated Using Tabular Characteristics	58
3.3	A Preliminary Study of Analytical Modelling	60
3.3.1	Curve Fitting By a General Polynomial	61
3.4	Motivation from the Previous Study	64
3.4.1	Need for a Multi-Objective Algorithm	64
3.5	Characterisation of Model Qualities	65
3.5.1	Characterisation of a Monotonic Behaviour Indicator	65
3.5.2	Characterisation of Error Indicator	67
3.5.3	Characterisation of the Predictability Indicator	68
3.6	Harmonisation of Performance Indicator	68
3.7	Global Criterion for Modelling	69
3.8	Application to the Compressors	70
3.8.1	Data Scaling	70
3.8.2	Transformation of Axes	72
3.8.3	Fitting of New Map of Compressor	74
3.8.4	Reconstructing Original Characteristics	74
3.8.5	Some Conclusions	79
3.9	Models for Compressors in Turbofan Engine	80
3.9.1	Fan Characteristics	80
3.9.2	IP Compressor Characteristics	85
3.9.3	HP Compressor Characteristics	90
3.10	Turbines Modelling	95

3.10.1	Turbine in the Single-Spool Engine	95
3.10.2	Transformed variables	97
3.10.3	Turbines in the Turbofan Engine	98
3.11	Conclusions	104
4	Digital Simulation of Gas Turbine Engines	105
4.1	Introduction	105
4.2	Performance Requirements of an Engine	106
4.3	Limitations to Thrust Response	107
4.4	Interpretation on the Compressor Characteristic	108
4.5	Acceleration Fuel Schedule	109
4.5.1	Scheduling as a Function of Pressure Ratio	109
4.5.2	Determination of K_s	111
4.6	Definition of Surge Margin and Turbine Inlet Temperature Limit .	111
4.7	Computation Procedure of Simulation	112
4.7.1	Numerical Integration	113
4.8	Single-Spool Turbojet Engine	113
4.8.1	Steady-State Operation	114
4.8.2	Transients At Sea Level, Mach Number 0.2	114
4.8.3	Transients At 10,000 m, Mach Number 0.8	120
4.8.4	Using Alternative Schedules	120
4.9	Two-Spool Turbofan Engine	125
4.9.1	Steady-State Operation	125
4.9.2	Transients At Sea Level, Mach Number 0.2	127
4.9.3	Transients At 10,000 m, Mach Number 0.8	135
4.10	Linearising the Nonlinear Models	141
4.10.1	Linearising a Nonlinear Model	142
4.10.2	Approximation Algorithm	145
4.10.3	Validating Linear Models	145

4.11	Conclusions	146
5	Nonlinear Controller Designs for Gas Turbine Engines	153
5.1	Introduction	153
5.2	Gain Scheduling Approach	155
5.2.1	Selection of Scheduling Variable	157
5.2.2	Controller Structure	158
5.2.3	Scheduling Functions	158
5.3	Performance Requirements for Control	159
5.3.1	Surge Line Tracking	161
5.4	Linear Controller Designs	163
5.4.1	Design Specifications	166
5.4.2	Selecting Design Model	168
5.4.3	Design Using Closed-loop Synthesis	168
5.5	Scheduled Nonlinear Controllers	176
5.6	Simulation and Comparisons	178
5.6.1	The Single-Spool Engine	178
5.6.2	The Two-Spool Engine	182
5.7	Alternative Way to Control Surge	182
5.8	Conclusions	189
6	Model-Based Control of Gas Turbine Engines	191
6.1	Introduction	191
6.2	Measurements and Disturbances	193
6.3	The Algorithm of a Model-Based Observer	193
6.4	Proportional Observer	195
6.4.1	Qualitative Deduction of Observer Gain	196
6.4.2	Design of Observer Gain K_p	197
6.5	Proportional and Integral(PI) Observer	198
6.5.1	Robust Properties of PI Observer	199

6.5.2	Robust Design of PI Observer	201
6.5.3	Augmenting Integrators	202
6.6	Control Strategy	203
6.7	Single-Spool Turbojet Engine	204
6.7.1	Open-Loop Observer Without Control	204
6.7.2	Closed-Loop Observer Without Control	206
6.7.3	Modelling Error and Use of PI Observer	206
6.7.4	Closed-loop Control	209
6.7.5	Inlet Flow Disturbance	209
6.8	Two-spool Turbofan Engine	212
6.9	Conclusions	221
7	Conclusions and Further Work	222
7.1	On Engine Modelling	222
7.2	On Engine Control	225
7.3	Direct Extension of the Present Work	226
7.4	Further Works in Modelling and Control	227
7.4.1	Real Time Identification	227
7.4.2	Nonlinear Modelling	227
7.4.3	Engine Control System Design	228
7.4.4	Engine Control Reliability	228
	Bibliography	229

List of Tables

2.1	The Volume Meaning for The Single-Spool Engine	35
2.2	The Volume Meaning for the Two-spool Engine	36
2.3	Choice of States, Controls and Outputs for The Single-Spool Engine	47
2.4	Choice of States, Controls and Outputs for The Two-Spool Engine	53
3.1	Coefficients From the Polynomial Fitting	63
3.2	Lists of Possible Choice of Transformations	73
3.3	The Performance Index Values From the Compressor Models . . .	95

List of Figures

1.1	The Procedure of Modelling and Control of Gas Turbine Engine	2
1.2	Diagram of Control Law Derivation	26
1.3	Control and Engine System	26
1.4	Model Following Control Structure	28
1.5	The Diagram of Internal Feedback Model Representations	29
1.6	The Control Scheme in Multi-Objective Optimisation Scheme	30
2.1	The Diagram of the Single-Spool Engine	34
2.2	The Diagram of the Two-spool engine	35
2.3	Energy Release Diagram	40
2.4	Information Flow Diagram for the Single-Spool Engine	46
2.5	Information Flow Diagram for the Two-Spool Engine	52
3.1	Pressure Ratio and Mass Flow Map of the Single-Spool Engine	59
3.2	Efficiency and Mass Flow Map of the Single-Spool Engine	59
3.3	Fitting Pressure Ratio Results Using Equations 3.1-4	61
3.4	Fitting Efficiency Results Using Equations 3.5-7	62
3.5	Fitting Results Using the Proposed Polynomial: Equation 3.8	63
3.6	Fitting Results Using the Proposed Polynomial: Equation 3.8	64
3.7	Fitting Mass Flow and Speed on the Surge Line	71
3.8	Fitting Pressure Ratio and Speed on the Surge Line	71
3.9	Transformed Pressure Ratio and Mass Flow Characteristic	72
3.10	Transformed Efficiency and Mass Flow Characteristic	73

3.11	Coefficients from Fitting Transformed Characteristic of Figure 3.9	74
3.12	Coefficients from Fitting Transformed Characteristic of Figure 3.10	75
3.13	Comparison of Results of Fitting Coefficients from Figure 3.11 . .	75
3.14	Comparison of Results of Fitting Coefficients from Figure 3.12 . .	76
3.15	Reconstructed X and Y Using the Above Equations	77
3.16	Reconstructed X and Y Using the Above Equations	78
3.17	Reconstructed Pressure Ratio/Mass Flow Characteristic	78
3.18	Reconstructed Efficiency/Mass Flow Characteristic	79
3.19	Normalised Fan Pressure Ratio/Mass Flow Characteristic	80
3.20	Normalised Fan Efficiency/Mass Flow Characteristic	81
3.21	Fitting Coefficients a_1 for Pressure Ratio/Mass Flow Map	82
3.22	Fitting Coefficients b_1 for Efficiency/Mass Flow Map	82
3.23	Fitting Transformed Fan Pressure Ratio/Mass Flow Characteristic	83
3.24	Fitting Transformed Fan Efficiency/Mass Flow Characteristic . .	83
3.25	Reconstructed Fan Pressure Ratio/Mass Flow Characteristic . . .	84
3.26	Reconstructed Fan Efficiency/Mass Flow Characteristic	84
3.27	Transformed IP Comp. Pressure Ratio/Mass Flow Characteristic	85
3.28	Transformed IP Comp. Efficiency/Mass Flow Characteristic . . .	86
3.29	Fitting Coefficients a_1 of Figure 3.27	86
3.30	Fitting Coefficients b_1 of Figure 3.28	87
3.31	Fitting Transformed IP Comp. Pressure Ratio/Mass Flow Charac- teristic	87
3.32	Fitting Transformed IP Comp. Efficiency/Mass Flow Characteristic	88
3.33	Reconstructed IP Comp. Pressure Ratio/Mass Flow Characteristic	88
3.34	Reconstructed IP Comp. Efficiency/Mass Flow Characteristic . .	89
3.35	Transformed HP Comp. Pressure Ratio/Mass Flow Characteristic	90
3.36	Transformed HP Comp. Efficiency/Mass Flow Characteristic . . .	91
3.37	Fitting Coefficients a_1 From Figure 3.35	91
3.38	Fitting Coefficients b_1 From Figure 3.36	92

3.39	Fitting Transformed HP Comp. Pressure Ratio/Mass Flow Characteristic	92
3.40	Fitting Transformed HP Comp. Efficiency/Mass Flow Characteristic	93
3.41	Reconstructed HP Comp. Pressure Ratio/Mass Flow Characteristic	93
3.42	Reconstructed HP Comp. Efficiency/Mass Flow Characteristic . .	94
3.43	Turbine Mass Flow Characteristic in the Single-Spool Engine . . .	96
3.44	Turbine Efficiency Characteristic in the Single-Spool Engine . . .	97
3.45	Transformed Turbine Mass Flow Characteristic	98
3.46	Transformed Turbine Efficiency Characteristic	99
3.47	LP Turbine Mass Flow Characteristic in the Turbofan Engine . .	99
3.48	LP Turbine Efficiency Characteristic in the Turbofan Engine . . .	100
3.49	HP Turbine Mass Flow Characteristic in the Turbofan Engine . .	100
3.50	HP Turbine Efficiency Characteristic in the Turbofan Engine . . .	101
3.51	Transformed LP Mass Flow Turbine Characteristic	102
3.52	Transformed LP Efficiency Turbine Characteristic	102
3.53	Transformed HP Mass Flow Turbine Characteristic	103
3.54	Transformed HP Efficiency Turbine Characteristic	103
4.1	A Hypothetical Transient Trajectory	108
4.2	Typical Fuel Flow Characteristic	110
4.3	Comparison of Steady-State Operating Points	115
4.4	Relation Between Thrust and Speed	115
4.5	Relation Between Thrust and Engine Pressure Ratio	116
4.6	Non-dimensional Fuel Schedule	116
4.7	Input Fuel Flow and Thrust Response	117
4.8	Responses of Engine States	118
4.9	Acceleration and Deceleration Trajectories	119
4.10	Variation of Compressor Surge Margin in Acceleration	119
4.11	Input Fuel Flow and Thrust Response	120

4.12 Responses of Engine States	121
4.13 Acceleration and Deceleration Trajectories	122
4.14 Variation of Compressor Surge Margin in Acceleration	122
4.15 Input Fuel Flow and Thrust Response	123
4.16 Responses of Engine States	124
4.17 Steady Running Line on Fan Characteristic	125
4.18 Steady Running Line on IP Compressor Characteristic	126
4.19 Steady Running Line on HP Compressor Characteristic	126
4.20 Relationship of HP and LP Shaft Speeds	127
4.21 Non-dimensional Fuel Schedule	128
4.22 Transient Responses At Sea Level, Mach Number 0.2	129
4.23 Transient Responses At Sea Level, Mach Number 0.2	130
4.24 Fuel Flow and Thrust Response	131
4.25 Relationship Between LP and HP shaft	132
4.26 Transient Trajectories on the Fan Characteristic	133
4.27 Transient Trajectories on IP Compressor Characteristic	134
4.28 Transient Trajectories on HP Compressor Characteristic	135
4.29 Variation of HP Compressor Surge Margin	136
4.30 Transient States Responses	137
4.31 Transient States Responses	138
4.32 Fuel Flow and Thrust Responses	139
4.33 Relationship Between LP and HP Shaft	139
4.34 Transient Trajectories on Fan Characteristic	140
4.35 Transient Trajectories on IP Compressor Characteristic	140
4.36 Transient Trajectories on HP Compressor Characteristic	141
4.37 Variation of HP Compressor Surge Margin	142
4.38 The structure for validating linear models	145
4.39 Comparing Linear and Nonlinear Model: Single-Spool Engine	147
4.40 Comparing Linear and Nonlinear Model: Single-Spool Engine	148

4.41	Comparing Linear and Nonlinear Model: Turbofan Engine	149
4.42	Comparing Linear and Nonlinear Model: Turbofan Engine	150
4.43	Comparing Linear and Nonlinear Model: Turbofan Engine	151
4.44	Comparing Linear and Nonlinear Model: Turbofan Engine	152
5.1	The Diagram Illustrating Gain Scheduling Scheme	156
5.2	Shaft Speed and Thrust Relationship of Single-Spool Engine	160
5.3	LP Shaft Speed and Thrust Relationship of Two-Spool Engine	161
5.4	The Possible Selection of Desired Responses	162
5.5	The Transient Tracking Trajectory of Single-Spool Engine	163
5.6	The Transient Tracking Trajectory of Two-Spool Engine	164
5.7	The Transient Tracking Trajectory of Single-Spool Engine	164
5.8	The Transient Tracking Trajectory of Two-Spool Engine	165
5.9	Tracking the Pressure Ratio on the Surge Line	165
5.10	The Closed-Loop System	166
5.11	Frequency Domain Design Specifications	167
5.12	The Singular Value Plot for Single-Spool Engine	169
5.13	The Singular Value Plot for Single-Spool Engine	169
5.14	Closed-Loop Frequency Response	171
5.15	Singular Value Plot of Loop Transfer Function	171
5.16	Singular Value Plot of Sensitivity Transfer Function	172
5.17	Singular Value Plot of Closed-Loop Transfer Function	172
5.18	Closed-Loop Frequency Response	174
5.19	Singular Value Plot of Loop Transfer Function	174
5.20	Singular Value Plot of Sensitivity Transfer Function	175
5.21	Singular Value Plot of Closed-Loop Transfer Function	175
5.22	Variations of Proportional Gains K_p with Non-dimensional Speed	176
5.23	Variations of Integral Gains K_i with Non-dimensional Speed	177
5.24	Variations of Proportional Gains K_p with Non-dimensional Speed	177

5.25	Variations of Integral Gains K_i with Non-dimensional Speed . . .	178
5.26	Comparison of Nonlinear Controller and Open-Loop Controller . .	179
5.27	Comparison of Nonlinear Controller and Open-Loop Controller . .	180
5.28	Tracking Performance Evaluation for the Single-Spool Engine . .	181
5.29	Tracking Performance Evaluation for the Single-Spool Engine . .	181
5.30	Comparison of Nonlinear Controller and Open-Loop Controller . .	183
5.31	Comparison of Nonlinear Controller and Open-Loop Controller . .	184
5.32	Comparison of Nonlinear Controller and Open-Loop Controller . .	185
5.33	Comparison of Nonlinear Controller and Open-Loop Controller . .	186
5.34	Comparison of Nonlinear Controller and Open-Loop Controller . .	186
5.35	Comparison of Nonlinear Controller and Open-Loop Controller . .	187
5.36	Comparison of Nonlinear Controller and Open-Loop Controller . .	187
5.37	Alternative Way to Control Compressor Surge	188
5.38	Comparisons of Transient Trajectory	188
5.39	The Variation of Compressor Inlet Guide Vane	189
6.1	The Structure of a Model-based Observer	194
6.2	The Structure of a PI Observer	199
6.3	The Structure of a Linear Quadratic Regulator	199
6.4	Responses of Open-Loop Observer Without Control	205
6.5	Responses of Open-Loop Observer Without Control	205
6.6	Responses of Closed-Loop Observer Without Control	206
6.7	Responses of Closed-Loop Observer Without Control	207
6.8	Responses Due to the Use of PI Observer	208
6.9	Responses Due to the Use of PI Observer	208
6.10	Responses of Closed-Loop Control and Observer	209
6.11	Responses of Closed-Loop Control and Observer	210
6.12	Closed-Loop Responses to Inlet Flow Disturbance	211
6.13	Closed-Loop Responses to Inlet Flow Disturbance	211

6.14	Closed-Loop Responses to Inlet Flow Disturbance	212
6.15	Closed-Loop Responses to Inlet Flow Disturbance	213
6.16	Open-Loop Observer and Closed-Loop Control	214
6.17	Open-Loop Observer and Closed-Loop Control	214
6.18	Open-Loop Observer and Closed-Loop Control	215
6.19	Open-Loop Observer and Closed-Loop Control	215
6.20	Open-Loop Observer and Closed-Loop Control	216
6.21	Open-Loop Observer and Closed-Loop Control	216
6.22	Closed-Loop Observer and Closed-Loop Control	217
6.23	Closed-Loop Observer and Closed-Loop Control	217
6.24	Closed-Loop Observer and Closed-Loop Control	218
6.25	Closed-Loop Observer and Closed-Loop Control	218
6.26	Closed-Loop Observer and Closed-Loop Control	219
6.27	Closed-Loop Observer and Closed-Loop Control	219
6.28	Closed-Loop Observer, Closed-Loop Control and Disturbance . . .	220
6.29	Closed-Loop Observer, Closed-Loop Control and Disturbance . . .	220
6.30	Closed-Loop Observer, Closed-Loop Control and Disturbance . . .	221

NOMENCLATURE

A_j	=	Propulsion nozzle area.
A_b	=	Bleed valve area.
a_i, b_i	=	Coefficients for a polynomial.
c_p, c_v	=	Specific heat capacities.
$cri1$ to $cri4$	=	Performance index.
F_{net}	=	Net thrust
$g\sigma$	=	Standard deviation.
$germ$	=	Relative error.
J	=	Shaft inertia
K_p	=	Observer gain vector.
K, k	=	Pressure loss coefficients.
K_d	=	Steady-state gain of thermal disturbances.
$Mach$	=	Mach number
\dot{m}	=	Mass flow rate.
\dot{m}_f	=	Fuel flow.
N	=	Engine shaft speed.
nc	=	Number of data points.
np	=	Number of data points used to construct model.
P	=	Stagnation pressure.
PLA	=	Power level angle.
PR	=	Pressure ratio.
q_1, \dots, q_4	=	Weighting coefficients.
s_{mag}	=	Normalized surge margin.
T	=	Stagnation temperature.
T_{lag}, τ	=	Time constants
R	=	Gas constant.
V	=	Intercomponent volume.
W	=	Power
γ	=	Ratio of specific heat.
η_{is}	=	Isentropic efficiency.
Δ	=	Deviation variable

SUBSCRIPT

- 1,2...13 = Station number.
- com* = Compressor.
- crit* = Critical.
- o* = Stagnation parameter.
- H or HP* = High pressure shaft.
- L or LP* = Low pressure shaft.
- tub* = Turbine.

Chapter 1

Modelling and Control of Gas Turbine Engines

SUMMARY

The interdisciplinary subject of modelling and control of gas turbine engines is introduced by means of a comprehensive literature survey. This provides particular insight into the operating problems that gas turbine engines face and the deficiencies of the existing approaches to modelling and control. After considering the performance requirements of gas turbine engines, a systematic modelling approach and control strategy are proposed. The layout and contributions of this thesis are given in the final section of this chapter.

1.1 Introduction

Gas turbine engines are thermodynamic machines which have been widely used as propulsion systems for a variety of civil and military aircrafts. From the aerothermodynamic viewpoint, the working processes in the gas turbine engines are very complex. As air flows through the engines, subjected to the extensive work and

heat transfers, its aerodynamic properties such as pressure and density and thermal properties such as temperature and entropy have significant spatial and temporal variations [1]. Such appreciable nonequilibrium and nonuniform conditions are present in every engine component. Furthermore, gas turbine engines have to regularly operate under a wide range of ambient conditions. In practice, this usually means that the design of an engine and its control system designs involves necessary compromises to provide acceptable performance for all expected duties. Indeed, most of today's aircraft gas turbine engines are equipped with sophisticated controls to allow constrained optimisation under all anticipated disturbances and further to permit orderly shutdown under extreme emergencies.

1.1.1 Modelling Gas Turbine Engines

By modelling a gas turbine engine, we provide a passage from a complex engine system to an abstract mathematical representation. This procedure is shown in Figure 1.1. Obviously, the engine dynamic analysis and controller design require

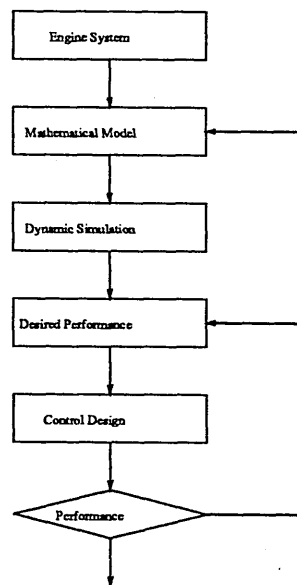


Figure 1.1: The Procedure of Modelling and Control of Gas Turbine Engine

a model in the form of a specific mathematical representation. This step, that of representing an engine by a substitute mathematical model, is certainly the most

crucial and probably the most difficult part of the analysis [2]. In the present application, the process of developing a model for an engine can be characterised in terms of the following sequential steps.

- Choice of level of detail and targeted objectives of the model.
- Collection and organisation of available information about the engine.
- Formulation of system equations for the engine and its components.
- Implementation of developed model via simulation. This may include computation of steady-state and transient behaviour.
- Model validation.

1.1.2 Control Objectives

The traditional and easiest approach to the control system design for a nonlinear systems involves linearising the nonlinear dynamics of the systems around steady-state points and applying linear control theory. It is obvious that the controller performance in this case will deteriorate as the systems operate away from the steady-state operating points around which the models were linearised.

Often the linear models employed for engine control system design are only very poor approximations to the real engine behaviour. While it is generally feasible to deal with mild nonlinearities just by using detuned linear controllers. In the presence of strong nonlinearities, design based on nonlinear models can offer distinct advantages.

Performance requirements imposed on a gas turbine engine dictate the needs for continuous monitoring and effective control of its performance variables. The main objectives of a gas turbine engine control system can be summarised as:

- Suppressing the influence of external disturbances.
- Stabilisation of an engine during its operations.

- Optimising the steady-state and transient performance.

Control systems which are capable of meeting these operational objectives have been actively pursued in the past [3]. The difficulties in designing effective controls for a gas turbine engine are related to its two inherent features; nonlinearities and the possibility of large magnitude variations in performance parameters. The nonlinearities are mainly due to the complex flow and the dynamic variations. Therefore, an accurate model of an engine is a prerequisite for studies into the control design problems.

1.2 An Overview of Engine Modelling

Many authors have worked on developing models for gas turbine engines. The models found in the open literature range from empirical ones for immediate use to abstract ones for qualitative general insight. The objective in developing a model is to utilise it either for engine design or for control studies. In the case of design, the nonlinear models may include every detail of the engine dynamics. These make it impractical to be used as control models. Linear empirical models, in the case of control, often result in detuned controllers which are inadequate to control the engine. Under the context of modelling and control, it is desirable to refine both linear and nonlinear models to enable them to be mutually complementary and reinforcing, each providing new sights for the other.

1.2.1 Linear Empirical Modelling

A linear empirical modelling approach is very useful whenever information regarding an engine's steady-state is available. An important assumption in this method is that around a steady-state operating point, the behaviour of an engine can be treated as that of a linear system. In this light, a single-spool engine was studied by Otto and Taylor [4] and a two-spool turbojet engine by Novik [5].

In Otto and Taylor's work, a single-spool engine was studied with fuel flow used as the only control. The torque exerted on the engine shaft is assumed to be a function of shaft speed and fuel flow:

$$Q = Q(N, \dot{m}_f) \quad (1.1)$$

Linearising Equation 1.1 at the design point, the following equation in terms of deviation variables (departure from steady-running condition) is obtained:

$$\Delta Q = \frac{\partial Q}{\partial N} \Delta N + \frac{\partial Q}{\partial \dot{m}_f} \Delta \dot{m}_f \quad (1.2)$$

Applying Newton's second law to the rotating shaft, the deviation of torque can be related to the deviation of shaft speed as:

$$\Delta Q = I \frac{d\Delta N}{dt} \quad (1.3)$$

Substituting Equation 1.2 into Equation 1.3, we obtain:

$$I \frac{d\Delta N}{dt} = \frac{\partial Q}{\partial N} \Delta N + \frac{\partial Q}{\partial \dot{m}_f} \Delta \dot{m}_f \quad (1.4)$$

It should be noted that Equation 1.4 holds only for one flight condition, e.g. a fixed ambient condition and Mach number [6]. Because shaft speed, fuel flow and torque can all be corrected to the engine inlet condition, the above equation can be rearranged into the normalised form as:

$$I\sqrt{T_1} \frac{d\Delta(N/\sqrt{T_1})}{dt} = P_1 \frac{\partial(Q/P_1)}{\partial(N/\sqrt{T_1})} \Delta(N/\sqrt{T_1}) + \frac{1}{\sqrt{T_1}} \frac{(\partial Q/P_1)}{\partial(\dot{m}_f/P_1\sqrt{T_1})} \Delta \dot{m}_f \quad (1.5)$$

where P_1 and T_1 are the engine inlet pressure and temperature. Transforming Equation 1.5 into Laplace form and rearranging the resultant equation, we have:

$$\Delta\left(\frac{N}{\sqrt{T_1}}\right) = \frac{k_s}{\tau s + 1} \Delta \dot{m}_f \quad (1.6)$$

where time constant τ and steady-state gain k_s are equal to:

$$\tau = -\frac{I\sqrt{T_1}}{P_1} \frac{1}{\partial(Q/P_1)/\partial(N/\sqrt{T_1})} \quad k = \frac{1}{P_1\sqrt{T_1}} \frac{\partial(N/\sqrt{T_1})}{\partial(\dot{m}_f/P_1\sqrt{T_1})} \quad (1.7)$$

For a specific engine where steady-state relationship between speed, fuel flow and torque is given, it is clear from Equation 1.7 that;

- At a given $N/\sqrt{T_1}$, the actual fuel flow to the engine is proportional to $P_1\sqrt{T_1}$.
- The engine time constant τ is proportional to $\sqrt{T_1}/P_1$.
- Steady-state k_s is inversely proportional to $P_1\sqrt{T_1}$.

Because P_1 and T_1 vary considerably over the flight envelope, the engine response is slower and consumes less fuel at high altitudes than at sea level for the same non-dimensional shaft speed $N/\sqrt{T_1}$.

The above model for a single spool engine was validated on a digital computer by Ketchum and Craig [7], and on an analogue computer by Pack and Phillips [8]. Their results agreed with the engine test results.

A linear model of a two-spool turbojet engine was firstly developed by Novik [5]. Following the same assumption as above, he obtained time constants for each shaft in terms of partial derivatives by assuming that engine dynamics are mainly dominated by shaft inertias. Fuel flow \dot{m}_f and propulsion nozzle A_j area are used as controls and states are two shaft speeds N_L and N_H . The resultant equations are summarised as follows:

$$Q_L = Q_L(N_L, N_H, \dot{m}_f, A_j) \quad (1.8)$$

$$Q_H = Q_H(N_L, N_H, \dot{m}_f, A_j) \quad (1.9)$$

$$\Delta Q_L = \frac{\partial Q_L}{\partial N_L} \Delta N_L + \frac{\partial Q_L}{\partial N_H} \Delta N_H + \frac{\partial Q_L}{\partial \dot{m}_f} \Delta \dot{m}_f + \frac{\partial Q_L}{\partial A_j} \Delta A_j \quad (1.10)$$

$$\Delta Q_H = \frac{\partial Q_H}{\partial N_L} \Delta N_L + \frac{\partial Q_H}{\partial N_H} \Delta N_H + \frac{\partial Q_H}{\partial \dot{m}_f} \Delta \dot{m}_f + \frac{\partial Q_H}{\partial A_j} \Delta A_j \quad (1.11)$$

Using equation $\Delta Q_L = I_L d\Delta N_L/dt$, $\Delta Q_H = I_H d\Delta N_H/dt$ and defining the time constants for each shafts as $\tau_L = -I_L \partial Q_L / \partial N_L$ and $\tau_H = -I_H \partial Q_H / \partial N_H$, the resultant equations are:

$$\Delta N_L = \frac{k_{mf}}{(\tau_L s + 1)(\tau_H s + 1)} \Delta \dot{m}_f + \frac{k_{Aj}}{(\tau_L s + 1)(\tau_H s + 1)} \Delta A_j \quad (1.12)$$

$$\Delta N_H = \frac{k_{mf}}{(\tau_{HS} + 1)(\tau_{LS} + 1)} \Delta \dot{m}_f + \frac{k_{Aj}}{(\tau_{HS} + 1)(\tau_{LS} + 1)} \Delta A_j \quad (1.13)$$

Determination of the parameters in the above equations depends on the availability of steady-state information about the engine.

It is obvious that the steady-state information about an engine is vital in determining whether this approach should be used. The later development is to find quick and efficient algorithms for estimating engine time constants associated with the shafts. Gold and Rosenzweig [9] proposed a simple method to calculate the rotor time constant for a single-spool engine. The only information needed in their approach was the shaft inertia and the knowledge of the variations in airflow and compressor temperature rise with respect to the engine speed. This method gave good correlation for engines with a centrifugal compressor. It was shown in [10] that the agreement was not very good for an engine with axial-flow compressor. A good approximate method was proposed by Lawrence and Powell [11]. In their study, the main assumption is : following a step change in fuel flow, the turbine torque changes but the compressor torque does not. As a result, the time constant of a single-spool engine was obtained as:

$$\tau = \frac{1.05 \times 10^{-8} IN}{1 - T_4/T_3} \frac{dN}{d\dot{m}_f} \quad (1.14)$$

All parameters in the expression can be readily obtained from the steady-state test, making the method a convenient and efficient way to estimate the time constant.

Several limitations are inherent in this method. Treating an engine as a linear system is valid only when the engine operates around the steady-state operating points. Although an analytical linear expression can be obtained, it will be useless without knowledge about steady-state. If the control is mainly to regulate engine operations around steady-state points, in particular around the design point, then effective control can be designed based on the linear empirical models. One important aspect of this approach is that a set of linear models generated in this way provides a potential for nonlinear gain-scheduled controller design [12]. A

disadvantage is that the transient information about compressors is lost due to the linear assumption.

An empiric model for a turbofan has been described by Barker et al [28]. The model comprises eight nonlinear sub-models which generate eight measurable outputs from the single control input, fuel flow. Two of the measurable outputs, low pressure spool speed and high pressure spool speed, are the state variables used in the model. A specific feature of the model is the use of nineteen tables of nonlinear functions which account for the parameters influencing engine performance.

1.2.2 Identifying Dynamic Models

One important aspect of modelling is the identification of dynamic models from the engine test data. Of particular interest is the real time identification with time-varying parameters using closed-loop test data. This allows an engine model to be updated in real-time as the engine moves from one flight condition to another. This kind of research could lead to a self-tuning or adaptive engine control system. The structure of such a control could be fixed, but the nominal model parameters within the structure would be constantly updated based upon real-time knowledge about the specific engine dynamics. The models obtained by means of identification techniques are certainly valid over a larger range than the linear empirical models generated as above [13]. In applying system identification techniques on gas turbine engines, extensive insights about the engine operations are necessary. Furthermore extensive experimental results are also required in order to lead to a successful model.

Michael and Farrar [14] proposed an algorithm based on the least-squares estimation technique. Nonlinear dynamic filtering was used to identify the parameters of a fixed structure multivariable model for the F-100 turbofan engine. Noise was introduced to simulate stochastic input-output data. Parameters of the multivariable model were identified from the simulated stochastic input-output open-loop

engine test data. The work by DeHoff [15] reported a technique used to determine a single-input engine model from closed-loop flight data using a maximum likelihood parameter search approach. It was assumed that there was no process noise and the parameter search was accomplished off-line. In the work of Merrill [16], the engine dynamics of the F-100 engine was identified using actual closed-loop input-output engine altitude test data. The parameters were identified using a recursive instrumental variable approach that, although applied off-line, could be implemented on-line to continually update the model parameters as the engine test evolves. In another work by Farrar [17], a two-input model was obtained using the “method of models” and this model was then used in several studies into engine condition monitoring. DeHoff and Hall [18] deduced an F-100 engine model from an engine simulation using the offset derivative approach and the output error identification technique.

A multivariable model for a turbofan engine was obtained by Merrill [19] as a time domain realisation of single-input single-output transfer function. The realisation was constructed by retaining the engine’s centralised fixed modes and eliminating all others. The single-input single-output transfer function was identified by the extended, adjustable parameter vector recursive identification technique. In another paper, Merrill [20] used a time series analysis method to find the model structure which is equivalent to Kalman filters for a single-input engine. Warner and Ward [21] introduced a filtered sequential regression parameter identification technique to derive the engine model. This is feasible for on-line digital computer implementation on gas turbine engines.

1.2.3 Nonlinear Aerothermodynamic Models

A nonlinear aerothermodynamic model has been developed by applying various aerothermodynamic principles to a gas turbine engine. Such a general model involves the equations of conservation of mass, conservation of momentum, and

conservation of energy. A model due to this approach, was found in the work by Schobeiri [22], [23]. To reduce the computer load, he simplified the resulting equations based on the following unsteady quasi one-dimensional flow assumptions as:

- The flow through an engine is axisymmetric and inviscid.
- The flow properties such as velocity, pressure, density, temperature and entropy are approximately uniform in any plane normal to the flow direction.
- There are no body forces or external forces. The ideal gas law, $p = \rho RT$ holds.

The resultant equations are expressed in terms of density, mass flow rate and stagnation temperature.

$$\frac{\partial \rho}{\partial t} = -\frac{\partial(\dot{m}/A)}{\partial x} \quad (1.15)$$

$$\frac{\partial \dot{m}}{\partial t} = -\frac{\partial(\dot{m}A)}{\partial x} - \frac{\partial(pA)}{\partial x} - (\dot{m}V + pA)\frac{1}{A}\frac{\partial A}{\partial x} - c_f\frac{\dot{m}V}{2D_h} \quad (1.16)$$

$$\frac{\partial T}{\partial t} = \frac{K}{c_p} \frac{\dot{m}}{\rho A} \frac{\partial(c_p T)}{\partial x} - \frac{(K-1)}{c_p} \left(\frac{1}{\rho} \frac{\partial(\dot{m}/A)}{\partial x} \right) \left(c_p T + \frac{1}{2} \left(\frac{\dot{m}}{\rho A} \right)^2 \right) + \frac{\dot{m}}{\rho^2 A^2} \frac{\partial \dot{m}}{\partial t} - \frac{K}{\rho c_p} \delta c_p \quad (1.17)$$

The next step is to apply these equations to each engine component, which results in a set of nonlinear differential equations as the model for a gas turbine engine. It is obvious such a model is impractical for use as a control model because it will be of very high order.

1.2.4 Nonlinear Thermodynamic Models

In a nonlinear thermodynamic model, it is essential to have the engine component characteristics, which are generally available as the result of engine design and test. Given the engine layout, the interactions between the components and thermodynamic cycle of the entire engine is consequently defined. This powerful approach to modelling gas turbine engines was first proposed by Dugan and Fillipi

[24] who were motivated to consider engines as nonlinear systems. Following a large step change in fuel flow, accelerations of a two-spool turbojet engine over the entire operating range were studied. This was done by finding a series of engine operating points for which flow compatibility, but not work compatibility, was satisfied; from the resulting torque imbalance the rotor acceleration rate and the engine speed response could be found. From the modelling viewpoint, this method was further characterised by:

- Method of Continuity of Mass Flow (CMF).
- Method of Intercomponent Volumes (ICV).

The differences between these two methods are due to the number of states used in the model. In the CMF method, it is assumed that at any instant, the mass flow through the engine is the same in the gas path. That is there are no dynamic lags associated with pressurisation of the component volumes. As a result, a low-order nonlinear model is obtained with only shaft speeds as state variables. Extensive iterative loops will exist in a digital simulation to satisfy necessary flow matching conditions between the components, and this makes simulation time relative longer. In the ICV method, the physical meanings were attached to the intercomponent volumes, and pressures and temperatures can be selected as state variables in addition to engine shaft speeds. A significant advantage of this approach is that the high-frequency dynamics can be easily included in a model and model reduction can be carried out based on the insight about frequency range over which the controls are supposed to work.

1.2.5 The Lumped Continuity Model

A model has been named as “The lumped continuity model” because of the manner in which compressors and turbines and their intercomponent volumes are represented. The underlying assumptions when developing such a model are made by Onions and Foss [26]:

- Momentum effects associated with much shorter time scales than those exhibited by the other equations, assuming them to be instantaneous, have little effect on the engine dynamics and therefore can be ignored.
- Little or no energy is added to the gas stream during its passage through the intercomponent volumes. Conservation of energy can therefore be approximated by assuming adiabatic conditions in characteristics.

Onions and Foss [26] have demonstrated that compressor simulation, constructed by assuming quasi-steady measured stage characteristics linked by stage volumes described by unsteady flow equations, can exhibit surge-like instabilities in the appropriate operating region. National Gas Turbine Establishment (NGTE) have adopted this approach in modelling several gas turbine engines [26]. The simulation work was reported for a two-shaft turbofan having a bypass pressure ratio 4:1 with no mixing, and includes an eight stage version of an experimental research compressor, containing three rows of variable geometry.

In Onions and Foss's work, they separate the effects of the momentum equation from the stage by stage approach by a lumped momentum continuity model. The additional momentum equation takes the form:

$$\frac{d}{dt}\dot{m} = \frac{K_3 A}{L}(P_{in} - P_{out}) - \frac{F_{net}}{L} \quad (1.18)$$

where F_{net} would, in a gas turbine, represent the sum of the pressure forces acting on the walls and drag force.

In steady-state:

$$F_{net} = \frac{K_3 A}{L}(P_{inss} - P_{outss}) \quad (1.19)$$

Now the pressure ratio can be obtained from the compressor characteristic:

$$Pr = \frac{P_{outss}}{P_{inss}} = f\left(\frac{\dot{m}\sqrt{T_{in}}}{P_{in}}, \frac{N}{\sqrt{T_{in}}}\right) \quad (1.20)$$

Hence:

$$F_{net} = \frac{K_3 A}{L} P_{outss} \left(\frac{1}{Pr} - 1\right) \quad (1.21)$$

In a similar fashion to Corbett and Elder, it was assumed that the above steady-state expression for F_{net} is also satisfied transiently, i.e the net force is equal to that experienced in steady-state for similar inlet conditions. In terms of mass flow rate, the resultant equation of momentum becomes:

$$\frac{d}{dt}\dot{m} = \frac{K_3 A}{L} [(P_{in} - P_{inss}) + (P_{out} - P_{outss})] \quad (1.22)$$

1.2.6 The Stage-Stacked Momentum Continuity Model

The objective of this model [26] is to study the performance of the HP compressor and therefore the remainder of the simulation has been kept as simple as possible. This led to the following simplifications:

- No internal air bleed or power offtake.
- Components, other than the HP compressor, have fixed efficiencies.
- Specific heats are constant for each component.
- Pressure loss in the combustion chamber, by-pass duct and jet pipe are constant percentage.
- Combustion efficiency is constant.
- Nozzle discharge coefficients are constant.
- Isentropic flow with $\gamma = 1.4$ occurs in the final nozzle.

This model has been used to simulate the compressor as a single entity using overall steady-state characteristics. The stage-stacked model uses the momentum continuity approach but simulates each stage of the HP compressor separately using the individual steady-state stage characteristics. Thus the model becomes complex in terms of computation as the compressor is now represented by eight sets of equation as opposed to the one for the previous analysis.

This model has two main advantages. Firstly it allows the compressor stage to be transiently mismatched, which leads to the possibility of simulating the onset of surge, and predicting the transient movement of the surge line. Secondly the simulation should be capable of being used to determine the optimum settings for the variable geometry both under the steady-state conditions and transiently.

1.2.7 Bond Graph Models

It must be mentioned here that some effort has already been made to apply the systematic bond graph modelling technique to a gas turbine engine. The only publication in this aspect of bond graph application is by Krikelis and Papadakis [27]. In the paper, only the general strategy is discussed.

1.2.8 Remarks on Modelling

The models mentioned above were used for predicting engine performance. Among various performance and safety considerations, compressor surge is a major consideration in the design of gas turbine engines and their control systems. The compressor designer must provide adequate surge margin between engine working line and surge line, and the control system must ensure that sufficient of that margin is retained during transients, in particular during a slam acceleration. The prediction of surge margin and working line variation during transients is therefore of major importance [25].

To provide sufficient surge margin at off-design conditions, variable geometry or bleed valve may be used. It is likely that greater advantage may be achieved from these variables if their controls, either closed-loop or scheduled, were integrated within the overall engine control scheme and could constitute a major contribution to surge avoidance.

The control strategy required to achieve this is not yet understood, and no satisfactory basis exists for optimising advanced control systems for surge avoidance.

This is not a task that can be undertaken by experiments on some long-suffering engine due to the high costs involved and the possibility of damage. Recourse must be made to simulation as the only practical alternative.

1.3 An Overview of Engine Control

1.3.1 Linear Design Model

A complete mathematical description of a gas turbine engine is exceedingly complex and highly nonlinear. The control synthesis procedure is dependent on the selection of a set of design models that may be used to formulate a control law for application throughout the engine operating range. Therefore a critical step in the control design procedure is the generation of tractable design models [29], [30]. Linear models are one class of such design models and can be effectively integrated to provide a nonlinear control function. Linear models have been used in most of the publications tackling engine control problems [31].

1.3.2 Model Reduction

Once nonlinear engine dynamics has been linearised, some method may be required to analyze the linear models and establish simpler design models which include only dynamic elements important to the desired control function. Without such simplification, design could result in highly complex and parameter sensitive controlled systems. Towards this end, the modal decomposition method has been used by DeHoff [32], [33] and Skira [34], and the multivariable residue method was used by Athans [35]. This provides one framework for reducing arbitrary linear models to design models containing an appropriate parameterisation.

1.3.3 Control Mode and Structure Analysis

Since the main control performance variables for the gas turbine engines cannot be measured, the problem of control mode selection must be studied to lead to an effective design. The objective of the control mode study is to select a mode that will indirectly control thrust while maintaining adequate compressor surge margin and engine temperatures within limits. Control mode analysis has been performed by many researchers and reported, for example, in the work of Brown [36]. They used the GE Aircraft Engines computer programme, called Control Mode Evaluation of Temperature Margin (COMET), to select control structure. This programme uses statistical variations between engines due to manufacturing tolerances, actuator and sensor tolerances, and changes in efficiency and flow functions due to engine deterioration with time.

In the analysis of control structure, The Relative Gain Array (RGA) described by McAvoy [37] and Morari [38] has been widely used. The RGA provides a measure of interaction between sensed and manipulated variables in a multivariable control system. It emphasises what manipulated variables and sensed variables can be paired and what simplified control structure can be used for closed-loop design without significant performance deterioration. The Singular Value Decomposition (SVD) method has been used by [39] to find out appropriate pairing between manipulated variables and sensed variables. The SVD method, by the use of the relative magnitude of the singular values, provides a clear insight into relative controllability between the selected controls and outputs. This play a very important role in helping to make decisions on the type of control structure that should be used. The topic of multivariable control structure and analysis has been systematically discussed by Nett [40] and Spang [41].

1.3.4 Control Design Methods

Designing control systems for gas turbine engines using modern control theory began to gain momentum in the late 1970s' when the U.S. Air Force first put forward the Pratt and Whitney F-100 Engine as a design example. Since then, efforts have been made to evaluate various modern control design techniques for the engine control problems. The motivation for these activities is that the ever-increasing performance requirements imposed on gas turbine engines, such as high cycle efficiency, fast dynamic response, reduced specific fuel consumption and safe operation cannot be fulfilled by the traditional control systems. Furthermore, the engine manufacturing technology has made it possible for variable geometries to be used as potential controls. Modern control applications on gas turbine engines are also stimulated by the improvements in microprocessor technology, which make it easy for control algorithms to be implemented. Because performance optimisation requires a control system to vary all control inputs simultaneously, the task of designing a control algorithm for such an engine becomes a formidable problem. Traditional single-input, single-output techniques can be used, but are often inadequate and require many interactions to get even close to a suitable engine control law. Efforts have also been made to evaluate various modern control design techniques on engine control problems.

Systematic control theory has existed since about the 1930s. The classical frequency-domain design and analysis methods of Nyquist, Bode, Nichols, and others led to the dominant methods of the late 1960s and the generalised Nyquist methods of the mid-1970s. However, classical methods and their extension are, in these forms, neither methodical nor easy to automate, nor do they, in general, result in an overall system exhibiting a high degree of robustness [42].

Modern control methods reduce at least some of the deficiencies in classical methods. The most common methods, termed "Linear Quadratic" (LQ), optimise system performance. The major benefit of the modern control methods is the

ability to guarantee the robustness of the closed-loop system, given full state availability.

In the early 1980s, a number of researchers shifted their emphasis to new methods. The most common of these methods are the unstructured uncertainty methods (H_∞) and their more complicated cousins, the structured uncertainty methods (μ -analysis). Whereas LQ methods seek performance optimisation at one loop point, methods based on (H_∞) and (μ -analysis) seek performance optimisation at multiple loop points simultaneously.

1.3.5 Proposed Engine Control Problem

All gas turbine engines have strict performance requirements at the steady-state operating points. These requirements specify the power output at a given mass flow rate in order to match the aircraft power requirements. In addition, the engine must operate efficiently from idle to take-off condition over a wide range of ambient conditions.

In addition to satisfactory steady-state operation, engines must move from one condition to another safely and rapidly. Engine safety is a predominant concern because most modern propulsion systems operate at the limit of their performance capability. The engine protection criteria limit temperatures, speeds and pressures. Limits are also required to ensure stable compressor flow without surge. Disturbances in the form of inlet airflow distortion and pressure transients must be suppressed. The engine controller must sense ambient conditions and critical engine parameters in response to the operator's demand. It must provide the logics and computations necessary to modulate the engine thrust throughout its operating range.

In general, the aim of the control is to define engine thrust level and response rate in response to a pilot's command. This requirement has to take into consideration several factors:

1. Desired response characteristics (e.g. engine acceleration rate).
2. Component operating point matching to provide high operating efficiency.
3. Ambient conditions.
4. Engine stability constraints such as airflow limits and stall avoidance.
5. Component performance limitations such as maximum actuator slew rates.

1.3.6 Multivariable Frequency Domain Methods

Controller design using Multivariable Frequency Domain approaches has been widely used on gas turbine engines. One of the earliest applications of the well-known Inverse Nyquist Array (INA) method was to a gas turbine engine [43]. Rosenbrock and Munro [44] used the INA method to investigate the flexibility of approximate decoupling on a linear model of F-100 engine. The model has three inputs, three outputs and sixteen states. The frequency domain concept of diagonal dominance is introduced as a means of assessing and reducing interactions between the loops, and further used to develop graphical stability criteria. As the result, the Gershgorin band and Ostrowski band were used to aid in studying the level of interactions, and the extent to which feedback gains can be varied. The resultant controller performed well in the sense of stability, fast response and small interaction. However, sensor and actuator dynamics had been neglected in the design. A later paper by Engell and Munro [45] tried to improve the control designed above by introducing actuator and sensor dynamics. They also give some guidance into the relationship between the open-loop frequency response and the closed-loop performance.

Spang [46] presented a paper which dealt with the application of INA method to the F-100 engine. His purpose was mainly to gain some insight into the controlled behaviour of the model with four inputs, four outputs, and five state variables, which brought a higher degree of interaction. The design was conducted

at one operating point for linear regulation. No attempt was made to achieve the design which would be capable of controlling the engine over the full power range. MacFarlane et al[47] presented results of applying INA and Characteristic Locus methods to a gas turbine engine model. They developed and described the generalisation of classical Nyquist-Bode and Root-Locus methods. The concept of duality between characteristic frequency and characteristic gain is used to relate the generalised Nyquist-Bode and the generalised Root-Locus methods to the standard state-space description. In particular, the paper shows how basic singularities of the transfer function involved are related to state-space model parameters. During the work of generalisation and design, use of well-established “inner” and “outer” loops in the feedback system design gives a natural framework within which one can weld the various techniques associated with generalised complex-variable methods into a unified design approach.

Edmunds [48] published another paper, which studied control systems using closed-loop Nyquist and Bode arrays. The resultant control schemes had closed-loop frequency response as close as possible, in a least squares sense, to a desired closed-loop response. Using the gain loci to ensure system stability, the closed-loop Bode array gave easily understood information about the controlled system in terms of bandwidth, speed of response, resonance and interaction. The closed-loop Nyquist array could be used to indicate the robustness of the control scheme for sensor failure. It can also predict the extent to which input noise will be suppressed, and the behaviour of the controlled system with actuator failure. The bands of Gershgorin and Ostrowski circles are used to indicate the behaviour for change in the characteristics of more than one sensor at a time. The verification of the method was conducted on a linear model of a jet engine. A study by Hoffmann et al[49] show that extension of classical frequency domain synthesis for single input and single output (SISO) systems to multiple input and multiple output (MIMO) systems. It involves identification of numerators of higher kinds than the first kinds, which result in an enormous simplification of the expressions

for closed-loop multivariable systems. Their design goals are:

1. Thrust response shall be rapid and free from overshoot.
2. Response in turbine inlet temperature and shaft speeds shall be rapid and free from overshoot.
3. Steady-state turbine inlet temperature shall be unchanged and transient increase in temperature shall be minimised.
4. Steady-state fan and compressor surge margins shall be unchanged.

The closed-loop transfer function they obtained was approximately established by the fact that numerators of all kinds can be interpreted as characteristic polynomials for the system under the constraints of infinite-gain control laws.

At the 1977 NEC forum, Kouvaritakis and Edmonds [50] presented a paper which describes how both multivariable Root-Locus and characteristic locus techniques were used to design a three-input and three-output controller for the F-100 engine. In addition, they considered a three-input problem in which estimates of the key unmeasurable variables (thrust, airflow and turbine inlet temperature) were used as feedback variables.

Leininger [51] reported on work using the Multivariable Nyquist Array (MNA) which treats dominance design as a problem of numerical optimisation of a fixed compensator structure. The main idea is to use conjugate direction minimisation algorithms to manipulate the set of unspecified parameters in the open-loop compensator matrices, and define a measure of the dominance levels for each row and column of the system transfer function. The concept of dominance sharing for the Multivariable Nyquist Array, together with a set of sufficient conditions, will direct the adjustment of crossed-coupled system interaction levels. In the 1980s, Leininger [52] further elaborated his work on dominance optimisation and sharing. An application of dominance-sharing concepts appears in his report in 1982 covering the MNA design of a two-input control for a general electric quiet

clean short-haul experimental engine. The design was evaluated over the full engine power range at the sea level static condition on both linear models and a nonlinear simulation. The paper by Schafer and Sain [53] presents a method which uses dynamic input compensation to achieve the column dominance which is a way of attaining diagonal dominance by use of frequency dependent, dynamic compensation. A graphical approach called Complex Acceptability Region for Diagonal Dominance is introduced to guide the design. The plots have the advantage that they can indicate whether it will be possible to realise dominance by simple, lead-lag compensators, rather than simply real compensators.

Work on the frequency domain design was carried out by Brown [54]. He describes the use of MacFarlane's CLADP package [55] to design multivariable regulators for an advanced variable-cycle engine for a V/STOL aircraft. The engine is quite complex, having 12 input variables. Approximate diagonalisation was achieved through use of the so-called KQ method and the resultant designs were evaluated on a nonlinear digital simulation.

Recently, Perez et al[56] have used the optimisation techniques to reducing the interactions between the loops. A precompensator was designed and its parameters are determined by minimising the interactions between the loop. Once this is achieved, the controllers can be designed for each loop on the basis of SISO design techniques.

The effort made by Baker [57] is to use a compensator to decouple the loops. The design starts by augmenting the plant state variables through adding states which are defined as the error between the set point and control output.

Other published references included Sain's method [58] which described the application of MacFarlane's Characteristic Locus method to a simple turbofan engine model. Gejji and Sain [59] also applied matrix polynomial design to engine control using a somewhat different frequency domain approach.

In 1986, Polley [60] designed a controller for the GE16/J11A6 variable-cycle

engine using Edmunds' KQ method (K - matrix compensator, Q - desired response). The design was validated for a single operating point. In 1989, Polley [61] extended his work to design an engine compensator for full flight operation. Controllers are designed for the selected operating points over the flight envelope using the KQ method. Thereafter, a nonlinear controller was obtained by scheduling gains of the linear compensators to the selected normalised engine variables. The nonlinear simulation at the flight condition of 36,000 feet and Mach number 1.2 has shown the satisfactory performance of the resultant nonlinear scheduled controller.

1.3.7 Control Using Linear Quadratic Methods

In the field of the control of gas turbine engines, the method that has been more actively pursued is that based on the Linear Quadratic Regulator (LQR). The first application of LQR methods to engine control was by Michael and Farrar [62]. They developed a control structure for handling large signal inputs and applied their control to a simulation of the F-100 engine at the sea level static condition. The six fifth-order linear models used in the design were derived at points from idle to intermediate power using a least-squares fit of engine test data. Control inputs were fuel flow, exhaust nozzle area, variable fan and compressor inlet guide vanes. With four controls, the four independent variables used to define the equilibrium point were thrust, turbine inlet temperature, and two geometry position schedules. In their method, the design model is augmented by control rates to achieve integral action. The four setpoint variables are defined as outputs, y_s , and the output perturbation is referenced to a command value of the setpoints as:

$$\Delta y = y_s - y \quad (1.23)$$

Beattie and Spock [63] had extended the work of Michael and Farrar to a two-spool, variable-area turbine engine with eight states, five controls and five outputs. This engine has variable turbine nozzle areas which affect the engine's response

characteristics. The control law is modified to include lead compensation in place of the pure derivative. The lead time constant is designed using classical bandwidth and noise amplification criteria. The engine setpoints are specified by a measured group of component variables. Cost function sensitivity to gain elements is used to simplify the feedback matrices. The study concluded that an additional procedure is needed to provide large transient reference trajectories for the output and control variables. Open-loop optimisation studies showed dramatic response improvement for this type of engine. Practical implementation is still of concern.

Work included in the reports by Stone et al[64] demonstrated the design and sea level testing of an LQR-based control for the GE J-85 engine. The primary control was fuel flow, with limited control of the exhaust nozzle area and scheduled control of the compressor bleed and the inlet guide vane. The control structure uses state feedback augmented with integral control of shaft speed. Model-following is used to accommodate large transients. The model represents a desired first order speed response. Temperature and pressure limits produce a command which overrides the fuel requirement during transients, i.e, the fuel requirement is selected as the minimum of three control law outputs derived to regulate shaft speed, pressure and temperature. The design model used in this study included many unsteady aerodynamic states, in addition to the simple first order lag associated with the shaft inertia.

Bowles [65] developed an optimal control law for the GE J-85 at sea level using a second order model with one control. The dynamics were associated with the shaft inertia and fuel pump responses. State feedback gains were calculated. An optimal feedforward gain was found for a step input. The engine operating line was separated into three linear regions and the gains to optimise the response were calculated for the control law.

$$u = c_x x + c_y y \quad (1.24)$$

where the control law quantities are absolute quantities. The gain, c_x , optimises the transient responses and gain, c_y , is used to satisfy the equilibrium conditions.

In the design by Elliott and Seitz [66], three engine states and one actuator lag were used with two control inputs (fuel flow and nozzle area) in the sea level static intermediate power model. State feedback was designed using integrals of shaft speed and exhaust temperature to specify steady-state. An interesting approach was used for the set point and transition logic. The control law has the form

$$u_i = K_{i1}\Delta N + K_{i2}\Delta T + K_{i3}\Delta P \quad (1.25)$$

Where $u_i, i = 1, 2$ are fuel flow and nozzle area. K_{ij} represents proportional and integral gains, $\Delta N, \Delta T$ and ΔP are errors in shaft speed, exhaust temperature and burner pressure respectively. The error signals are calculated as:

$$\Delta N = N - f_1(PLA) \quad (1.26)$$

$$\Delta T = T - f_2(N) \quad (1.27)$$

$$\Delta P = P - f_3(N) \quad (1.28)$$

where f_1 is a function of the power lever input (PLA), f_2 and f_3 are derived schedules which relate the temperature and pressure to the shaft speed. Accurate steady-state tracking is obtained as well as temperature and pressure limiting. The gains are determined from an augmented plant design. The overall dynamic response is determined by the linear feedback and the nonlinear effects are due to the slopes of the schedules.

Weinberg et al [67] have produced a series of reports illustrating the use of modelling and optimal synthesis techniques on the F-100 turbofan engine and a twin-spool, variable-area turbine derivative engine. The F-100 engine model has three engine states, four control variables and eight performance outputs. The model is augmented by the control rates. The control law is written as follows:

$$u = \int [c_x(x - x_o) + c_u(u - u_o)]dt \quad (1.29)$$

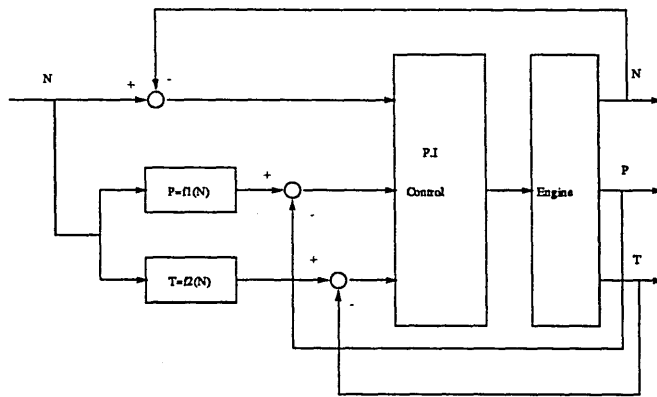


Figure 1.2: Diagram of Control Law Derivation

where x_o, u_o are derived from a set of sea-level operating line schedules as a function of power level. There are two models used in the design for low and middle power at sea level, static conditions. The gain matrices are interpolated in the transition region. Large transients are accommodated by rate limiting of the command. Merrill [68] documented the use of a discrete output regulator to control

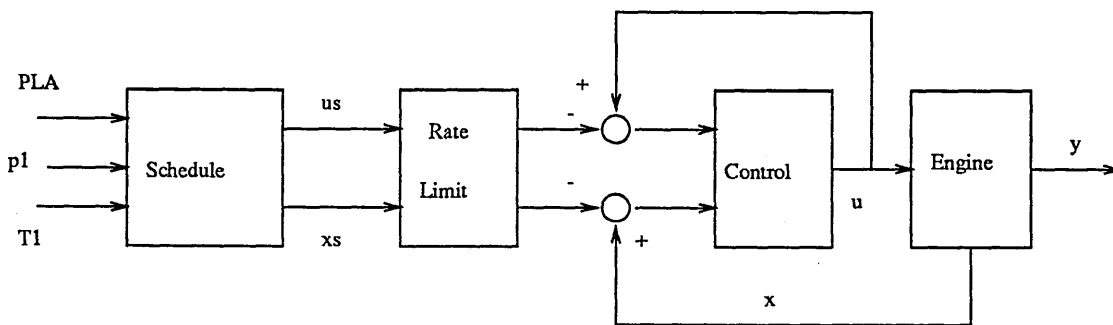


Figure 1.3: Control and Engine System

a simple turbojet engine simulation. He also investigated further applications of the output feedback regulator to the F-100 engine. A comparison between LQR results has shown essentially the same behaviour. The output regulator design allows a greater flexibility for direct fixed structure optimisation and multiplant design unavailable in LQR procedure. The importance of this procedure is that high order linear models do not penalise the control law with redundant and difficult estimates of feedback terms. The procedure can be used to validate designs produced by LQR synthesis.

Harvey and Stein [69] employed a new procedure for selecting weighting matrices to achieve desired asymptotic modal characteristics. The procedure is based on asymptotic modal characteristics of multivariable linear-quadratic regulators as control weights tend to zero. The asymptotic behaviour of both eigenvalues and eigenvectors is used to define a unique performance index.

The design methods summarised above resulted in a control law for engines of varying complexity. Control law synthesis seems a common routine. The major differences in control structure are due to

1. Engine model differences.
2. Setpoint schedule design.
3. Large transition logic and protection considerations.

Recently, an extended design method called Linear Quadratic Regulator and Linear Quadratic Transfer Recovery (LQR/LTR) has found a successful application in turbine engine control system design. This method adopts an integrated frequency and time-dominance approach to multivariable feedback control synthesis so as to meet stability robustness, command following and disturbance rejection specifications. The LQG/LTR methodology requires direct measurement of only the output variables that must be independently controlled to meet the posed command following and disturbance rejection specifications. Athans et al [70] described a design procedure using the linear model of the F-100 engine. The design starts with using the residue for model reduction and the resultant model was used to demonstrate that the neglected dynamics successfully accounted for by the design method in the description of the modelling uncertainties as well as stability robustness of the reduced-order model. Integral action has been forced into each channel to meet steady-state specifications.

Following their work on F-100 engine, Pfeil and Athans [71] further demonstrated the application of LQR/LTR on a GE-T700 engine. Designs were shown

on three different linear models. One is a SISO model which uses fuel flow to control power turbine speed and the other two are MIMO models using fuel flow and nozzle area to control gas generator speed and power turbine speed. LQR/LTR design for SISO model was used to demonstrate the improvements over the classical design, and MIMO design was used to show the success in achieving stability robustness and disturbance rejection which are both very important in this type of engine.

1.3.8 Control Using Alternative Methods

Work has also found on applying alternative control design methods on gas turbine engines. Monopoli [72] reported his work of applying model-following control approach to design a nonlinear controller for a gas turbine engine. The method shows the potential of eliminating or reducing the requirement for designing at a number of different operating points and yielding a good engine response under all operating conditions. The resultant control system forces certain engine variables to track the corresponding variables of an ideal model of the engine which is specified by the designer. Liapunov's Direct Method which is specifically intended to deal with nonlinear, time-varying systems, is the basis for the controller synthesis. The control structure is shown in Figure 1.4;

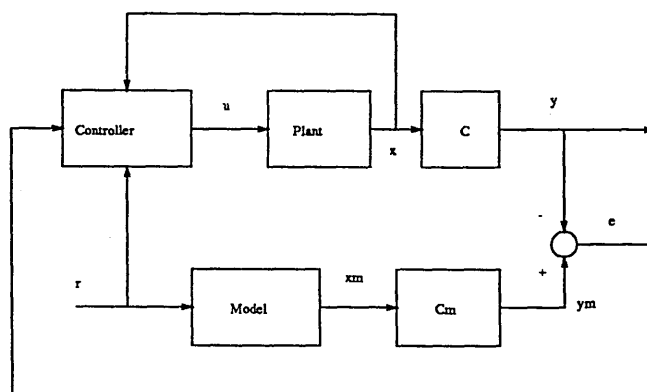


Figure 1.4: Model Following Control Structure

A feasibility study of the F-100 engine control system design was carried out

by Taiwo [73] who employed Zakian's Method of Inequalities to design a simple controller for the linear engine model. The method allows the designer to express each aspect of desired performance and each constraint as a separate inequality and therefore has the advantage of not being limited only to problems whose performance can be expressed by a single performance index. The design was conducted on two models of different complexity.

In 1990, Moellenhoff and Rao [74] published a paper which described the importance of robust controller design for a gas turbine engine. The design method is the Parameter Robust Linear Quadratic Gaussian with Loop Transfer Recovery (PRLQR/LTR) which demonstrated good robust properties with respect to both unstructured uncertainties in the frequency domain and the structured parameter variations in the time domain. This method uses an internal feedback loop to achieve robust with respect to structured parameter variations in the state-space model representations. The block diagram is given in Figure 1.5.

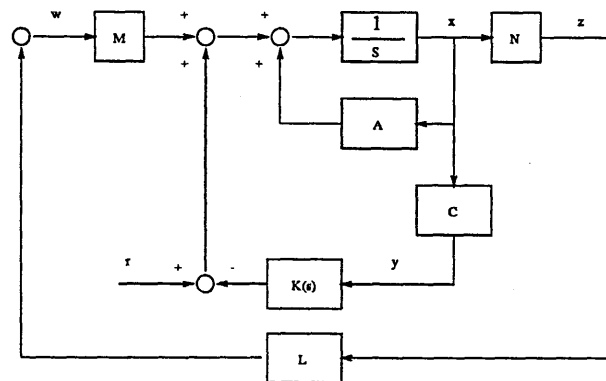


Figure 1.5: The Diagram of Internal Feedback Model Representations

The optimisation techniques have also been used to synthesise controllers for gas turbine engines. The work by Hancock and Fleming [75] used the multi-objective optimisation techniques to find out the parameter of a fixed structure controller. The performance objective was formulated as the desired time domain response. The diagram reported in their work is shown in Figure 1.6.

A similar method was found in the work by Hiesener[76].

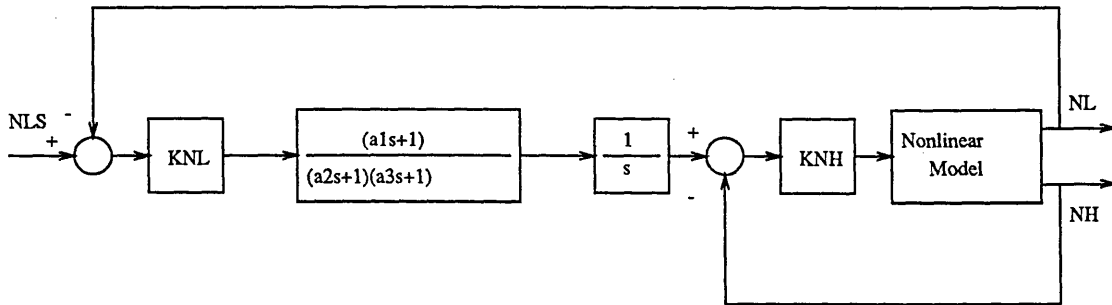


Figure 1.6: The Control Scheme in Multi-Objective Optimisation Scheme

1.4 Modelling Approach and Control Strategy

Following the review of the previous work described above, this section presents the approach which has therefore been adopted in the present study.

The nonlinear thermodynamic approach is used to model gas turbine engines. This is because in such models, the thermodynamic variables which govern each component are clearly defined and the lumped structures are very flexible to be used as a generic approach for modelling gas turbine engines. The achieved features of the models are:

- They are capable of predicting an engine's steady-state and transient performance with an acceptable accuracy and less computation time.
- Linear models can be directly generated from this model.
- The model can be used for nonlinear controller synthesis.

Using this modelling approach, the transient information about compressors is modelled and variable geometries as controls included.

Two control strategies considered in this work are nonlinear control and model-based control. In the present work, in spite of the ignorance of the high frequency dynamics in modelling an engine, linear models generated from the thermodynamic model represent the engine dynamics at the various operating conditions.

There are a number of performance variables on a real engine such as surge margin, turbine inlet temperature and thrust that cannot be directly measured, but must be monitored and controlled. In this situation, two solutions are possible with the aid of engine models. In the one case, indirect controls methods can be used which measure certain variables having close connections with the unmeasured outputs, for example, the inter turbine temperature is a clearly indication of turbine inlet temperature and behaviour of jet pipe pressure is a measure of engine thrust. On the other hand, a mathematical model can be used to estimate those unmeasured outputs to realise the direct control.

1.5 Contribution of This Thesis

The work presented in this thesis and the contributions by the author are laid as follows:

- Development of the nonlinear thermodynamic models for a single-spool turbojet engine (Avon RA-29) and a two-spool turbofan engine (RB-183). These models are based on the tested components' characteristics. The modelling process used by previous workers has been refined, and justifications are given as to the assumptions made and selection of state variables. This is described in Chapter 2.
- Proposition by author of a computationally efficient algorithms for approximating compressors and turbine characteristics. Characterisation of model qualities and criteria for model quality evaluation are defined. This is detailed in the Chapter 3.
- Prediction by digital simulations of the dynamic characteristics of the engines using the open-loop fuel controllers designed by the author. Furthermore, effects of variable geometries on an engine's dynamic responses are discussed. This is described in Chapter 4.

- The author has designed nonlinear controllers for the gas turbine engines using the gain scheduling approach. Using the closed-loop synthesis approach, the robust properties of the nonlinear controllers are discussed with respect to the selected scheduling variable. This is described in Chapter 5.
- Model-based control schemes have been proposed elsewhere. The author has applied the technique for the effective control of a gas turbine engine. The concept of a model-based observer is discussed and algorithms proposed. Direct control of unmeasured outputs are achieved by means of a robust PI observer design by the author. This is described in Chapter 6.
- Some conclusions based on the conducted research are drawn in Chapter 7, and further works in this area are suggested.

Chapter 2

Thermodynamic Models for Gas Turbine Engines

SUMMARY

The development of nonlinear thermodynamic models for a single-spool turbojet engine (Avon RA-29) and a two-spool turbofan engine (RB-183) is described in this chapter. At the component level of modelling, the most efficient and practical approach is selected among various alternatives. This has led to structurally compact models for the engines which are convenient for the subsequent performance analysis and control system design. Various assumptions made in the modelling process are discussed. Justifications are also given as to the way of selecting state variables.

2.1 Introduction

The method of modelling that allows greater insight into the dynamic behaviour of a gas turbine engine is based upon the characteristics for each of the engine components. A gas turbine engine comprises a number of components, and the

behaviour of each of these is well understood. The interactions between the components is fixed by the physical layout of the engine. Thus, for a given engine, if all component characteristics and the engine layout are known, then the gas turbine engine is precisely defined and its dynamic behaviour can be expressed mathematically.

This approach to developing the model for a gas turbine engine has many advantages. Estimates of the component characteristics could be available at as early as the design stage. The model is valid over the entire operating range and effects such as bleed flow and variable geometry can be easily included. Furthermore, a model of this type is a true representation of the thermodynamic process in the engine, and allows the behaviour of any engine performance parameter during transients to be determined by simulation. This method is also flexible to allow additional dynamics to be included, for example, investigations can be made on the effects of the thermal characteristics of the components [77].

2.2 System Description

2.2.1 Single-Spool Engine

The AVON RA-29 is a single-spool turbojet engine, as shown in Figure 2.1. Its

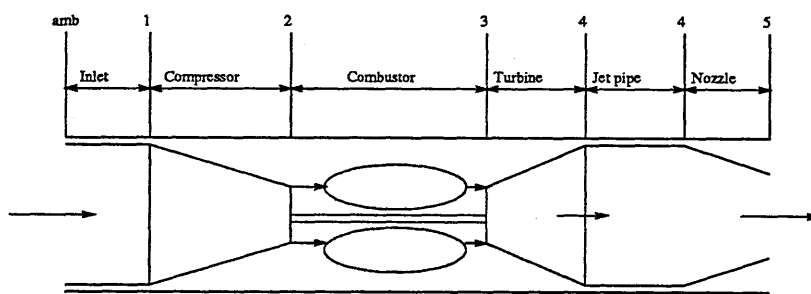


Figure 2.1: The Diagram of the Single-Spool Engine

components include: an inlet ($amb \rightarrow 1$), a 16 stage compressor ($1 \rightarrow 2$), a combustor ($2 \rightarrow 3$), a 3 stage turbine ($3 \rightarrow 4$), jet pipe ($4 \rightarrow 4$), and the propulsion nozzle ($4 \rightarrow 5$). For this engine, the steady-state characteristics for the compressor

Volume name	Physical meaning	Size
V_2	Compressor + Combustor	0.10 m^3
V_4	Turbine volume + Jet pipe + Nozzle	0.15 m^3

Table 2.1: The Volume Meaning for The Single-Spool Engine

and turbine are available. In developing the model, two intercomponent volumes are introduced and are assumed to locate at station number 2 and 4. The physical meaning of these volumes are given in table 2.1.

2.2.2 Typical Modern Turbofan Engine

This engine is a typical turbofan engine, which represents the modern state-of-the-art of Rolls-Royce in design and manufacturing. The diagram of this engine is shown in Figure 2.2.

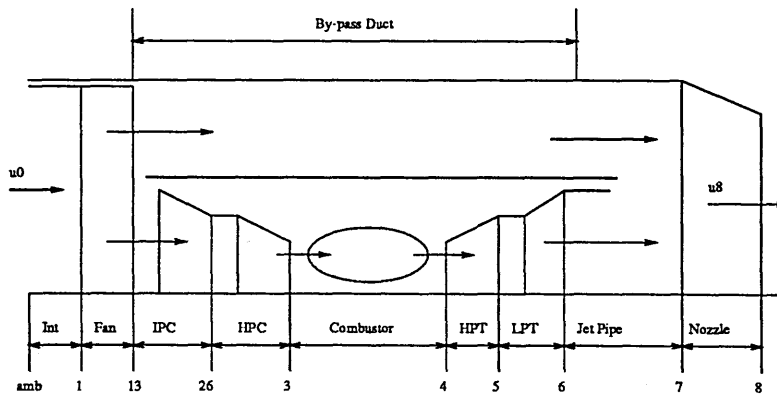


Figure 2.2: The Diagram of the Two-spool engine

The engine has a by-pass ratio of 3, which significantly reduces the engine noise [78]. Its components include; inlet ($amb \rightarrow 1$), a long chord fan ($1 \rightarrow 13$), intermediate pressure(IP) compressor ($13 \rightarrow 26$), high pressure(HP) compressor ($26 \rightarrow 3$), combustor ($3 \rightarrow 4$), high pressure(HP) turbine($4 \rightarrow 5$), low pressure(LP) turbine ($5 \rightarrow 6$), jet pipe ($6 \rightarrow 7$), by-pass duct ($13 \rightarrow 6$), and propulsion nozzle ($7 \rightarrow 8$). LP turbine is used to drive the fan and IP compressor, therefore they are on the same shaft. The HP turbine drives HP compressor through a concentric shaft and this combination is sometimes called a gas generator. There are five intercomponent volumes which are lumped to represent the dynamic effects of the

Variable	Physical meaning	Size
V_{13}	Fan + $\frac{1}{2}$ IP Compressor + $\frac{1}{2}$ By-pass Duct	0.50 m^3
V_{26}	$\frac{1}{2}$ IP Compressor + $\frac{1}{2}$ HP Compressor	0.10 m^3
V_3	$\frac{1}{2}$ HP Compressor + Combustor	0.20 m^3
V_5	HP Turbine + $\frac{1}{2}$ LP Turbine	0.10 m^3
V_7	$\frac{1}{2}$ LP Turbine + $\frac{1}{2}$ By-pass Duct + Jet pipe + Nozzle	0.5 m^3

Table 2.2: The Volume Meaning for the Two-spool Engine

components. The definitions of these volumes are given in the table 2.2.

2.3 Gas Turbine Modelling

In this section, The functions of each component in a gas turbine engine are described and different treatments in modelling are discussed.

2.3.1 Inlet

The purpose of the inlet duct is to recover the ambient pressure and temperature to the inlet of the following component (fan or compressor) at flight conditions. The airflow is decelerated in this component. The total pressure loss due to flow friction is relatively small. There are three different ways to model the process:

- Assuming isentropic flow [79].
- Using the isentropic efficiency to account for the pressure loss [80].
- Using a pressure recovery coefficient for pressure loss . [81], [82].

2.3.2 Fan and Compressors

Theoretically, there are two ways of modelling a fan and a multistage compressor. One is to use stage performance map, e.g. using the functional relationship between the pressure rise coefficient, temperature rise coefficient and flow coefficient. These relationship could either be obtained from single-stage test results or

estimated using general aerothermodynamic laws [83]. With this method, mass and energy storage in the compressor are modelled by taking into account of the physical volumes between the stages. The other method is to use the overall characteristic of the compressor. Effects of mass and energy storage in the compressor are lumped into a single volume. The functional relationship between pressure ratio, non-dimensional mass flow and isentropic efficiency are used [84], [85]. Modelling a compressor in this way is equivalent to ignoring the detailed dynamics inside the compressor. The mass flow rate through the compressor at any instant could be read from the steady-state characteristics even when the engine is under transient operation. This method has the advantage that computing load is less heavy than with the stage-to-stage modelling technique, at the same time without losing too much insight into compressor performance during transients.

2.3.3 Combustion Chamber Model

In modelling the combustion chamber, pressure loss, heat addition and combustion efficiency are the three factors that must be considered [86].

Total Pressure Loss

The total pressure loss across the combustion chamber can be attributed to flow friction and momentum loss due to heat addition and mixing process. The analytical representation is generally based on the assumption that the combustion chamber can be divided into equivalent fluid friction and heat addition zones. The air enters the combustion zone and experiences a total pressure loss due to flow friction. This pressure loss corresponds to the actual mixing loss that occurs without combustion, which can be determined experimentally and correlated with theory. Momentum pressure loss is assumed to occur in the combustion zones with the addition of heat to the air. This loss is assumed to occur after the friction loss. The overall pressure loss is then formed from the sum of the two losses. The

resulting expression is:

$$\Delta P_{loss} = \frac{\dot{m}_{in}^2}{P_{in}}(K_{cold}T_{in} + K_{hot}T_{out}) \quad (2.1)$$

where K_{cold} is friction loss coefficient and found from non-combustion flow tests, and K_{hot} determined from combustion flow tests [87].

Whenever the above information is not available, a simple approach is to assume that the total pressure loss is a fixed percentage of the combustor inlet total pressure [88], [89].

Combustion Efficiency

The actual combustion involves processes such as atomisation, vapourisation, mixing, and chemical reaction. These processes are gradual in time and space. For combustor simulation, however, it is only necessary to determine relations between initial and final condition of the gas.

Since variation in specific heat due to composition and temperature changes can introduce significant errors, variable specific heat is considered in the combustion temperature evaluation. Because of the complexity of the combustion process, no exact analytical treatment of combustion efficiency was attempted. For the purposes of obtaining a simple model, combustion efficiency was approximated by a correlation of the form:

$$\eta_{cc} = F_{cc}(P_{out}\Delta T) \quad (2.2)$$

The efficiency η_{cc} is defined as that portion of the heat of combustion that is available for gas temperature rise. The parameter $P_{out}\Delta T$ is based on the ideal combustion temperature rise and includes the effects of fuel-to-air ratio and inlet pressure variations but neglects the effect of inlet temperature variations [90].

The above modelling considerations involve detailed combustor tests. To use a simple model, a fixed combustion efficiency can be used [91].

2.3.4 Turbines

Based on the characteristics of a turbine, two alternative treatments can be used. One is to include the effects of the shaft speeds [22]. This procedure was adopted in the present work when modelling the two-spool engines. The other is to use a single line relating pressure ratio to non-dimensional mass flow [92]. This was followed when modelling the single-spool engines.

2.3.5 Propulsion Nozzle Model

In the propulsion nozzle, flow is accelerated to provide a high velocity jet for the thrust requirement. The pressure loss due to flow friction is taken into account using an isentropic efficiency. Therefore, the equations of mass flow, temperature for adiabatic flow can be used [93].

2.4 Dynamic Equations

2.4.1 State Selections

In the present work, state selections (i.e. locations and associated pressures and temperatures) are based on the following criteria:

- State is necessary because the volume is large and dynamics are significant.
- State is necessary because it is necessary to avoid iterative loop.

In most of the intercomponent volumes, pressures are used as state variables. This is because if there is no work or heat transfers, total temperature is constant. Furthermore the pressure is more easily measured than the temperature. Another factor neglected in the present work is the dynamics associated with fuel flow transport, which can be modelled using a first order lag with a dead time as:

$$\frac{\dot{m}_{f_{out}}}{\dot{m}_{f_{in}}} = \frac{e^{-\tau_d s}}{T_{lag}s + 1.0} \quad (2.3)$$

The process can be explained as following; referring to Figure 2.3, suppose fuel inject through the nozzles into combustion primary zones at time $t = 0$, it will continuously pick up heat from its surroundings and reach the hot regime of the recirculation zone. This will take a time interval of Δt_1 . In the subsequent interval Δt_2 , it is being prepared for combustion by evaporation. A further interval Δt_3 , will be taken between the ignition and maximum energy release. Therefore, the time interval $\Delta t_1 + \Delta t_2$ can be treated as dead time and Δt_3 can be treated as time lag. Thus, $\tau_d = \Delta t_1 + \Delta t_2$ and $T_{lag} = \Delta t_3$. The τ can be evaluated with acceptable accuracy using the following equation:

$$\tau_d = K_a * P_{in}^{K_b} \quad (2.4)$$

Thomson suggests the following values for the constant referred as above: $K_a \approx 0.02$, $K_b \approx -0.3$ and $T_{lag} \approx 0.05$.

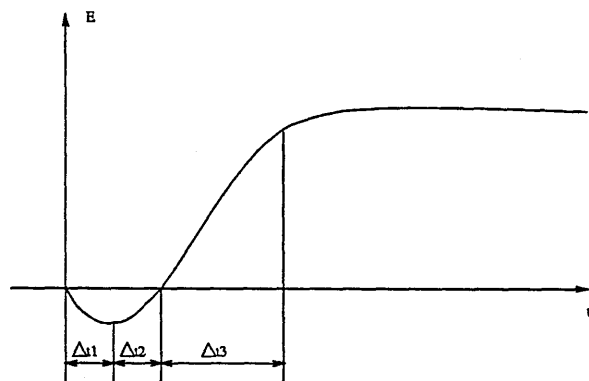


Figure 2.3: Energy Release Diagram

2.4.2 Lumped Volume Dynamics

The following approximations are made in deriving dynamic equations for the lumped volumes in gas turbine engines. The verifications can be found, for example, in reference [94].

- The process in the volume is isentropic.

- The flow velocity is very small, so that the static properties can be approximated by stagnation properties.

The continuity equation for the volume is:

$$V \frac{d}{dt} \rho = \sum \dot{m}_{in} - \sum \dot{m}_{out} \quad (2.5)$$

Because the process in the volume is assumed isentropic, the density change can be related to the change in pressure by:

$$\frac{d}{dt} \rho = \frac{1}{\gamma RT} \frac{d}{dt} P \quad (2.6)$$

Substituting equation 2.4 into equation 2.3:

$$\frac{d}{dt} P = \frac{\gamma RT}{V} (\sum \dot{m}_{in} - \sum \dot{m}_{out}) \quad (2.7)$$

For the volume in which there is no heat or work transfer, the total temperature will be spatially constant. The energy balance equation is:

$$\frac{d}{dt} (m c_v T) = \sum \dot{m}_{in} c_p T_{in} - \sum \dot{m}_{out} c_p T$$

2.4.3 Shaft Inertia

In the present application, it is assumed that there is no mechanical loss in the transmission system, therefore the dynamic equations due to the shaft inertia can be written as:

$$JN \frac{d}{dt} N = \sum W_{turbine} - \sum W_{compressor} \quad (2.8)$$

where J is shaft inertia, and N is in the unit of *rad/s*.

2.5 Effects of Variable Geometry

Referring to Figure 2.2, the fan and compressor inlet guide vanes (if fitted) modify the direction of air flow entering the rotating blades and, as a result, affect the airflow level and surge margin of both components and also the power required to drive them. Compressor bleed flow also affects airflow level, surge margin and

required power. Changing the vane angle of the high-pressure turbine (if this can be done) changes the effective flow area and hence the flow capacity of the turbine. Thus the high-pressure turbine can be used to regulate the back pressure on the high-pressure compressor which effects its surge margin and power requirement. In a similar manner, the low-pressure turbine area controls the back pressure on the high-pressure turbine and, as a result, can be used to regulate the work split between the two turbines, thereby affecting both rotor speeds. The propulsion nozzle area controls the back pressure on the low-pressure turbine and, as a result, affects the total power outputs from both turbines which in turn affects both rotor speeds and the overall pressure ratio and thrust level [95]

2.5.1 Compressor Characteristic with Variable Geometry

The variable geometry features considered in the present work are compressor inlet guide vane, compressor bleed valve area and propulsion nozzle area. In the case of the two-spool engine, the variable geometry is referring to those associated with the HP compressor. As far as compressor characteristics concerned, there is a difference between those with variable geometry and these without it. For the compressor with variable geometry, the steady-state characteristics of stages can be represented by:

$$\left(\frac{\dot{m}_{in}\sqrt{T_{in}}}{P_{in}}\right)_i = F_{cm}\left(\frac{N}{\sqrt{T_{in}}}, \frac{P_{out}}{P_{in}}, \alpha\right), \quad i = 1, 2, \dots, n \quad (2.9)$$

where the vane angle α can be varied.

2.5.2 A Simple Model for Considering Variable Geometry

Because the compressor characteristics in the present work had been obtained without the effects of variable geometry, therefore it is necessary to introduce a

model to allow its effects to be studied. The simple method is to use a non-dimensional coefficient β to modify the inlet non-dimensional mass flow to the compressor, and its effective range is restricted [25].

$$\left(\frac{\dot{m}_{in}\sqrt{T_{in}}}{P_{in}}\right)_{actual} = \beta * \left(\frac{\dot{m}_{in}\sqrt{T_{in}}}{P_{in}}\right)_{map}, \quad 0.8 \leq \beta \leq 1.2 \quad (2.10)$$

2.6 Thermodynamic Modelling of Engines

The general procedure for thermodynamic modelling of gas turbine engines was introduced in section 2.3. In this section, the detailed procedure is described for both the single-spool engine and the two-spool engine. Each component in this engine have been lumped as an element according to its specific function.

2.6.1 The Single-spool Engine

Component A is the inlet. In this component, it is assumed that flow is adiabatic. Using an isentropic efficiency to account for the pressure loss, the inlet condition to the compressor can be calculated using the following equations:

$$T_{01} = T_{amb} \left(1.0 + \frac{\gamma + 1}{2} Mach^2\right) \quad (2.11)$$

$$T_{01,s} = T_{amb} + \eta_{is}(T_{01} - T_{amb}) \quad (2.12)$$

$$P_{01} = P_{amb} \left(\frac{T_{01,s}}{T_{amb}}\right)^{\gamma-1/\gamma} \quad (2.13)$$

Component B is the compressor. It is modelled empirically using its steady-state characteristic, which gives the non-dimensional mass flow rate as a function of pressures, temperature and shaft speed.

$$\frac{\dot{m}_c\sqrt{T_{01}}}{P_{01}} = \beta * F_c(N, P_{02}, P_{01}, T_{01}) \quad (2.14)$$

The total temperature rise is found by using the isentropic efficiency η_c in the following manner:

$$T_{02} = T_{01} \left[1 + \frac{1}{\eta_c} \left(\left(\frac{P_{02}}{P_{01}}\right)^{\gamma-1/\gamma} - 1\right)\right] \quad (2.15)$$

Component C is the volume 2. Here it is assumed that the flow is adiabatic and reversible and the flow properties are spatially uniform. The discretised continuity equation combined with the isentropic relation results in:

$$\frac{d}{dt}P_{02} = \frac{\gamma RT_{02}}{V_2}(\dot{m}_c - \dot{m}_b - \dot{m}_t + \dot{m}_f) \quad (2.16)$$

Component D is the compressor bleed valve. It is modelled with an empirical orifice relation, which gives:

$$\dot{m}_b = A_b \sqrt{\frac{2P_{amb}}{RT_{amb}}(P_{02} - P_{amb})} \quad (2.17)$$

Component E is the combustor. In the combustor, the total pressure loss is assumed to be a fixed percentage of its inlet pressure P_{02} , which gives:

$$P_{03} = k_{loss}P_{02} \quad (2.18)$$

The total temperature rise is given by the dynamic equation, which is derived by considering the energy storage in a one-dimensional volume:

$$\frac{dT_{03}}{dt} = \frac{\gamma RT_{03}}{P_{03}}(\dot{m}_c T_{02} + \dot{m}_f T_{01} - \dot{m}_b T_{02} + \dot{m}_t T_{03} + \frac{\dot{Q}}{c_p} + T_{03}(\dot{m}_c + \dot{m}_f - \dot{m}_b - \dot{m}_t)) \quad (2.19)$$

Component F is the turbine. It is modelled empirically with the steady-state turbine performance map, which gives the nondimensional mass flow across the turbine, thus:

$$\frac{\dot{m}_t \sqrt{T_{03}}}{P_{03}} = F_t(N, T_{03}, P_{03}, P_{04}) \quad (2.20)$$

The total temperature drop is found by using the isentropic efficiency, η_T , in the following manner:

$$T_{04} = T_{03} \left(1 - \eta_T \left(\left(\frac{P_{04}}{P_{03}} \right)^{\gamma-1/\gamma} - 1 \right)\right) \quad (2.21)$$

Component G is the volume 4. As in the case of volume 2, the exit total pressure P_4 is modelled using the dynamic equation as:

$$\frac{d}{dt}P_{04} = \frac{\gamma RT_{04}}{V_4}(\dot{m}_t - \dot{m}_n) \quad (2.22)$$

Component H is the propulsion nozzle. Here it is assumed that the flow is adiabatic. By using an isentropic efficiency factor to account for flow loss, the algebraic continuity equation can be put into the form:

$$\frac{\dot{m}_n \sqrt{T_4}}{P_4} = \frac{u_5}{\sqrt{T_{04}}} \frac{A_p}{R} \frac{P_5}{P_{04}} \frac{T_{04}}{T_5} \quad (2.23)$$

where

$$\frac{u_5}{\sqrt{T_{04}}} = \sqrt{2c_p \eta_n \left(1 - \left(\frac{P_5}{P_{04}}\right)^{\gamma-1/\gamma}\right)} \quad (2.24)$$

and

$$\frac{T_{05}}{T_{04}} = \left(1 - \eta_n \left(1 - \left(\frac{P_{05}}{P_{04}}\right)^{\gamma-1/\gamma}\right)\right) \quad (2.25)$$

The preceding equations hold only if the nozzle is not choked. If the nozzle is choked, i.e. $P_5/P_4 \leq P_{crit}/P_4$, then

$$\frac{\dot{m}_n \sqrt{T_{04}}}{P_{40}} = \frac{u_5}{\sqrt{T_{04}}} \frac{A_p}{R} \frac{P_{crit}}{P_{04}} \frac{T_{04}}{T_{crit}} \quad (2.26)$$

where

$$\frac{P_{crit}}{P_{04}} = \left(1 - \frac{1}{\eta_n} \left(\frac{\gamma-1}{\gamma+1}\right)^{\gamma/\gamma-1}\right) \quad (2.27)$$

and

$$\frac{T_{crit}}{T_{04}} = \frac{2}{\gamma+1} \quad (2.28)$$

and

$$\frac{u_5}{\sqrt{T_{04}}} = \frac{2\gamma R}{\gamma+1} \quad (2.29)$$

Using the momentum equation applied to the entire engine and ignoring the unsteady terms which are negligible compared to the momentum flux term, an estimate of thrust of the engine is calculated.

$$F_{net} = \dot{m}_n u_5 - \dot{m}_c u_0 + A_p (P_5 - P_{amb}) \quad (2.30)$$

Component I is the compressor/turbine spool. This dynamic equation comes from a power balance on the spool which gives:

$$JN \frac{d}{dt} N = W_t - W_c \quad (2.31)$$

where $W_c = \dot{m}_c c_p (T_{02} - T_{01})$ and $W_t = \dot{m}_t c_p (T_{03} - T_{04})$. The governing equation is therefore

$$JN \frac{d}{dt} N = \dot{m}_t c_p (T_{03} - T_{04}) - \dot{m}_c c_p (T_{02} - T_{01}) \quad (2.32)$$

An information flow diagram for the model described above is given in Figure 2.4, which shows where the parameters and inputs enter into the model structure.

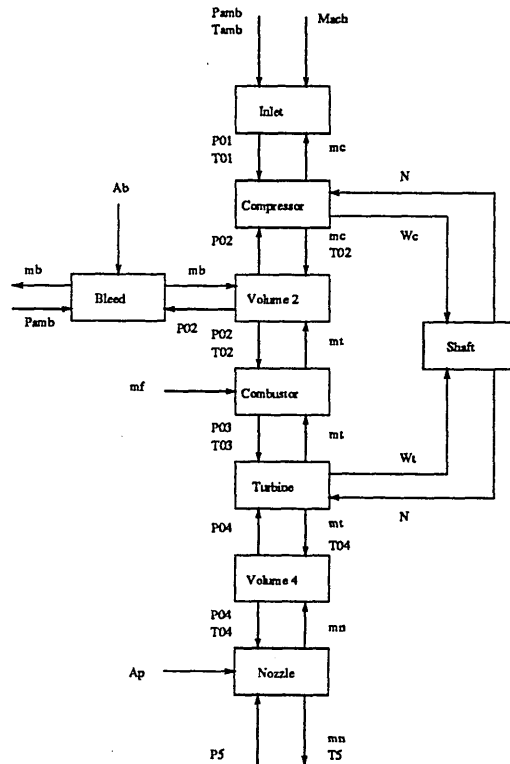


Figure 2.4: Information Flow Diagram for the Single-Spool Engine

2.6.2 The Two-spool Turbofan

The states and properties which have been considered significant in this model are shown in table 2.3.

Component A is the inlet. In this component, as before, it is assumed that flow is adiabatic. Using an isentropic efficiency to account for the pressure loss. The inlet conditions to the fan can be calculated using the following equations:

$$T_{01} = T_{amb} \left(1.0 + \frac{\gamma + 1}{2} Mach^2 \right) \quad (2.33)$$

Variable name	Physical meaning	Measurements	Unit
States			
P_{02}	Compressor exit pressure	Measurable	KN/m^2
T_{03}	Turbine inlet Temperature	Unmeasurable	K
P_{04}	Jet pipe pressure	Measurable	KN/m^2
N	Engine shaft speed	Measurable	rad/s
Controls			
\dot{m}_f	Engine fuel flow	Measurable	Kg/s
A_p	Propulsion nozzle area	Measurable	m^2
A_b	Bleed valve area	Measurable	m^2
α	Compressor inlet guide vane	Measurable	%
Outputs			
T_{04}	Jet pipe temperature	Measurable	K
S_{mag}	Compressor surge margin	Unmeasurable	%
F_{net}	Engine net thrust	Unmeasurable	N

Table 2.3: Choice of States, Controls and Outputs for The Single-Spool Engine

$$T_{01,s} = T_{amb} + \eta_{is}(T_{01} - T_{amb}) \quad (2.34)$$

$$P_{01} = P_{amb} \left(\frac{T_{01,s}}{T_{amb}} \right)^{\gamma-1/\gamma} \quad (2.35)$$

Component B is the fan. It is modelled empirically using the fan steady-state performance map, which gives the non-dimensional mass flow rate across the fan:

$$\frac{\dot{m}_{fan} \sqrt{T_{01}}}{P_{01}} = F_f(N_L, P_{013}, P_{01}, T_{01}) \quad (2.36)$$

The total temperature rise is found by using the isentropic efficiency, η_{fan} , in the following manner:

$$T_{013} = T_{01} \left(1 + \frac{1}{\eta_{fan}} \left(\left(\frac{P_{013}}{P_{01}} \right)^{\gamma-1/\gamma} - 1 \right) \right) \quad (2.37)$$

Component C is the volume 13. Here it is assumed that the flow is adiabatic and flow properties were spatially uniform. The discretised continuity equation combined with the isentropic relation results in:

$$\frac{d}{dt} P_{013} = \frac{\gamma R T_{013}}{V_{13}} (\dot{m}_{fan} - \dot{m}_{ipc} - \dot{m}_{bp}) \quad (2.38)$$

Component D is the IP compressor. It is modelled empirically using the steady-state performance map, which gives the non-dimensional mass flow rate

across the IP compressor:

$$\frac{\dot{m}_{ipc}\sqrt{T_{013}}}{P_{013}} = F_{ipc}(N_L, P_{026}, P_{013}, T_{013}) \quad (2.39)$$

The total temperature rise is found by using the isentropic efficiency, η_{ipc} , in the following manner:

$$T_{026} = T_{013}\left(1 + \frac{1}{\eta_{ipc}}\left(\left(\frac{P_{026}}{P_{013}}\right)^{\gamma-1/\gamma} - 1\right)\right) \quad (2.40)$$

Component E is the volume 26. Here it is assumed that the flow is adiabatic and flow properties were spatially uniform. The discretised continuity equation combined with the isentropic relation results in:

$$\frac{d}{dt}P_{026} = \frac{\gamma RT_{026}}{V_{26}}(\dot{m}_{ipc} - \dot{m}_{hpc}) \quad (2.41)$$

Component F is the HP compressor. It is modelled empirically using the steady-state performance map, which gives the non-dimensional mass flow rate across the compressor:

$$\frac{\dot{m}_{hpc}\sqrt{T_{026}}}{P_{026}} = \beta * F_{hpc}(N_H, P_{03}, P_{026}, T_{026}) \quad (2.42)$$

The total temperature rise is found by using the isentropic efficiency, η_{hpc} , in the following manner:

$$T_{03} = T_{026}\left(1 + \frac{1}{\eta_{hpc}}\left(\left(\frac{P_{03}}{P_{026}}\right)^{\gamma-1/\gamma} - 1\right)\right) \quad (2.43)$$

Component G is the volume 3. Here it is assumed that the flow is adiabatic and flow properties are spatially uniform. The discretised continuity equation combined with the isentropic relation results in:

$$\frac{d}{dt}P_{03} = \frac{\gamma RT_{03}}{V_3}(\dot{m}_{hpc} - \dot{m}_{hpt} - \dot{m}_b + \dot{m}_f) \quad (2.44)$$

Component H is the HP compressor bleed valve. It is modelled with an empirical orifice relation which gives:

$$\dot{m}_b = A_b \sqrt{\frac{2P_{amb}}{RT_{amb}}(P_{03} - P_{amb})} \quad (2.45)$$

Component I is the combustor. In the combustor, the total pressure loss is assumed to be a fixed percentage of its inlet pressure P_{03} , which gives:

$$P_{04} = k_{loss}P_{03} \quad (2.46)$$

The total temperature rise is given by the dynamic equation, which is derived by considering the energy storage in a one-dimensional volume.

$$\begin{aligned} \frac{dT_{04}}{dt} = \frac{\gamma RT_{04}}{P_{04}V_3} & (\dot{m}_{hpc}T_{03} - \dot{m}_fT_{01} - \dot{m}_{hpt}T_{04} - \dot{m}_bT_{03} + \frac{\dot{Q}}{c_p}) \\ & + T_{04}(\dot{m}_{hpc} + \dot{m}_f - \dot{m}_{hpt} - \dot{m}_b) \end{aligned} \quad (2.47)$$

Component J is the HP turbine. It is modelled empirically with the steady-state turbine performance map, which gives the non-dimensional mass flow across the turbine, thus:

$$\frac{\dot{m}_{hpt}\sqrt{T_{04}}}{P_{04}} = F_{hpt}(N_H, T_{04}, P_{04}, P_{05}) \quad (2.48)$$

The total temperature drop is found by using the isentropic efficiency, η_{hpt} , in the following manner:

$$T_{05} = T_{04}(1 - \eta_{hpt}((\frac{P_{05}}{P_{04}})^{\gamma-1/\gamma} - 1)) \quad (2.49)$$

Component K is the volume 5. As in the case of compressor volume, the exit total pressure P_{05} is modelled using the dynamic equation as:

$$\frac{d}{dt}P_{05} = \frac{\gamma RT_{05}}{V_5}(\dot{m}_{hpt} - \dot{m}_{lpt}) \quad (2.50)$$

Component L is the LP turbine. It is modelled empirically with the steady-state turbine performance map, which gives the non-dimensional mass flow across the turbine, thus:

$$\frac{\dot{m}_{lpt}\sqrt{T_{05}}}{P_{05}} = F_{lpt}(N_L, T_{05}, P_{05}, P_{06}) \quad (2.51)$$

The total temperature drop is found by using the isentropic efficiency, η_{lpt} , in the following manner:

$$T_{06} = T_{05}(1 - \eta_{lpt}((\frac{P_{06}}{P_{05}})^{\gamma-1/\gamma} - 1)) \quad (2.52)$$

Component M is the by-pass duct. It is modelled using the one-dimensional compressible flow equation, which gives:

$$\frac{\dot{m}_{bp}\sqrt{T_{013}}}{P_{013}} = \sqrt{\frac{2r}{(r-1)R}} \left(\frac{P_{07}}{P_{013}}\right)^{1/\gamma} \sqrt{1 - \left(\frac{P_{07}}{P_{013}}\right)^{\gamma-1/\gamma}} \quad (2.53)$$

Because there is no work or heat transfer in this component, the total temperature is constant.

Component N is the volume 7. the exit total pressure P_{07} is modelled using the dynamic equation as:

$$\frac{d}{dt}P_{07} = \frac{\gamma RT_{07}}{V_7} (\dot{m}_{bp} + \dot{m}_{lpt} - \dot{m}_{noz}) \quad (2.54)$$

The total temperature in this volume is given by the steady energy equation when two stream join together:

$$T_{07} = \frac{\dot{m}_{bp}T_{013} + \dot{m}_{lpt}T_{06}}{\dot{m}_{bp} + \dot{m}_{lpt}} \quad (2.55)$$

Component P is the propulsion nozzle. The treatment is same for the propulsion nozzle of the single-spool engine (component I). Again, it is assumed that the flow is adiabatic. Using an isentropic efficiency to account for flow loss, the algebraic continuity equation can be put into the form:

$$\frac{\dot{m}_n\sqrt{T_{07}}}{P_{07}} = \frac{u_8}{\sqrt{T_{07}}} \frac{A_8}{R} \frac{P_8}{P_{07}} \frac{T_{07}}{T_8} \quad (2.56)$$

where

$$\frac{u_8}{\sqrt{T_{07}}} = \sqrt{2c_p\eta_n \left(1 - \left(\frac{P_8}{P_{07}}\right)^{\gamma-1/\gamma}\right)} \quad (2.57)$$

and

$$\frac{T_8}{T_{07}} = \left(1 - \eta_n \left(1 - \left(\frac{P_8}{P_{07}}\right)^{\gamma-1/\gamma}\right)\right) \quad (2.58)$$

The preceding equations hold only if the nozzle is not choked. If the nozzle is choked, i.e. $P_8/P_{07} \leq P_{crit}/P_{07}$, then

$$\frac{\dot{m}_n\sqrt{T_{07}}}{P_{07}} = \frac{u_8}{\sqrt{T_{07}}} \frac{A_8}{R} \frac{P_{crit}}{P_{07}} \frac{T_{07}}{T_{crit}} \quad (2.59)$$

where

$$\frac{P_{crit}}{P_{07}} = \left(1 - \frac{1}{\eta_n} \left(\frac{\gamma - 1}{\gamma + 1}\right)^{\gamma/\gamma-1}\right) \quad (2.60)$$

and

$$\frac{T_{crit}}{T_{07}} = \frac{2}{\gamma + 1} \quad (2.61)$$

and

$$\frac{u_8}{\sqrt{T_{07}}} = \frac{2\gamma R}{\gamma + 1} \quad (2.62)$$

Using the momentum equation applied to the entire engine and ignoring the unsteady terms which are negligible compared to the momentum flux term, an estimate of thrust of the engine is calculated:

$$F_{net} = \dot{m}_n u_8 - \dot{m}_c u_0 + A_8(P_8 - P_{amb}) \quad (2.63)$$

Component Q is the HP spool which is a concentric shaft connecting HP compressor and HP turbine. The dynamic equation is based on the power balance on the shaft, which gives:

$$J_H N_H \frac{d}{dt} N_H = W_{hpt} - W_{hpc} \quad (2.64)$$

where $W_{hpc} = \dot{m}_{hpc} c_p (T_{03} - T_{026})$ and $W_{hpt} = \dot{m}_{hpt} c_p (T_{04} - T_{05})$. The governing equation is therefore:

$$J_H N_H \frac{d}{dt} N_H = \dot{m}_{hpt} c_p (T_4 - T_5) - \dot{m}_{hpc} c_p (T_{03} - T_{026}) \quad (2.65)$$

Component R is the LP spool, through which the power produced by LP turbine is used to drive the fan and IP compressor. The dynamic equation comes from a power balance applied on this spool, which gives:

$$J_L N_L \frac{d}{dt} N_L = W_{lpt} - W_{ipc} - W_{fan} \quad (2.66)$$

where $W_{fan} = \dot{m}_{fan} c_p (T_{013} - T_{01})$, $W_{ipc} = \dot{m}_{ipc} c_p (T_{026} - T_{013})$ and $W_{lpt} = \dot{m}_{lpt} c_p (T_{05} - T_{06})$. The governing equation is therefore:

$$J_L N_L \frac{d}{dt} N_L = \dot{m}_{hpt} c_p (T_{05} - T_{06}) - \dot{m}_{ipc} c_p (T_{026} - T_{013}) - \dot{m}_{fan} c_p (T_{013} - T_{01}) \quad (2.67)$$

An information flow diagram for the model described above is given in Figure 2.5, which shows where the parameters and inputs enter into the model structure.

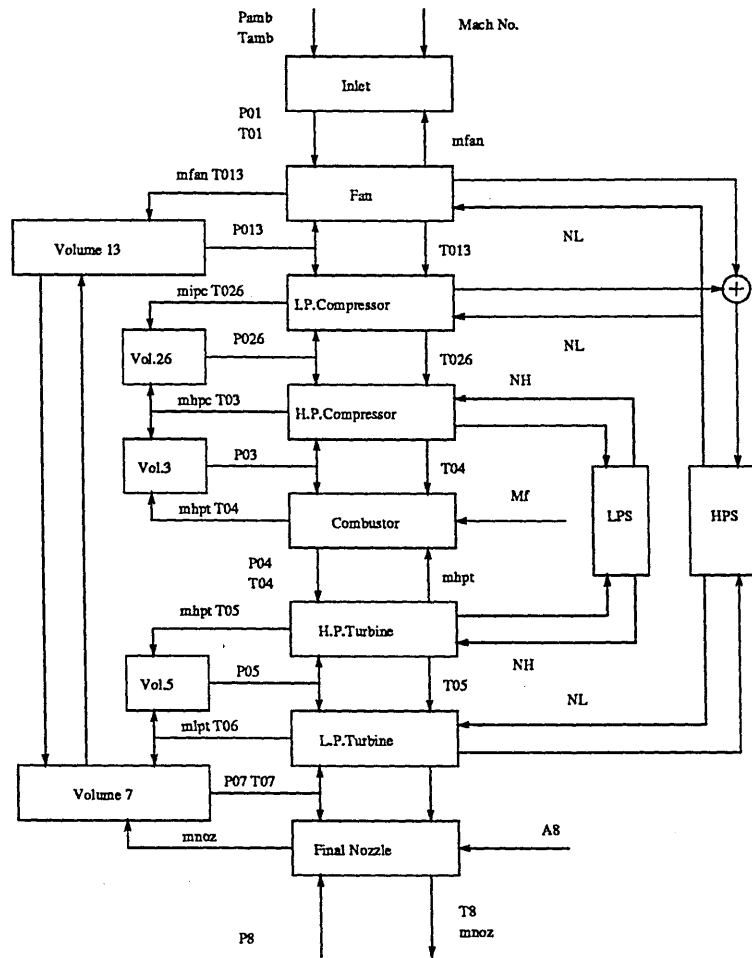


Figure 2.5: Information Flow Diagram for the Two-Spool Engine

Variable name	Physical meaning	Measurements	Unit
States			
P_{013}	Fan exit pressure	Measurable	KN/m^2
P_{026}	IP Compressor exit pressure	Measurable	KN/m^2
P_{03}	HP Compressor exit pressure	Measurable	KN/m^2
T_{04}	Turbine inlet Temperature	Unmeasurable	K
P_{05}	HP Turbine exit pressure	Measurable	KN/m^2
P_{07}	Jet pipe pressure	Measurable	KN/m^2
N_L	LP Shaft speed	Measurable	rad/s
N_H	HP Shaft speed	Measurable	rad/s
Controls			
\dot{m}_f	Engine fuel flow	Measurable	Kg/s
A_8	Propulsion nozzle area	Measurable	m^2
A_b	HP Compressor Bleed valve area	Measurable	m^2
α	HP Compressor inlet guide vane	Measurable	$\%$
Outputs			
T_{05}	Inter-turbine temperature	Measurable	K
S_{mag}	Compressor surge margin	Unmeasurable	$\%$
F_{net}	Engine net thrust	Unmeasurable	N

Table 2.4: Choice of States, Controls and Outputs for The Two-Spool Engine

2.7 Transient Thermal Characteristics

The thermal effects in a gas turbine engine transient can be summarised as follows:

- Heat absorption in fan, compressor, turbines and combustion chamber
- Changes in characteristics of compressors due to the heat transfer
- Changes in efficiencies of compressors and turbines due to the tip clearances.
- Air flows through seals differing from design proportions due to seal clearances during the transient differing from design values.

These effects on the transient response have been extensively investigated, particularly by Maccallum and Pilidis [96],[97] [98]and various models exist to account for these effects. The general conclusions from their studies are:

- The predicted transient responses are slowed down whenever such effects are considered, and these predictions are then much closer to real engine behaviour.

- The pressures and temperatures at the conclusion of a speed transient deviate from steady-state values by 2 – 5%.

In the present work, to model these secondary effects without using the complicated models, these effects were treated as slow disturbances on the temperatures and pressures, which give:

$$D(s) = \frac{K_d}{\tau_d s + 1} \quad (2.68)$$

where K_d and τ_d are related to the shaft speed and temperature difference across the component.

2.8 Handling of the Fan and Turbine Characteristics

In the present work, a single characteristic has been used to represent the performance of the fan, rather than using the separate characteristics for Inner and Outer Fan. This simplifies the resultant model without losing too much of accuracy, as shown by Petrides [99].

The turbine characteristics has been modified from the way that they are handled in Maccallum's work [100], where the turbine "working factor" has been used as an independent variable in addition to non-dimensional shaft speed. To adapt the unified modelling approach, discussed in the next chapter, the pressure ratio across the turbine has been computed and used instead of "working factor". This is done by using a specific heat, in the present case, $c_p = 1.33$ and calculating the pressure ratio corresponding to each working factor. A similar approach has been followed in the work of Nawrocki [101].

Chapter 3

A Method for Approximating Compressor and Turbine Characteristics

SUMMARY

An algorithm is proposed to derive mathematical representations for compressor and turbine, given their steady-state performance characteristics. This method is the result of our continuous efforts devoted to find a systematic approach to modelling compressor and turbine, so as to obtain quick and efficient estimations of their transient values. Motivated by some mathematical concepts in statistics, several performance indices are defined and used to evaluate the qualities of the resultant models.

3.1 Introduction

Numerous problems have been encountered in realising a adequate real-time model for an gas turbine engine [102]. Among them, one of the difficulties is due to the way that compressor and turbine characteristics are used in the simulations.

Although the performance characteristics used in the models are considered as accurate representations of these components, unrealistic transient values could result due to the numerical algorithms used for interpolation [103].

In the past, various numerical interpolation methods have been used in engine digital simulations and the accuracy of transient predictions is generally acceptable [104]. However this is achieved only by using narrow time steps to guarantee the reliable estimations [97].

In order to increase the efficiency of simulations, it is necessary to develop a systematic approach to modelling compressor and turbine, using the given performance characteristics. Unfortunately relatively little work has been carried out on this aspect of modelling. Most of the work reported on gas turbine engine modelling and simulation used numerical algorithms to obtain transient performance values of compressors, and as a result, the simulation time is relatively longer. To overcome this problem, Cockshutt [105] has suggested a simple treatment of a compressor characteristic. He assumed compressor pressure ratio is only dependent on non-dimensional speed, and his simulation has shown that accuracy of the predicted transient values has been sacrificed to a certain degree, this being especially the case in the low speed ranges on the characteristics. The simulation time saved due to this simple treatment can not justify the loss of accuracy. Thomson [106] also suggested the linear approximation of the relationship between the pressure ratio, non-dimensional mass flow and non-dimensional speed, but this are found to be useful only for the compressor with 8 stages or less. The polynomial approximation approach used in the work [107] seems to lack theoretical basis and the accuracy of his fitting is heavily dependent on the reliability of the given data.

In this chapter, a systematic approach to approximating the characteristics of the compressor and turbine is proposed, and validity of this method is established by applying it to the compressors and turbines used in the present study. The objective of this algorithm can be summarised as: given compressor characteristic

and turbine characteristics, derive simple mathematical representations for these components, which will be easily used to obtain efficient and quick estimations of their values in transient calculations. Obviously there are many such methods that can be potentially applied, and there are no general criteria to judge the efficiency of various methods. In this situation, it is necessary to define performance indices which will provide a framework for the model evaluations.

3.2 Compressor Models and their Problems

3.2.1 Compressor Models

Modelling a compressor requires formulation of the functional relations that exist between compressor performance variables. There are basically two methods that can be used to model multistage compressors. The first uses individual component performance, and as a result, the aerothermodynamic performance of a compressor can be given in several ways:

1. Relations between pressure ratio, efficiency, mass flow, and shaft speeds [108]
2. Relations between flow coefficient, work coefficient, loss, and a pseudo-flow Mach Number in terms of “backbone” and “off-backbone” curves [109].

Engine transient predictions are of the utmost importance. The potential performance enhancement of a gas turbine engine depends to a great extent on the accuracy and reliability attached to the estimates of engine transient paths. Determination of these transient paths followed by the engine operating point requires knowledge of the compressor characteristics, and particularly of the momentary compressor angular velocity [110].

A compressor model has to present our knowledge of the compressor in a usable form [111]. If a real-time simulation is to be considered, a detailed approach or a complete mathematical description of the compressor behaviour is not appropriate, rather a simple and efficient model is desired. Thus, a model form is

usually assumed, and a suitable technique is used to extract information from available compressor characteristics.

3.2.2 Problems Associated Using Tabular Characteristics

The two methods which may be used are:

- Interpolation.
- Polynomial curve fitting.

In the interpolation method, the algorithm may be linear or quadratic, but for accurate estimates in some area, narrow data steps are required. For polynomial fitting, suitable relations must first be found.

Error limits for the model outputs are guaranteed at the originally given data points, while errors at intermediate points do not have such a guarantee. The reproduced engine characteristics at these intermediate points usually suffer unreal values of the predicted model parameter at these points, due to the inconsistency of the interpolation algorithm or the adopted variation of the estimated coefficients.

To obtain better polynomial model outputs, the coefficients in the polynomial relationship should, ideally be monotonic [112]; these are to be used in conjunction with a consistent interpolation algorithm.

Figure 3.1 and 3.2 show the compressor characteristics used in the single-spool engine. Since we are concerned with fitting the compressor characteristics, a global examination of these characteristics draws our attention to the following potential troubles:

They are:

- Curve shapes which cannot be easily identified.
- The non-uniqueness problem (for some fan characteristics), especially in the area of the high speed curves.

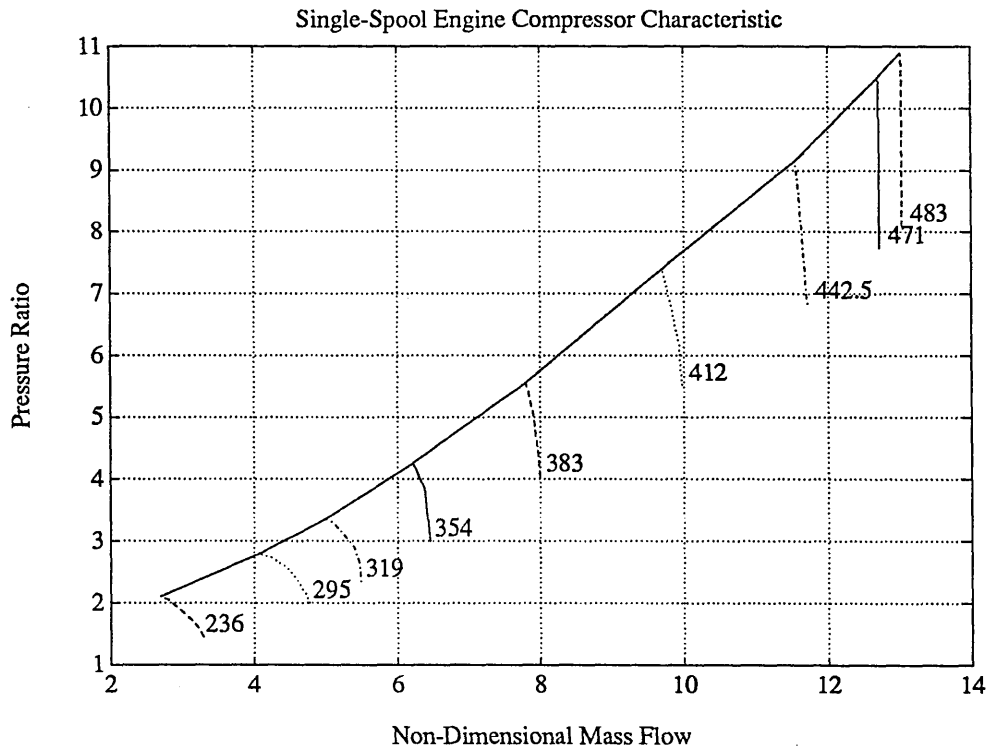


Figure 3.1: Pressure Ratio and Mass Flow Map of the Single-Spool Engine

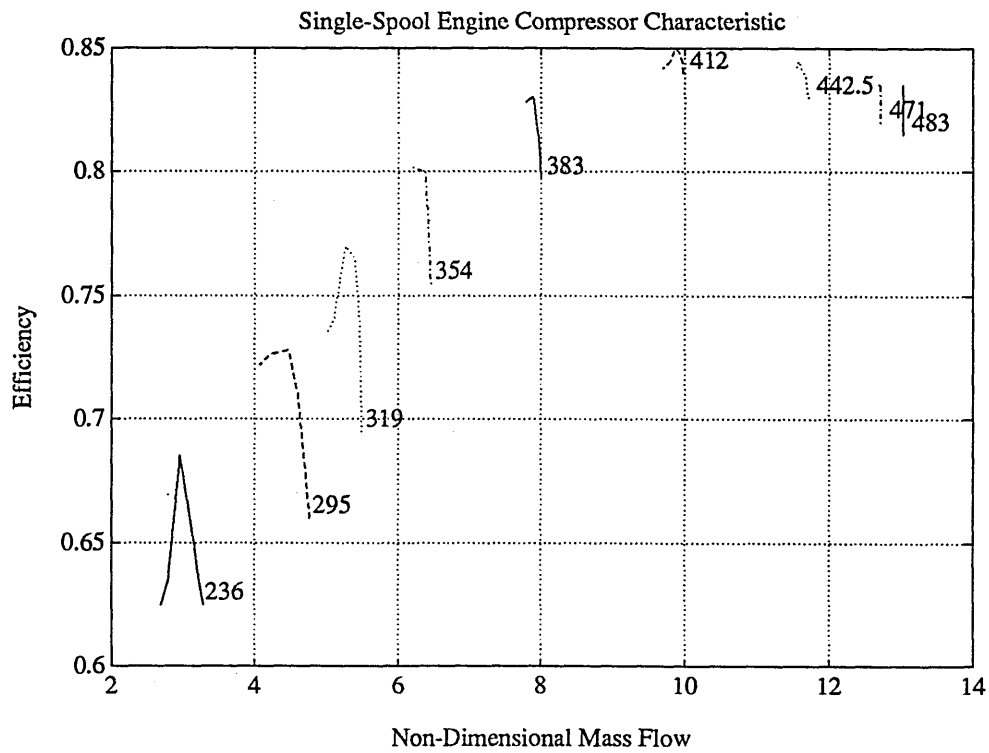


Figure 3.2: Efficiency and Mass Flow Map of the Single-Spool Engine

- The ill-conditioning problem, where small changes in the variable of one coordinate produce large changes in the other coordinate variable.
- The large variation encountered in the variables if a full envelope of compressor (engine) working area is desired.
- The difference in the order of magnitude of coefficients in the polynomial fitting.

Strongly related to these problems is the need for different functions to fit the low and high-speed portions of the characteristics, along with a methodology for switching from one function to the other.

3.3 A Preliminary Study of Analytical Modelling

An alternative to interpolation or polynomial fitting of tabular characteristic data is to develop a closed form of analytical expression relating the appropriate parameters.

In a preliminary study, Maccallum [113] obtained an empirical expression to represent the given characteristics in the single-spool engine. The resultant equations for the non-dimensional mass flow are:

$$K_1 = 1.50 + 1.8 * 10^{-10} \left(\frac{N}{\sqrt{T}} \right)^4 - \frac{50}{508 - N/\sqrt{T}} \quad (3.1)$$

$$K_2 = 1.05 - 4.44 * 10^{-4} \left(\frac{N}{\sqrt{T}} \right) + 4.44 * 10^{-6} \left(\frac{N}{\sqrt{T}} \right)^2 \quad (3.2)$$

$$K_3 = 2.13 + 5.538 * 10^{-9} \left(\frac{N}{\sqrt{T}} \right)^{3.5} - \frac{53}{500 - N/\sqrt{T}} \quad (3.3)$$

$$\frac{\dot{m}\sqrt{T}}{P} = K_3 \left[1 + \left(\frac{1}{K_2} \right)^{10} + \left(\frac{Pr}{K_1 K_2} \right)^{10} \right] \quad (3.4)$$

For the isentropic efficiency:

$$F_1 = 29.33 - 5.33 * 10^{-2} \left(\frac{N}{\sqrt{T}} \right) \quad (3.5)$$

$$F_2 = \left\{ \left[1.01 - \left(\frac{K_1}{10Pr} \right)^2 \right] \left[1.01 - \left(\frac{Pr}{10K_1} \right)^2 \right] \right\}^{F_1} \quad (3.6)$$

$$\eta_{is} = F_2 \left[0.86 - 8.46 * 10^{-4} \left(\frac{N}{\sqrt{T}} - 430 \right) \right] \quad (3.7)$$

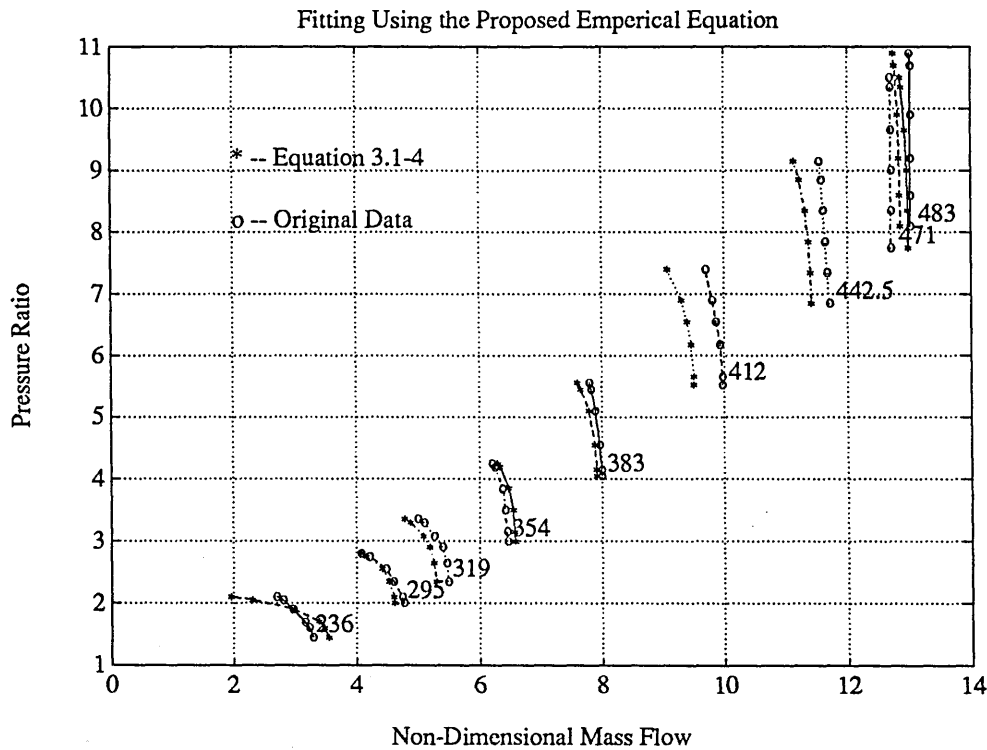


Figure 3.3: Fitting Pressure Ratio Results Using Equations 3.1-4

Using the above equations to reconstruct the characteristics, the results are shown in Figure 3.3 and Figure 3.4. It can be seen from figures that the the fittings are reasonably good only at the low speed ranges. This is because in this range, the shapes of characteristics are well rounded. In the Figure 3.4, the fitting of isentropic efficiency is relatively poor, and this is mainly due to the large variations in its magnitude.

3.3.1 Curve Fitting By a General Polynomial

In the present work, effort has been made to Effort has been made to find a general nonlinear polynomial to fit to the given compressor characteristics. Motivated by

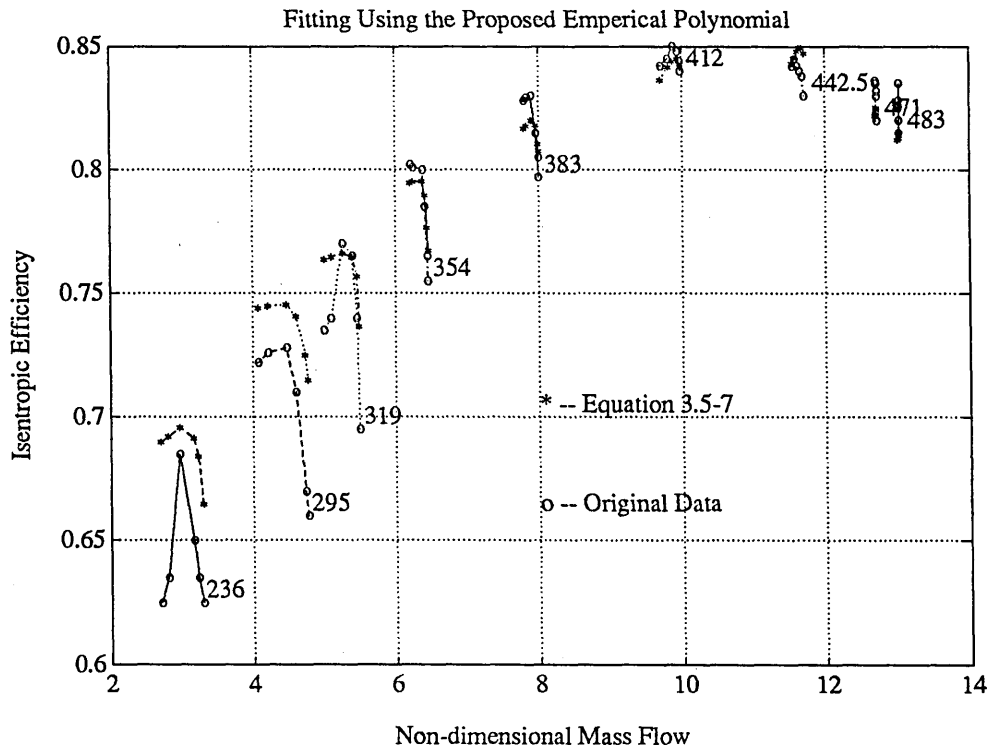


Figure 3.4: Fitting Efficiency Results Using Equations 3.5-7

the idea introduced in [114], the following polynomial is used:

$$z = a_0 + a_1x + a_2y + a_3x^2 + a_4y^2 + a_5xy + a_6x^2y + a_7xy^2 + a_8x^2y^2 \quad (3.8)$$

Here, the independent variables, x and y represent non-dimensional speed and pressure ratio, respectively. The dependent variable; namely non-dimensional mass flow or isentropic efficiency is represented by z . The coefficients of fitting this polynomial to the single-spool characteristic are listed in Table 3.1, and the reconstructed characteristics are shown in Figure 3.5 and 3.6. It is obvious that some improvements have been made in the low speed ranges compared with Maccallum's results, however the fitting still cannot be considered satisfactory, especially in the high speed ranges.

Experience has taught us that direct fitting from the given data will always result in error and doubt in the estimates in the intermediate points on the characteristics. The polynomial fitting has resulted in a set of coefficients which range

Coefficient a_i	$\frac{\dot{m}\sqrt{T}}{P}$	η_{is}
a_0	3.6484e+00	6.4229e-01
a_1	-1.4552e+00	-1.3005e-01
a_2	-7.5913e-03	-7.7943e-04
a_3	-2.1175e+00	-7.0034e-02
a_4	2.5018e-05	2.7240e-07
a_5	1.4563e-02	1.9090e-03
a_6	8.3590e-03	1.7677e-04
a_7	-1.7179e-05	-2.9863e-06
a_8	-8.5946e-06	-8.5131e-08

Table 3.1: Coefficients From the Polynomial Fitting

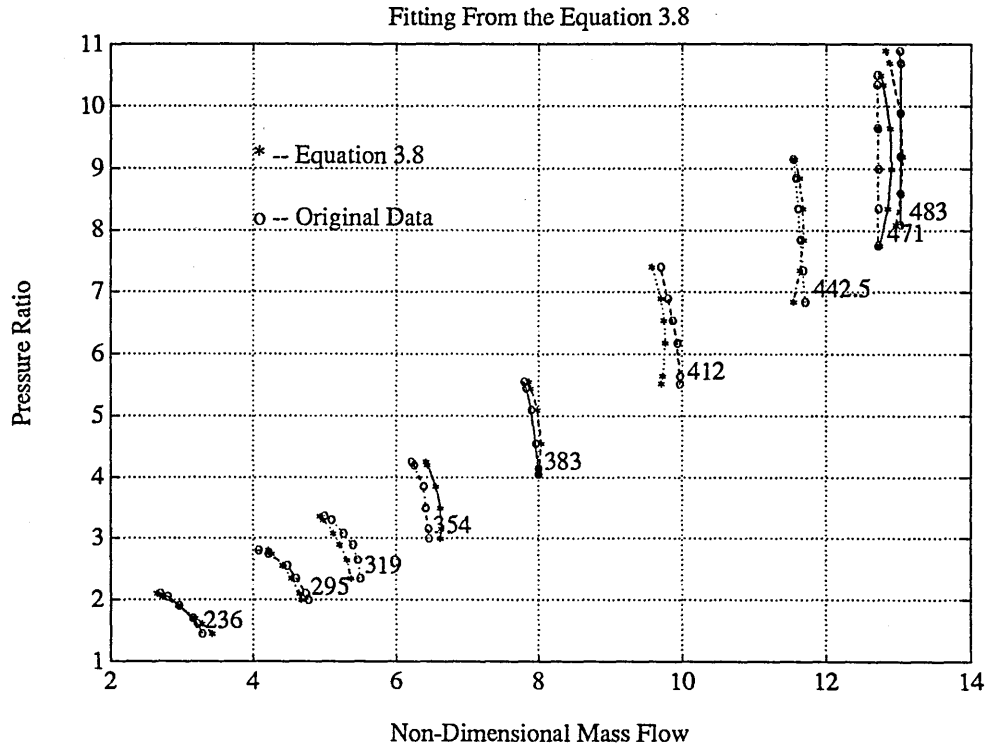


Figure 3.5: Fitting Results Using the Proposed Polynomial: Equation 3.8

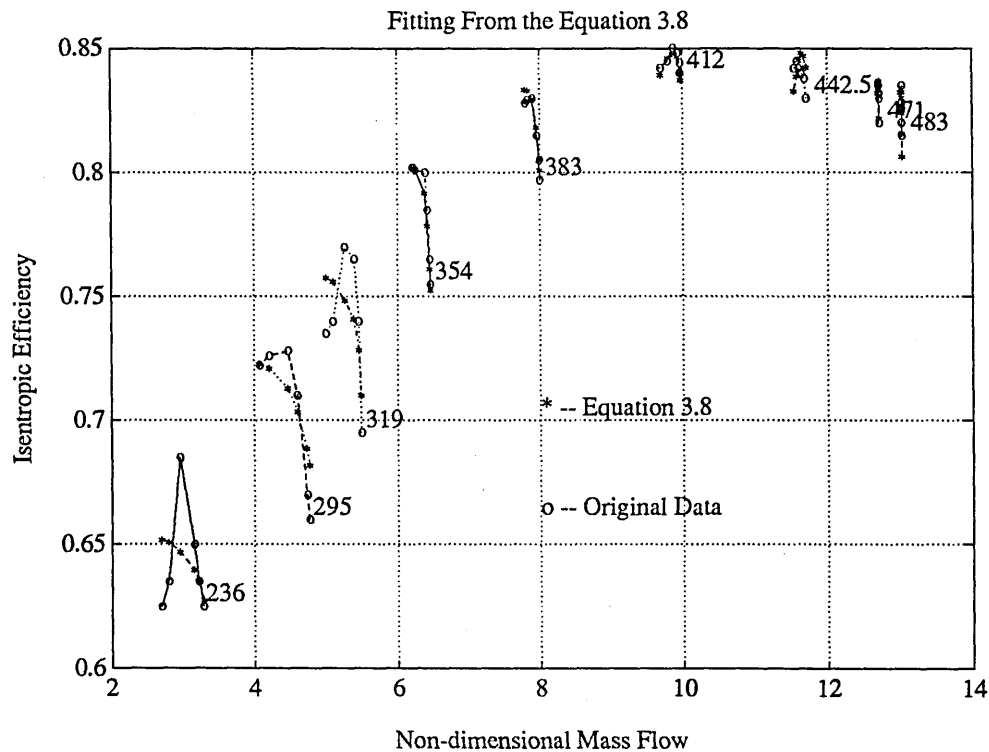


Figure 3.6: Fitting Results Using the Proposed Polynomial: Equation 3.8

from 10^{-8} to 10^{-1} , which may easily cause numerical problems in transient calculations. This is partly due to the variation of the shape of each curve on the characteristics, which requires polynomials having different orders [115].

3.4 Motivation from the Previous Study

3.4.1 Need for a Multi-Objective Algorithm

Modelling techniques usually focus on one type of model performance measure. This often narrows the designer's overall view of system model performance. On the other hand, modelling has to be considered as a multi-objective process. Besides the well-known error limitations usually considered, a model and modelling algorithm have to guarantee the following:

- Accurate prediction of engine error and also real-time execution capability, in order to cope with the new role attached to engine simulations.

- Monotonic variation of the model parameters, in order to ease the complexity of the analytical models of the components.

An exact quantitative specification of model objectives is rarely available in practice. In order for the modelling process to proceed in a systematic way, it is necessary that each of the model qualities be rated quantitatively, by means of a suitable defined performance index. In this way, it may be possible to take care of modelling objectives. Besides, the model performance indices should clearly reveal the ability of the model to predict engine behaviour, as well as the qualities of that prediction, at all engine operating points.

3.5 Characterisation of Model Qualities

In the following, the adequate quantitative rating and mathematical formulation of model qualities are considered. The investigated ratings include:

- Error rating
- Rating of parameters' monotonic behaviour.
- Predictability rating.
- Global model performance rating.

3.5.1 Characterisation of a Monotonic Behaviour Indicator

Here it is intended:

- To find an analytical tool for checking the monotonic behaviour of a given data set along a specified interval.
- To establish a proper scale for evaluating the discrepancy of the data set from the monotonic.

Thus if

$$sld_i = sl_{i,i+1} - sl_{i-1,i} \quad (3.9)$$

where $sl_{i,i+1}$ is the slope value in the interval $(i,i+1)$, and sld_i is the difference of the slope values at point i . If we sum up the sld_i :

$$slo = \sum_1^{no} |sld_i| \quad (3.10)$$

where no is the number of turning or inflection points, and slo is the slope-attitude-variation indicator of a parameter, the slo can be regarded as a representative of the total slope oscillations, which may be used as an indicator for derivations of parameter values from the monotone. Furthermore, if the curve monotonic behaviour indicator (CMI) is defined as:

$$CMI = \frac{slo}{((nc - 1) - 1)(|aix - ain|)} \quad (3.11)$$

where aix and ain are the maximum and minimum values, respectively, of the model parameter a_i , then CMI gives an unbiased normalised indicator in the sense that it does not depend on the number of data points, nor on the order of magnitude of the parameter considered. If a parameter sdp is defined by:

$$sdp_i = \sum_i^{nai} CMI \quad (3.12)$$

where nai is the number of terms for fitting the parameter a_i , then sdp will reflect the monotonic behaviour of the complete set of model parameters. It also correlates with the deterioration from monotonic behaviour resulting from the increase in the number of parameters. In this way, it is possible to evaluate the behaviour of any parameter set analytically, and thus to evaluate and compare the monotonic behaviour associated with various models, even if different data sets or different numbers of parameters are used.

3.5.2 Characterisation of Error Indicator

Usually, an error measure is used to assess a good fit. However, the least-squares error has two serious deficiencies as an indicator of a good fit. It can be large, because the number of data points is large, even if the fit is fairly good. More important, it depends on the scale used for the data values [116]. We are concerned with a general scale that can be used both for evaluating model performance and for comparing different models (even if different data sets are used). The intended measure of error has to compensate for the changeable number of data points, and for the scale variations.

In order to analyze the discrepancy between the predicted data values and their original values, we may use:

1. Relative errors.
2. Mean absolute relative error.
3. Standard deviation.

These measures are evaluated for each curve in the characteristic, as well as for the considered characteristic as a whole. Thus a relative error, $germ$, and a standard dervation, $g\sigma$, can be defined by:

$$germ = \frac{\sum_1^{nc} \sum_1^{np} |er|}{\sum_1^{nc} np} \quad (3.13)$$

$$g\sigma = \sqrt{\frac{\sum_1^{nc} \sum_1^{np} |er|^2}{\sum_1^{nc} (np - 1)}} \quad (3.14)$$

where nc is the number of data points on a parameter curve and np is the number of these points used to form the model. Evaluation of the standard deviation gives a picture of the error dispersion about the considered data mean. Also it is useful if we know about the encountered maximum error values, as indicated by $germ$.

3.5.3 Characterisation of the Predictability Indicator

To obtain a possible definition for a model predictability, it is considered that the available data are divided into two distinct sets, with the first set used for model deduction, and the second set used for measuring the deduced model predictability. If the error measure evaluated for the first set is $mgerm$, and for the second set is $pgerm$, the form, a predictor indicator, $crit4$, may be given by:

$$crit4 = 1 - \frac{2pgerm}{(1 + pgerm + mgerm)} \quad (3.15)$$

This definition meets the proper logic requirements:

- It has a constant value of unity when the prediction error ($pgerm$) is zero, whatever the value of modelling error is.
- It weights the effect of modelling error $mgerm$ even when its value is equal to $pgerm$.
- The departure of its value from the ideal value of unity increase as the predicted error increases.
- Its value is bounded even at the zero value of the prediction error $pgerm$.

This form of predictor indicator is also useful as a measure of validity of a model.

3.6 Harmonisation of Performance Indicator

As a result of the model performance characterisation, various factors have to be included. These factors usually represent competing objectives, and the intended model has to make necessary compromise to trade-off one against another. Thus it is useful if the previously mentioned factors are combined into adequate mathematical formulation. Having indicators x and y that have to be included together to formulate a suitable measure, it is appropriate if the form $(1 + x)(1 + y)$ is

adopted for that purpose. Besides other advantages, this form keeps the information content related to nonzero factors even when there is a possible zero for the other factor (x, y etc).

Accentuating the model qualities of interest, previously introduced, and the proposed harmonisation procedure, the following performance measures are defined:

$$cri1 = (1 + germ)(1 + g\sigma) \quad (3.16)$$

$$cri2 = (1 + germ)(1 + sdp) \quad (3.17)$$

$$cri3 = (1 + germ)(1 + g\sigma)(1 + sdp) \quad (3.18)$$

$$cri4 = 1 - \frac{2pgerm}{(1 + mgerm + pgerm)} \quad (3.19)$$

3.7 Global Criterion for Modelling

Using the $cri3$ measure enables grasping the resultant interaction of the mean error, maximum error, standard deviation, and monotonic behaviour of parameters. If we combine this measure together with the predictability indicator in the form of:

$$cri5 = \frac{cri4}{cri3} \quad (3.20)$$

we got a global modelling criterion that measure the overall model behaviour. In the ideal case the predictability $cri4 = 1$ and $cri1 = 1$; therefore the departure $cri5$ from the value of unity will reflect the deviation of the model from the ideal. We are now in a position to evaluate and compare various models, even if they possess small differences in different performance indices. This is achieved in a well-defined and mathematically precise way.

3.8 Application to the Compressors

In this section, the proposed performance indices are applied to the representation of the characteristics used in the present study. To simplify the exposition, the characteristics of the single-spool engine are used as an illustrative example, and the results using the characteristics of the two-spool engine are presented.

3.8.1 Data Scaling

The largest error in the design chain is likely to arise because the original process data is not sufficiently representative [117]. For modelling, it is of utmost importance to keep the data to be modelled free from corruption until they are introduced to the model. Mathematical operation may cause distortion to the information content of the original data, and this is especially true if the variables are likely to have large magnitude variations. It is necessary to keep the same order of magnitude for all the variables to be manipulated, as these variables change their values over the entire range of compressor operation. This may require the re-scaling of the original data before they are mathematically manipulated. From possible re-scaling strategies, it is clear that using the constant speed line parameter in its relative form, while re-scaling the abscissa and ordinate variables with respect to the corresponding surge line values is the most convenient strategy. This what has been referred to as “dynamic scaling”. In reality, we are searching for an appropriate moving origin for handling data on each of the speed lines. A second-order estimate of the surge line for the compressor in the present work is found to be adequate. For modelling in this case, the surge line pressure ratio, efficiency and non-dimensional mass flow as functions of the non-dimensional speed are fitted and plotted in Figure 3.7 and 3.8.

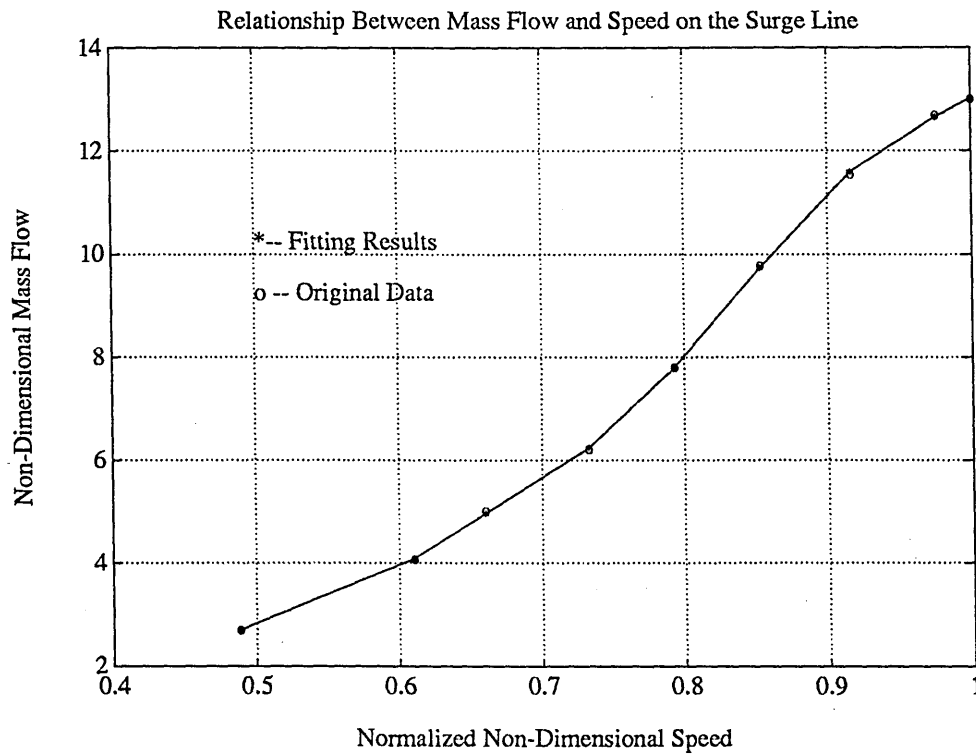


Figure 3.7: Fitting Mass Flow and Speed on the Surge Line

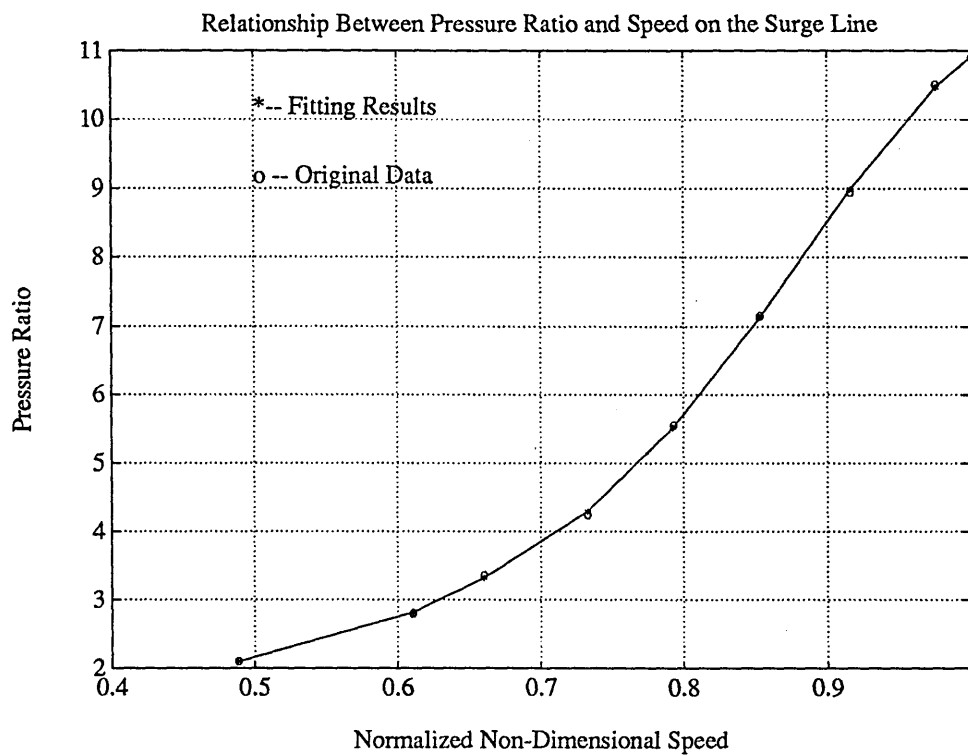


Figure 3.8: Fitting Pressure Ratio and Speed on the Surge Line

3.8.2 Transformation of Axes

For a good model we have to preserve a degree of the compressor internal behaviour and cross couplings. This is accomplished through a superficial or external transformation by regrouping the compressor variables into new lumps. These lumps maintain various shapes for connecting variables and preserving interactions in compressor representation according to their individual form.

In order to realise the intended monotonic behaviour of parameters, the previously explained concepts of bundling up variables is exercised with various transformation. Table 3.2 presents the final transformations that have been tested.

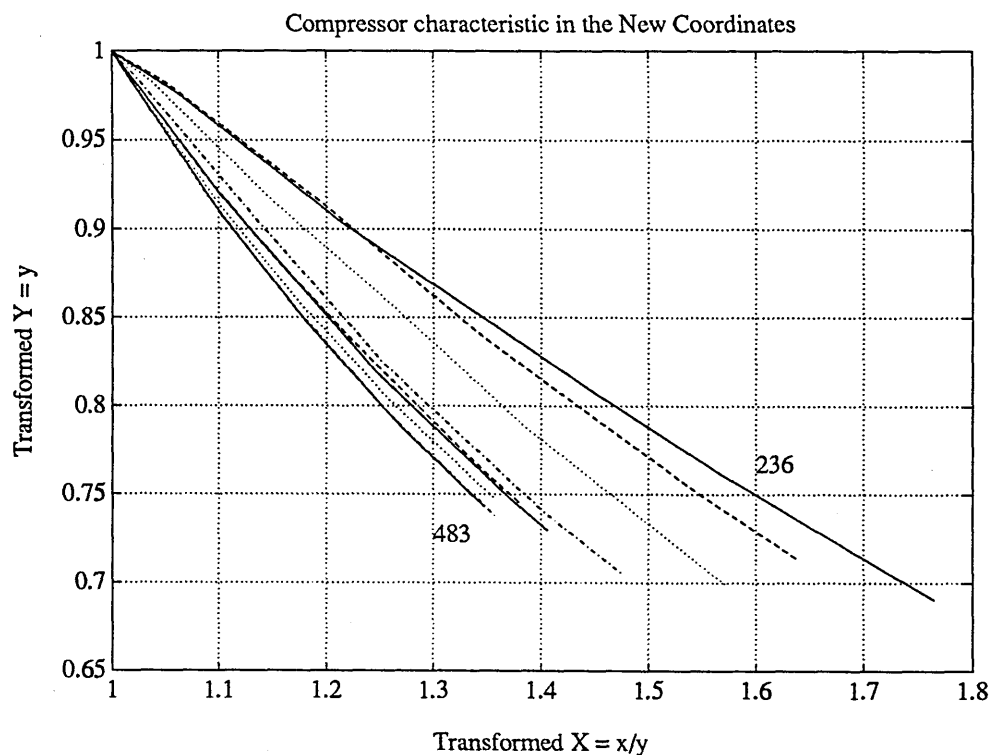


Figure 3.9: Transformed Pressure Ratio and Mass Flow Characteristic

Thus it is possible to combine all the different transformations. For each case, a function is guessed, with increasing numbers of terms, to determine the optimum lumping with compatible parameters.

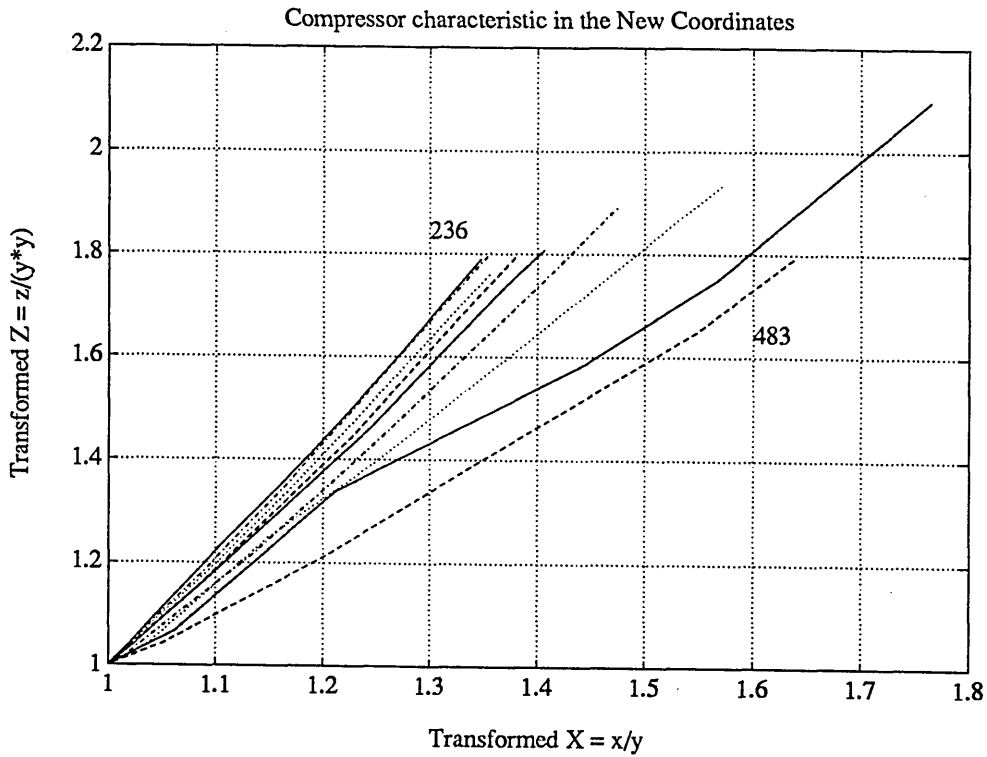


Figure 3.10: Transformed Efficiency and Mass Flow Characteristic

Index	New X coordinate
1	x/y
2	$x/(y * \bar{n})$
3	$x * y$
4	$x * y * \bar{n}$
5	$x + y$
6	$(x + y) * x$
7	$(x + y)^2$

Table 3.2: Lists of Possible Choice of Transformations

3.8.3 Fitting of New Map of Compressor

For the new re-scaled characteristics as shown in Figure 3.9 and 3.10, it is obvious that we have a data set that can be well fitted by a guessed function whose graph is monotonic over the entire range. Two parameters are generally sufficient to achieve a good fit in this case. Figure 3.11 and 3.12 show the variations of the coefficients found for this fitting.

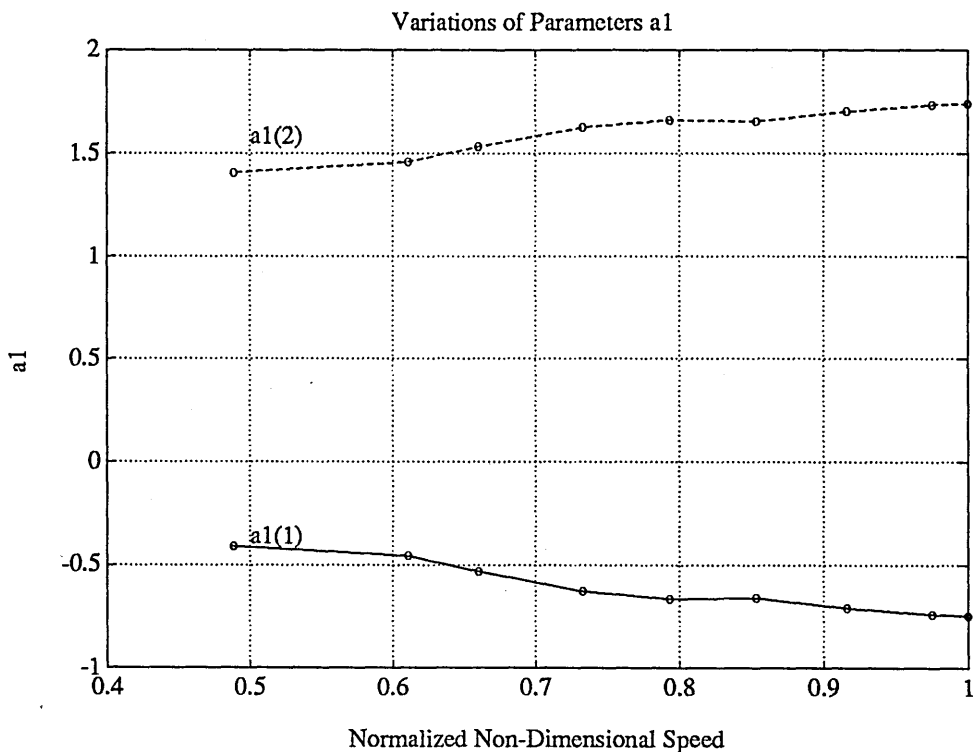


Figure 3.11: Coefficients from Fitting Transformed Characteristic of Figure 3.9

For more complex cases, a more general form for the guessed function would be:

$$Y(X) = \sum_i^n a_i X^{i-1} \tag{3.21}$$

3.8.4 Reconstructing Original Characteristics

It is clear from Figure 3.11 and 3.12 that the monotonic variation of these parameters makes it easier to fit them to the non-dimensional speed. The results from such fitting are shown in Figure 3.13 and 3.14. The derived analytical equations

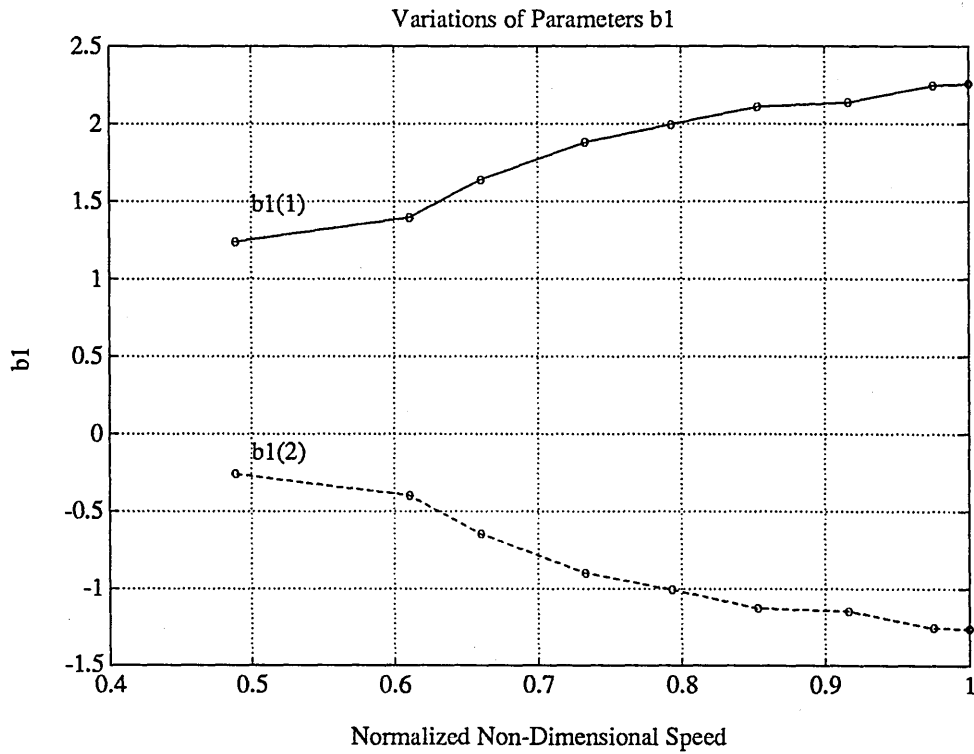


Figure 3.12: Coefficients from Fitting Transformed Characteristic of Figure 3.10

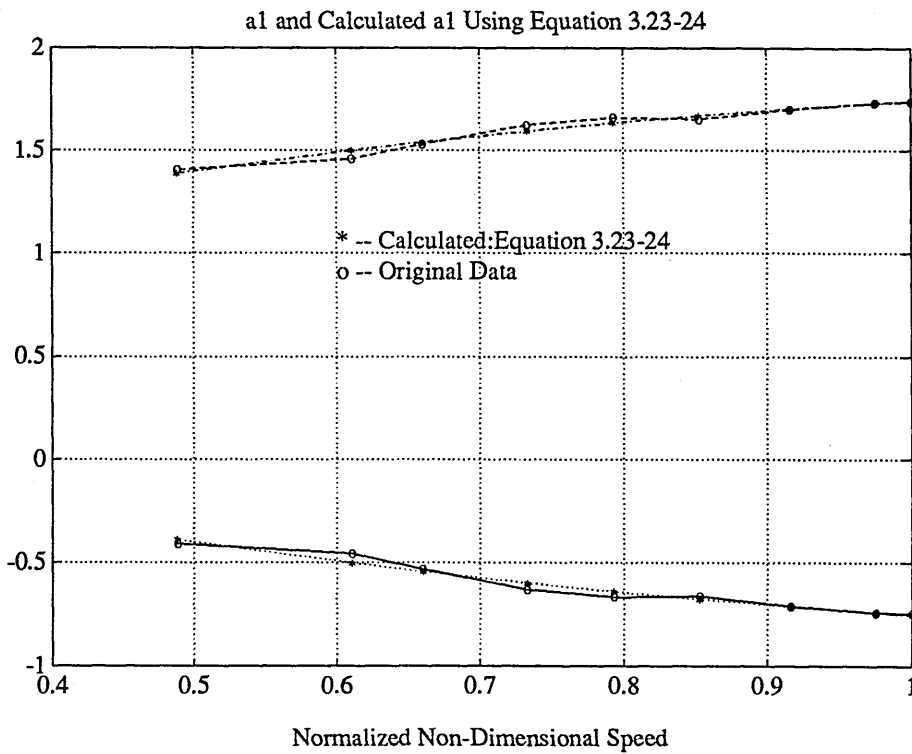


Figure 3.13: Comparison of Results of Fitting Coefficients from Figure 3.11

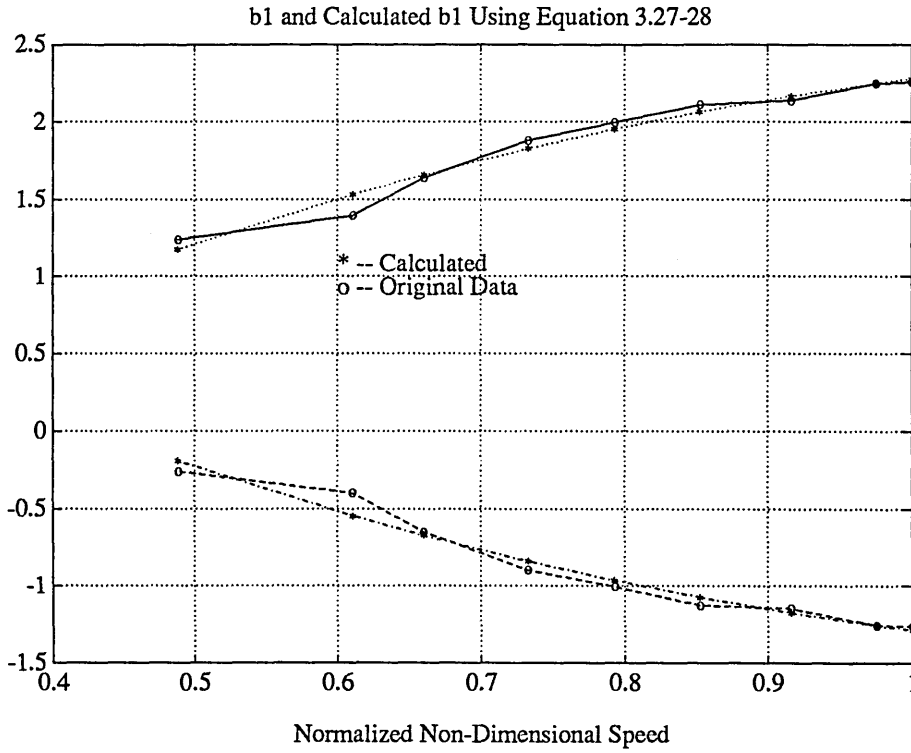


Figure 3.14: Comparison of Results of Fitting Coefficients from Figure 3.12

to represent the compressor used in the single-spool engine are given as follows.

For the non-dimensional mass flow:

$$Y_1 = a_1(1) + a_1(2)X \quad (3.22)$$

$$a_1(1) = -0.566\bar{n}^2 + 1.5328\bar{n} + 0.7753 \quad (3.23)$$

$$a_1(2) = 0.5587\bar{n}^2 - 1.5387\bar{n} + 0.2288 \quad (3.24)$$

$$(3.25)$$

Similarly the equations for the isentropic efficiency are:

$$Y_2 = b_1(1) + b_1(2)X \quad (3.26)$$

$$b_1(1) = 1.9249\bar{n}^2 - 5.0055\bar{n} + 1.7940 \quad (3.27)$$

$$b_1(2) = -1.9268\bar{n}^2 + 5.0208\bar{n} - 0.8156 \quad (3.28)$$

where $X = x/y$, $Y_1 = y$, $Y_2 = x/y^2$ and \bar{n} is the normalised non-dimensional speed.

The above equations have been used to reconstruct the characteristics and Figure 3.15 and 3.16 show the relationships between the X and Y in the transformed coordinates. Figure 3.17 and 3.18 show the reproduced compressor characteristics. Figure 3.17 and 3.18 show the reproduced compressor characteristics. It

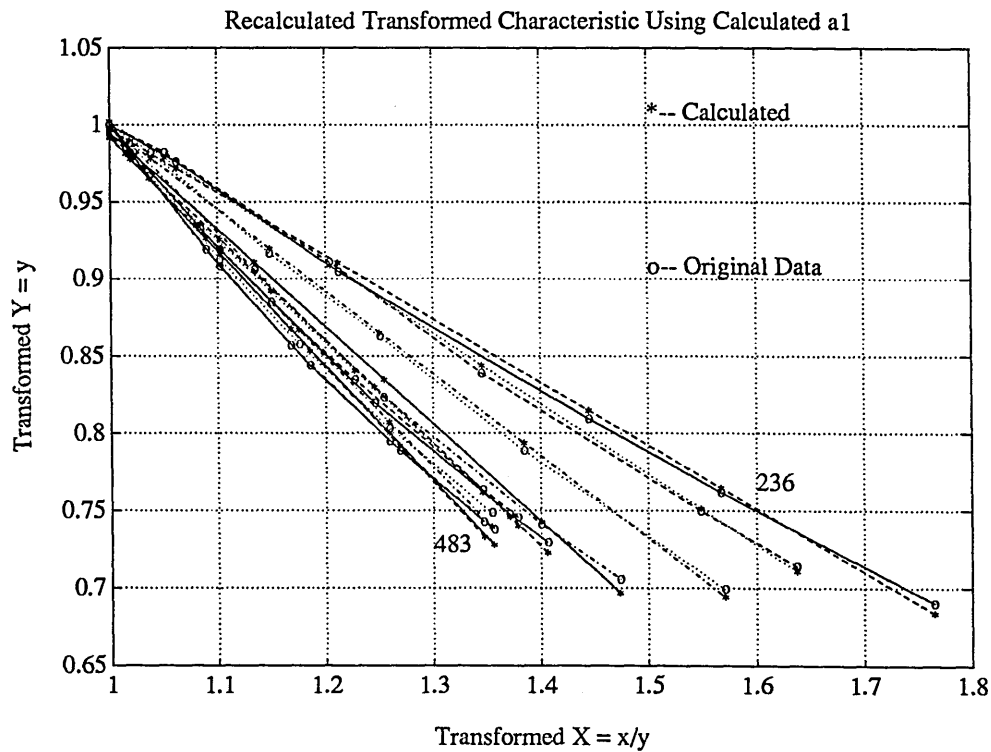


Figure 3.15: Reconstructed X and Y Using the Above Equations

is seen from the Figures that, for the non-dimensional mass flow, such fitting has produced very good results, there are almost no visible errors between the original characteristic and the reproduced characteristic. For efficiency as shown in Figure 3.18, it is seen that for the first and second constant speed lines, errors exist. It is clear from the coefficient fitting in Figure 3.14 that this is due to the errors in fitting coefficients b_1 . The accuracy can certainly be increased by using higher order polynomial for fitting b_1 .

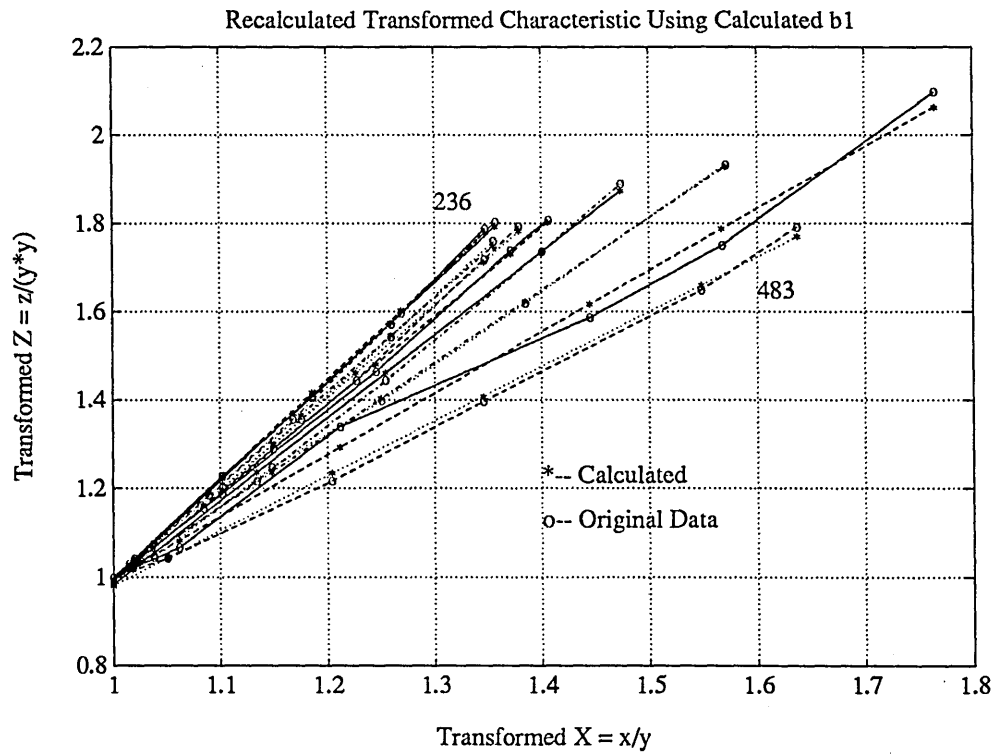


Figure 3.16: Reconstructed X and Y Using the Above Equations

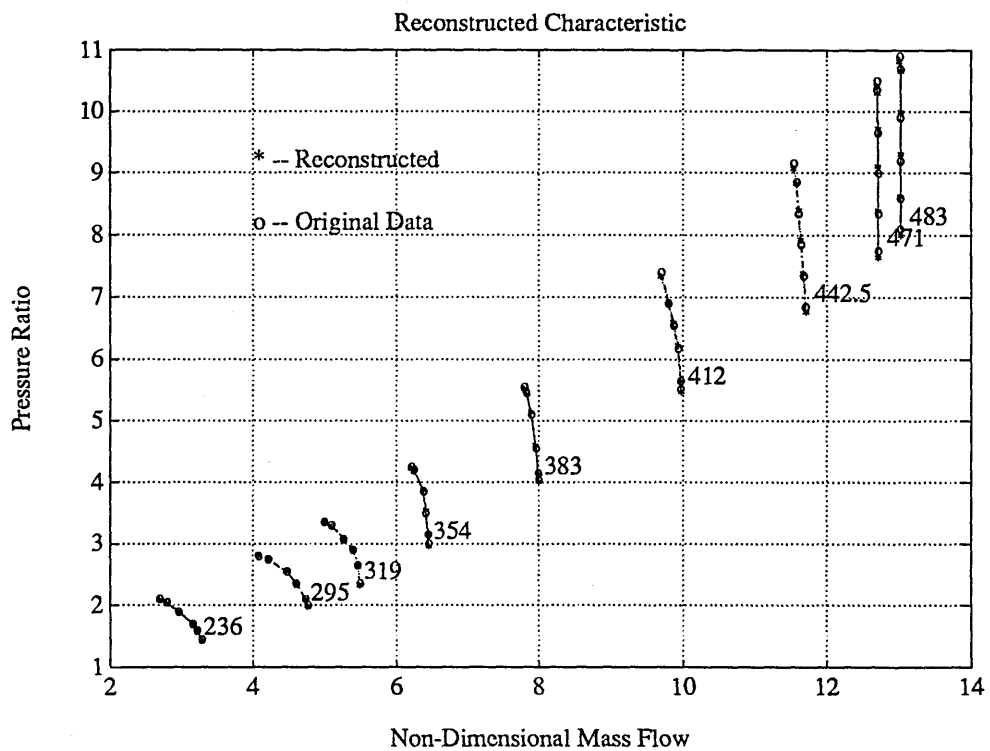


Figure 3.17: Reconstructed Pressure Ratio/Mass Flow Characteristic

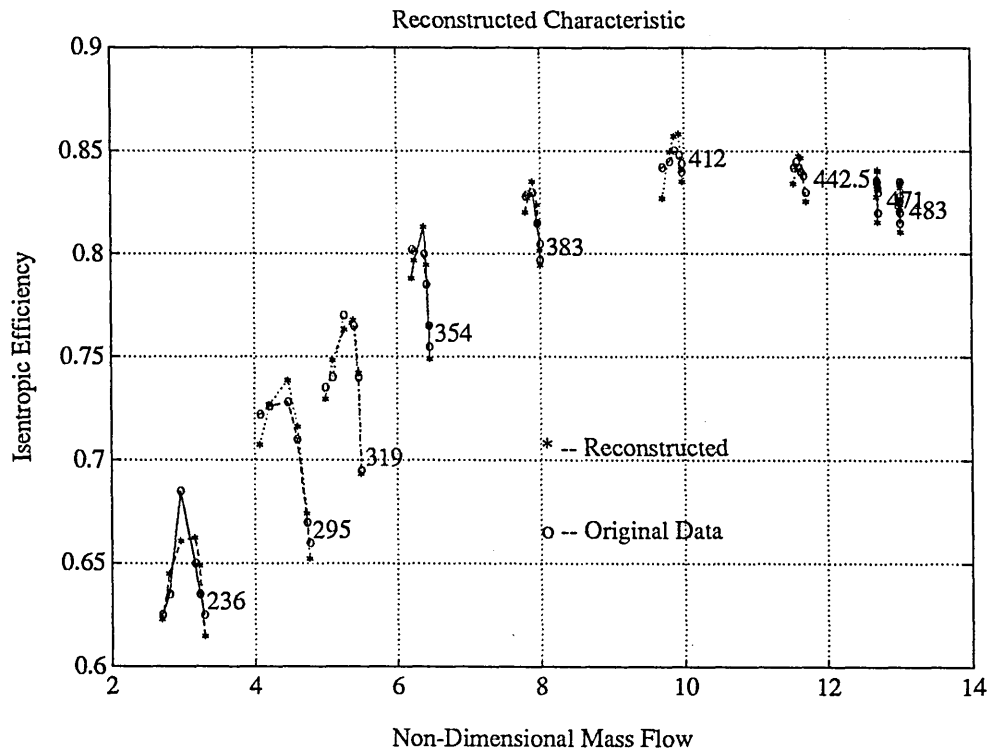


Figure 3.18: Reconstructed Efficiency/Mass Flow Characteristic

3.8.5 Some Conclusions

No matter how models with lower sdp are obtained, it is not easy through a trial-and-error process to attain the model that guarantees the intended monotonic behaviour of parameters. Besides, the major difficulty when trying to implement real-time engine simulation on digital computers is that the time taken to evaluate all the required parameters is longer than real-time. The following should be noted:

1. Measurements are made with real, and thus imperfect instruments. Thus there is no justification for requiring that model parameters have to be exactly the identified ones.
2. The model structure and model parameters form a compatible set; for another model structure, the system information content may be redistributed between the new model constitutions and its related parameters [118].

3. Simulation is an objectively oriented process. Therefore, the information content of the engine characteristics has to be fitted to an adequately usable form.

Therefore, especially for the real-time simulation, it may be valuable if closed analytical form are used for the model parameters.

3.9 Models for Compressors in Turbofan Engine

3.9.1 Fan Characteristics

The Figure 3.19 through to Figure 3.26 show the results of applying the proposed method to the fan characteristics used in the turbofan engine. It is clear from

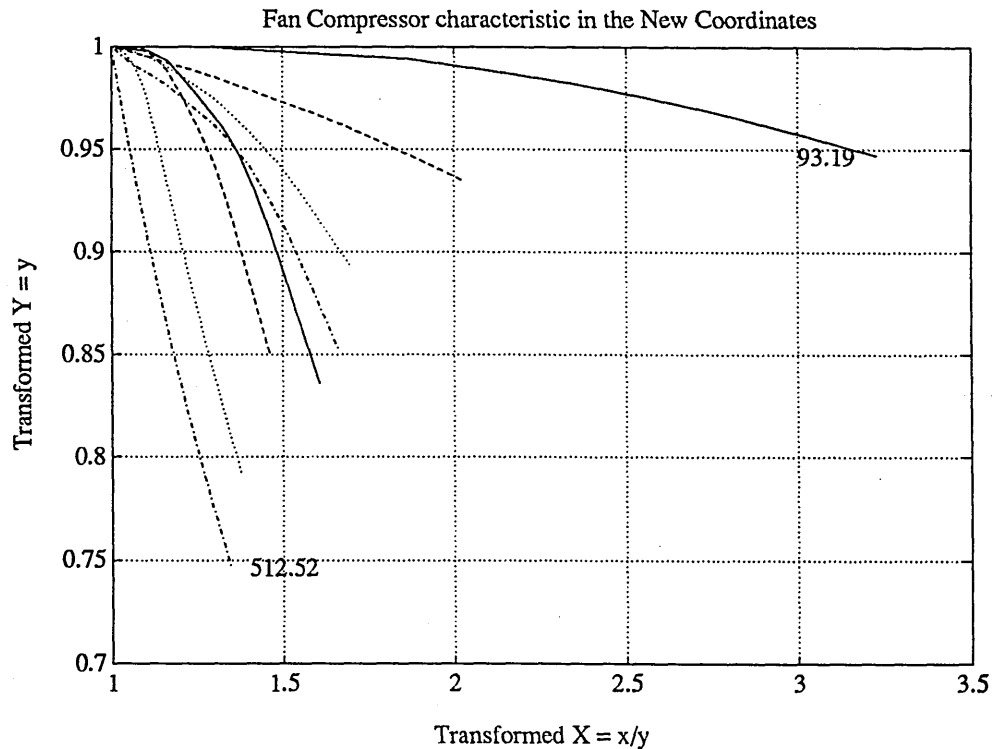


Figure 3.19: Normalised Fan Pressure Ratio/Mass Flow Characteristic

the Figure 3.19 and 3.20 that a set of second order polynomial are necessary to fit

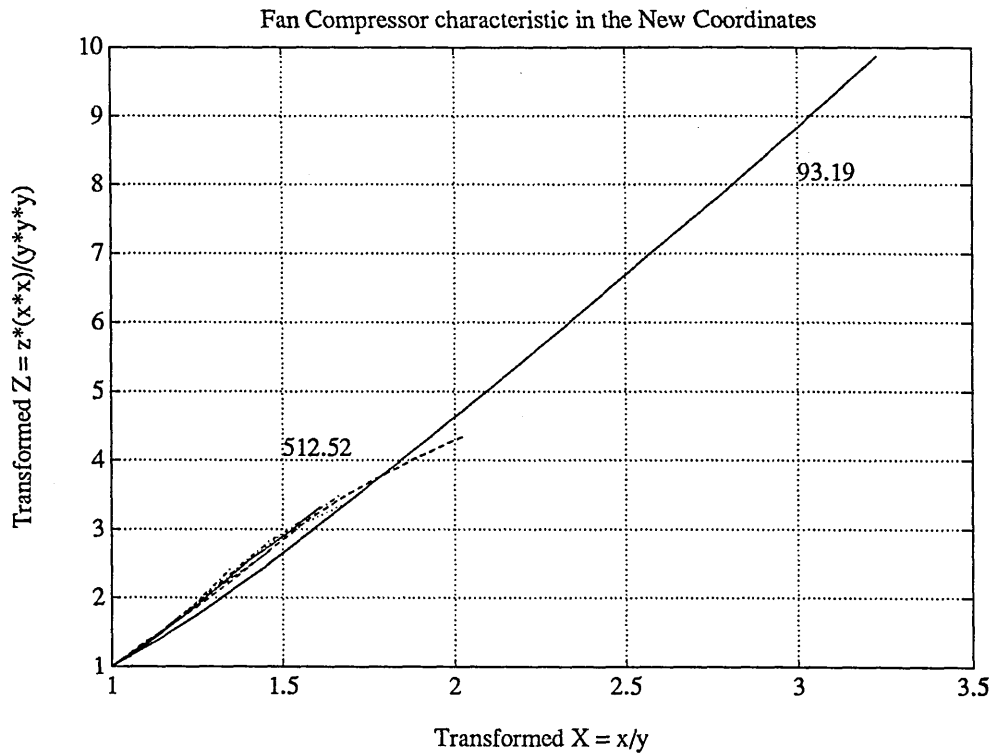


Figure 3.20: Normalised Fan Efficiency/Mass Flow Characteristic

to the transformed curves, therefore function a_1 and b_1 will have three coefficients. Figure 3.21 and 3.22 show the results of fitting to a_1 and b_1 , a set of second order polynomials as functions of normalised speed \bar{n} . Figure 3.23 and 3.24 show the results of using the fitting coefficients to reproduce the transformed characteristics, and Figure 3.25 and 3.26 show the reconstructed fan characteristics.

It is seen that the non-dimensional mass flow characteristic has been almost exactly reproduced. The equations which represent the fan mass flow characteristics are given as:

$$Y_1 = a_1(1) + a_1(2)X + a_1(3)X^2 \tag{3.29}$$

$$a_1(1) = 1.8008\bar{n}^2 - 0.4721\bar{n} - 0.7608 \tag{3.30}$$

$$a_1(2) = 4.0011\bar{n}^2 - 2.7416\bar{n} + 0.3937 \tag{3.31}$$

$$a_1(3) = -0.8851\bar{n}^2 + 2.2366\bar{n} - 0.2644 \tag{3.32}$$

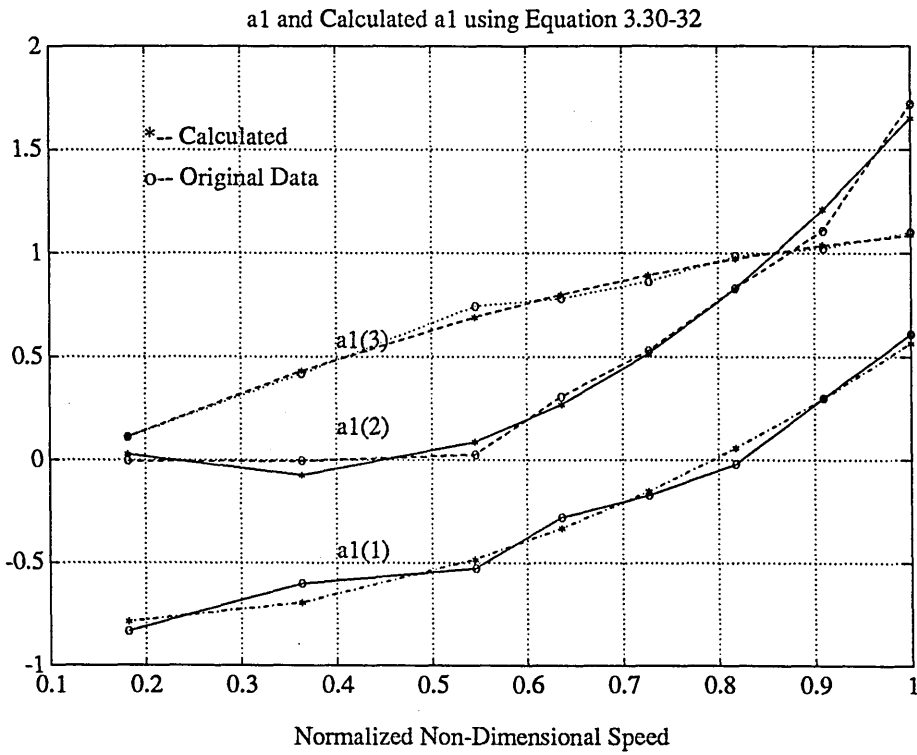


Figure 3.21: Fitting Coefficients a_1 for Pressure Ratio/Mass Flow Map

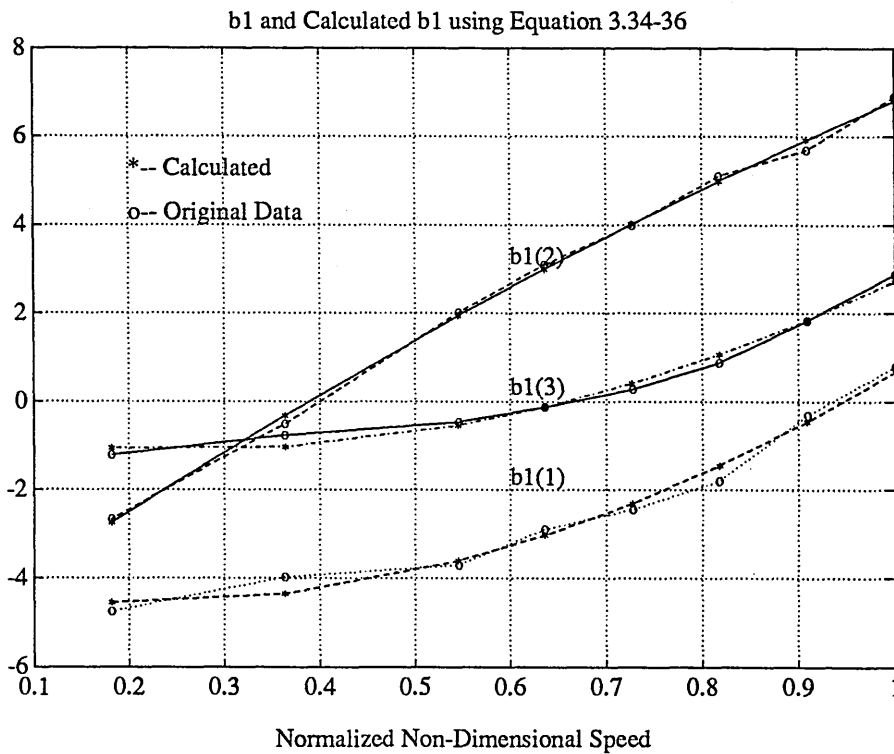


Figure 3.22: Fitting Coefficients b_1 for Efficiency/Mass Flow Map

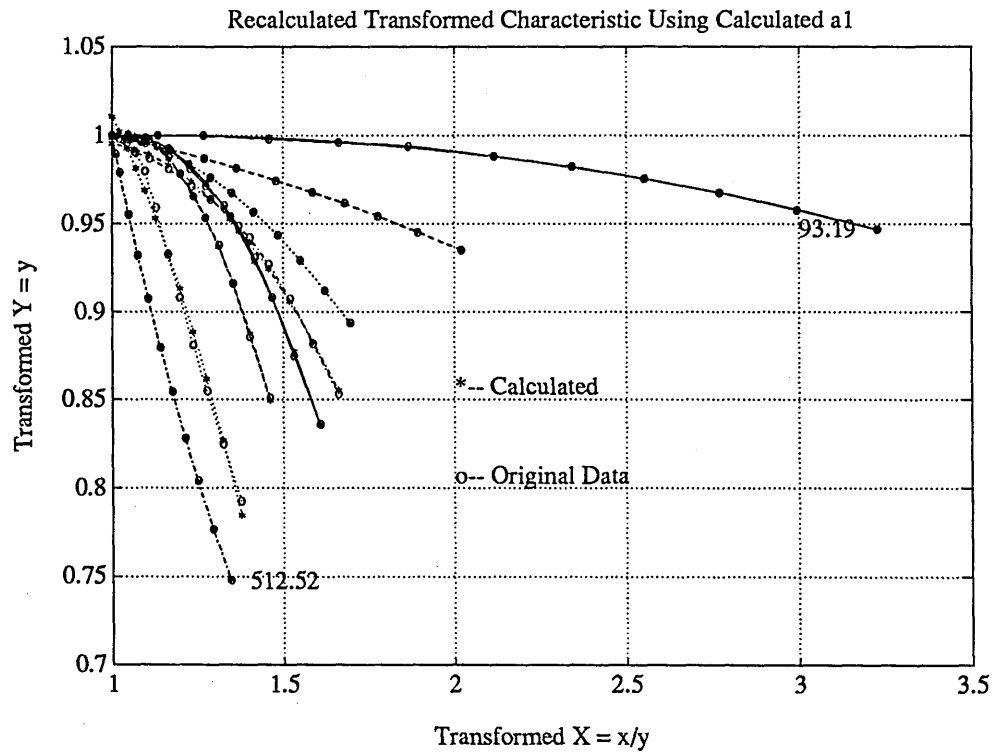


Figure 3.23: Fitting Transformed Fan Pressure Ratio/Mass Flow Characteristic

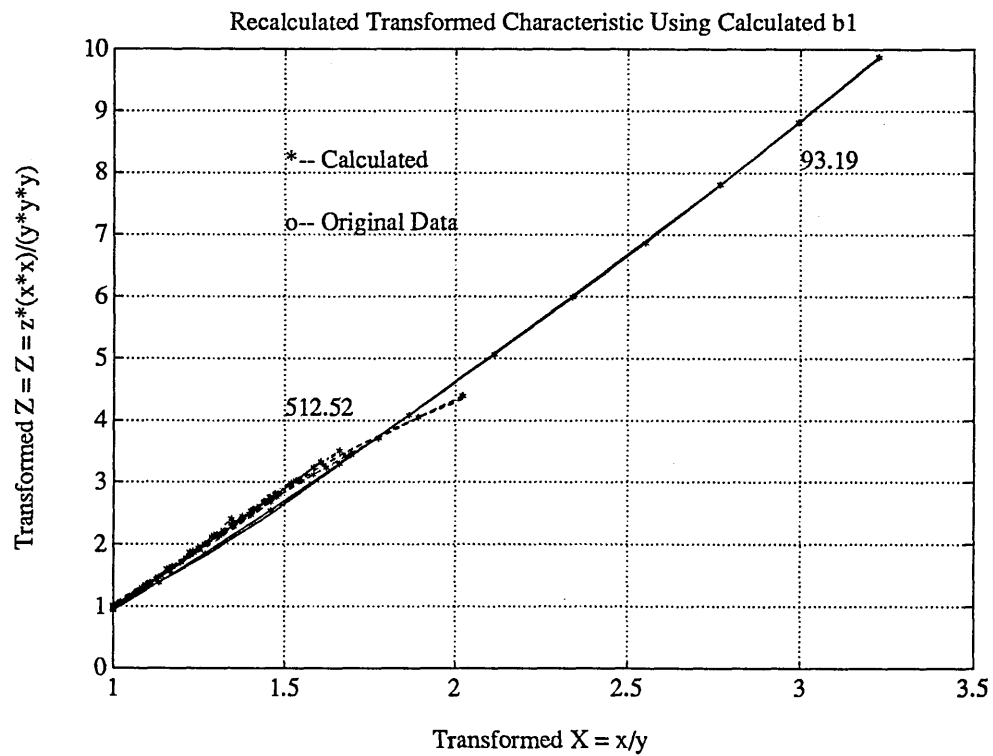


Figure 3.24: Fitting Transformed Fan Efficiency/Mass Flow Characteristic

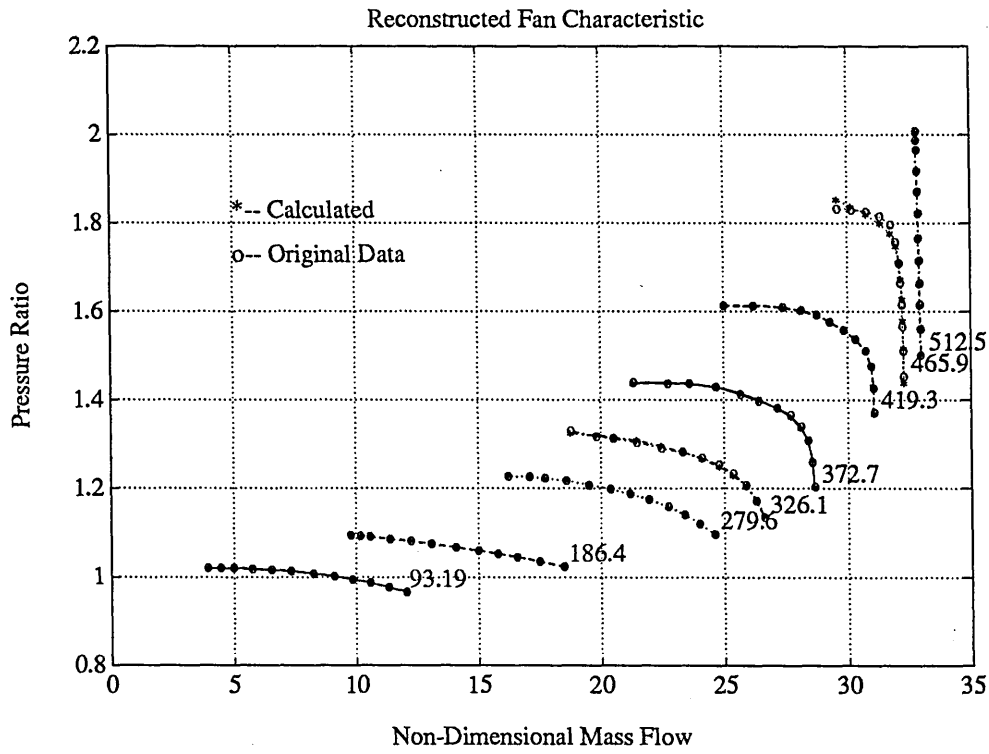


Figure 3.25: Reconstructed Fan Pressure Ratio/Mass Flow Characteristic

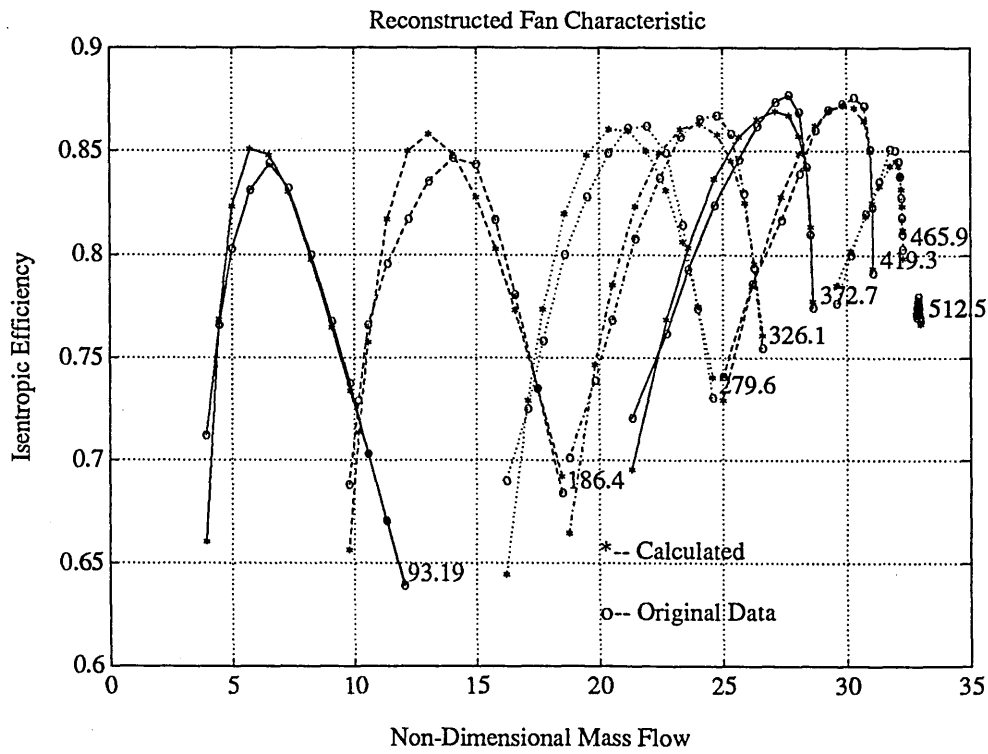


Figure 3.26: Reconstructed Fan Efficiency/Mass Flow Characteristic

For the isentropic efficiency:

$$Y_2 = b_1(1) + b_1(2)X + b_1(3)X^2 \quad (3.33)$$

$$b_1(1) = 7.0326\bar{n}^2 - 3.6901\bar{n} - 0.6204 \quad (3.34)$$

$$b_1(2) = -2.5961\bar{n}^2 - 14.741\bar{n} - 5.3338 \quad (3.35)$$

$$b_1(3) = 8.3109\bar{n}^2 - 3.4387\bar{n} - 4.1983 \quad (3.36)$$

3.9.2 IP Compressor Characteristics

The procedure of applying the proposed approach to the IP compressor is the same as above and the Figure 3.27 to Figure3.34 show the results of the fitting:

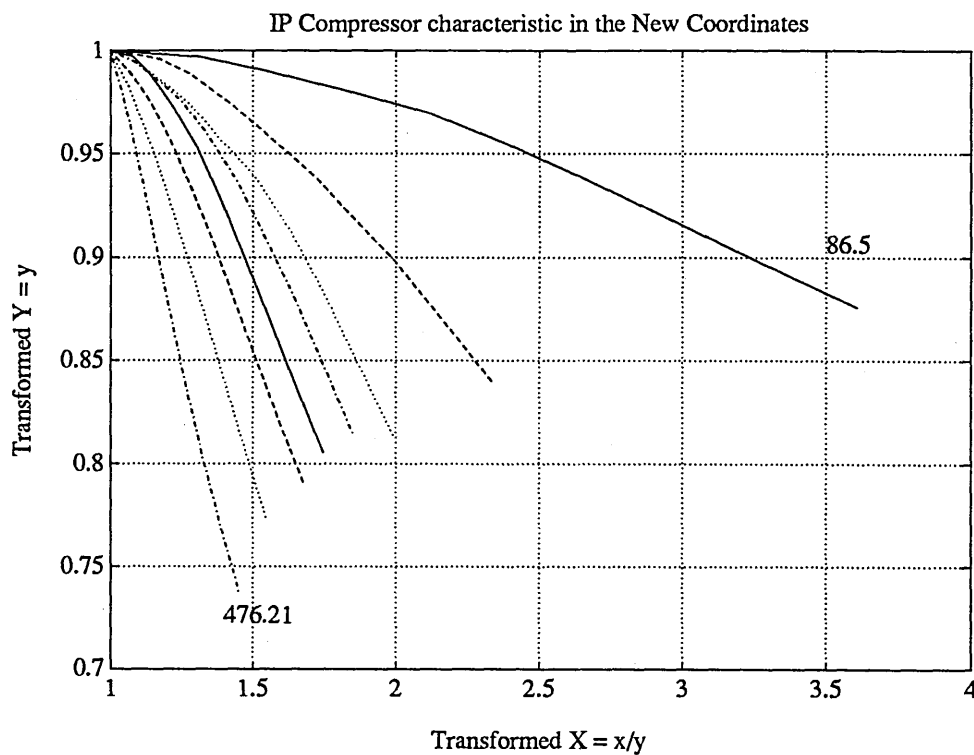


Figure 3.27: Transformed IP Comp. Pressure Ratio/Mass Flow Characteristic

The equations used to describe the IP compressor mass flow are:

$$Y_1 = a_1(1) + a_1(2)X + a_1(3)X^2 \quad (3.37)$$

$$a_1(1) = 0.7256\bar{n}^2 - 0.5133\bar{n} - 0.1234 \quad (3.38)$$

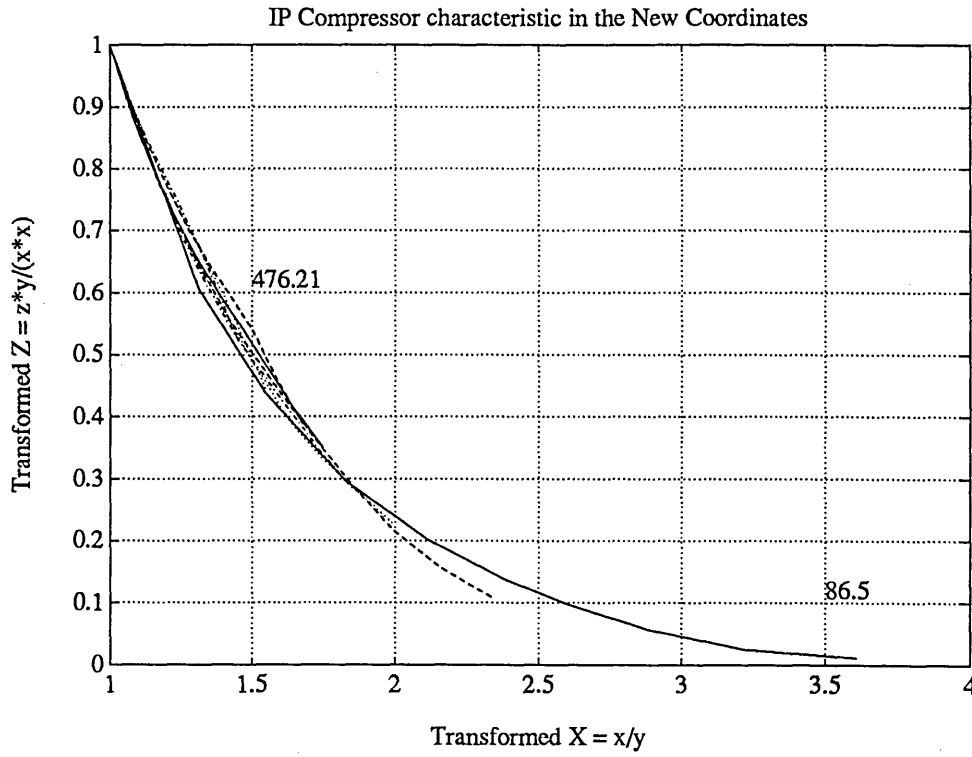


Figure 3.28: Transformed IP Comp. Efficiency/Mass Flow Characteristic

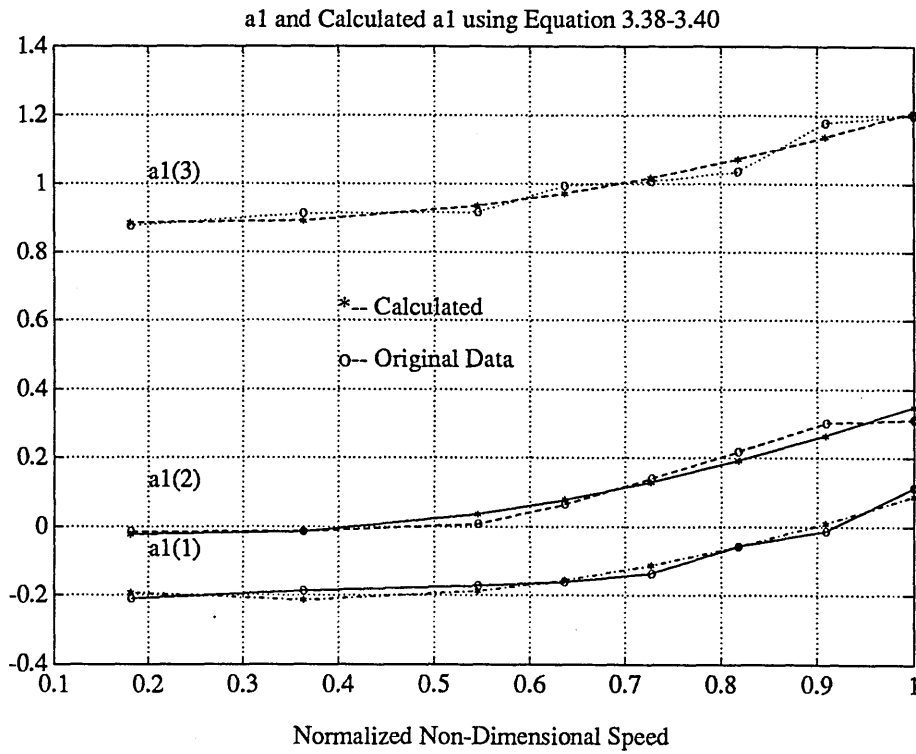


Figure 3.29: Fitting Coefficients a_1 of Figure 3.27

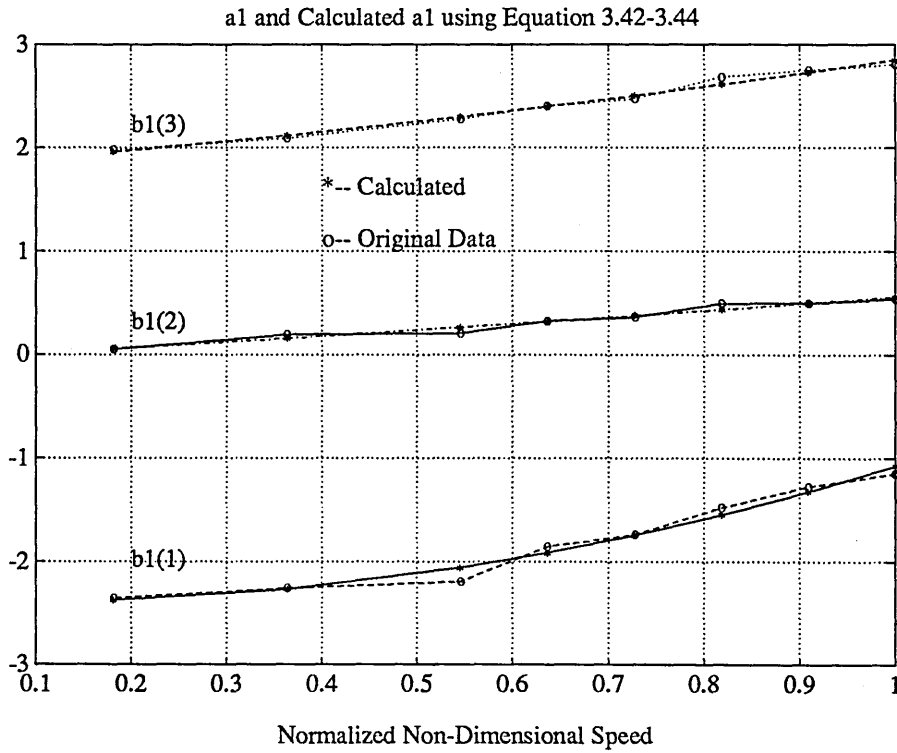


Figure 3.30: Fitting Coefficients b_1 of Figure 3.28

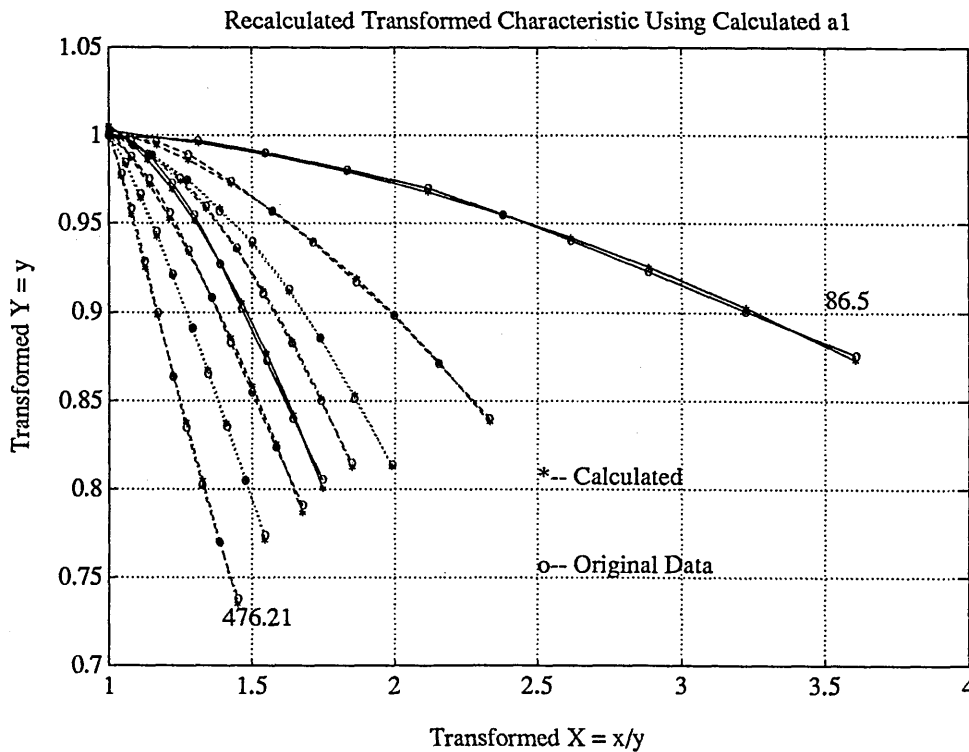
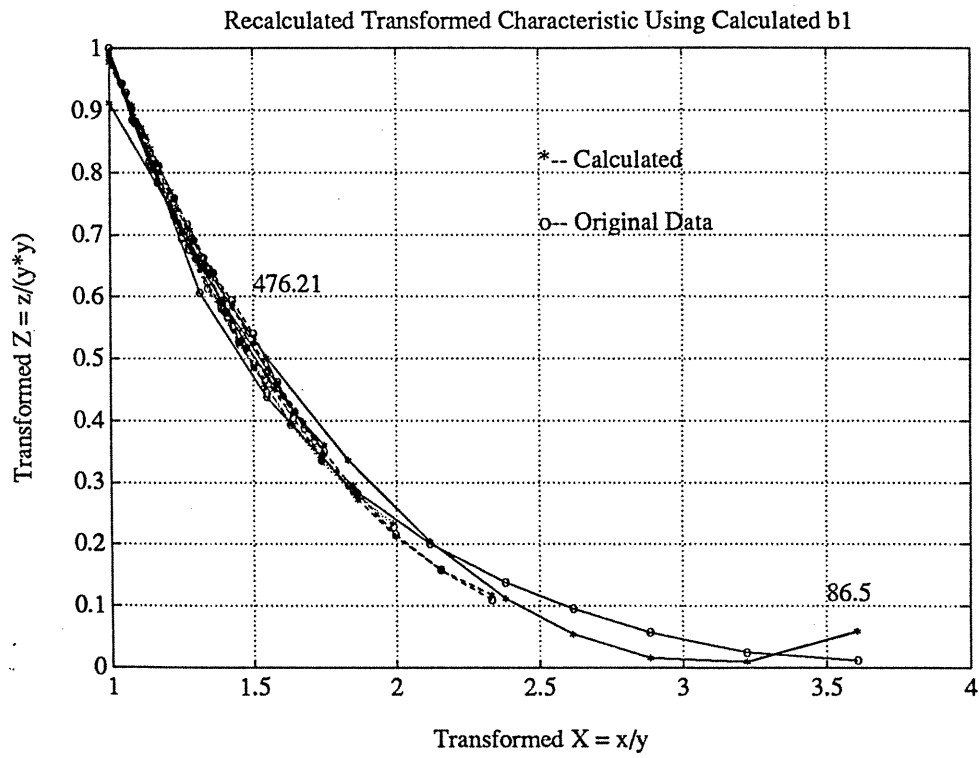
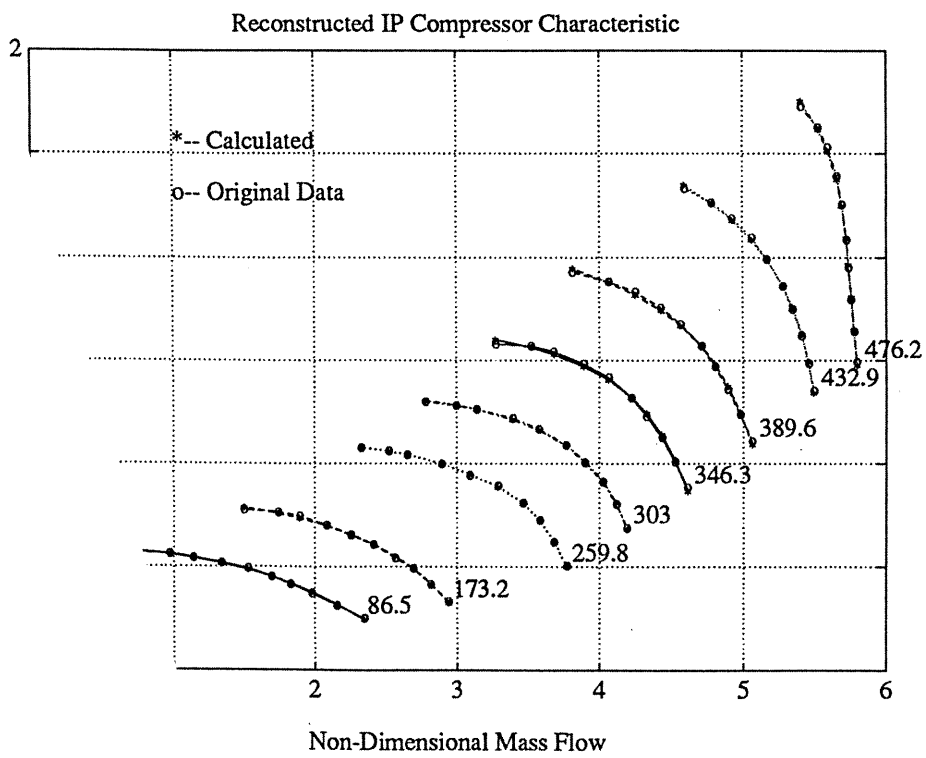


Figure 3.31: Fitting Transformed IP Comp. Pressure Ratio/Mass Flow Characteristic



3.32: Fitting Transformed IP Comp. Efficiency/Mass Flow Characteristic



ted IP Comp. Pressure Ratio/Mass Flow Characteristic

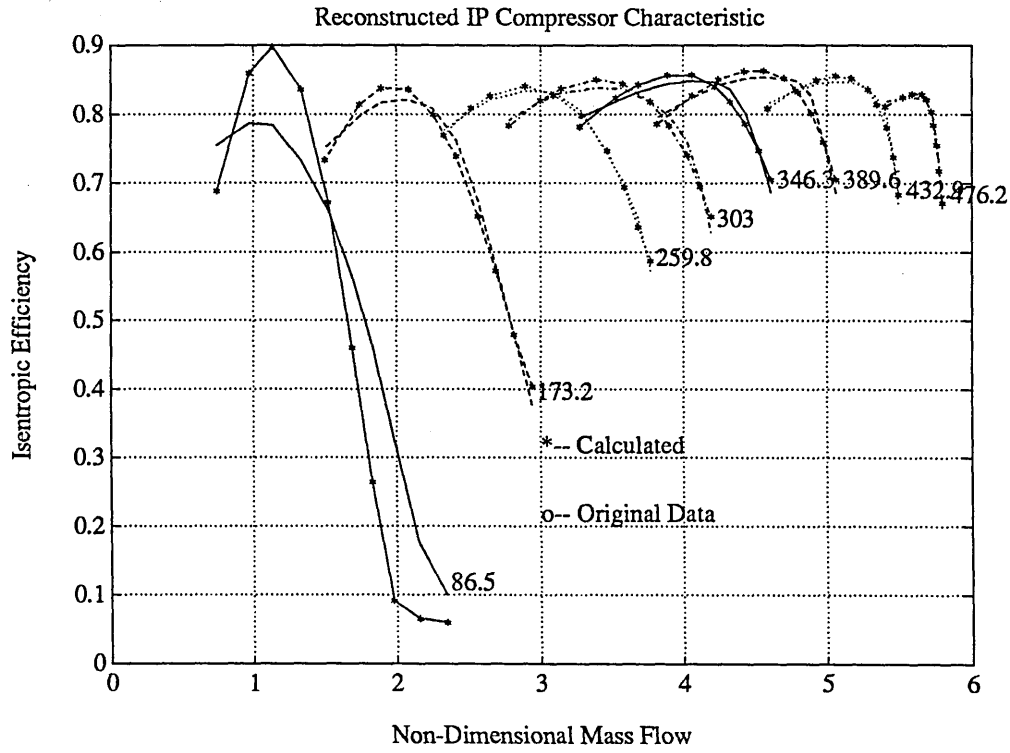


Figure 3.34: Reconstructed IP Comp. Efficiency/Mass Flow Characteristic

$$a_1(2) = 0.6405\bar{n}^2 - 0.3015\bar{n} + 0.0105 \quad (3.39)$$

$$a_1(3) = 0.5673\bar{n}^2 - 0.2747\bar{n} + 0.9178 \quad (3.40)$$

For the isentropic efficiency:

$$Y_2 = b_1(1) + b_1(2)X + b_1(3)X^2 \quad (3.41)$$

$$b_1(1) = 0.1053\bar{n}^2 + 0.4930\bar{n} - 0.0370 \quad (3.42)$$

$$b_1(2) = 1.5744\bar{n}^2 - 0.2698\bar{n} - 2.3783 \quad (3.43)$$

$$b_1(3) = 0.3571\bar{n}^2 + 0.6660\bar{n} + 1.8265 \quad (3.44)$$

It should be noted from the Figure 3.34 that the reconstructed IP compressor efficiency characteristic has some discrepancy in the first curve, i.e at the low speed. Because these are only local errors in zones not encountered during transients, they should not affect the results of transient calculations as a whole.

3.9.3 HP Compressor Characteristics

For the HP Compressor, the Figure3.34 to Figure3.42 show the results of HP compressor.

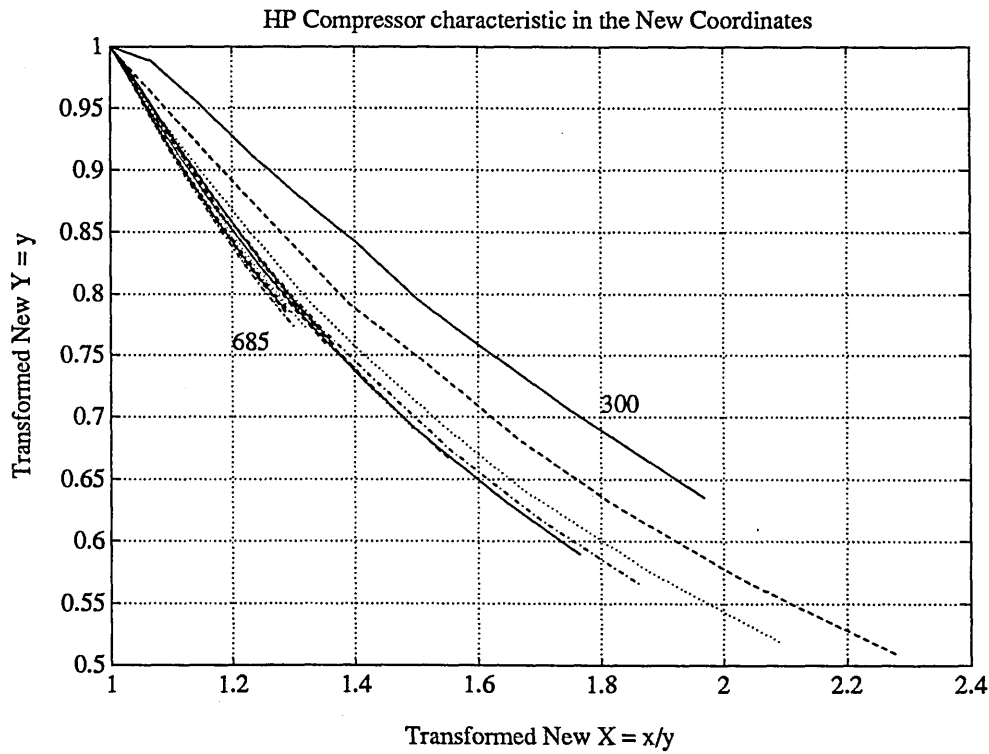


Figure 3.35: Transformed HP Comp. Pressure Ratio/Mass Flow Characteristic

The equations used to express this component are, for non-dimensional mass flow:

$$Y_1 = a_1(1) + a_1(2)X + a_1(3)X^2 \quad (3.45)$$

$$a_1(1) = 1.3164\bar{n}^2 - 1.0030\bar{n} + 0.2757 \quad (3.46)$$

$$a_1(2) = 6.8196\bar{n}^2 - 7.5277\bar{n} - 0.0458 \quad (3.47)$$

$$a_1(3) = 1.2226\bar{n}^2 - 0.0272\bar{n} + 1.33503 \quad (3.48)$$

For the isentropic efficiency:

$$Y_2 = b_1(1) + b_1(2)X + b_1(3)X^2 \quad (3.49)$$

$$b_1(1) = -12.0982\bar{n}^2 + 24.0804\bar{n} - 8.9079 \quad (3.50)$$

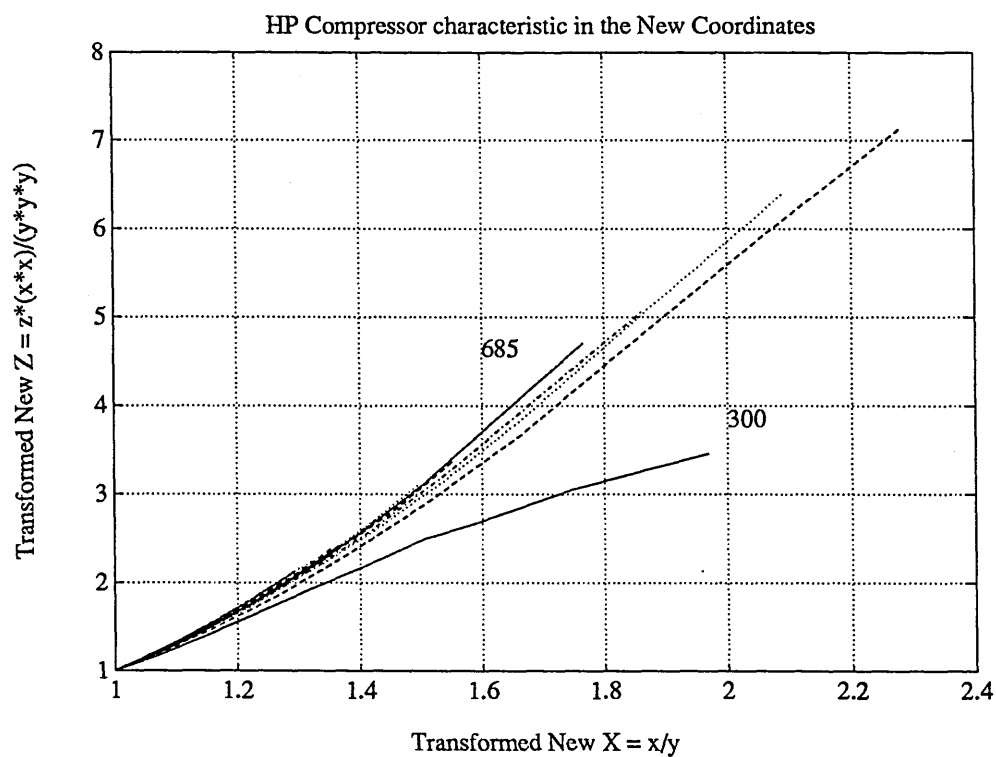


Figure 3.36: Transformed HP Comp. Efficiency/Mass Flow Characteristic

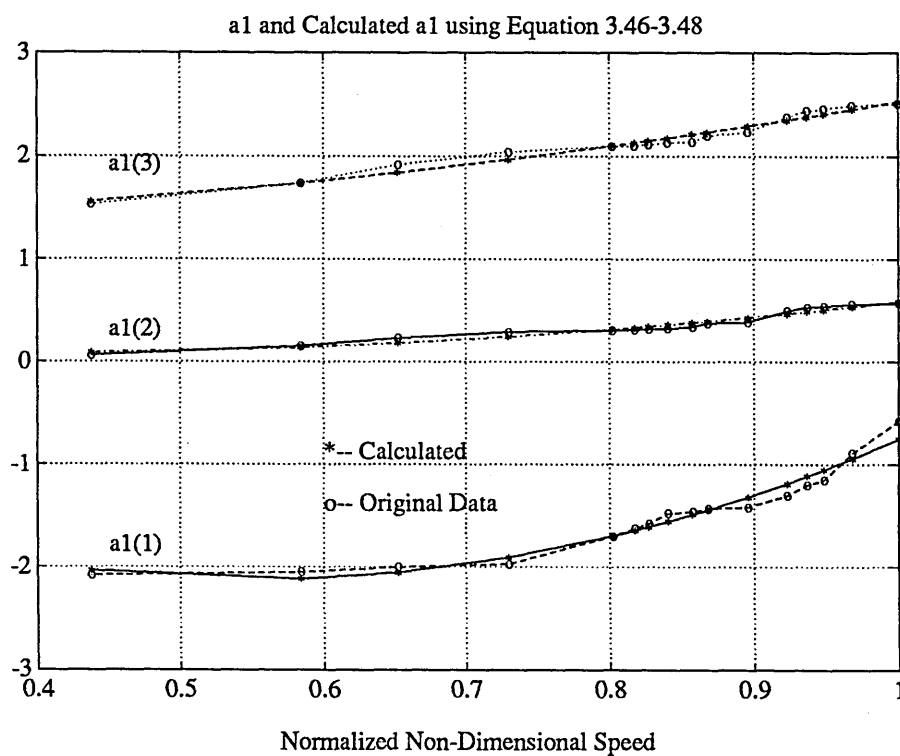


Figure 3.37: Fitting Coefficients a_1 From Figure 3.35

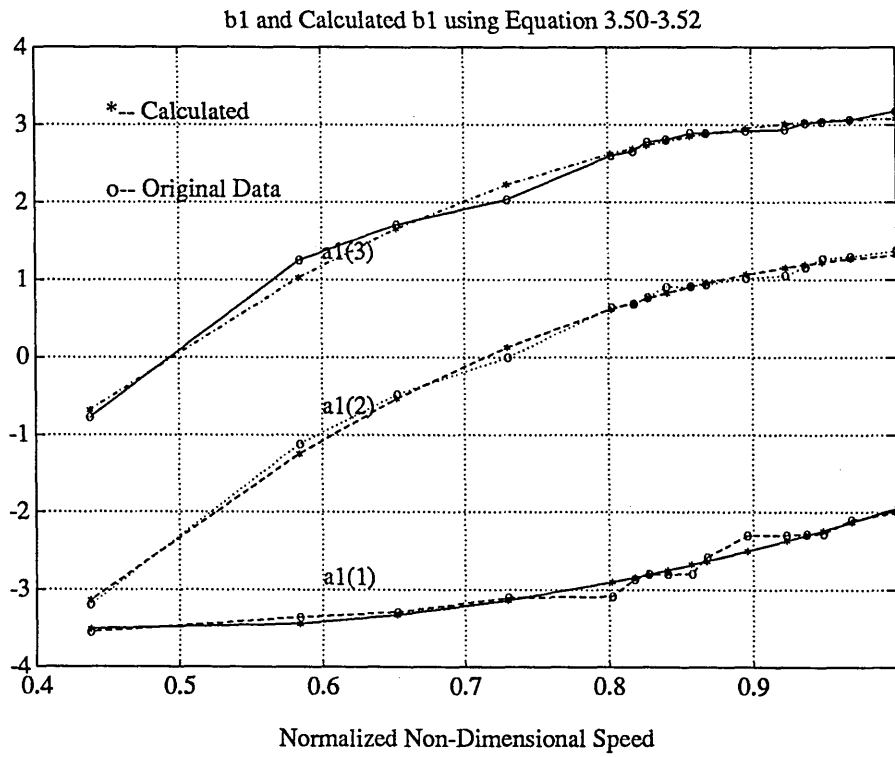


Figure 3.38: Fitting Coefficients b_1 From Figure 3.36

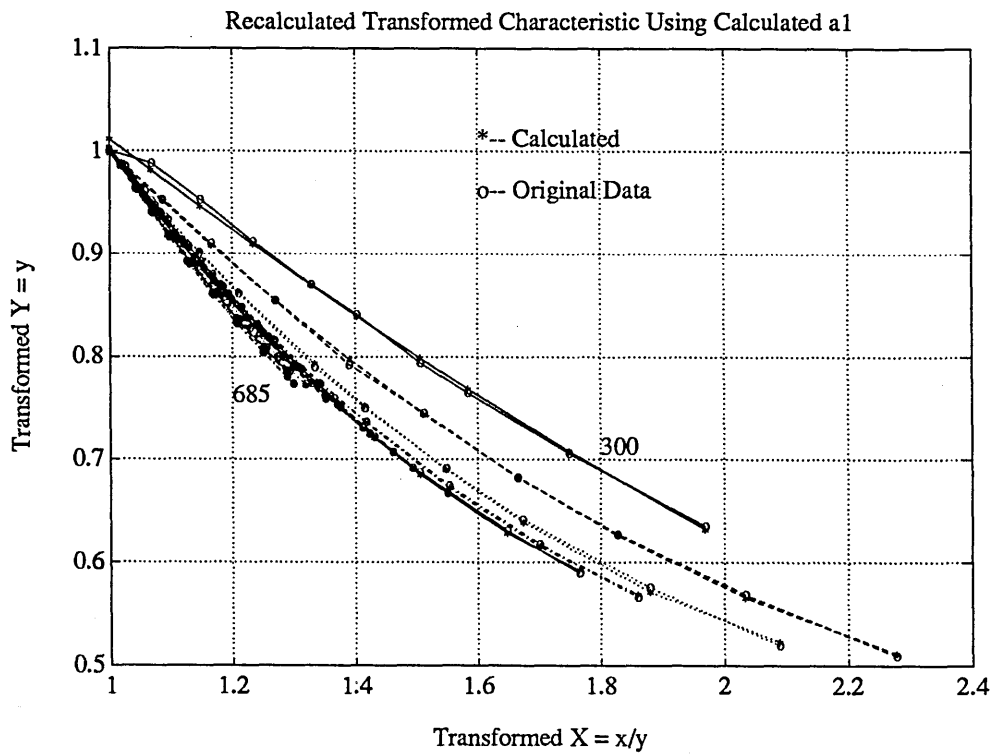


Figure 3.39: Fitting Transformed HP Comp. Pressure Ratio/Mass Flow Characteristic

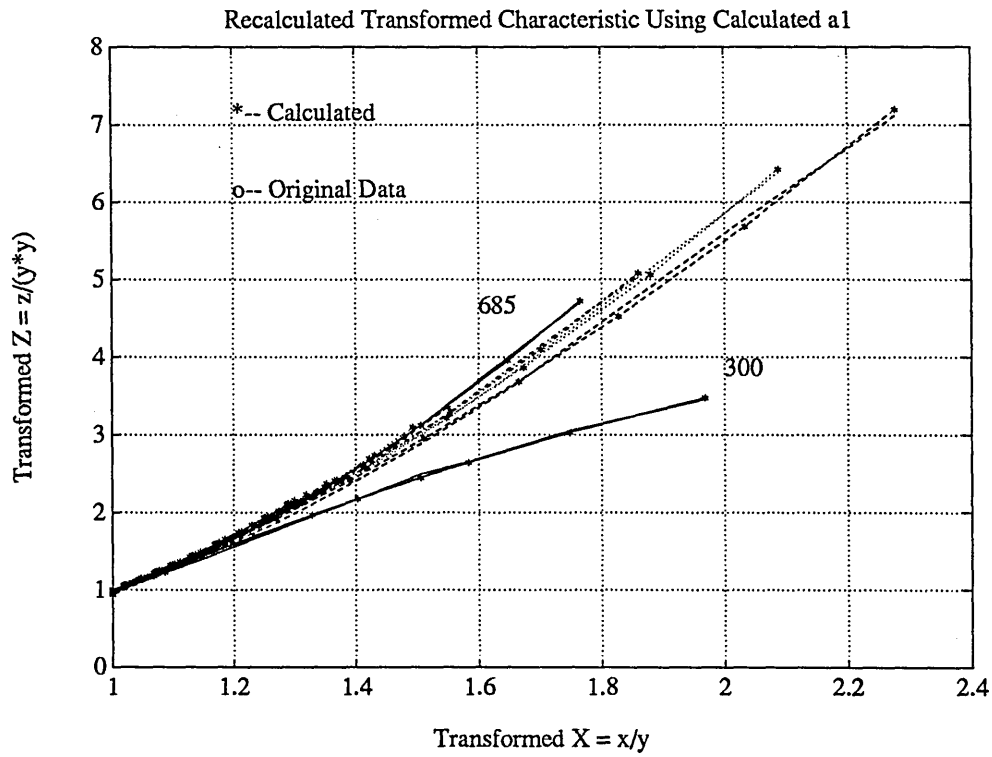


Figure 3.40: Fitting Transformed HP Comp. Efficiency/Mass Flow Characteristic

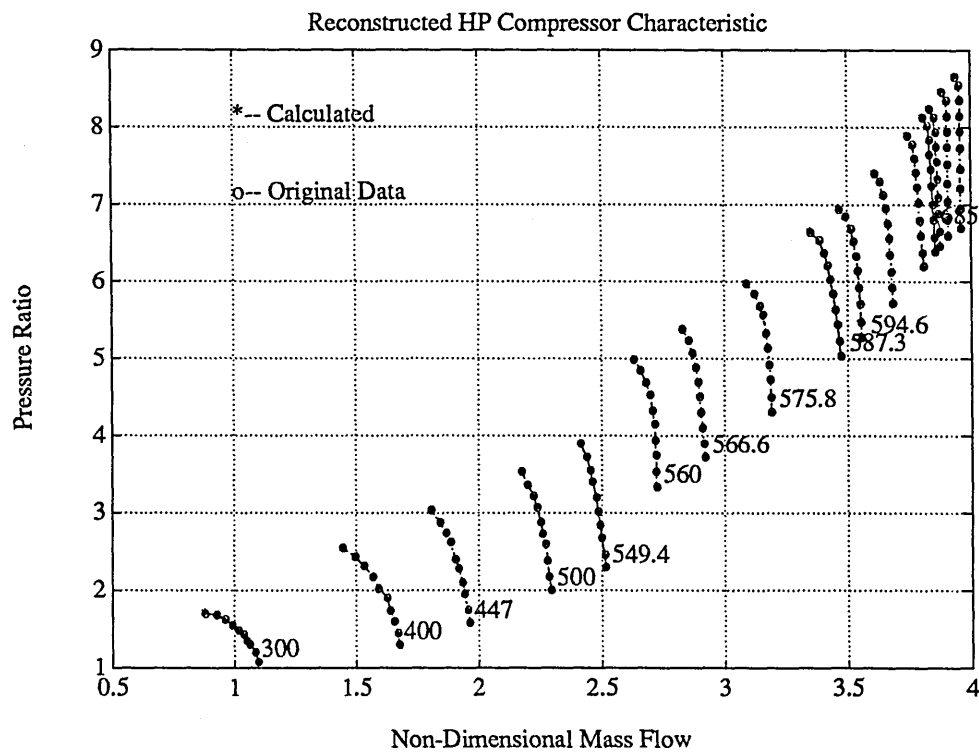


Figure 3.41: Reconstructed HP Comp. Pressure Ratio/Mass Flow Characteristic

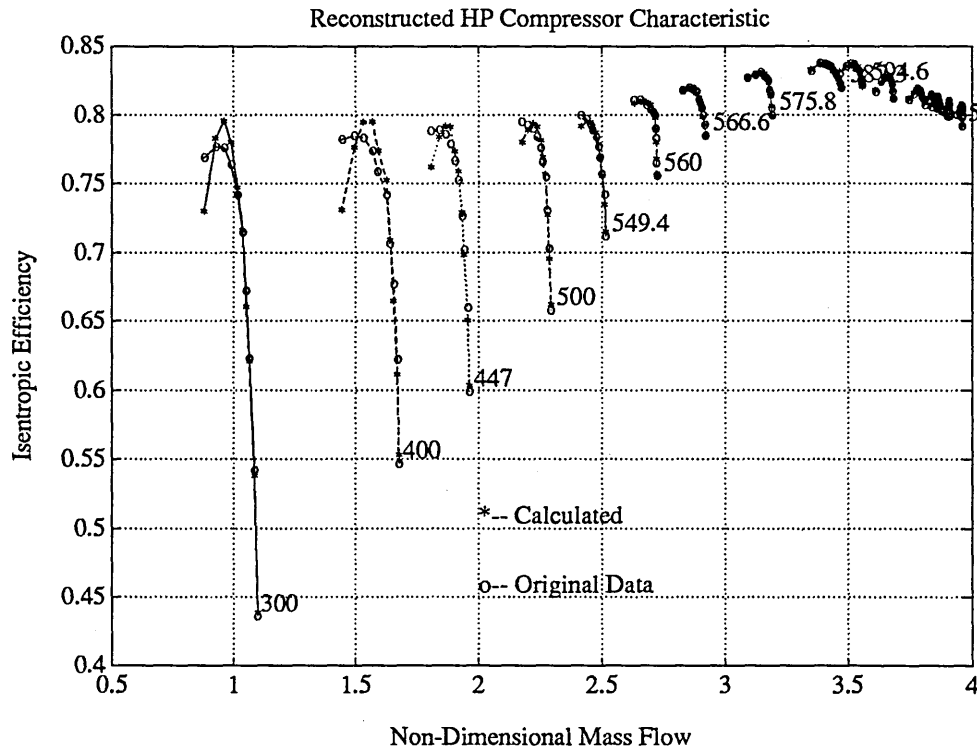


Figure 3.42: Reconstructed HP Comp. Efficiency/Mass Flow Characteristic

$$b_1(2) = 5.5853\bar{n}^2 - 5.2558\bar{n} - 2.2719 \tag{3.51}$$

$$b_1(3) = -12.0834\bar{n}^2 + 25.2889\bar{n} - 11.8921 \tag{3.52}$$

It should be mentioned that in obtaining these models, some difficulties were encountered in deriving an appropriate transformation for the HP compressor pressure ratio/mass flow characteristic due to the variation in the surge line. This is clearly shown in the Figure 3.41. The bleed valve gradually closes in the non-dimensional speed range of 545 to 568, causing discontinuities to occur in the surge line. This gives rise to difficulties for fitting the relationship on the surge line.

Table 3.3 has listed the transformations and the values of the corresponding performance indices. It is seen that IP compressor has the highest performance index which means that the analytical models are more reliable. In the fan representation, although there are relatively small values of error indices, the values for

Details of Models for Compressors in Turbofan Engine						
Function	Fan		IP Compressor		HP Compressor	
	$\dot{m}\sqrt{T}/P$	η_{is}	$\dot{m}\sqrt{T}/P$	η_{is}	$\dot{m}\sqrt{T}/P$	η_{is}
New X	x/y	x/y	x/y	x/y	x/y	x/y
New Y	y	zx^2/y^3	y	zx/y^2	y	zx^2/y^3
Mon. index	0.213	0.112	0.331	0.314	0.568	0.455
Error index	0.258	0.213	0.466	0.123	0.286	0.465
Pred. index	0.787	0.886	0.911	0.929	0.941	0.965

Table 3.3: The Performance Index Values From the Compressor Models

the predictability indices are poor. This may be due to the way that the characteristics have been used to represent the whole fan, which have large variation in the non-dimensional mass flow. This, from another point of view, suggests that it is more reasonable to have separate representations for the “inner” and “outer” fans. The analytical representation for the HP compressor is acceptable and the resultant indices show that the model has the good predictability number which means that the transient path on the characteristic is trustworthy. However the monotonic indices values are relatively large, which indicates that the parameter variations are less monotonic. The reasons for this have been given as above.

3.10 Turbines Modelling

The modelling objective here is to transform the given turbine characteristics into a form from which a simple relationship between the transformed variables can be derived.

3.10.1 Turbine in the Single-Spool Engine

Turbine non-dimensional mass flow and isentropic efficiency are given as functions of pressure ratio and non-dimensional speed as:

$$\frac{\dot{m}_t\sqrt{T_{in}}}{P_{in}} = f_{TM}\left(\frac{N}{\sqrt{T_{in}}}, \frac{P_{out}}{P_{in}}\right) \quad (3.53)$$

$$\eta_{is} = f_{TE}\left(\frac{N}{\sqrt{T_{in}}}, \frac{P_{out}}{P_{in}}\right) \quad (3.54)$$

Here the index *in* and *out* represent the variables at the inlet and exit of the turbine. The turbine characteristics used in the single-spool model are shown in Figure 3.45 and 3.46.

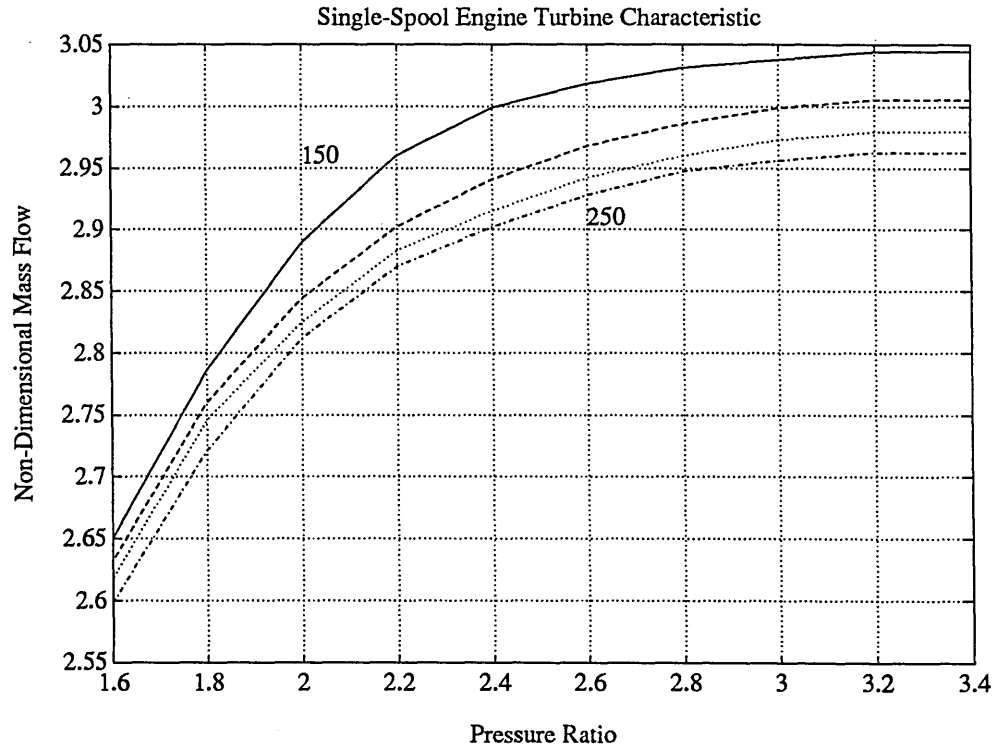


Figure 3.43: Turbine Mass Flow Characteristic in the Single-Spool Engine

Examination of the turbine characteristics in Figure 3.45 and 3.46 suggests that the well known nozzle flow parameter :

$$\frac{\dot{m}\sqrt{T}}{P} = K_N f_N \left(\frac{P_{out}}{P_{in}} \right) \quad (3.55)$$

could be used to correlate the characteristic as a function of a single variable.

Since a turbine consists of alternating stator blades or nozzles and rotating blades, expansion occurs in the stators and may also occur in the rotors. Thus, the flow through a turbine stage can be represented by:

$$\frac{\dot{m}_t \sqrt{T_{in}}}{P_{in}} = K_d \left(\frac{P_{out}}{P_{in}} \right)^{1/\gamma} \sqrt{1 - \left(\frac{P_{out}}{P_{in}} \right)^{\gamma-1/\gamma}} \quad (3.56)$$

$$\frac{\dot{m}_t \sqrt{T_{in}}}{P_{in} f_p(P_{out}/P_{in})} = K_d \quad (3.57)$$

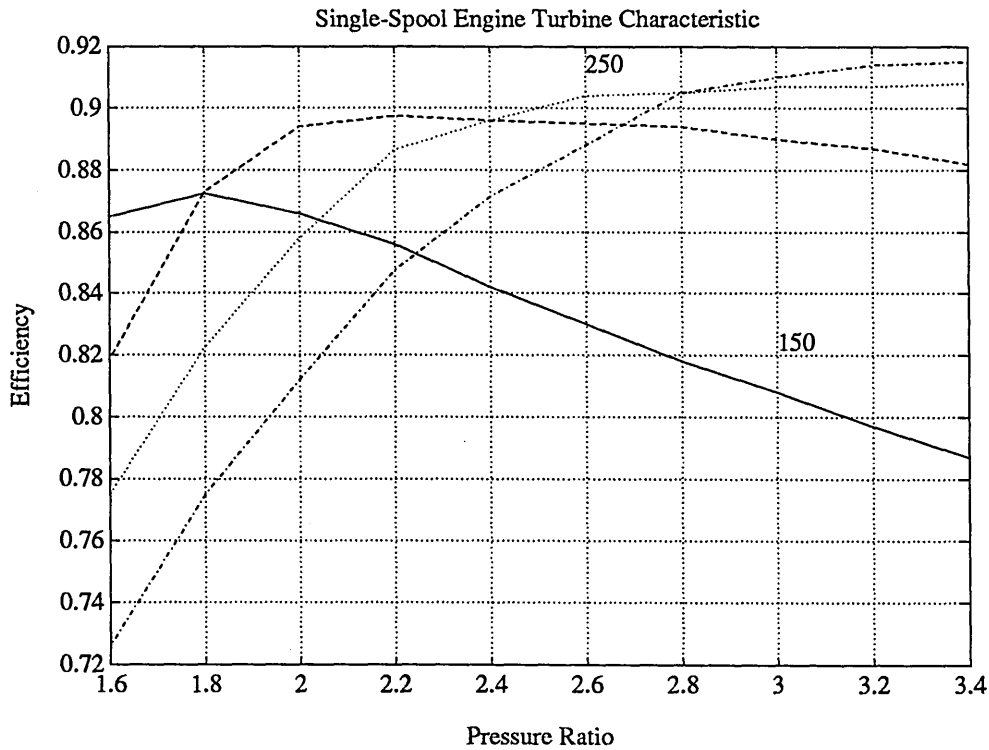


Figure 3.44: Turbine Efficiency Characteristic in the Single-Spool Engine

However, it has been shown experimentally [119] that this flow correlation varies as a function of the speed parameter $N/\sqrt{T_{in}}$. We have, finally, a correlation of the form:

$$\frac{\dot{m}_t \sqrt{T_{in}}}{P_{in} f_p(P_{out}/P_{in})} = f_n\left(\frac{N}{\sqrt{T_{in}}}\right) \quad (3.58)$$

In most of the engine operating regime, the turbine is in the choked condition. The choked non-dimensional mass flow does not significantly vary. However, in the low pressure ratio range, the non-dimensional speeds do effect the function.

3.10.2 Transformed variables

By using the following transformations, the turbine characteristics have been transformed into the form as shown in Figure 3.47 and 3.48.

$$K_{tpr} = \sqrt{1 - \left(\frac{P_{out}}{P_{in}}\right)^{\gamma-1/\gamma}} \quad (3.59)$$

$$X_1 = \frac{\bar{n}}{\sqrt{1 - (P_{out}/P_{in})^{\gamma-1/\gamma}}} \quad (3.60)$$

$$X_2 = \frac{\bar{n}}{(P_{out}/P_{in})^{1/\gamma} \sqrt{1 - (P_{out}/P_{in})^{\gamma-1/\gamma}}} \quad (3.61)$$

$$Y_1 = \frac{x}{\bar{n}} \quad (3.62)$$

$$Y_2 = \frac{z * \sqrt{1 - (P_{out}/P_{in})^{\gamma-1/\gamma}}}{\bar{n}} \quad (3.63)$$

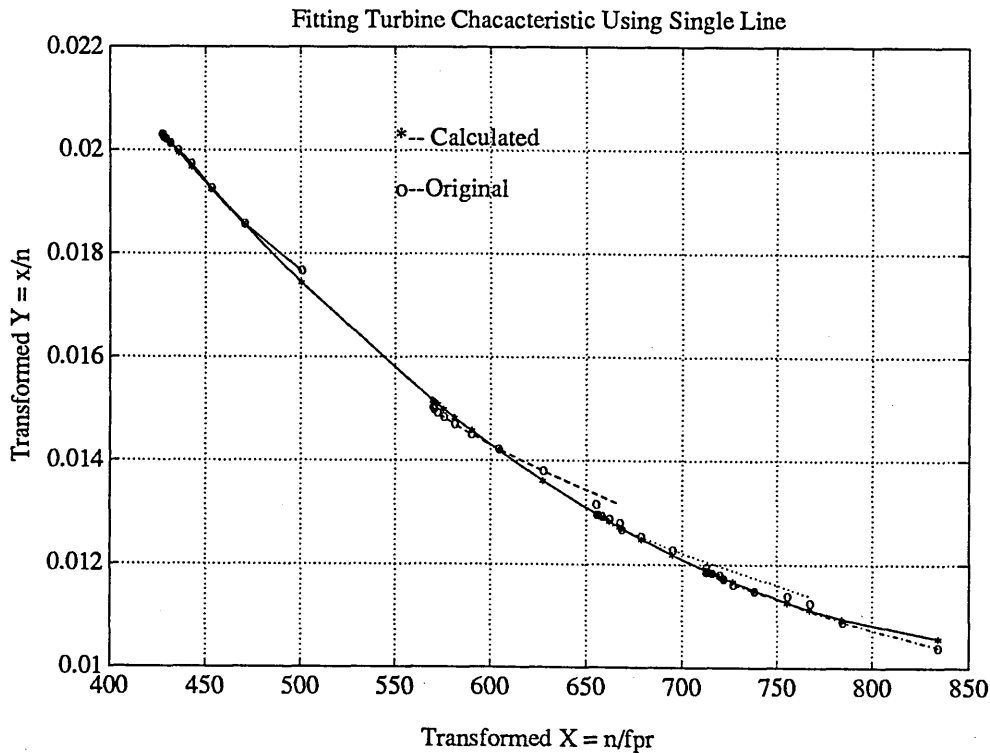


Figure 3.45: Transformed Turbine Mass Flow Characteristic

The relations show that the turbine performance can be expressed as a function of a single parameter. This make it most amenable to simulations.

3.10.3 Turbines in the Turbofan Engine

The modelling of the turbines used in the turbofan engine follows in the same fashion as above. The characteristics for the LP turbine and HP turbine are shown in

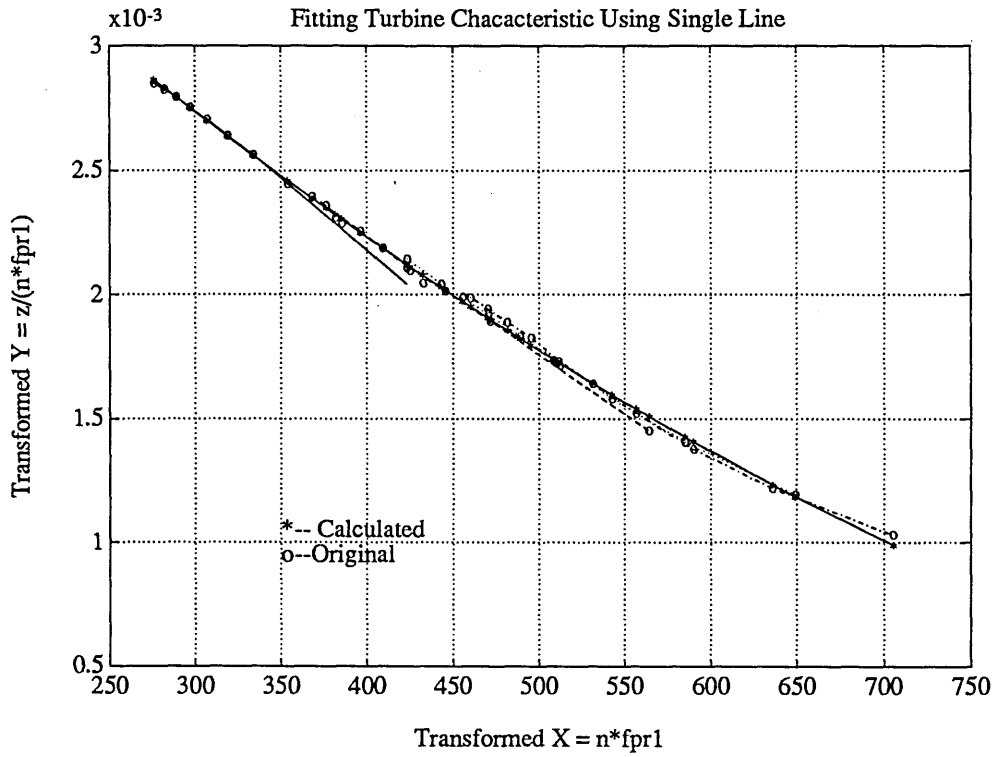


Figure 3.46: Transformed Turbine Efficiency Characteristic

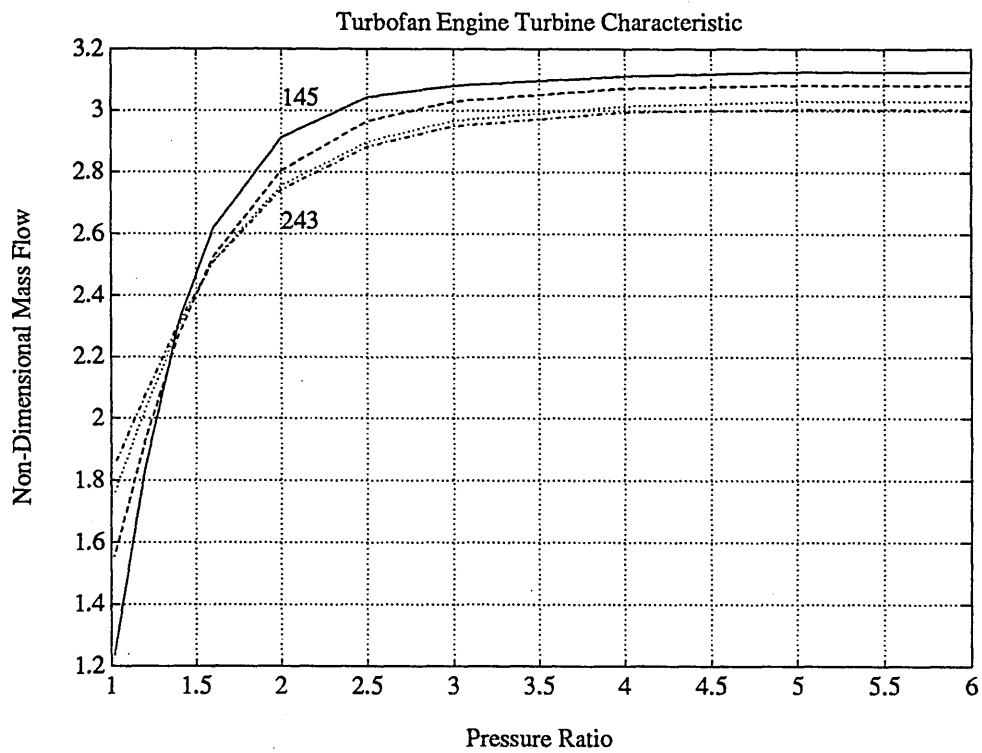


Figure 3.47: LP Turbine Mass Flow Characteristic in the Turbofan Engine

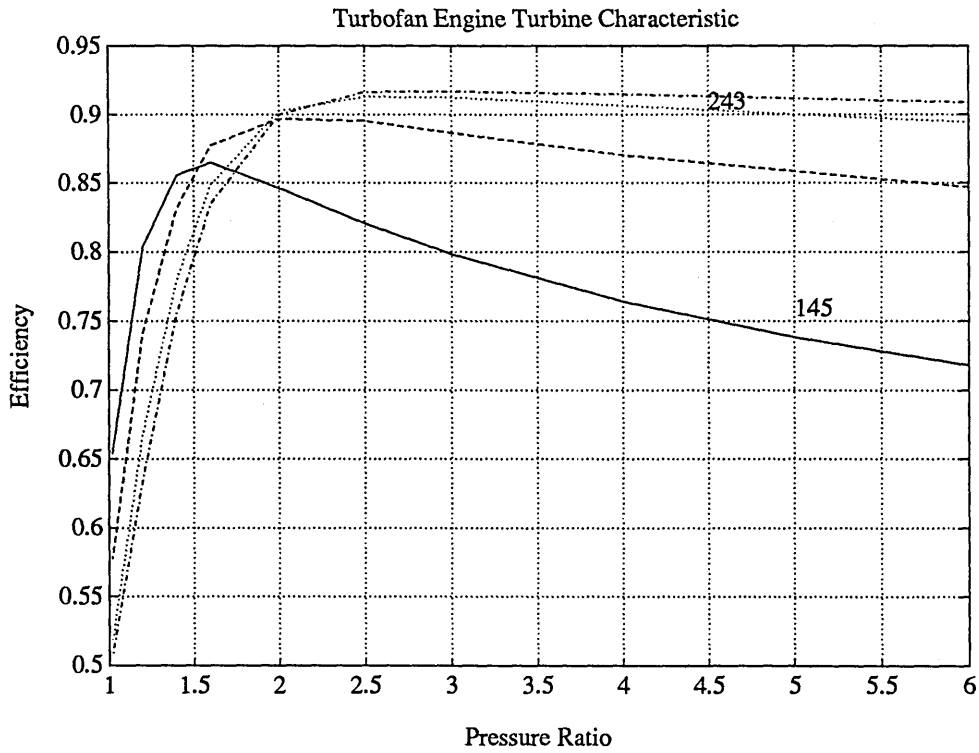


Figure 3.48: LP Turbine Efficiency Characteristic in the Turbopan Engine

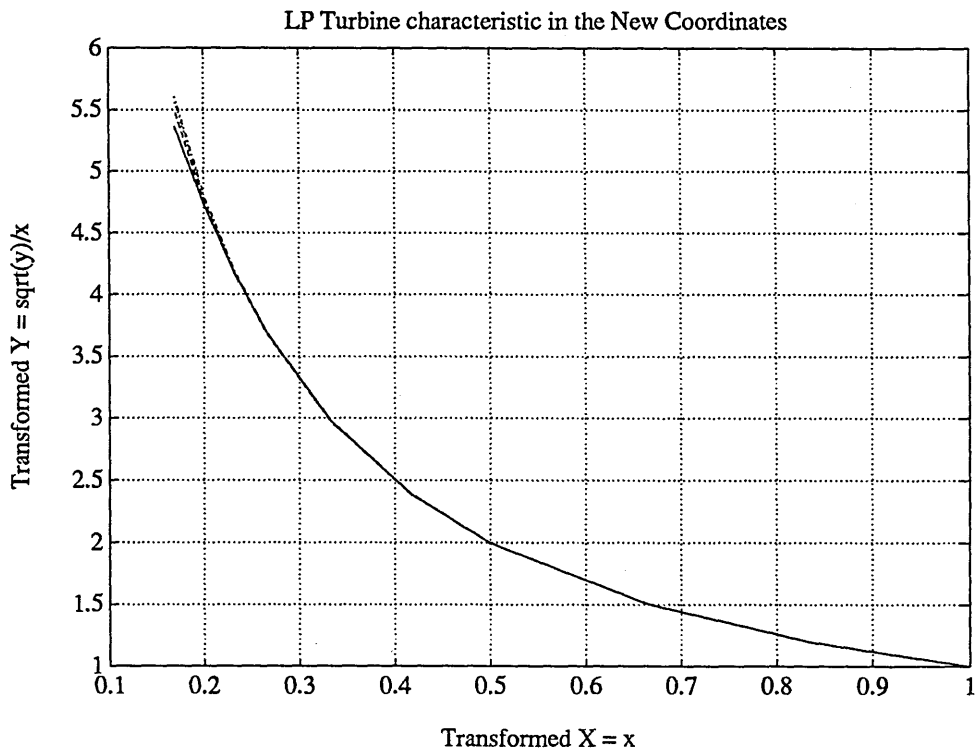


Figure 3.49: HP Turbine Mass Flow Characteristic in the Turbopan Engine

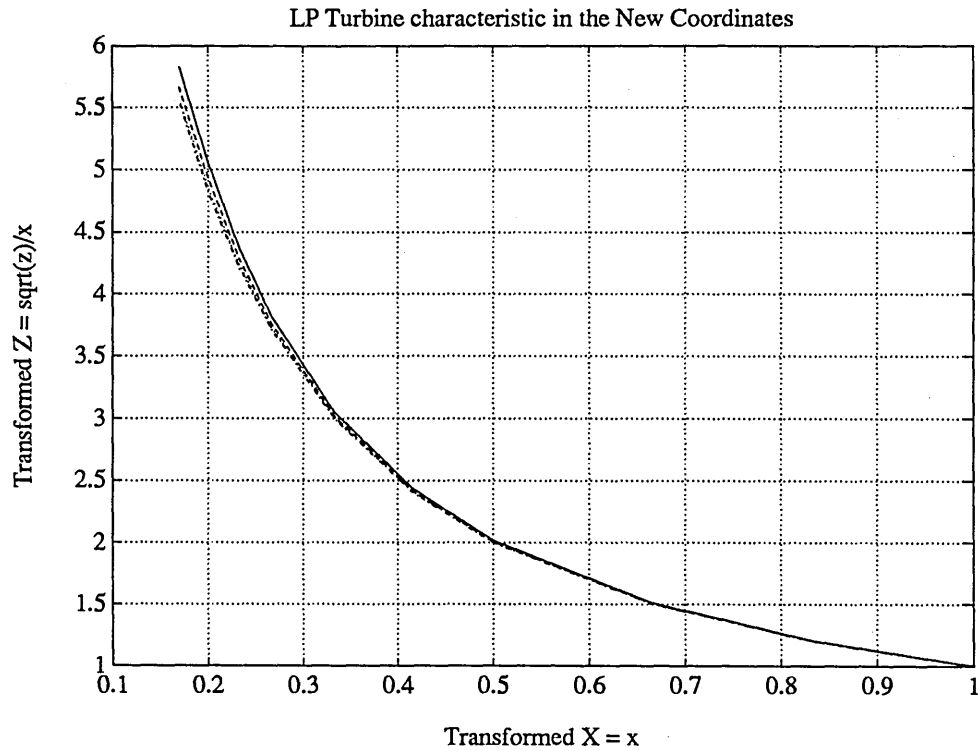


Figure 3.50: HP Turbine Efficiency Characteristic in the Turbofan Engine

Figure 3.49 to Figure 3.52. It is intended to transform these characteristics into the form which gives simple relationships in terms of the new coordinates. This has been achieved by normalising the non-dimensional mass flow, pressure ratio and the isentropic efficiency by the choking values and regrouping the normalised variables. Using x to represent the normalised pressure ratio, y the normalised non-dimensional mass flow and z the normalised isentropic efficiency; the transformations are found to be $X = x$, $Y = \sqrt{y}/x$ and $Z = \sqrt{z}/x$; Figure 3.53, 3.54 and Figure 3.55, 3.56 clearly show that the single relationship exists between Y and X and Z and X .

The equations used to represent the turbines are:

$$Y = a_1 + a_2X + a_3X^2 \tag{3.64}$$

$$Z = b_1 + b_2X + b_3X^2 \tag{3.65}$$

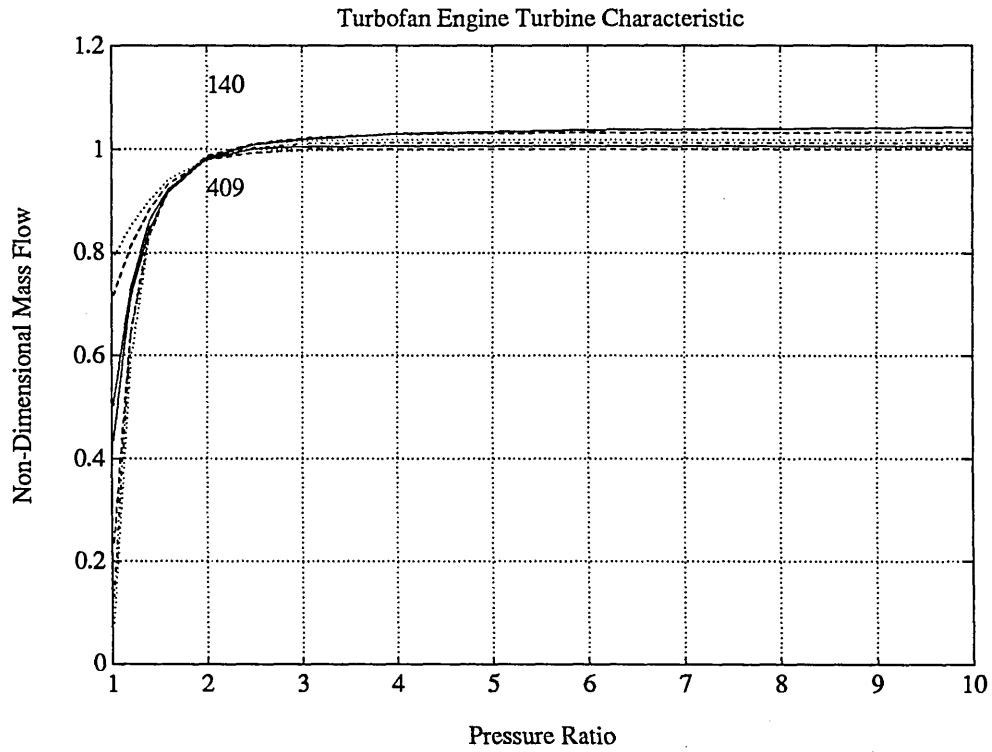


Figure 3.51: Transformed LP Mass Flow Turbine Characteristic

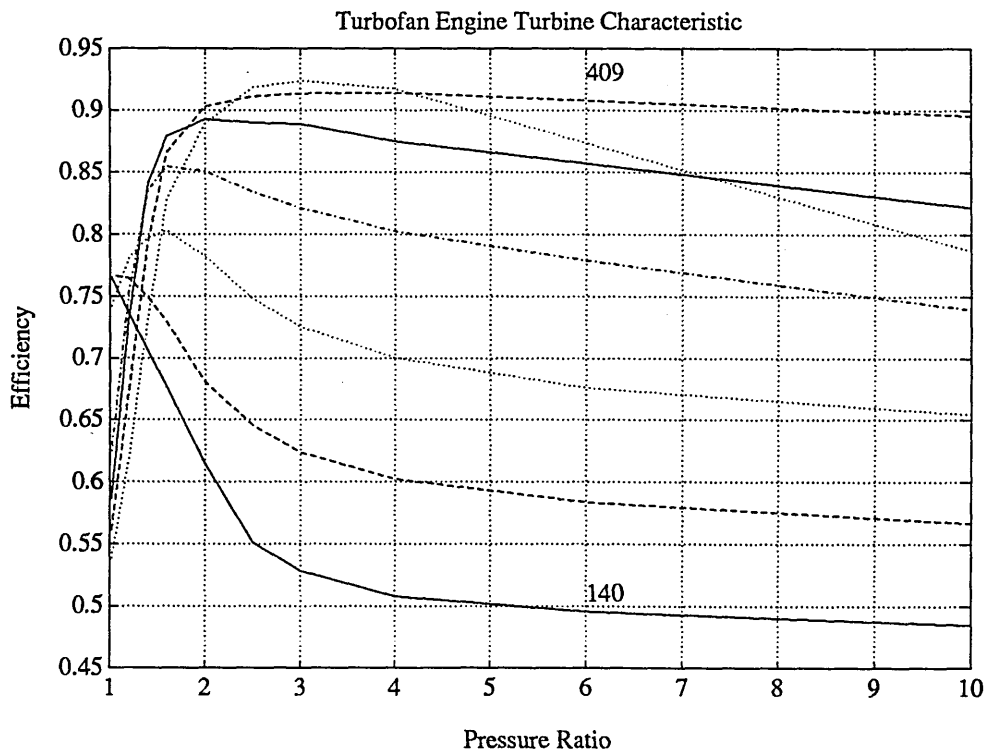


Figure 3.52: Transformed LP Efficiency Turbine Characteristic

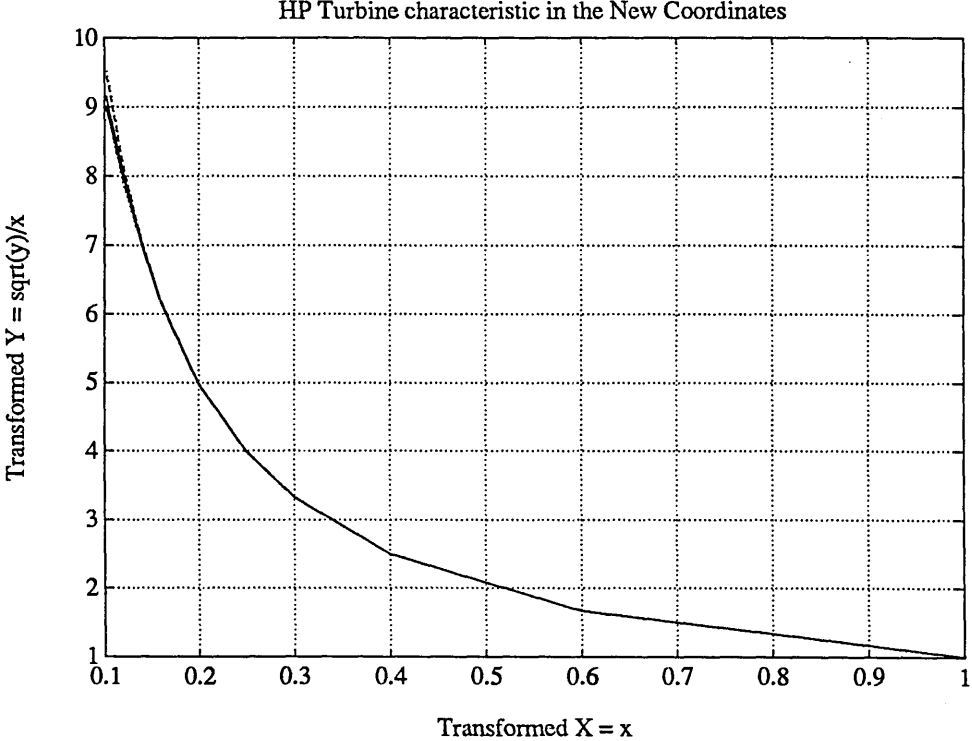


Figure 3.53: Transformed HP Mass Flow Turbine Characteristic

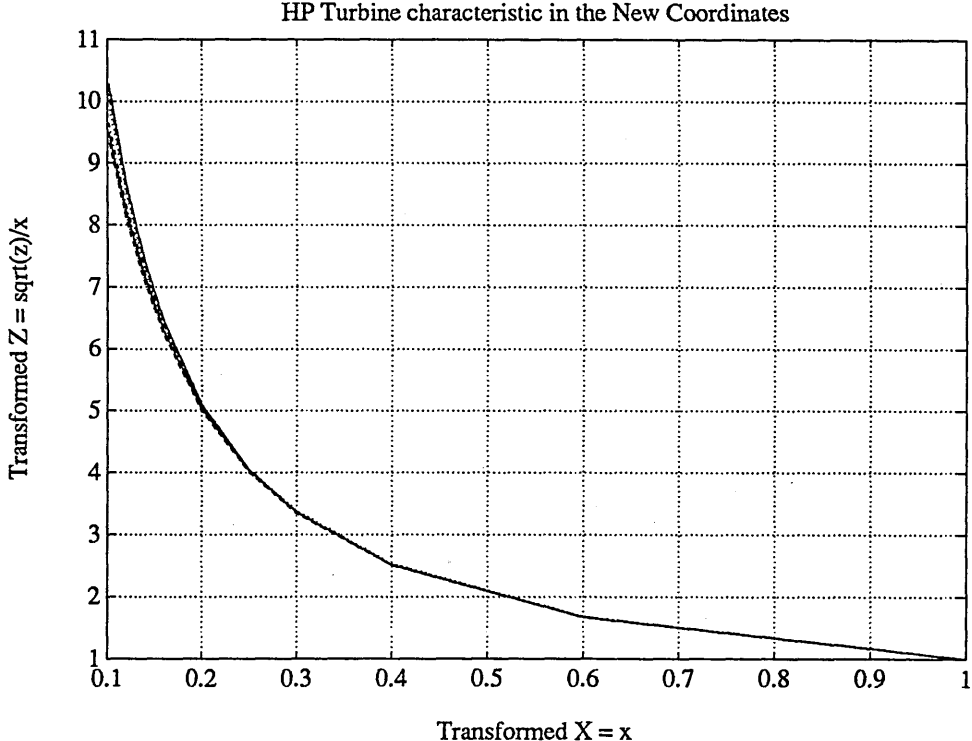


Figure 3.54: Transformed HP Efficiency Turbine Characteristic

The coefficients for these polynomials can be determined as in the case of compressor modelling and the results are shown in Table 3.3.

3.11 Conculsions

The proposed method has been described and applied to model the compressors and the turbines used in formulating the thermodynamic models. It is seen that our objective has been achieved; that is the simple mathematical representations have been obtained. The significance of this is the simulation efficiency will be increased and the model qualities can be evaluated and compared.

Chapter 4

Digital Simulation of Gas Turbine Engines

SUMMARY

The steady-state and transient performance of the gas turbine engines are predicted using the developed thermodynamic models which are validated by comparing the simulation results with these from the well-established model. The simulation results not only provide an insight into the dynamic characteristics of the gas turbine engines, and also demonstrate the difficulties in designing suitable control systems. A set of linear models for control system designs are generated and further validated against the results from the nonlinear simulation.

4.1 Introduction

Gas turbine engines are subjected to the most extensive transient operations during most of in-service time. The engines have frequently to accelerate from idling speed to maximum speed to enable aircrafts to take-off or vice versa to touch down. During transients, thrust response should be as fast as possible, and this must be achieved with complete safety. Therefore, it is very important to be able

to predict thrust response and performance during transients to ensure the engine is operating within the safety limits.

Mathematical modelling and simulation have been playing a very important role in designing gas turbine engines. When these are used as tools, engine dynamic responses can be studied even when an engine is at the design stage. As the result, the thrust response can be guaranteed to the customers. Also by this way, expensive wind-tunnel and flight test program can be minimised, and system problems may be avoided or minimised.

The development of a suitable control system requires a deep understanding about the transient responses. Simulation can provide valuable information as to the usage of compressor surge margin and turbine inlet temperature response during transients. Furthermore, control systems can be tested on simulation before being implemented on real engines.

The purpose of this chapter is to use the simulation technique to establish the validity of the developed models. The steady-state and transient performance of the gas turbine engines are predicted using the developed models. The simulation results for the single-spool engine are validated against the steady-state test data provided by the engine manufacture. For the two-spool engine, the model developed here is validated by comparing the simulation results with these in [100], [120], [99], [121],[122].

In the present work, the thermodynamic models are programmed using Matlab Software on the Sun work station. This provides an integrated environment for the active dynamic simulations and control system designs.

4.2 Performance Requirements of an Engine

American and British civil aviation authorities have required that an engine must be capable of acceleration from a low thrust, typically flight idle, to 95 percent rated take-off thrust in no more than 6 seconds [123]. This requirement on an

engine's thrust response is to guarantee that the engine has good handling quality during a take-off or a baulk landing. It is always desirable for an engine to have fast response rate, especially for V/STOL applications, where thrust response time is more crucial. Good dynamic responses can be achieved by the transient operations at turbine inlet temperatures greater than the design values, and this often results in transient running line close to the surge line on the compressor characteristic [124].

4.3 Limitations to Thrust Response

The thrust or power output from an engine depends, at its most basic level, on airflow through the engine. To obtain a significant and sustained change in thrust, it is necessary to increase airflow through the engine, and hence through the compressor. The most important factor in determining the ability to change thrust quickly is therefore the ability to change airflow quickly. Since airflow depends on the engine speed, therefore the rate of change of thrust is primarily governed by the rate of change of airflow with speed, and the rate of change of speed with time. The former is governed by airflow/speed characteristic of the compressor, and the latter by the spool inertia.

For an engine to start an acceleration, fuel flow and thus turbine inlet temperature have to be increased, providing an increase in turbine torque. This in turn results in an increase in spool speed, and hence airflow through the compressor. However, the shaft speed will not change instantaneously due to the inertia of the spool, and as the result, the rise in turbine inlet temperature must be matched by either a fall in airflow or a rise in compressor pressure ratio. This results in a movement of the transient running line on the compressor characteristic towards surge line along a constant non-dimensional speed line. Thus the surge line limits the ability of the engine to accept a rapid increase in fuel flow, and hence turbine inlet temperature, and thus , limits the increase of torque on the spool and the

rate of change of thrust.

4.4 Interpretation on the Compressor Characteristic

Limits to the acceleration rate are determined by compressor surge and turbine inlet temperature considerations. At low speeds, the permissible over-fuelling will be restricted by surge rather than temperature consideration. As the rotor time constant is relatively higher at the low speeds, it is important to utilise the maximum permissible fuel flow to get a reasonable initial acceleration rate [125]. At the higher speeds, the maximum allowable temperature will be reached before surge is encountered and the fuel flow will be limited by the temperature consideration. A hypothetical optimum trajectory on the compressor characteristic is shown in Figure 4.1. The point 1 on the surge line determines the initial maximum fuel flow

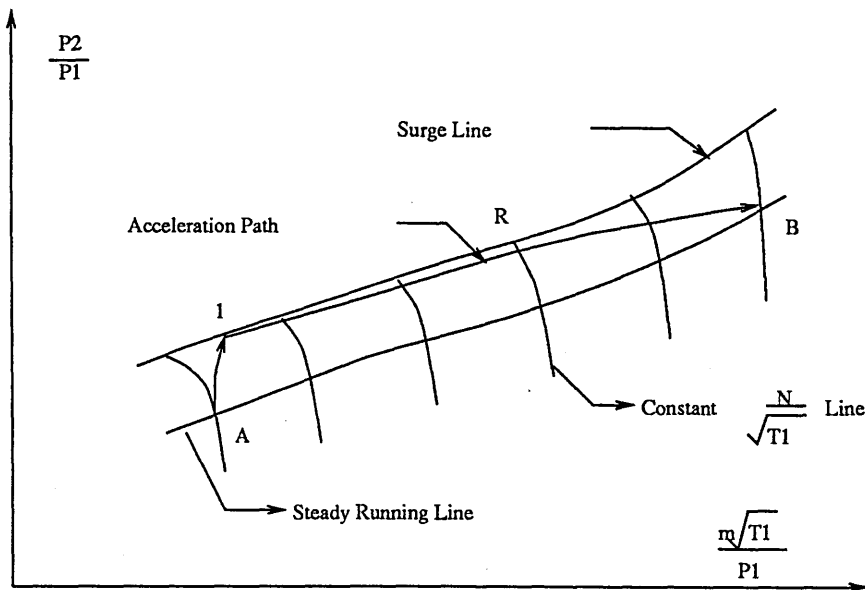


Figure 4.1: A Hypothetical Transient Trajectory

that can be added to the engine, and point R is to avoid the maximum turbine inlet temperature being exceeded. This clearly shows that some allowance would have to be made in practice to allow for possible deterioration of the surge line

due to intake flow distortion or deficiencies of the compressor. The actual trajectory followed on the compressor characteristic are determined by the acceleration schedule.

4.5 Acceleration Fuel Schedule

When using an open-loop fuel schedule to control transient operations, it has been a common practice to meter fuel flow to the engine as a function of compressor pressure ratio or non-dimensional shaft speed [126]. When the inlet conditions of pressure and temperature are altered, the fuel flow to accelerate or decelerate must be altered in order to follow the same transient trajectory on the compressor characteristics. This can be achieved by scheduling a non-dimensional fuel flow group as a function of compressor pressure ratio[6]. Such a group could be $\dot{m}_f/(P_1\sqrt{T_1})$.

Using such a group however will involve the measurement of inlet temperature which is generally slow in response compared with the measurements of speed and pressure. An alternative non-dimensional parameter could be obtained by dividing the above group by non-dimensional speed $N/\sqrt{T_1}$, which gives:

$$\frac{\dot{m}_f}{P_1\sqrt{T_1}} / \frac{N}{\sqrt{T_1}} = \frac{\dot{m}_f}{P_1N} \quad (4.1)$$

Using the fuel group of this form, only shaft speed and inlet pressure need to be measured. The fuel schedules are usually designed based on steady-state information [127].

4.5.1 Scheduling as a Function of Pressure Ratio

When the compressor pressure ratio is used as the scheduling variable, the open-loop fuel controller can be expressed as:

$$\frac{\dot{m}_f}{P_1N} = K_s f_{pr} \left(\frac{P_{out}}{P_{in}} \right) \quad (4.2)$$

The controller of this form is designed to guarantee the stable operation of the compressor at all flight conditions. In the two-spool engines, the HP compressor is more prone to surge during an acceleration than the LP compressor. Therefore, the parameters of HP compressor should be used to schedule fuel flow during transients. A typical non-dimensional fuel schedule as a function of pressure ratio is shown in Figure 4.2. It is shown that if it is desired to accelerate the engine

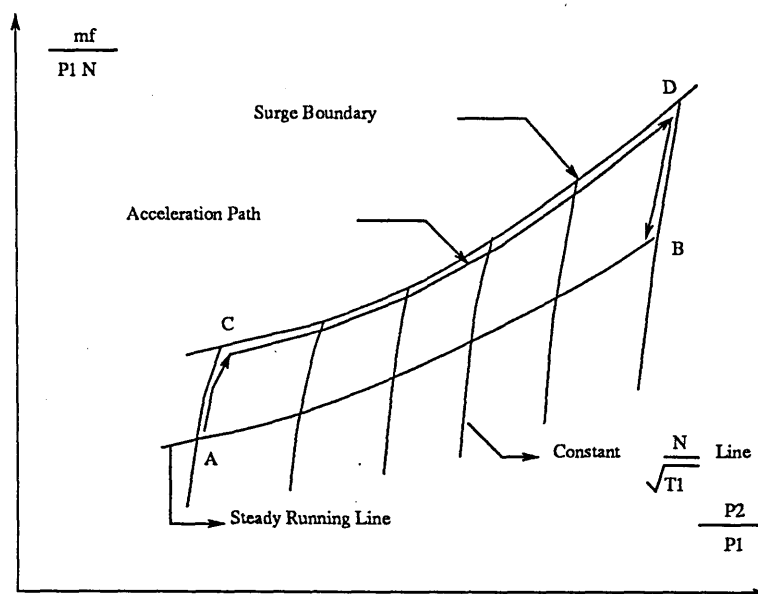


Figure 4.2: Typical Fuel Flow Characteristic

from the low power at the point A to high power setting B, the fuel flow must be increased. However the fuel flow must be limited to the value at point C, otherwise the engine will surge and acceleration becomes impossible. As the engine begin to accelerate, progressively more fuel flow can be admitted so that path of \dot{m}_f/P_1N follows just below the surge line until it reach point D. The fuel flow can then be reduced to the value corresponding to point B, and the engine will run steadily at this condition. Clearly, in order to avoid surge during accelerations, a system is required which controls the normalised fuel flow \dot{m}_f/P_1N or $\dot{m}_f/P_1\sqrt{T_1}$ according to one of the normalised compressor parameters.

Equivalently, fuel flow can be scheduled as a function of non-dimensional shaft

speed and resultant equation is:

$$\frac{\dot{m}_f}{P_1\sqrt{T_1}} = K_s f_N\left(\frac{N}{\sqrt{T_1}}\right) \quad (4.3)$$

4.5.2 Determination of K_s

It is seen from Equation 4.2 and 4.3 that coefficient K_s has to be determined for the schedule to be used in transients. Design using optimisation techniques has been carried out to determine this coefficient. The performance constraints are formulated based on the consideration of engine safety during transients, and the coefficient is determined by minimising the cost function, J , where J is given by:

$$J = q_1 \int (S_{mag} - 0.97)^2 dt + q_2 \int (T_{tub} - 1.2)^2 dt + q_3 \int (N - 1.0)^2 dt \quad (4.4)$$

$$+ q_4 \int \text{Max}[0, (S_{mag} - 0.97), (T_{tub} - 1.2), (N - 1.0)] dt$$

where $q_i, i = 1, 4$ are the weights, S_{mag} represent the compressor surge margin, T_{tub} the turbine inlet temperature and N the shaft speed.

4.6 Definition of Surge Margin and Turbine Inlet Temperature Limit

The compressor surge margin is a very important indication of compressor operation. Conceptually, it is defined based on the separation of the surge line from the transient running line. In the present work, two alternative definitions are adopted for the single-spool engine and two-spool engine.

For the single-spool engine:

$$S_{mag} = \frac{PR_{sg} - PR_{tr}}{PR_{sg} - PR_{ss}} \quad (4.5)$$

For the two-spool engine:

$$S_{mag} = 1.0 - \frac{PR_{tr}}{PR_{sg}} \quad (4.6)$$

where PR_{sg} , PR_{tr} and PR_{ss} are the surge pressure ratio, transient pressure ratio and steady-state pressure ratio at the constant non-dimensional speed line. It should be noted that both definitions have some inherent deficiency. The first definition is not applicable to the case when the compressor characteristics have flat shapes. While the second can only be considered as an indication of surge, but it is computing efficient.

The maximum turbine inlet temperature, T_{max} , is defined based on its design value, T_{deg} , which is given by:

$$\frac{T_{max}}{T_{deg}} \leq 1.2 \quad (4.7)$$

This specifies the maximum value of turbine inlet temperature allowed during any transient operation.

4.7 Computation Procedure of Simulation

The computation procedure of the simulations is based on the intercomponent volume method [128]. Some details are described in the following.

The first requirement for digital simulation of a gas turbine engine is the selection of the states and their initial conditions that together with the externally applied conditions of P_{amb} , T_{amb} , flight Mach number and fuel flow, will enable the operating point for each component to be found with one pass through the engine calculation. A gas turbine engine operating at a steady-state condition is defined by the state vector x_0 and control input u_0 , where x_0 includes the various pressures and temperatures and u_0 indicates the fuel flow and variable geometry. If the given x_0 , and the given external flight conditions correspond to a steady state operating point, then the condition of flow compatibility and work compatibility will be satisfied. That is, there will be no accumulation of mass at any point in the engine and no net torque on any shaft. Values of x_0 may also exist which correspond to flow compatibility being satisfied, but not work compatibility. For a general value of x_0 , however, neither flow nor work compatibility will be satisfied.

There will be work imbalance, which represents a rate of accumulation of mass at some point in the engine gas path. This will enable the eventual steady-running conditions to be determined.

If a change in fuel flow is made and the engine calculation performed still using x_0 , then there will be a flow and work mismatch. Engine operating states that have flow incompatibility are taken to be possible engine states during transient operation. The work mismatch is used to calculate the rotor acceleration rate and flow mismatch is used to obtain the rate of change of pressure at the various stations in the engine, therefore, the differential equation describing the engine dynamics behaviours can be solved:

$$\dot{x} = f(x, A_j, \dot{m}_f, \alpha) \quad (4.8)$$

where α represent flight condition.

4.7.1 Numerical Integration

In the present work, the integration method known as trapezoidal rule has been used. The state variables are calculated using iteration scheme:

$$x_{i+1} = x_i + \frac{1}{2}(f_i + f_{i+1})\Delta t \quad \text{where } f = dx/dt \quad (4.9)$$

Index i marks the iteration stage.

The application of the trapezoidal rule for solving nonlinear equations of the gas turbine engines demands a sufficiently small time interval Δt in order to avoid numerical instability as well guaranteeing a satisfactory accuracy.

4.8 Single-Spool Turbojet Engine

In this section, the predicted steady-state and transient performance of the single-spool engine are discussed.

4.8.1 Steady-State Operation

Before investigating the dynamic behaviour of the engine, it is necessary to compare the steady-state performance predicted by the simulation with that of the real engine. This is to ensure that the simulation is proceeding correctly and that the component characteristics used in the model are representative of the components in the engine. To obtain a steady-state engine operating point, an initial engine state vector x is fed to the simulation, together with values for the fuel flow, nozzle area and flight conditions. A “transient” is then carried out at constant fuel flow and nozzle area, and the engine state vector will adjust itself until it reaches the correct value for the given fuel flow and nozzle area. This “transient” has in general no physical significance, as it starts from an unrealistic value for the state vector. Once an equilibrium engine operating point has been reached the desired transient can be initiated.

The comparison between the simulation and the engine for steady-state operation is shown in Figure 4.3, which plots the predicted result and the test data (from engine manufacturer) on the compressor characteristic. It can be seen that there is good agreement right down to the low speed range. In the present work, the steady-state operating conditions are obtained by setting $dx/dt = 0$, and solving the set of nonlinear equations for x .

In Figure 4.4 and 4.5, the relationship between the shaft speed/thrust and engine pressure ratio/thrust are plotted.

4.8.2 Transients At Sea Level, Mach Number 0.2

In this section, results of the adiabatic acceleration and deceleration simulation at sea-level, Mach number 0.2 are presented. The solid line is for acceleration and dashed line for deceleration. The idling speed for the engine is 4027 *rpm* and take-off speed is 8194 *rpm*. The take-off thrust is 53875 *N*. The non-dimensional fuel schedule is shown in Figure 4.6.

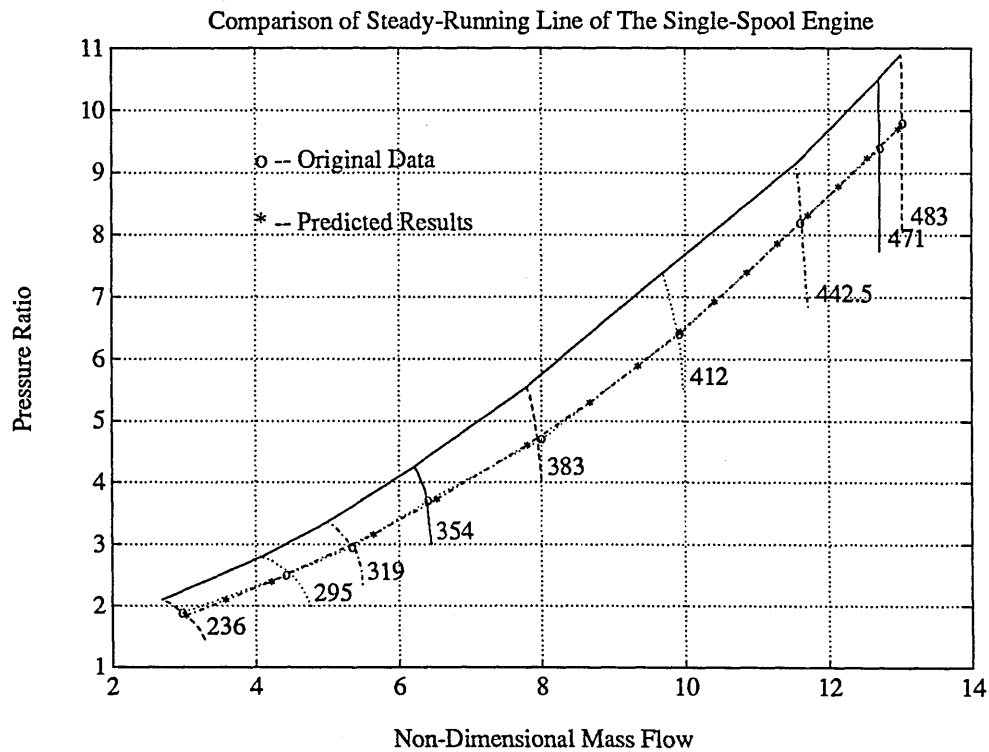


Figure 4.3: Comparison of Steady-State Operating Points

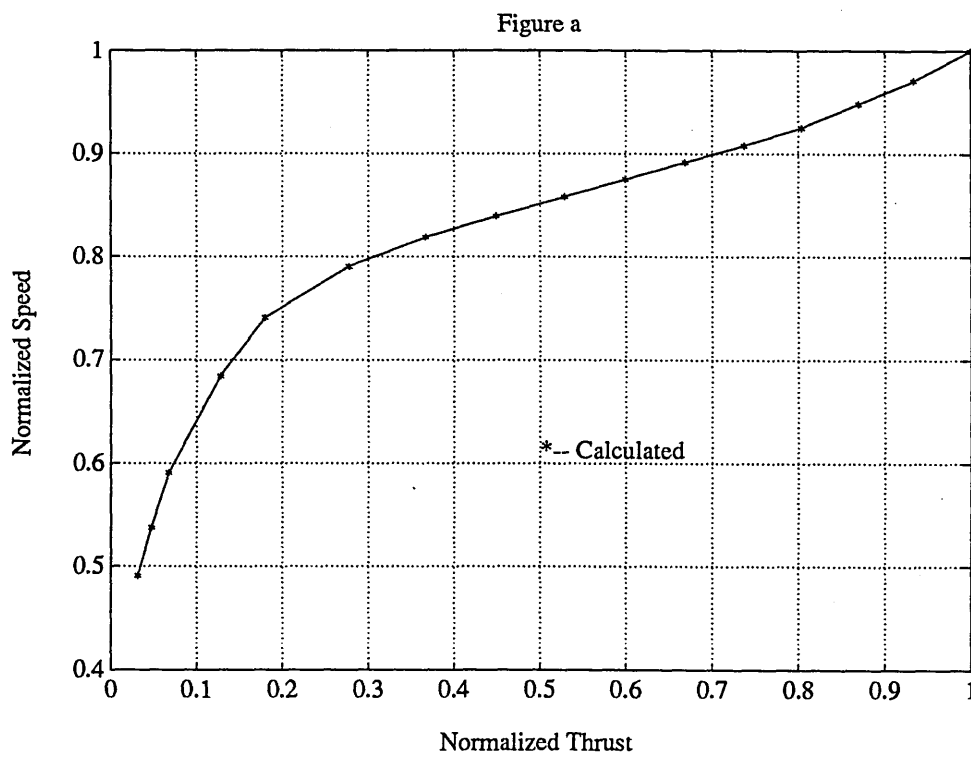


Figure 4.4: Relation Between Thrust and Speed

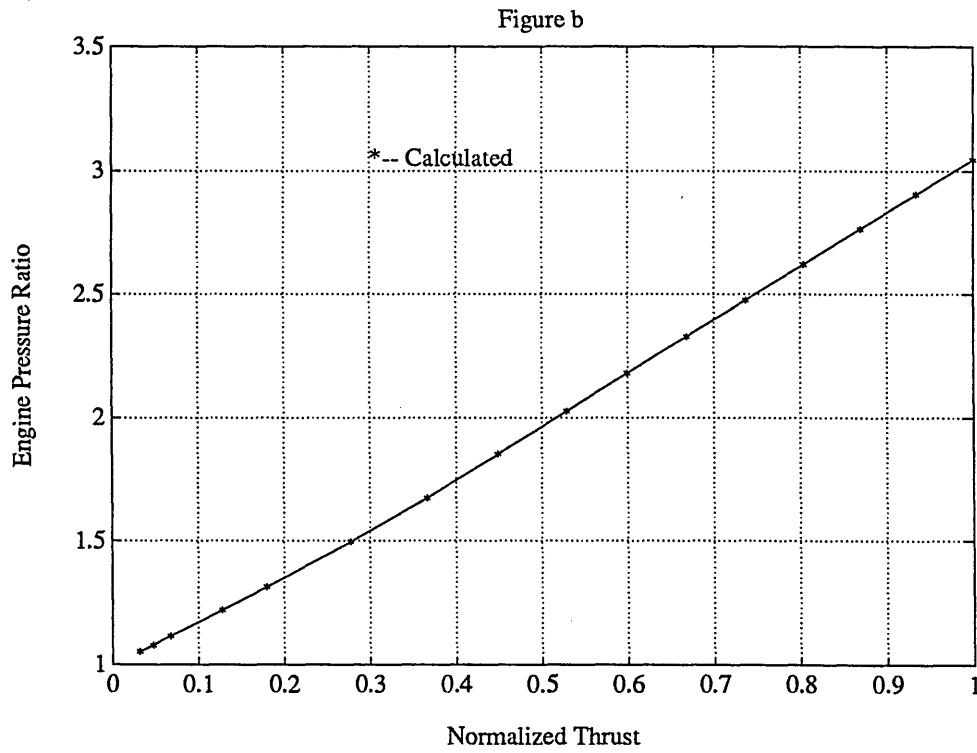


Figure 4.5: Relation Between Thrust and Engine Pressure Ratio

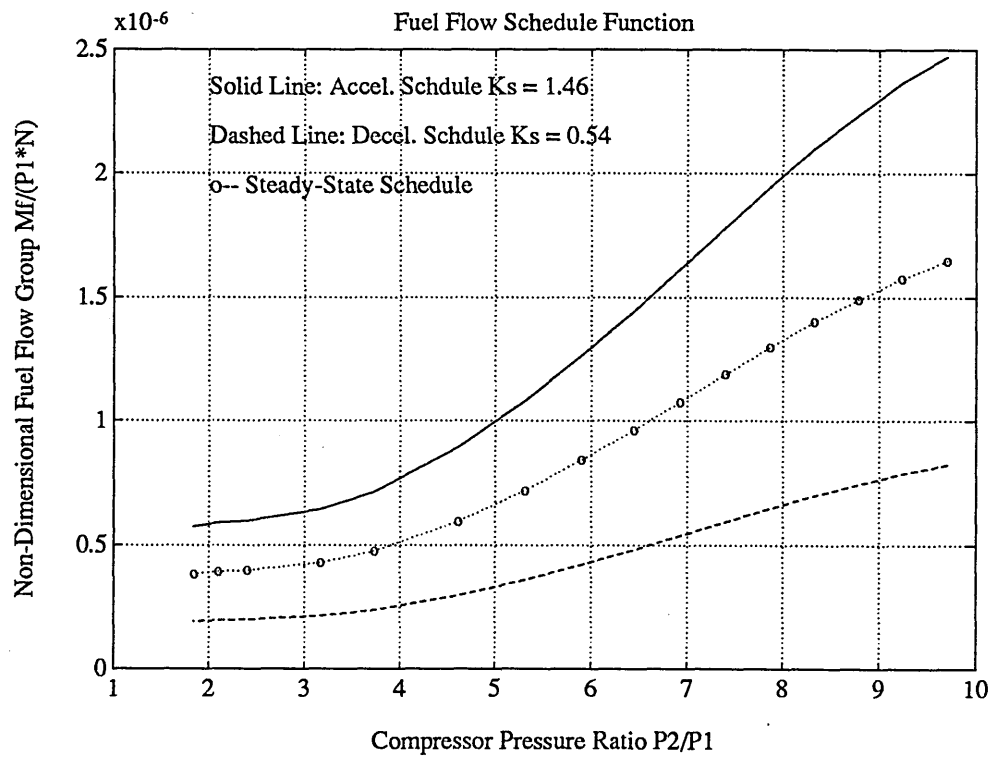


Figure 4.6: Non-dimensional Fuel Schedule

In the Figure 4.7, the variations of input fuel flow and thrust responses are shown.

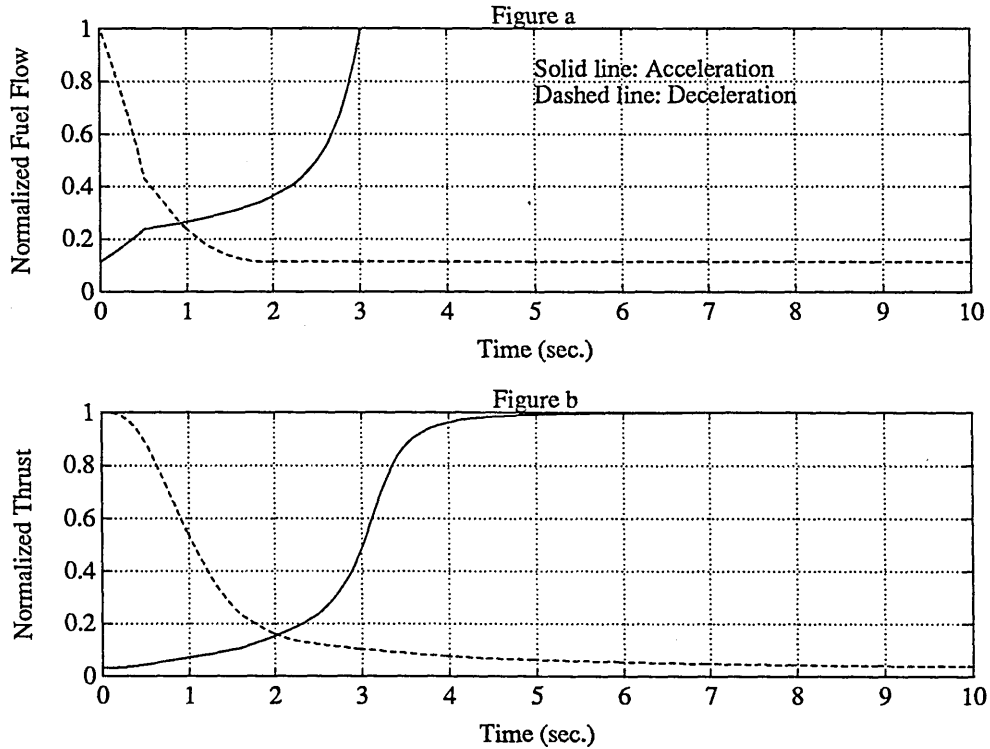


Figure 4.7: Input Fuel Flow and Thrust Response

As shown in Figure 4.7a fuel flow has been increased on a ramp for 0.5 seconds until it reaches the schedule line after which there is a gradual change until it reaches the maximum value. In Figure 4.7b, engine thrust responds fairly slowly in the first 2.5 seconds of the acceleration and then rises rapidly for another 2 seconds until maximum thrust is reached. In the Figure 4.8, the state responses are plotted, all the states are stabilised at about 5 seconds. In Figure 4.8b, it is clear that the normalised turbine inlet temperature is well below the maximum value allowed, which has the value of 1.2 for this engine. The trajectories on the compressor characteristic are shown in Figure 4.9. It is shown that these trajectories are acceptable. The surge margin is plotted in Figure 4.10, which shows that maximum 78% of the surge margin has been used in the first two seconds of acceleration, as the result, the fast thrust response is achieved.

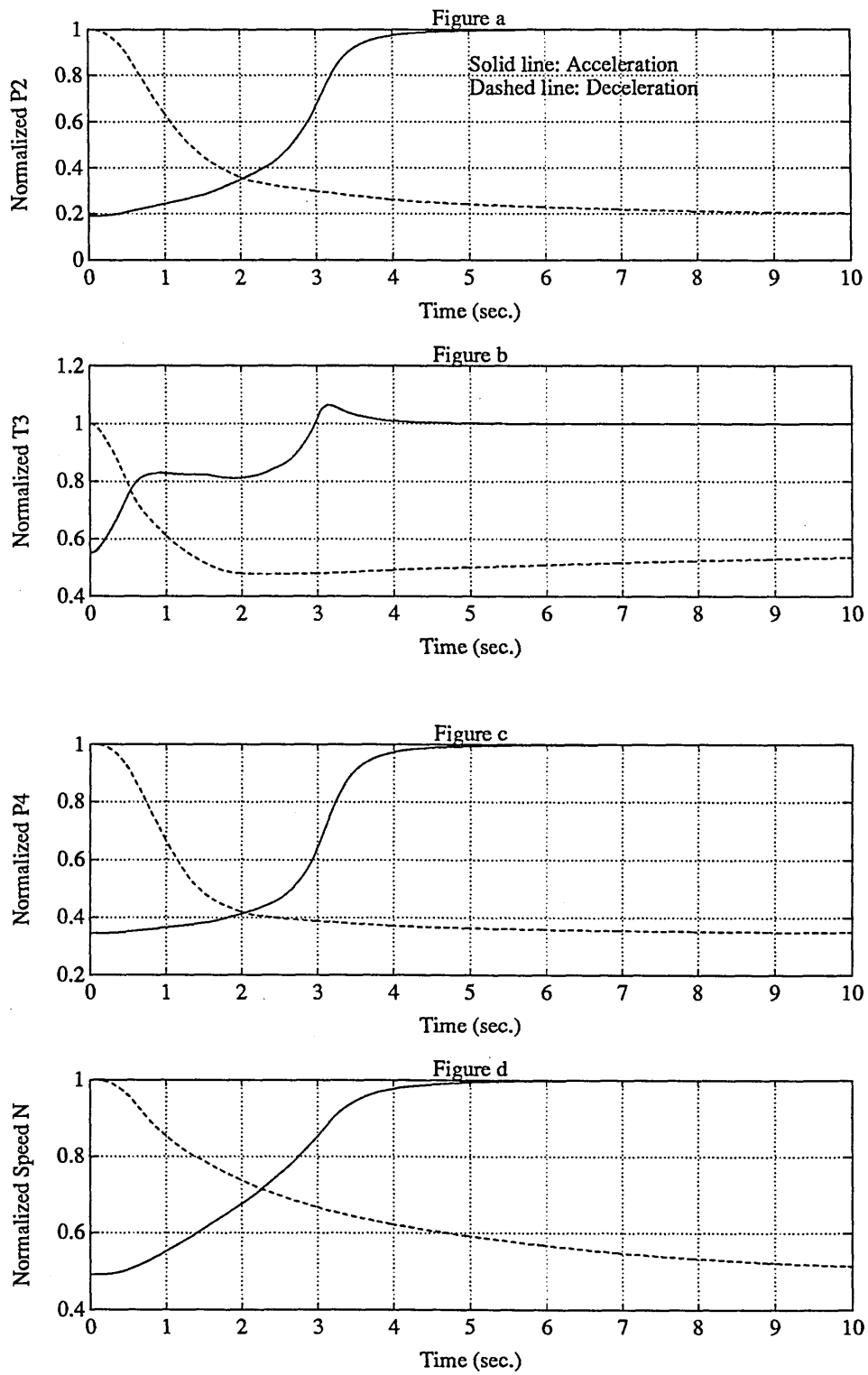


Figure 4.8: Responses of Engine States

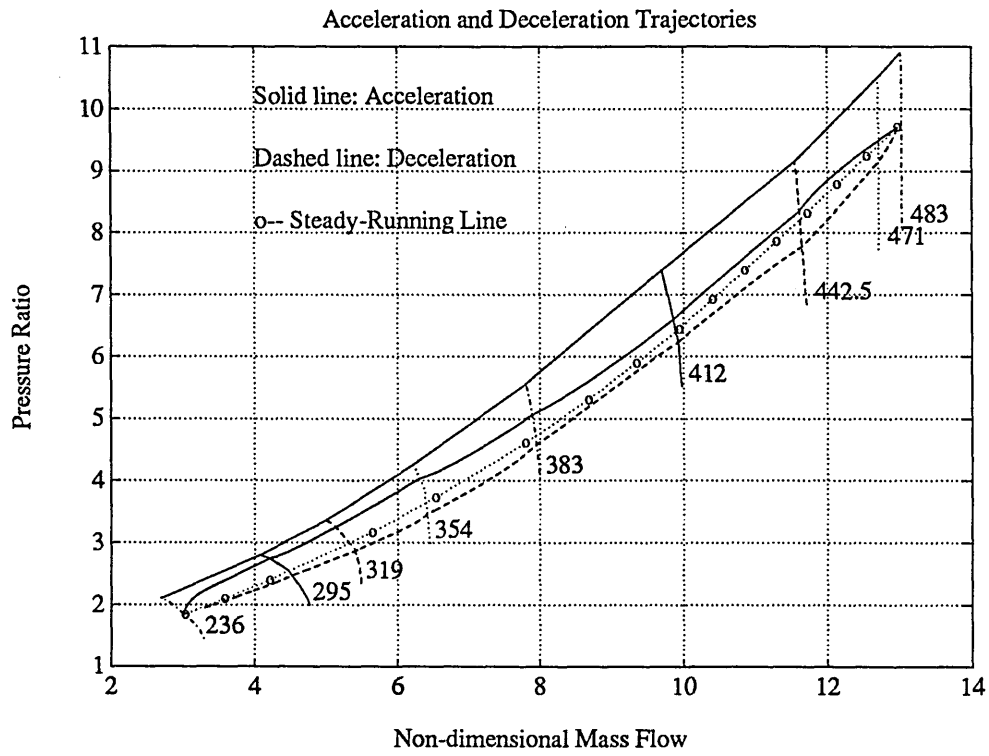


Figure 4.9: Acceleration and Deceleration Trajectories

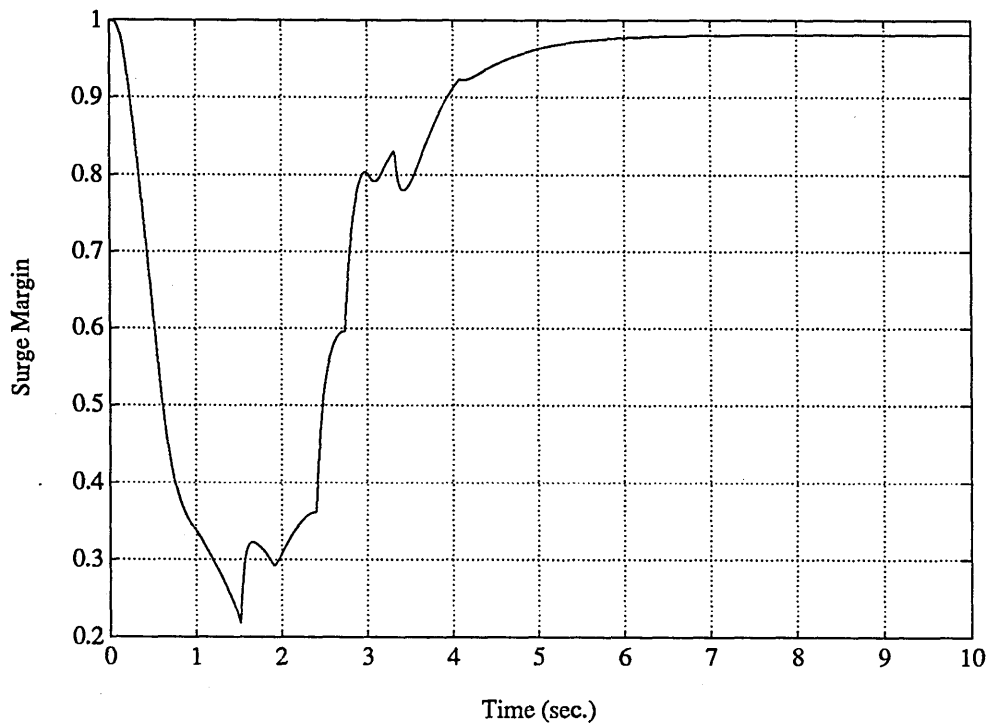


Figure 4.10: Variation of Compressor Surge Margin in Acceleration

4.8.3 Transients At 10,000 m, Mach Number 0.8

The transient performance of this engine at the 10,000 m altitude, Mach number 0.8 is also studied. Starting speed is 5012 rpm and the maximum speed is 7586 rpm. The maximum thrust is 17406 N. The minimum and maximum fuel flow are 0.04kg/s and 0.5kg/s respectively. The results are shown through Figure 4.11 to 4.14.

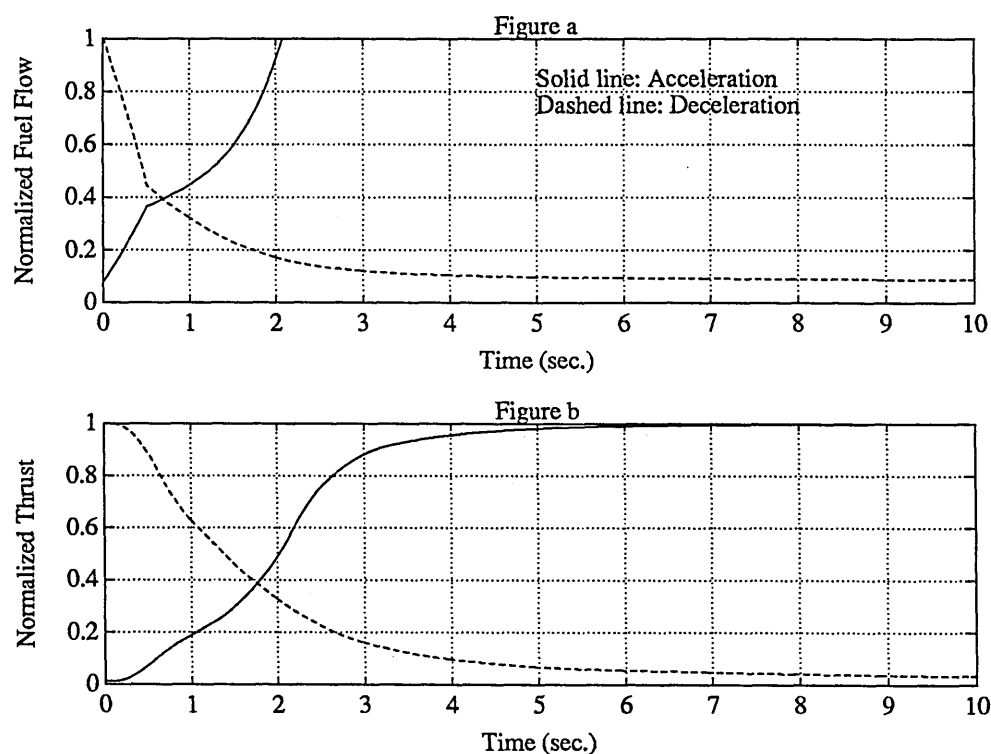


Figure 4.11: Input Fuel Flow and Thrust Response

By comparing the results in Figure 4.8 with these in Figure 4.12, it is obvious that at the altitude, the engine has the relative slower response than at the sea level condition, this is especially the case when the engine begins to stabilise towards the steady-state.

4.8.4 Using Alternative Schedules

Here it is intended to investigate the performance when using non-dimensional speed as the scheduling variable. The results are compared with those obtained

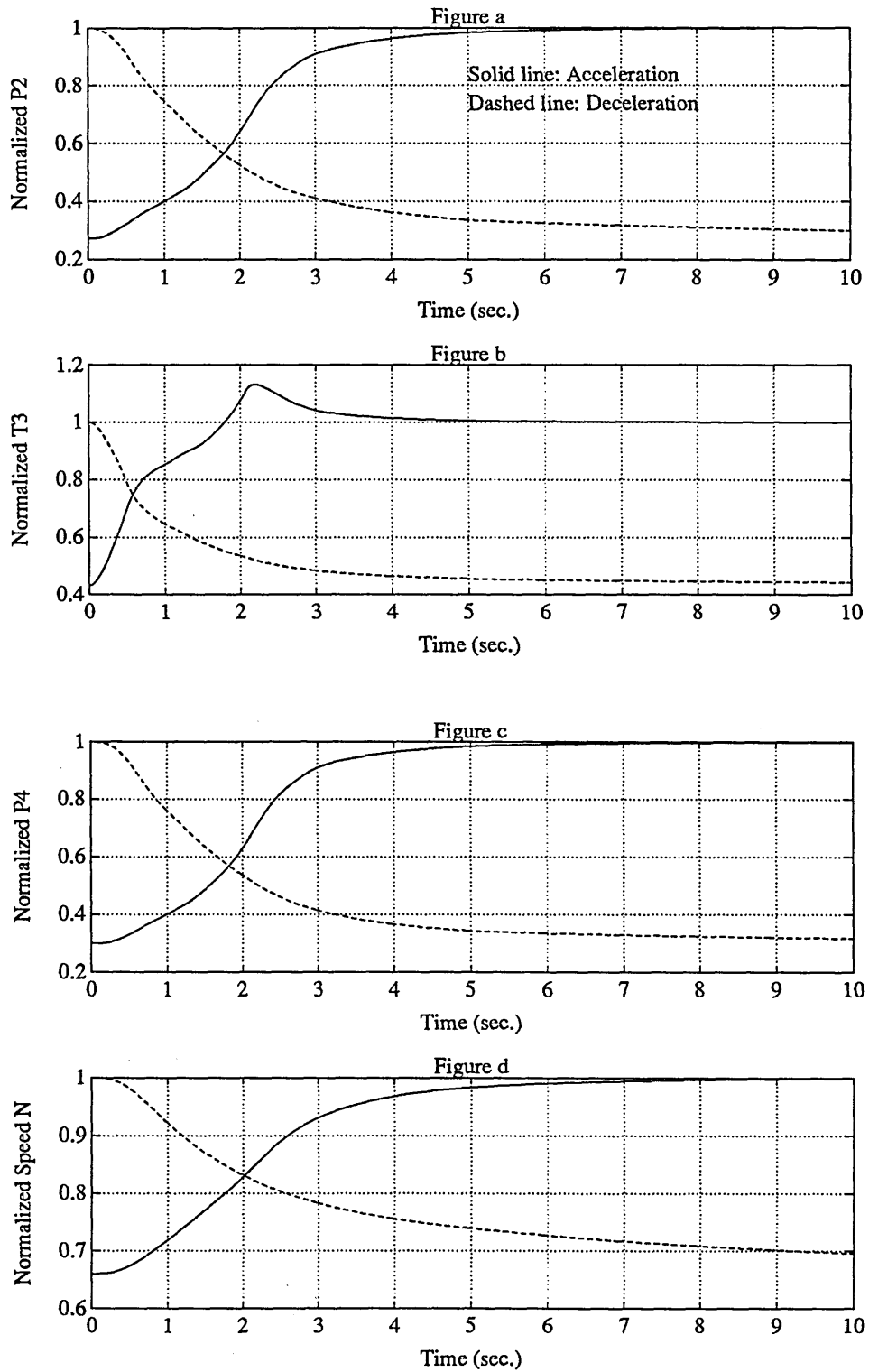


Figure 4.12: Responses of Engine States

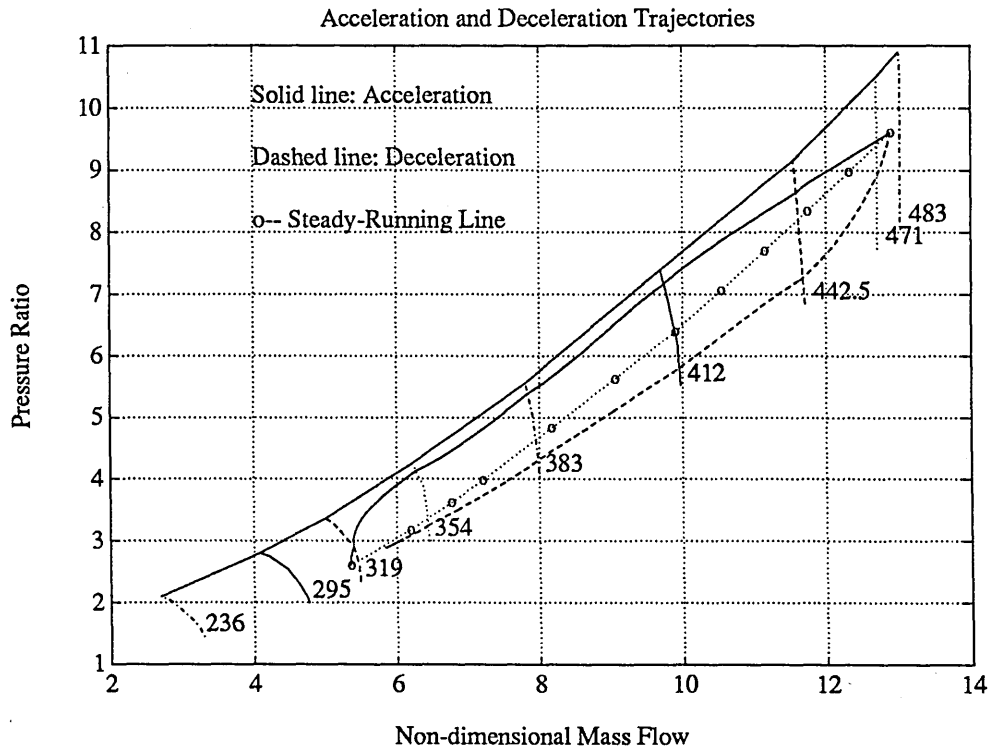


Figure 4.13: Acceleration and Deceleration Trajectories

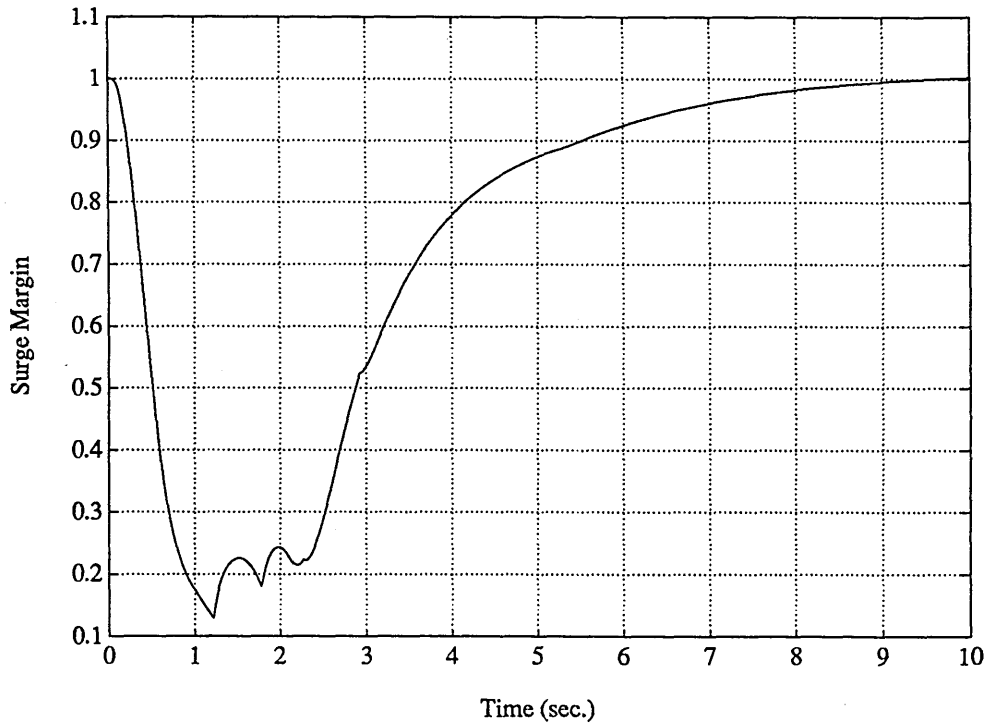


Figure 4.14: Variation of Compressor Surge Margin in Acceleration

when using pressure ratio. The comparisons are made by accelerations at the sea level, Mach number 0.2. Figure 4.15 and 4.16 show the results. The solid line is from results when using pressure ratio as the scheduling variable and the dashed line for the use of non-dimensional speed. It is seen from the Figures that schedul-

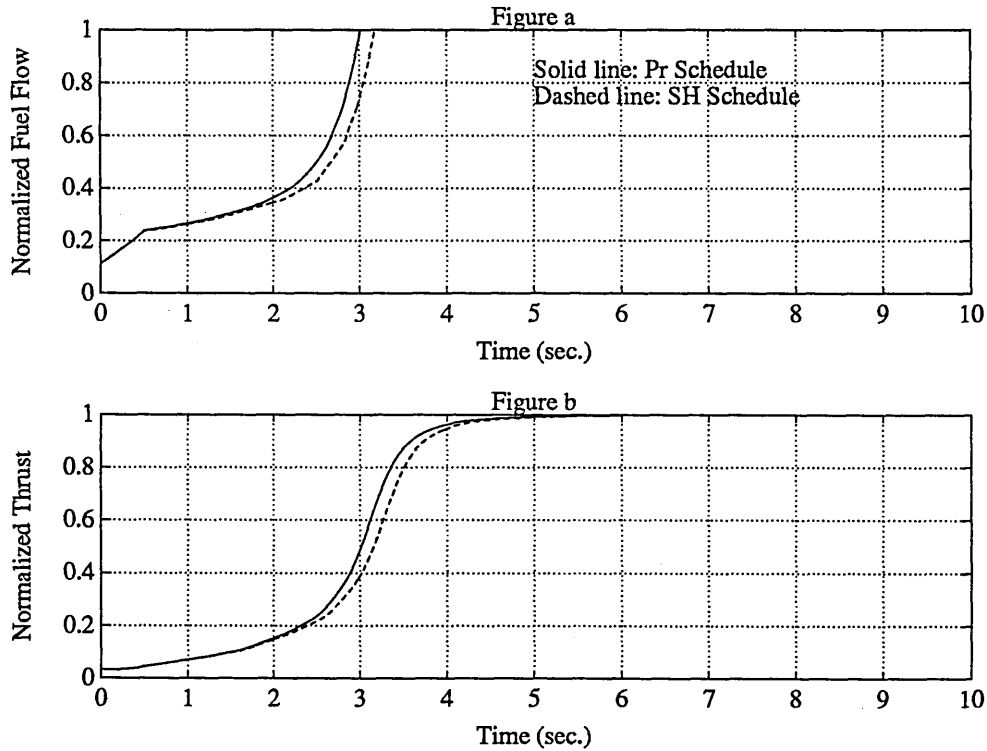


Figure 4.15: Input Fuel Flow and Thrust Response

ing using the non-dimensional speed results in slow response, compared with these using pressure ratio. The reason for this is at the constant non-dimensional speed, the pressure ratio used in the acceleration is higher than the steady-state value, whereas using the non-dimensional speed, this is the same as the steady-state value. If the acceleration factor is same for both schedules, which is the case in the present study, the fuel flow due to the pressure ratio scheduling will be higher than that due to the non-dimensional speed scheduling. From the dynamic analysis, it is also known that using the fast state as the scheduling variable will always produce faster responses. It is noted, though not illustrated here, that the fraction of the surge margin used when accelerating by the pressure ratio schedule was greater than the fraction used when on the non-dimensional speed schedule.

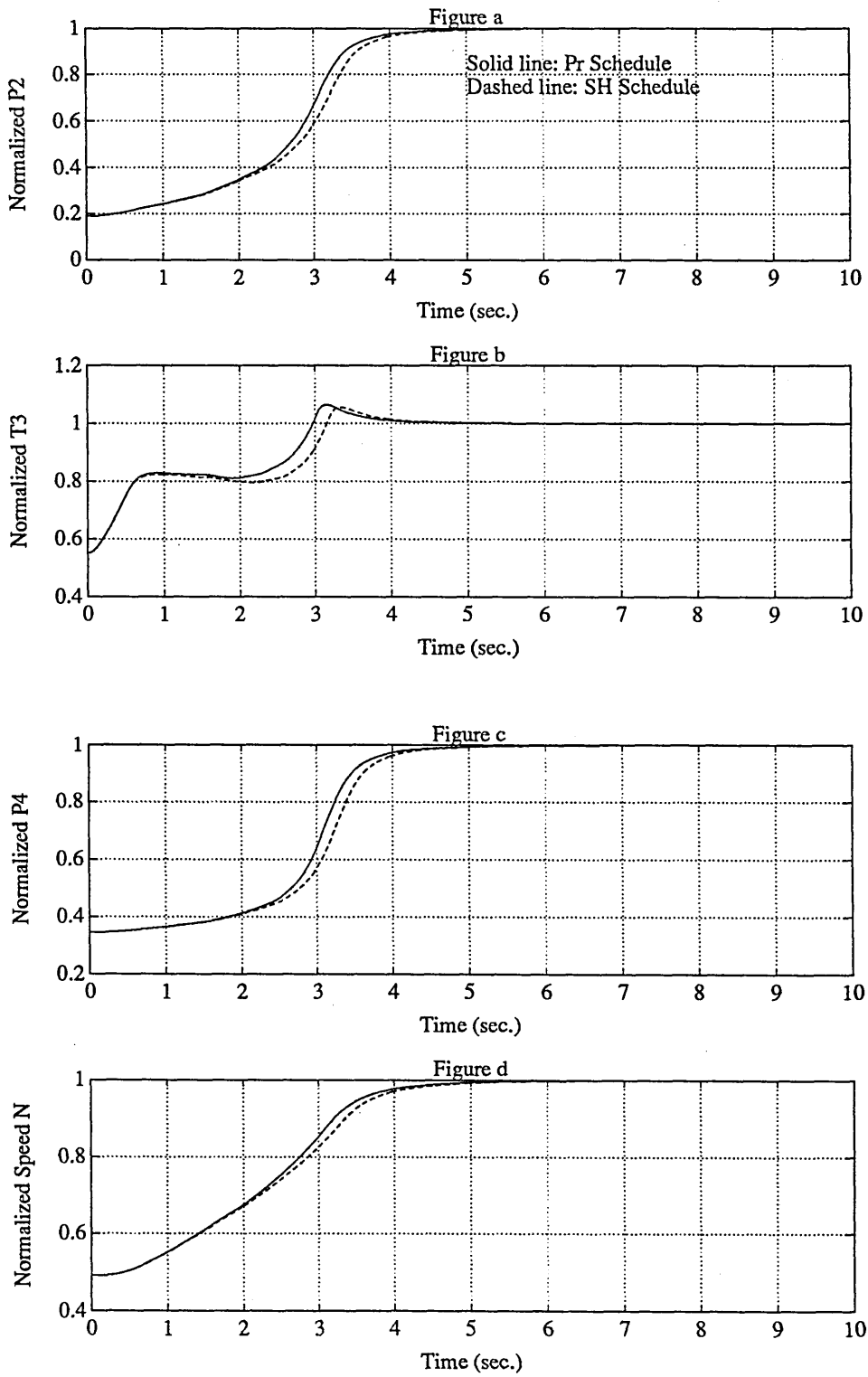


Figure 4.16: Responses of Engine States

4.9 Two-Spool Turbofan Engine

The simulation results for the turbofan engine are discussed in this section.

4.9.1 Steady-State Operation

The steady-state performance have been predicted using the developed models at the sea level, Mach number 0.2, and the results have been plotted on the compressor characteristics as shown from Figure 4.17 to 4.20. Also on the

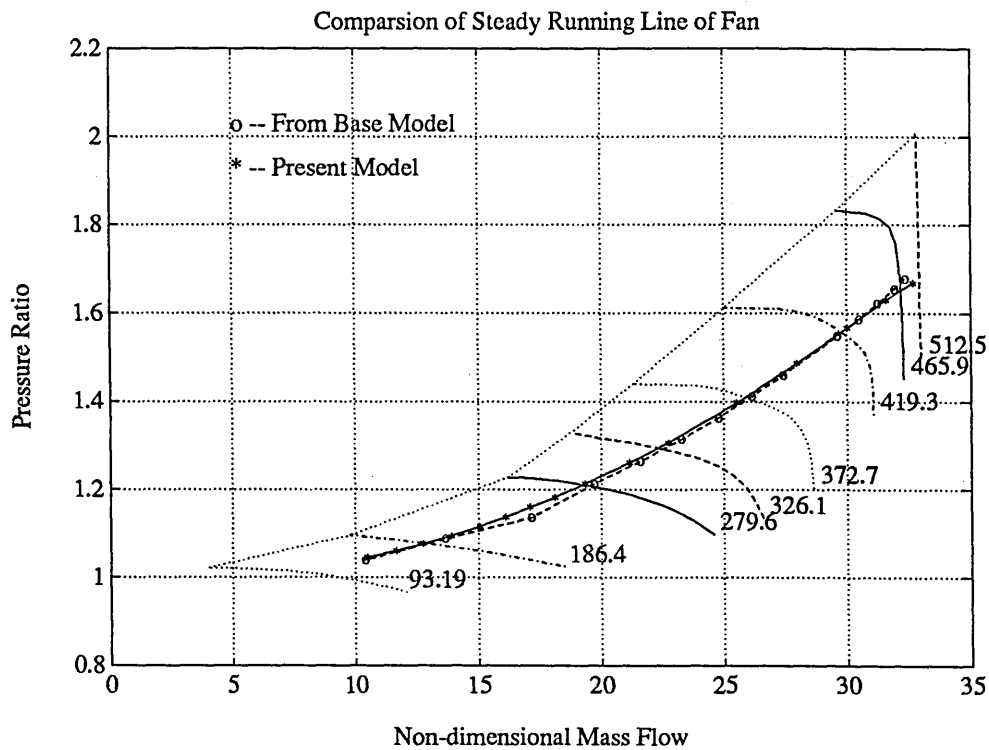


Figure 4.17: Steady Running Line on Fan Characteristic

plots, the data from Maccallum's model are shown to enable the comparison. The maximum and minimum fuel flow limits of 0.85kg/s and 0.08kg/s , respectively, have been used as the terminating conditions.

It is fruitful to examine the positions of the working lines on various compressor characteristics. It was found that the fan has a fairly flat steady-running line. The predicted steady-running line agrees well with that from the base model. The steady-running line on the IP Compressor characteristic presents a slight

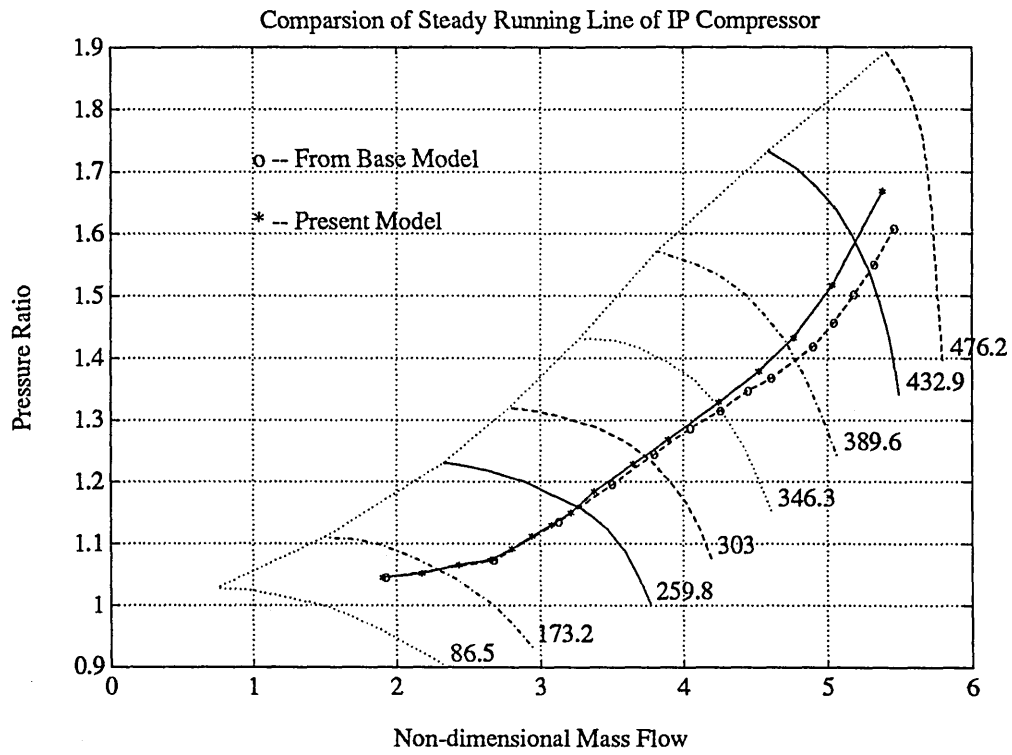


Figure 4.18: Steady Running Line on IP Compressor Characteristic

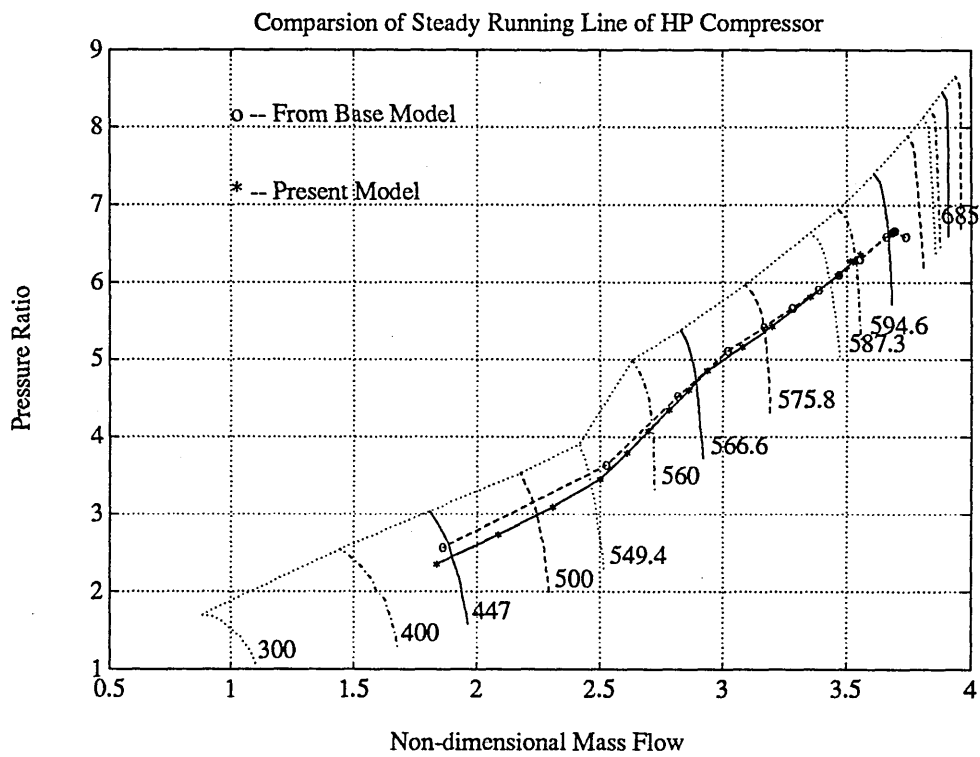


Figure 4.19: Steady Running Line on HP Compressor Characteristic

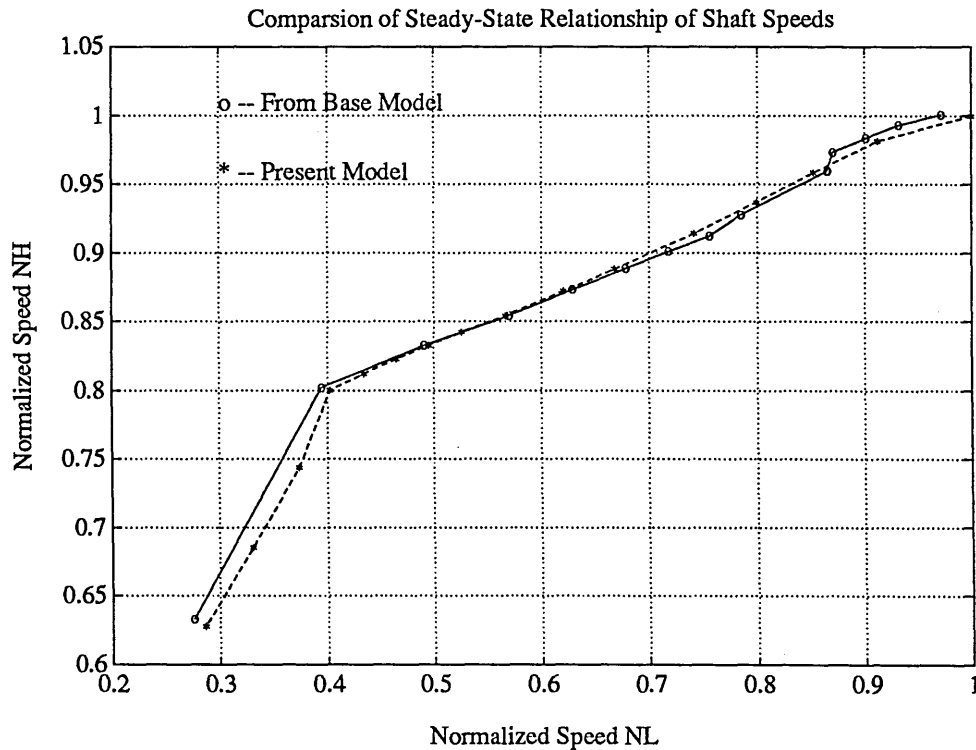


Figure 4.20: Relationship of HP and LP Shaft Speeds

discrepancy at the higher values of non-dimensional speed, compared to those predicted by Maccallum, and in fact, the working line deviates slightly towards surge at higher non-dimensional speed. Considering the steady running line on HP Compressor, the constant non-dimensional speed lines are almost vertical at high speed ranges and the corresponding mass flow is that given by choking condition. In this component, the steady running line agree well at the high speeds. In the low speeds, there are deviations for the model. Figure 4.20 shows that the model has correctly followed the base model.

4.9.2 Transients At Sea Level, Mach Number 0.2

The initial values of the LP and HP shaft speed are specified at the start, together with the fuel flow. This is fed into the combustion chamber by the fuel schedule used during this acceleration. The nature of the fuel schedule used depends on whether the transient is experienced at sea-level or at altitude conditions of flight.

The non-dimensional fuel schedule as functions of HP compressor pressure ratio are shown in Figure 4.21.

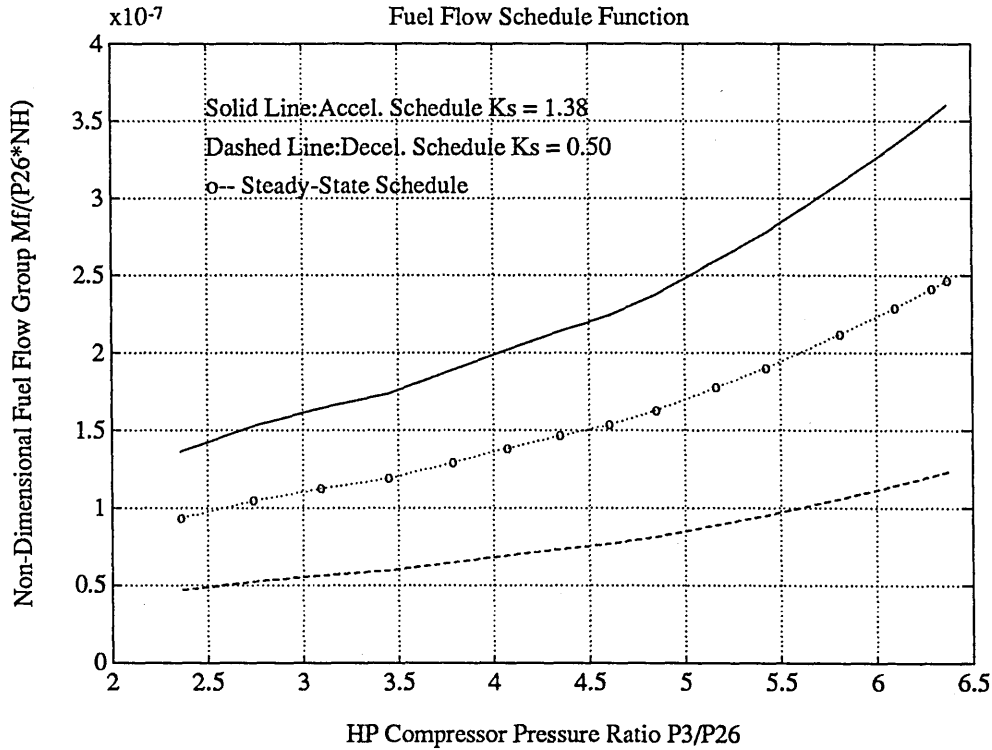


Figure 4.21: Non-dimensional Fuel Schedule

At sea level, Mach number 0.2, the transient performance of turbofan engine is predicted using the developed models. The idling speeds are 2185 rpm and 7376 rpm for LP and HP shafts respectively. The take-off speeds are 8455 rpm for the LP shaft, and 12065 rpm for the HP shaft. The maximum and minimum fuel flow are 0.85 kg/s and 0.08 kg/s. The heat transfer and thermal effects which are likely to occur during the transients are not taken into account in the present study. The simulation results are shown from Figure 4.22 to 4.30.

In the Figure 4.22 and 4.30, the responses of engine state variables are shown. It is seen that all the responses are very slow in the first 4 seconds, then rise rapidly due to the HP compressor bleed valve closing and the fuel flow thus quickly increasing. In the Figure 4.22d, the turbine inlet temperature is shown to be well below the maximum allowed values which is normalised to be 1.2. In Figure 4.23d, response of HP shaft speed exhibit a overshoot of 1.05 at 6.0 second. The

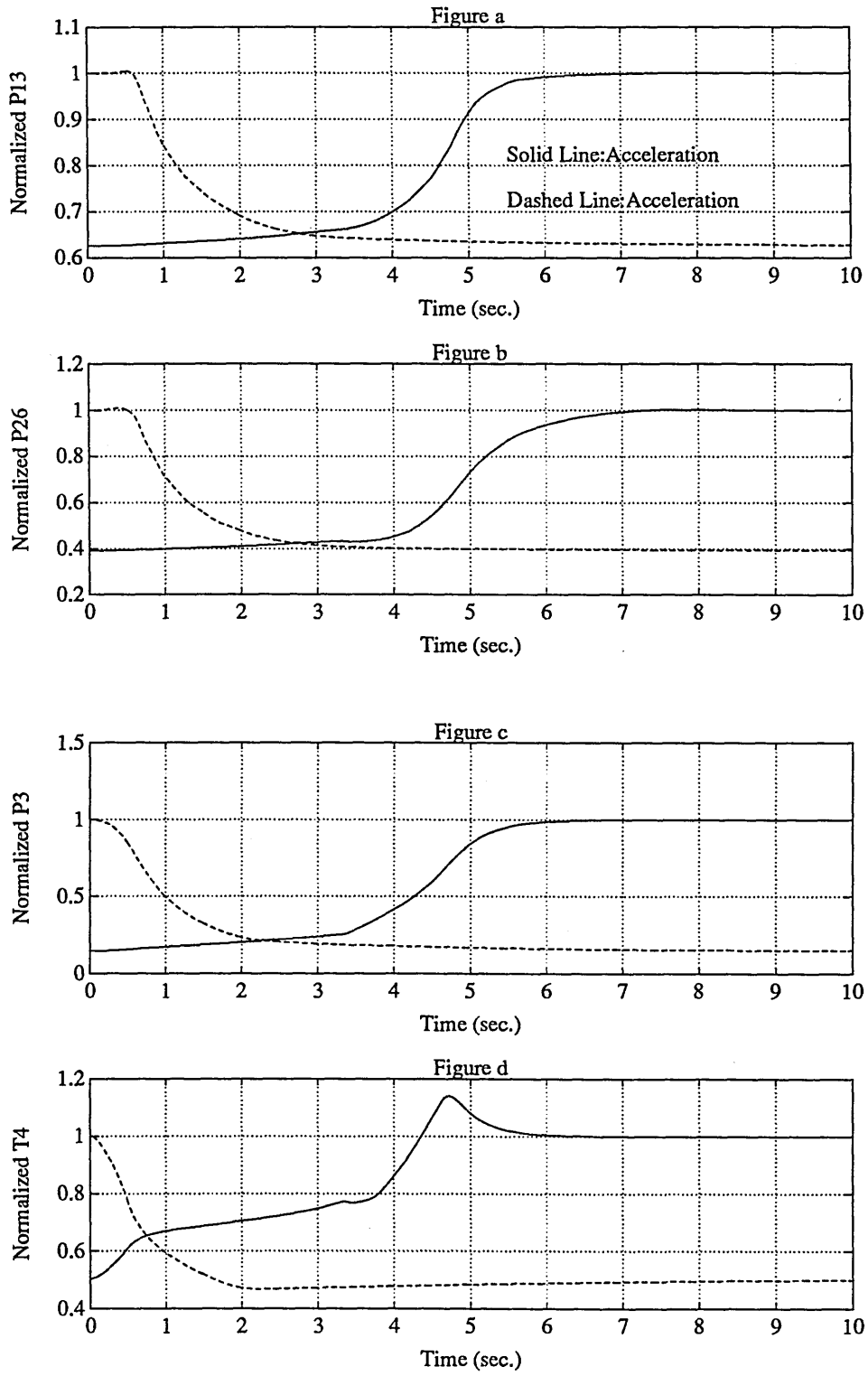


Figure 4.22: Transient Responses At Sea Level, Mach Number 0.2

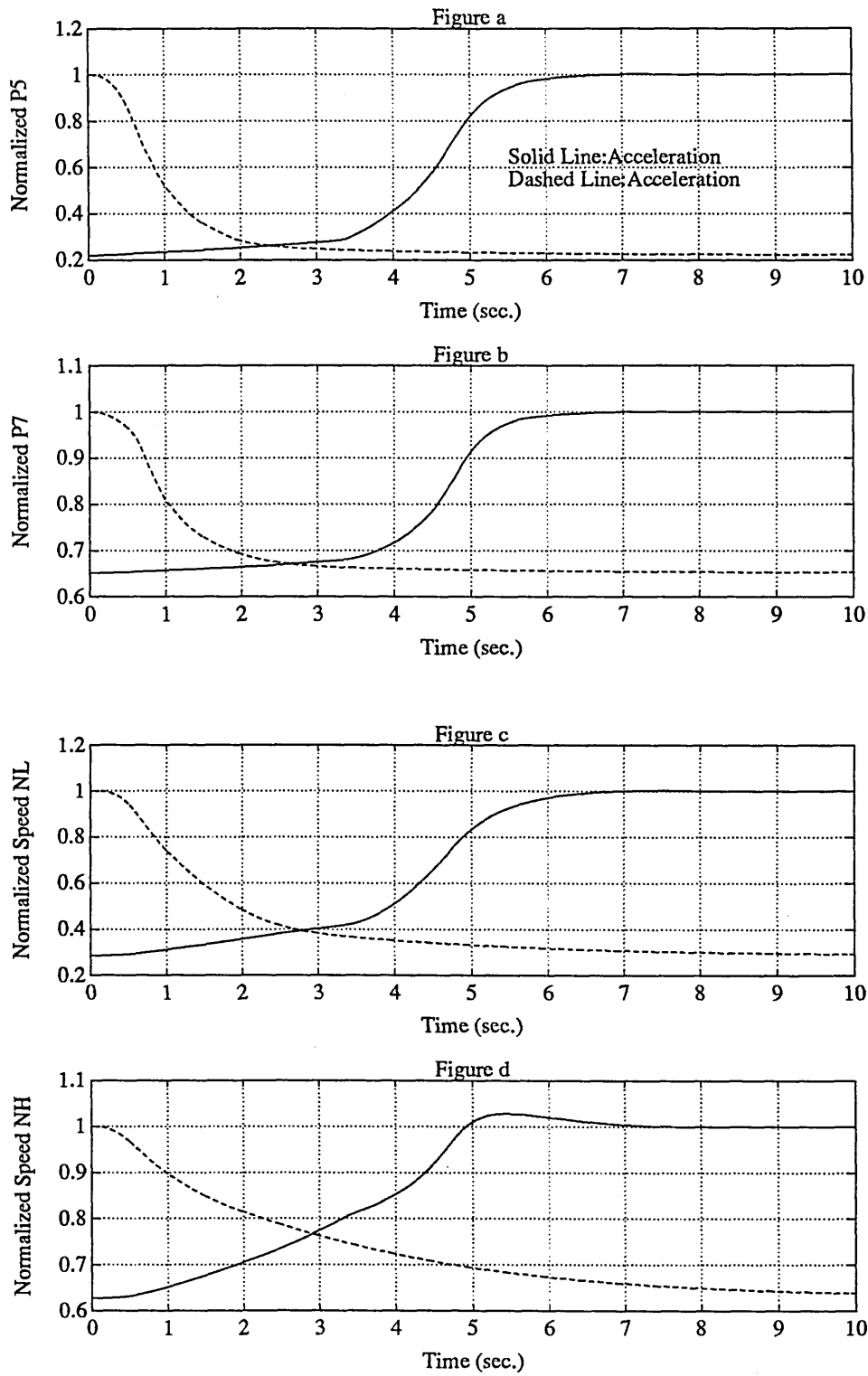


Figure 4.23: Transient Responses At Sea Level, Mach Number 0.2

deceleration in Figure 4.22a and 4.22b show that the pressure P_{13} and P_{26} increase slightly at the initial half second of the deceleration. This is due to the rapid deceleration of HP shaft and the closing of HP compressor inlet guide vane, as a result, HP compressor will admit much less $\dot{m}_{26}\sqrt{T_{26}}/P_{26}$

The acceleration and deceleration fuel flow are plotted in the Figure 4.24a, the fuel flow is controlled by the relationship shown in Figure 4.21.

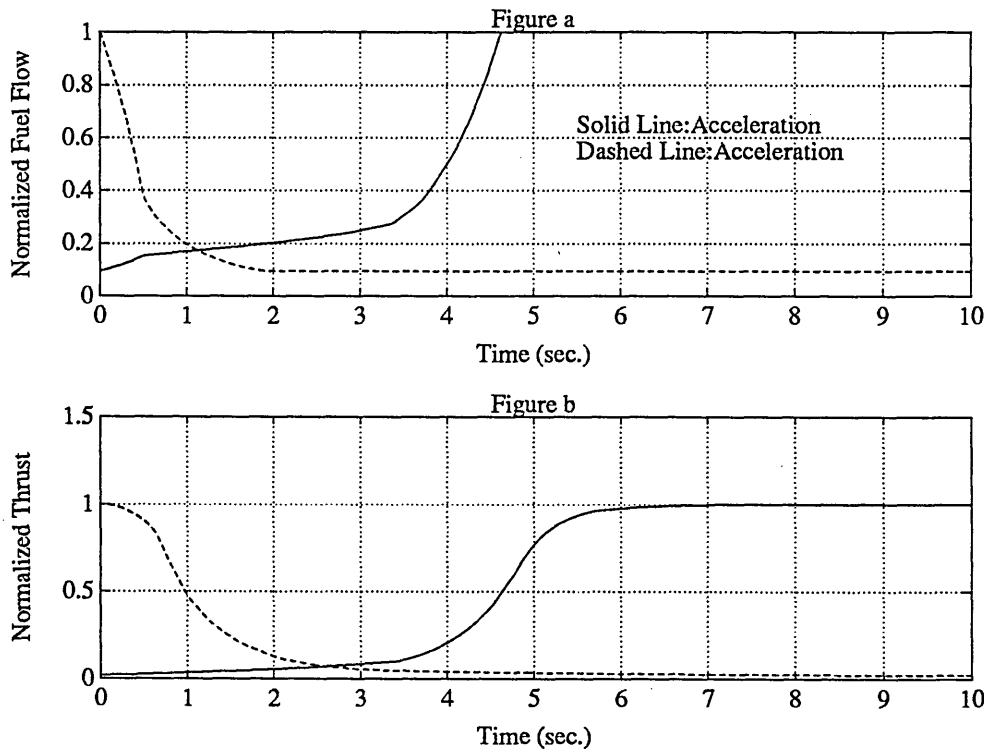


Figure 4.24: Fuel Flow and Thrust Response

The thrust response illustrated in Figure 4.24b shows that the thrust start at 4.0 per cent of its maximum and reaches 50 percent in 4.5 seconds. It is seen that the thrust rises fairly slowly in the first 4 seconds of the acceleration and then rises rapidly for about 1.5 seconds. The maximum fuel flow of 0.85 kg/s is reached at about 4.6 seconds. In the remaining part of the transient the engine is stabilising towards the speed corresponding to this maximum fuel flow. The change from the slow rate of thrust increase to the rapid rate, which occurs at 4 second, as explained earlier, is due to the HP compressor reaching the speeds when the 7th stage bleed starts to close. This makes the engine cycle become more efficient, and

thus the acceleration becomes more rapid, therefore more rapid thrust increase. It should be noted that while the LP and HP shaft speed relationships in acceleration and deceleration differ from the steady-running relationship, as shown in Figure 4.25, thrust response follows closely the response of the LP shaft speed. This is to be expected because the net thrust is approximately proportional to the total airflow through the engine, and this total airflow is primarily influenced by the LP shaft speed.

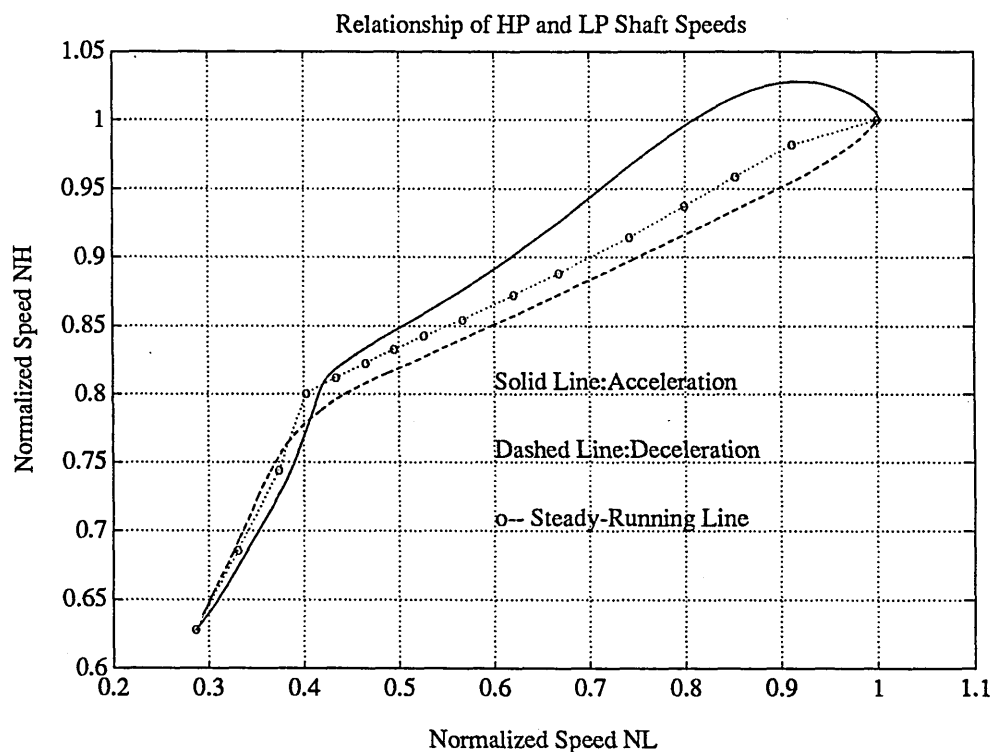


Figure 4.25: Relationship Between LP and HP shaft

The acceleration and deceleration trajectories on the fan characteristic are found to be very similar and move alongside the predicted steady running line. This is shown in Figure 4.26. Examining the movement of the transient trajectories on the components characteristics, the operating points predicted during the acceleration on the fan follow that of the steady-state operation. Therefore, no additional problems should be experienced during acceleration.

In the Figure 4.27, it is seen that the transient trajectories in the IP compressor

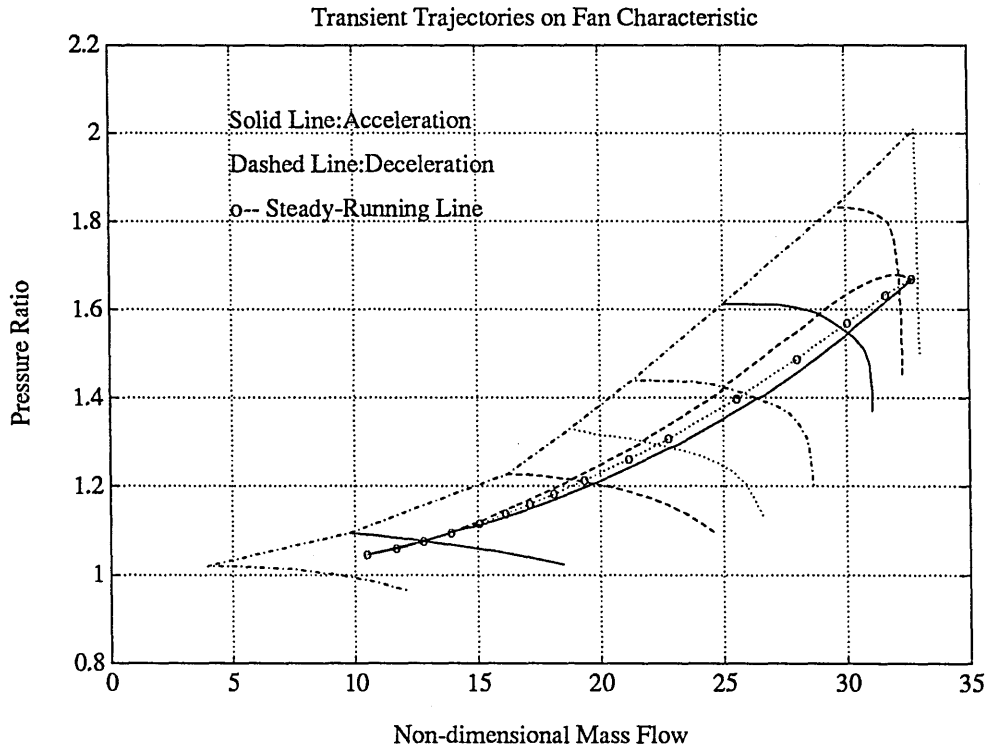


Figure 4.26: Transient Trajectories on the Fan Characteristic

in both the acceleration and deceleration move significantly away from the steady-running line. In the acceleration, the trajectory starts very close along the steady-running line and then suddenly drops below it. This sudden displacement away from the steady running line came at the same time as the change from the slow rate of increase of thrust to the rapid rate of increase. That change was associated with the 7th stage bleed in the HP compressor closing and IGV at the inlet of the HP compressor beginning to open, which brought about rapid rate of shaft speed increase. When the IGV at inlet to the HP compressor are opening, the air demand into that compressor rise rapidly. This tends to lower the pressure at delivery from the IP compressor in order to meet the non-dimensional mass flow requirements of HP compressor. In order to meet this requirement the pressure at delivery of the IP compressor is forced to drop, relative to steady-running line. The reverse process occurs in the deceleration and trajectories rise. In the present example, although about 75 percent of available surge margin is used, none of the present examples illustrated has meet this condition, which is obviously a real

danger.

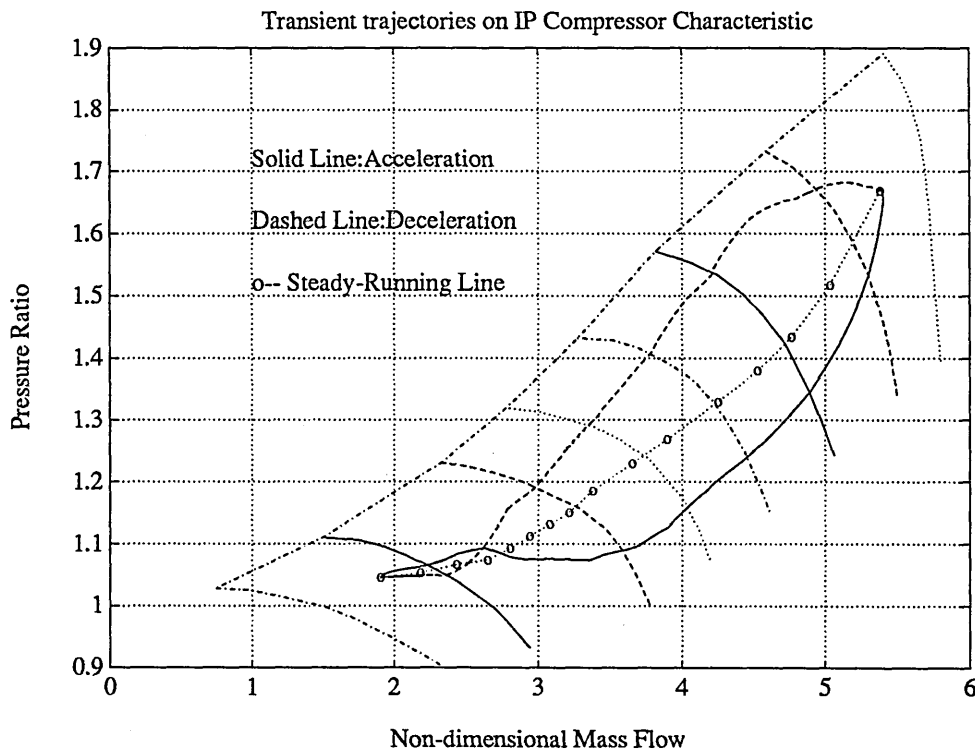


Figure 4.27: Transient Trajectories on IP Compressor Characteristic

In the Figure 4.28, the predicted acceleration and deceleration trajectories are plotted on the HP compressor characteristic. From idling to maximum speed the transient acceleration running line for the HP compressor is raised from the steady state towards surge. This is because, when the fuel flow is increased to accelerate the engine, turbine inlet temperature is increased. However the HP turbine capacity group has to remain almost constant, so to a first approximation the pressure at inlet to the HP turbine has to rise, thus the HP compressor delivery pressure and hence the HP compressor pressure ratio have to increase. It is noticed that the trajectory is still significantly below the surge line. It is very noticeable that there is a considerable overshoot in the non-dimensional speed before the engine finally stabilises. This is due to an overshoot in the HP shaft speed, and the lag of LP shaft which causes the increase of the temperature at delivery from the IP compressor to lag. The HP compressor surge margin defined in Equation 4.6 is plotted in Figure 4.28. Approximately 70% of this margin was already used

after which the trajectory moved away from the surge line, at the high values of speeds. It should be noted that the overshoot in non-dimensional mass flow means that under steady-running design point condition, the operating point will lie well inside the maximum non-dimensional mass flow capacity.

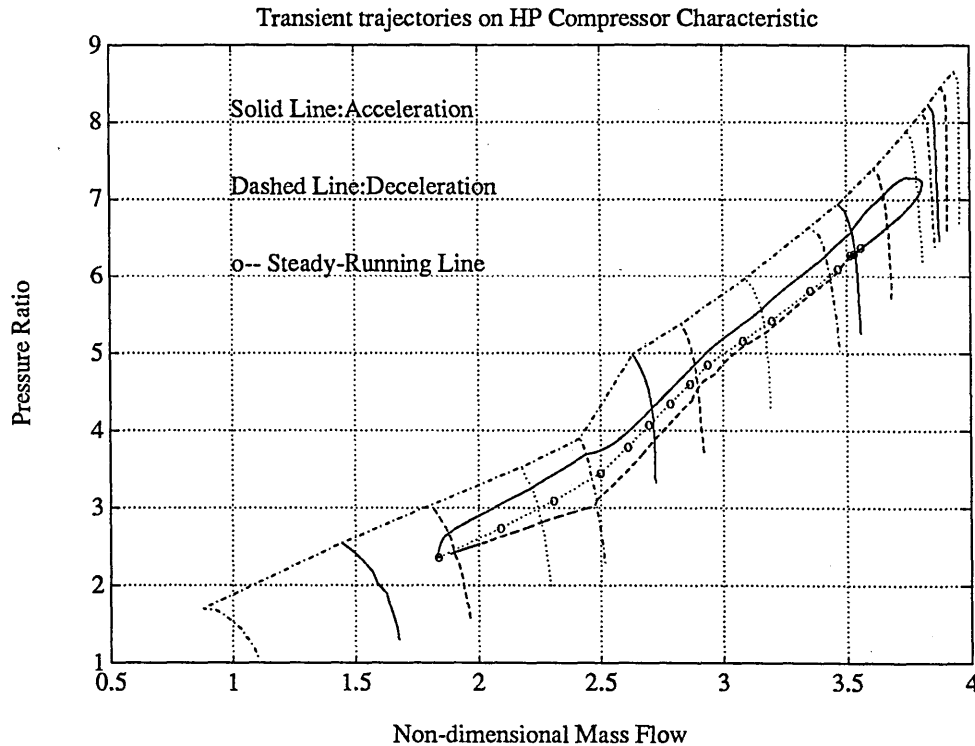


Figure 4.28: Transient Trajectories on HP Compressor Characteristic

4.9.3 Transients At 10,000 m, Mach Number 0.8

For an altitude of 10,000 m and Mach number 0.8, the performance of the simulation model has also been examined. For an acceleration, the starting speed for LP shaft is 4190 *rpm* and 9339 *rpm* for HP shaft. The maximum and minimum fuel flow adopted in this simulation were 0.25kg/s and 0.058kg/s. The fuel schedule used are the non-dimensional schedule plotted in Figure 4.21. The starting speeds for the deceleration are corresponding to the maximum condition of acceleration.

Figure 4.30 and 4.31 show that responses of the engine state variables. It is seen that states respond very quickly at the altitude.

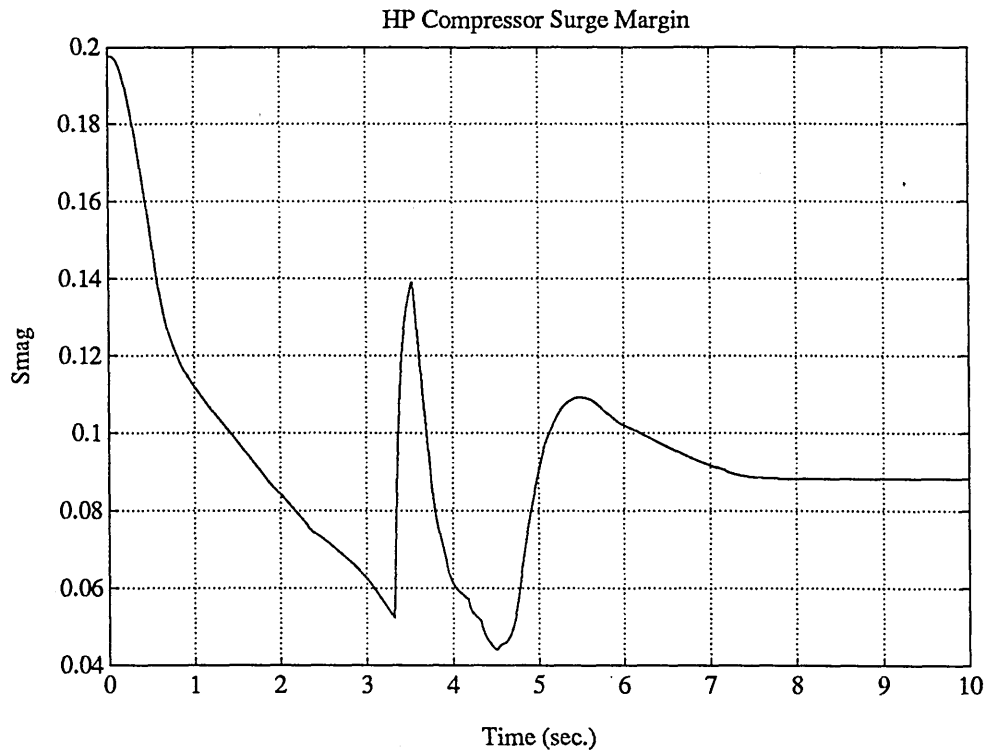


Figure 4.29: Variation of HP Compressor Surge Margin

The fuel flow input and the engine thrust responses are shown in Fig.4.31. Fig.4.32 show the relationship between LP and HP shaft.

In the Figure 4.35, it is seen that the acceleration and deceleration trajectories on the fan almost coincide with steady-running line and thus will clear of surge.

In Figure 4.35, the transient trajectories on the IP compressor are plotted. The transient deceleration, as in the sea level case, again approaches surge, using about 75 to 80 percent of the available surge margin. This is slightly more severe than at sea level. This small effect may be due to the lower Reynolds Number in the HP Compressor when at altitude. This causes thicker boundary layers and a resulting deterioration in the efficiency of the HP compressor which raises the working line.

In Fig.4.36, the transient trajectories on the HP compressor are plotted. The transient acceleration trajectories here is similar, within the range of engine running, to these at sea level shown in Figure 4.28. There is a small departure from the steady running line. The thrust start at 10 percent of the maximum and 50

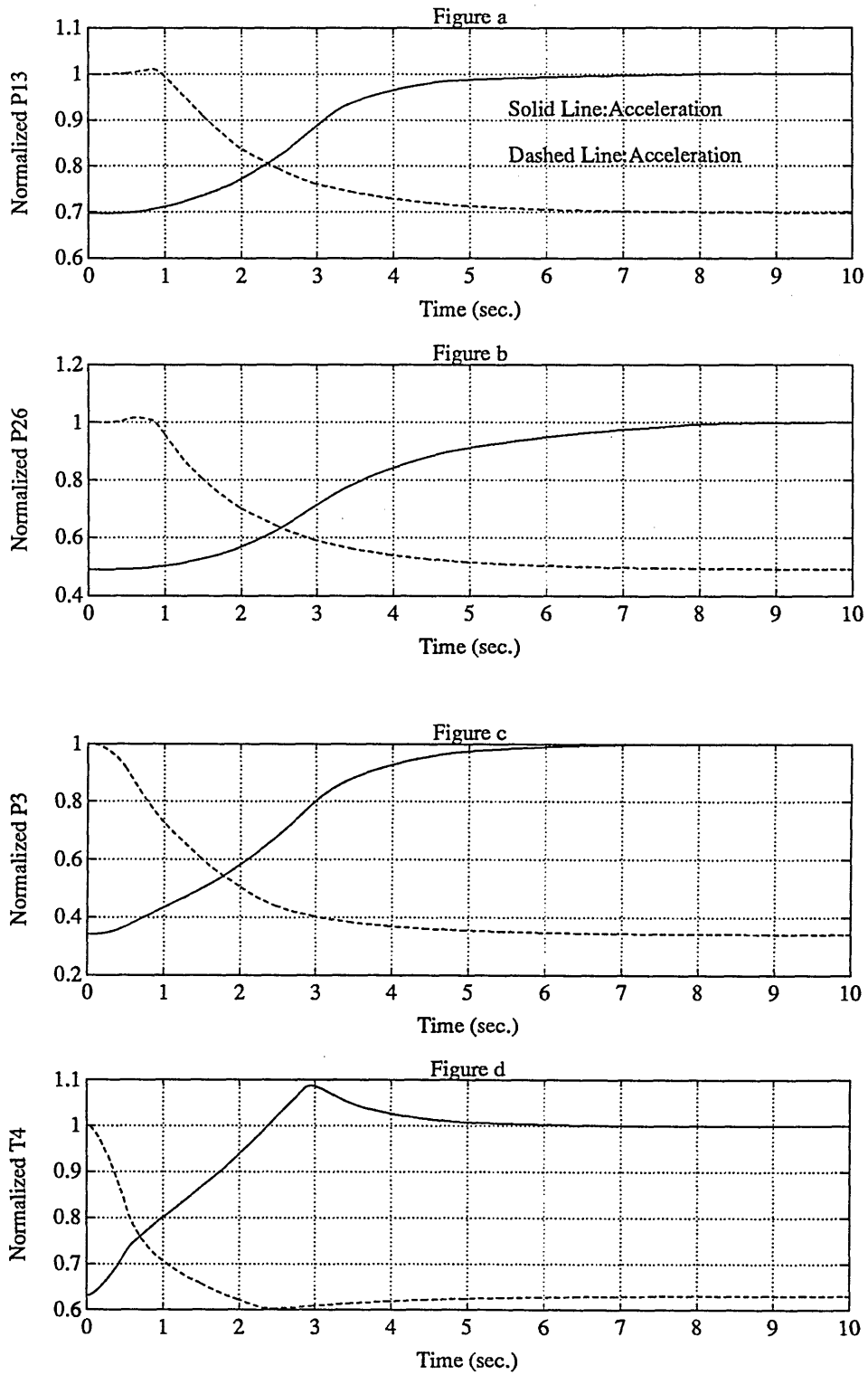


Figure 4.30: Transient States Responses

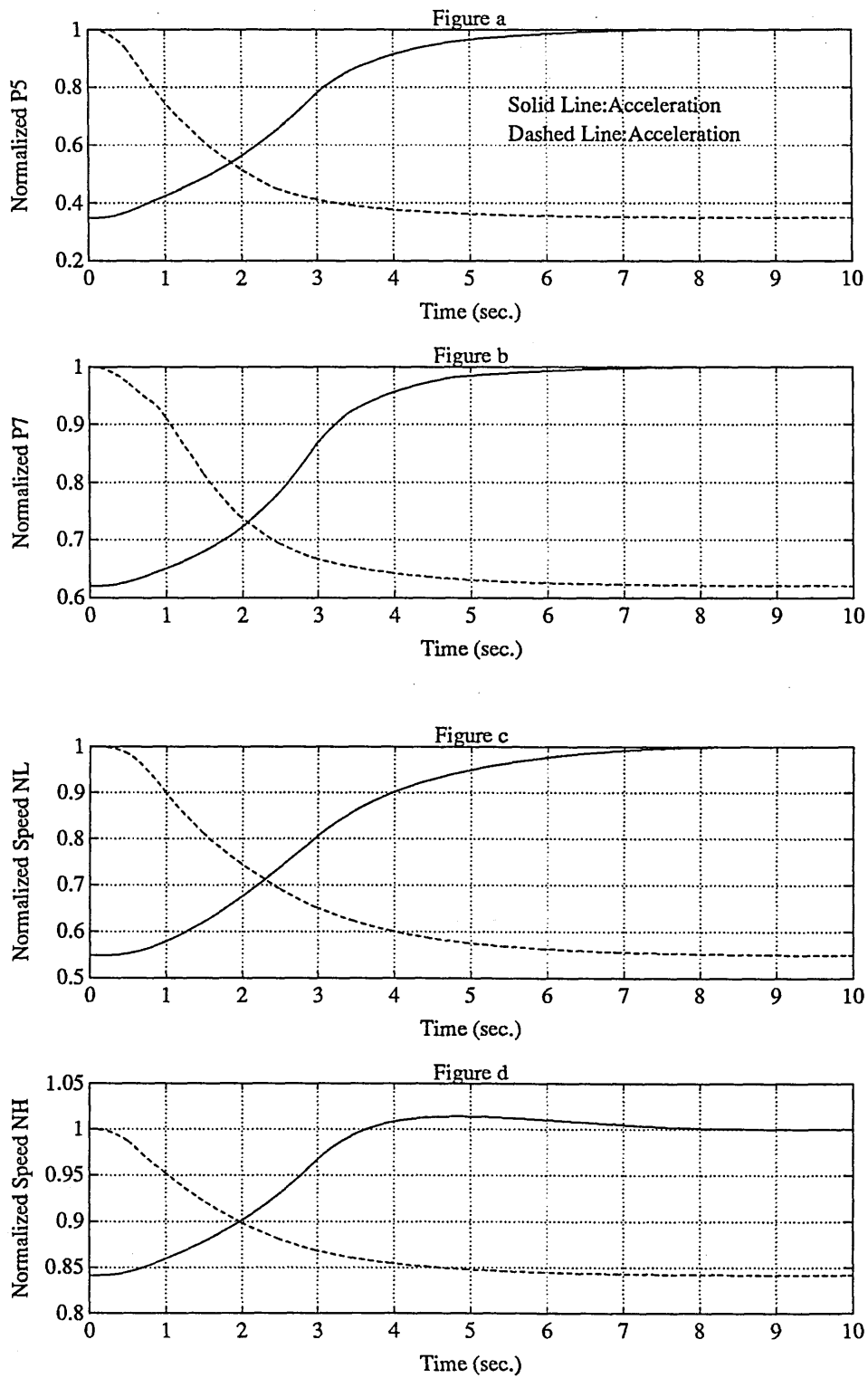


Figure 4.31: Transient States Responses

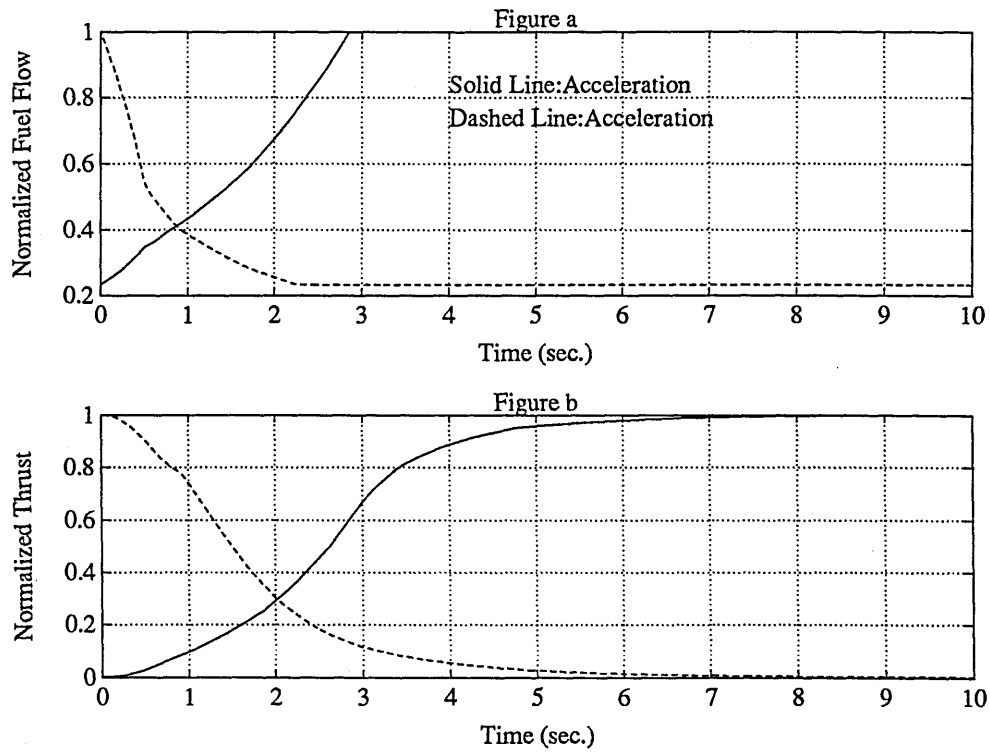


Figure 4.32: Fuel Flow and Thrust Responses

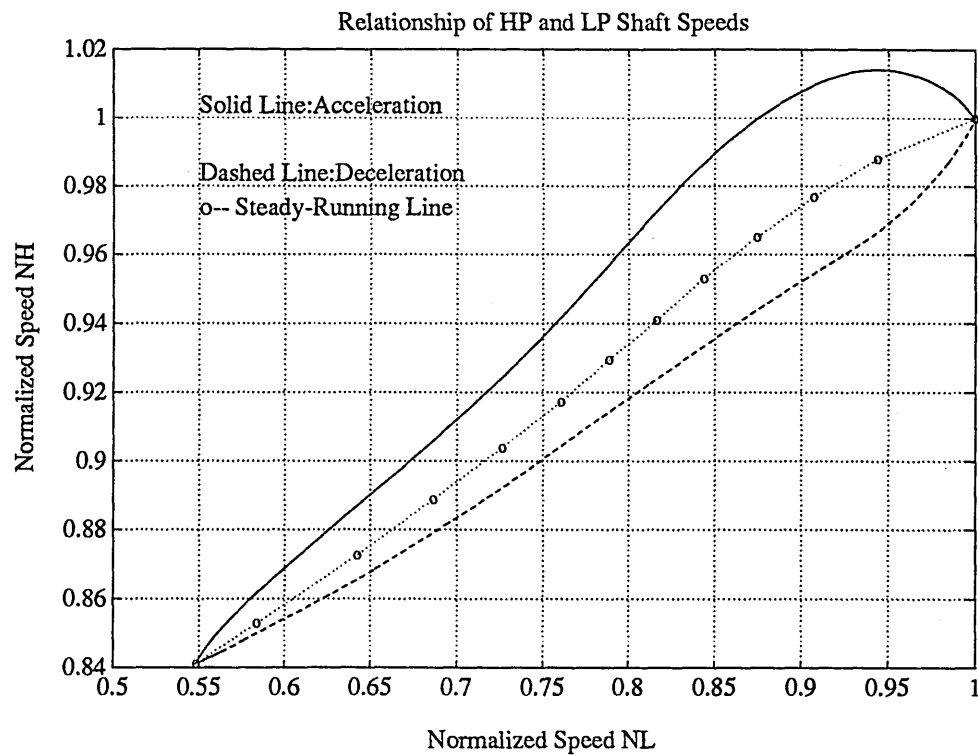


Figure 4.33: Relationship Between LP and HP Shaft

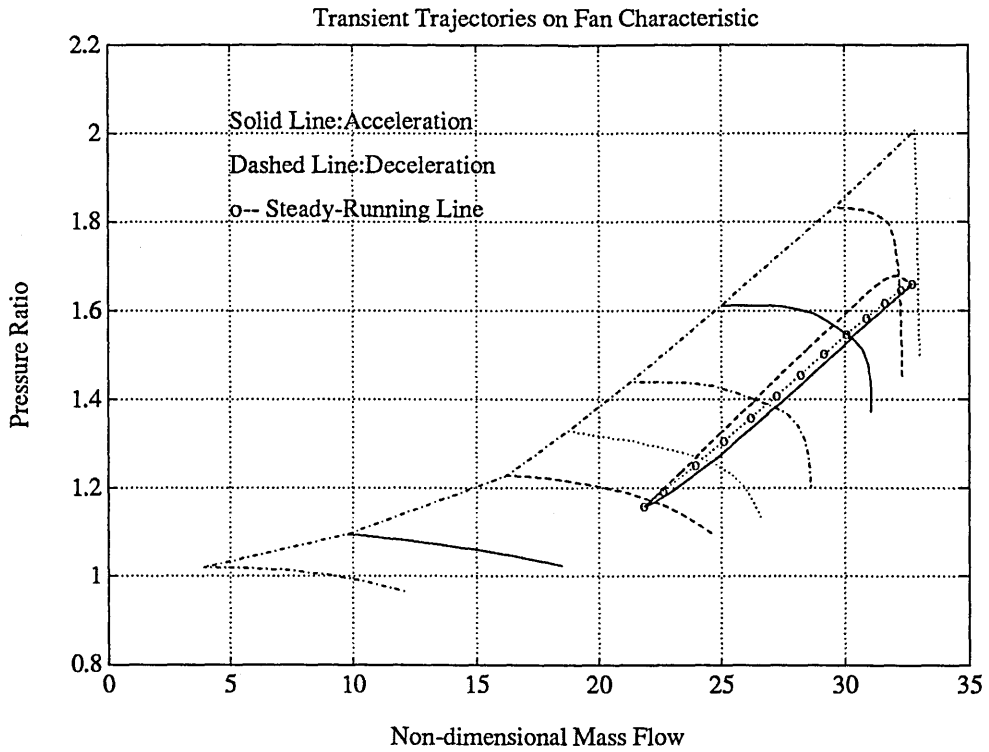


Figure 4.34: Transient Trajectories on Fan Characteristic

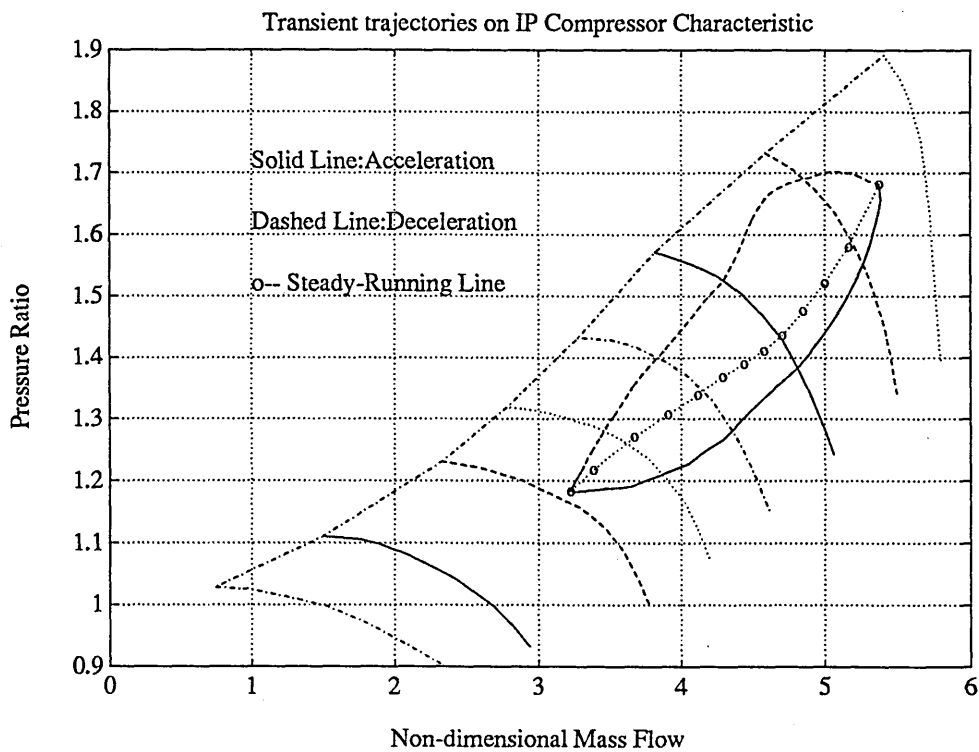


Figure 4.35: Transient Trajectories on IP Compressor Characteristic

and 50 percent thrust is reached in 1.5 seconds. In the deceleration, the thrust reduced to 50 percent in about 1.5 second

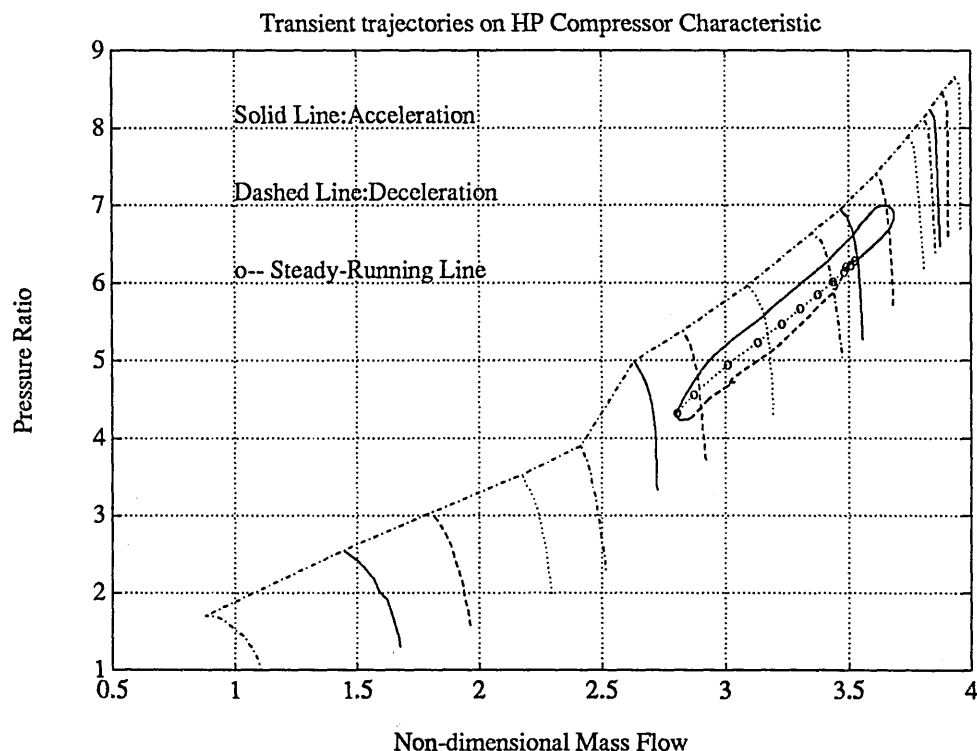


Figure 4.36: Transient Trajectories on HP Compressor Characteristic

In Figure 4.37, the variation of HP compressor surge margin during the acceleration are plotted.

4.10 Linearising the Nonlinear Models

It has been a common practice to generate linear models from nonlinear simulation for controller synthesis and this is especially the case when it comes to designing control systems for gas turbine engines. In the previous chapter, developed nonlinear models have been shown to be the accurate representations of gas turbine engines over operating envelope. However, these nonlinear models are not appropriate to be used in the procedure of controller synthesis. The reasons are that:

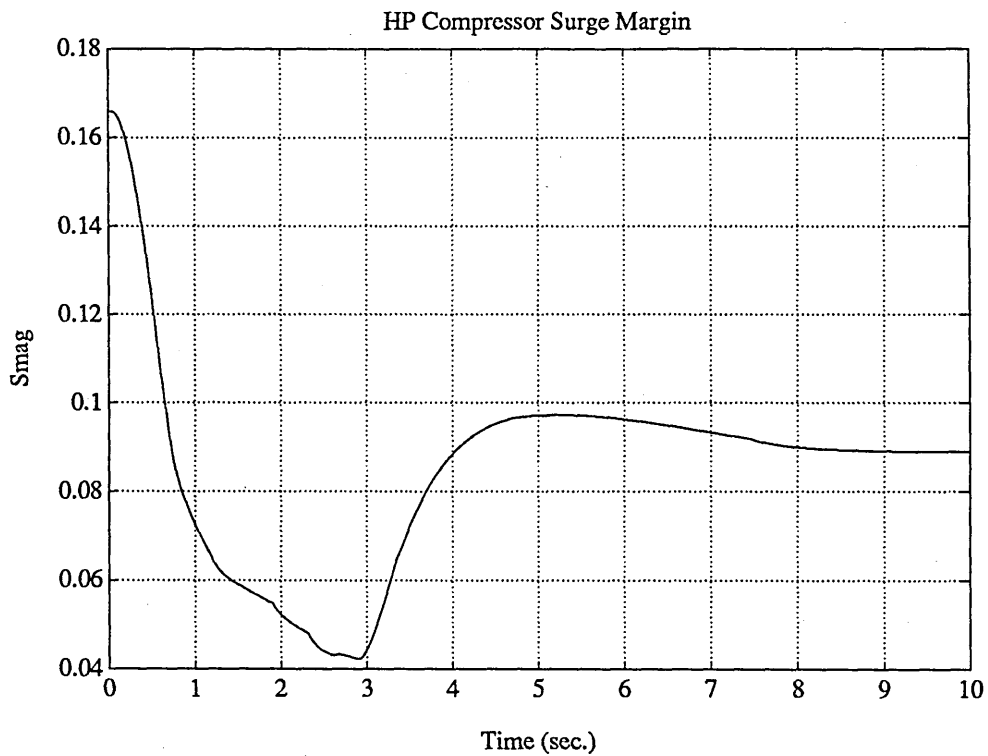


Figure 4.37: Variation of HP Compressor Surge Margin

- The nonlinear model itself is not analytical due to the way of modelling compressors and turbines using table characteristics.
- Lack of systematic procedure for nonlinear controller synthesis.

Because of the difficulties associated with nonlinear models, it is logical to analyze the system using the well established linear multivariable control theory. To this end, it is necessary to formulate the models in the form of state space equations or transfer function matrix.

4.10.1 Linearising a Nonlinear Model

Suppose a gas turbine engine can be represented by the following nonlinear differential and algebraic equations.

$$\dot{x} = F(x, u)$$

$$y = G(x, u) \quad (4.10)$$

In deriving linearised models, we assume that functions F and G are continuous and differentiable [129]. If the system described by equation 4.10 is in a steady state condition, i.e., constant input u_{ss} producing constant state x_{ss} and constant output y_{ss} , then the combination (u_{ss}, x_{ss}, y_{ss}) satisfies;

$$\begin{aligned} 0 &= F(x_{ss}, u_{ss}) \\ y_{ss} &= G(x_{ss}, u_{ss}) \end{aligned} \quad (4.11)$$

The point (u_{ss}, x_{ss}, y_{ss}) is termed a equilibrium or operating point of the gas turbine engine, and it may be stable or unstable. Perturbating the control input with δu results in state and output perturbation δx and δy , respectively and control input, state and output become $u = u_{ss} + \delta u$, $x = x_{ss} + \delta x$ and $y = y_{ss} + \delta y$, and the equation 4.10 follows;

$$\begin{aligned} \dot{x}_{ss} + \delta \dot{x} &= F(x_{ss} + \delta x, u_{ss} + \delta u) \\ y_{ss} + \delta y &= G(x_{ss} + \delta x, u_{ss} + \delta u) \end{aligned} \quad (4.12)$$

Because of the continuity requirements imposed on the functions of F and G , equation 4.12 can be expanded in a Taylor series about the point (u_{ss}, x_{ss}) , resulting in the following representation for the gas turbine engine;

$$\begin{aligned} \dot{x}_{ss} + \delta \dot{x} &= F(x_{ss}, u_{ss}) + A\delta x + B\delta u + \mu(\delta x, \delta u) \\ y_{ss} + \delta y &= G(x_{ss}, u_{ss}) + C\delta x + D\delta u + \nu(\delta x, \delta u) \end{aligned} \quad (4.13)$$

The constant matrices A , B , C , D have the dimensions of $n \times n$, $n \times m$, $r \times n$, $r \times m$ respectively and are given by;

$$A = \frac{\partial F_i}{\partial x_j} \quad B = \frac{\partial F_i}{\partial u_j} \quad C = \frac{\partial G_i}{\partial x_j} \quad D = \frac{\partial G_i}{\partial u_j} \quad i = 1, 2, \dots, n. \quad j = 1, 2, \dots, r. \quad (4.14)$$

with each partial derivative evaluated at the point $x = x_{ss}$, $u = u_{ss}$. The expressions $\mu(\delta x, \delta u)$, and $\nu(\delta x, \delta u)$ represent all the second and higher order terms in

the Taylor series expansion. Using the above equations, noting that $\dot{x}_{ss} = 0$, and retaining only first order terms in the Taylor series expansion of F and G leads to the perturbation equations;

$$\begin{aligned}\delta\dot{x} &= A\delta x + B\delta u \\ \delta y &= C\delta x + D\delta u\end{aligned}\tag{4.15}$$

This equation approximates the dynamic behaviour of the nonlinear gas turbine engine in a small region about the operating point ($u = u_{ss}$, $x = x_{ss}$).

Remark 1 : Linear models of a gas turbine engine can be generated in many ways, e.g. numerically from the nonlinear simulation, or directly from engine test data. A common method is to utilise a nonlinear hybrid or digital engine simulation. This procedure is computationally efficient; but often, linearised behaviour is dependent on the perturbation size. Alternatively, the time response of the measured outputs to engine inputs can be used with various system identification algorithms to develop models which accurately represent engine behaviour over a rather large range. These procedures tend to be computationally demanding and require extensive experience in their applications.

Remark 2 : Linear models generated numerically do not contain the most convenient parametrisation of dynamics and sometime contain far too complex a description to be practically utilised for design. It is likely that a design model including engine, actuator and sensor dynamics could be a high order system. In this case, model reduction will be the first important step to establish an effectively simple model which include only elements important to the desired control function.

Remark 3 : When using linear models for engine control, model reduction is dependent upon the control designer's estimate of the frequency range of the control function. For the turbine engine, the controller was designed primarily to modulate thrust in transient and steady state operation. The response frequency range is approximately from 0 to about 10 Hz, which is the bandwidth

of the primary actuator. This frequency range will be significantly different if, for example, the controllers were designed to modulate compressor surge margin with a high bandwidth variable area turbine actuator. The implication here is that all eigenvalues significantly outside the bandwidth of interest are assumed in equilibrium.

4.10.2 Approximation Algorithm

When approximating the partial derivatives using finite difference method, using the relative perturbation have been found to produce better results. This is the case especially when the nonlinear models have not been properly scaled and states and controls have different magnitudes. Using the relative perturbation could result in the uniform perturbed models which are less sensitive to the perturbation size [130]. In our cases, the relative perturbation $\epsilon = 0.001 - 0.01$ have been applied to all operating conditions and resultant linearised models are found to be robust to the perturbation size when $\epsilon \leq 0.01$.

4.10.3 Validating Linear Models

The structure for validating the linear models is shown in Figure 4.41 where linear and nonlinear models are subjected to the equal step change of fuel flow.

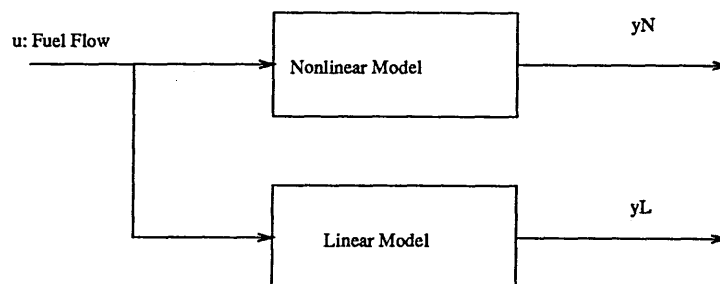


Figure 4.38: The structure for validating linear models

In Figure 4.42 through Figure 4.43, the simulations are shown when linear and nonlinear model are fed equal step change of fuel flow. The comparison of state variables show that linear model approximate the nonlinear model well between

the operating points, although the steady-state error exist. Such comparison establish the validity of the linear models and used for the controller design;

4.11 Conclusions

In this chapter, the developed models have been validated against the models, which have already been developed. The open-loop schedule control have been used to predict the transient performance for the comparison. Simulations have shown that the good agreement have been achieved. The linear model has been generated and also validated by simulation.

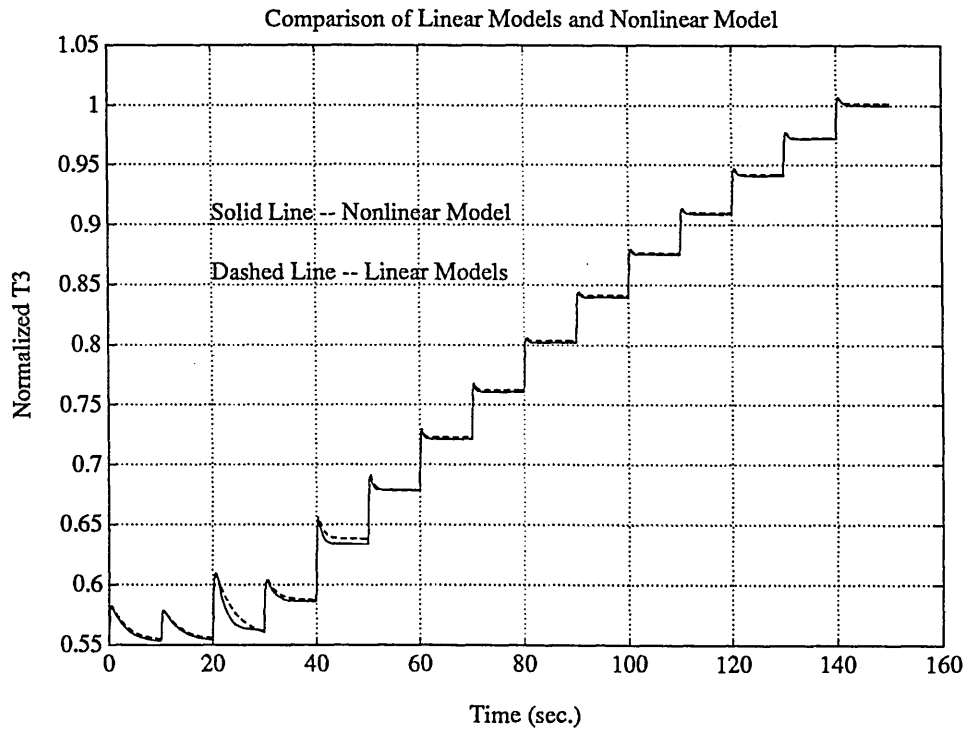
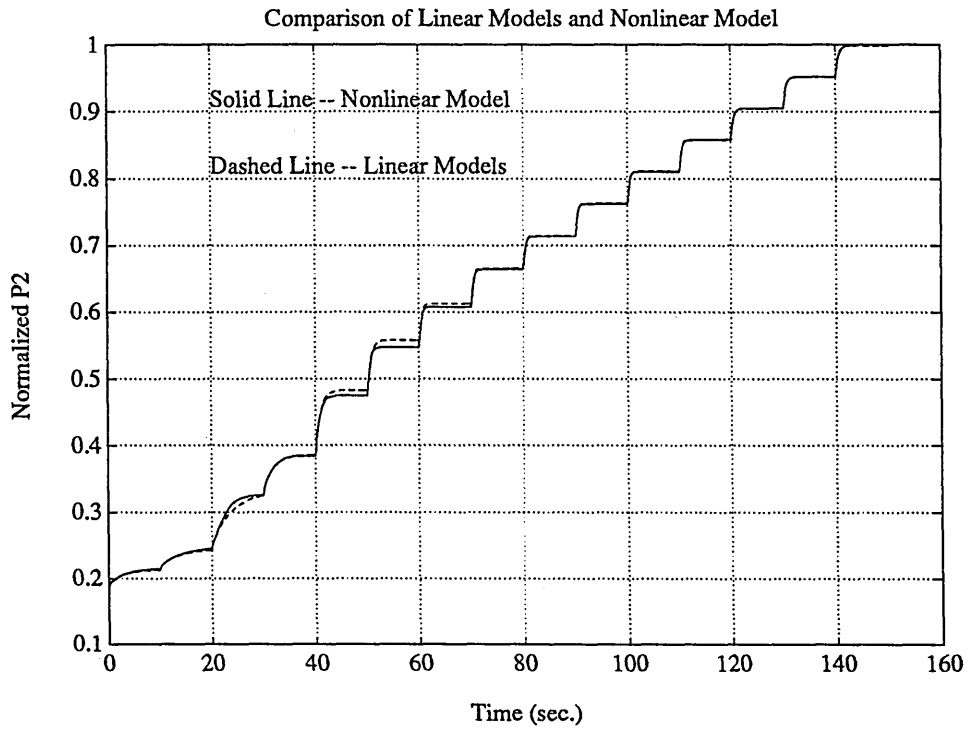


Figure 4.39: Comparing Linear and Nonlinear Model: Single-Spool Engine

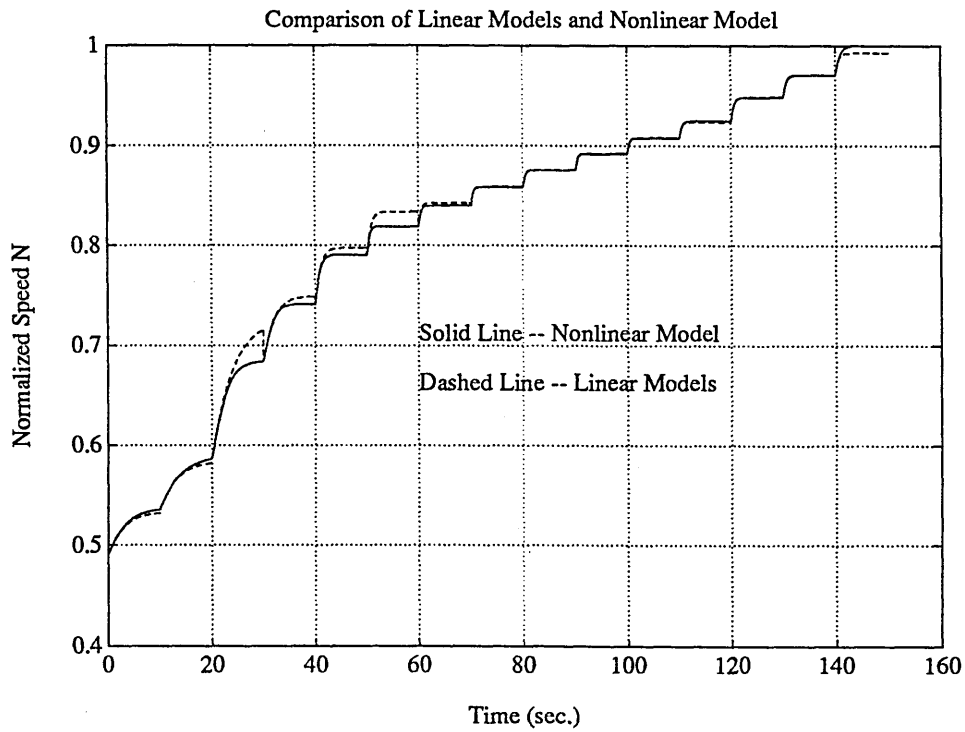
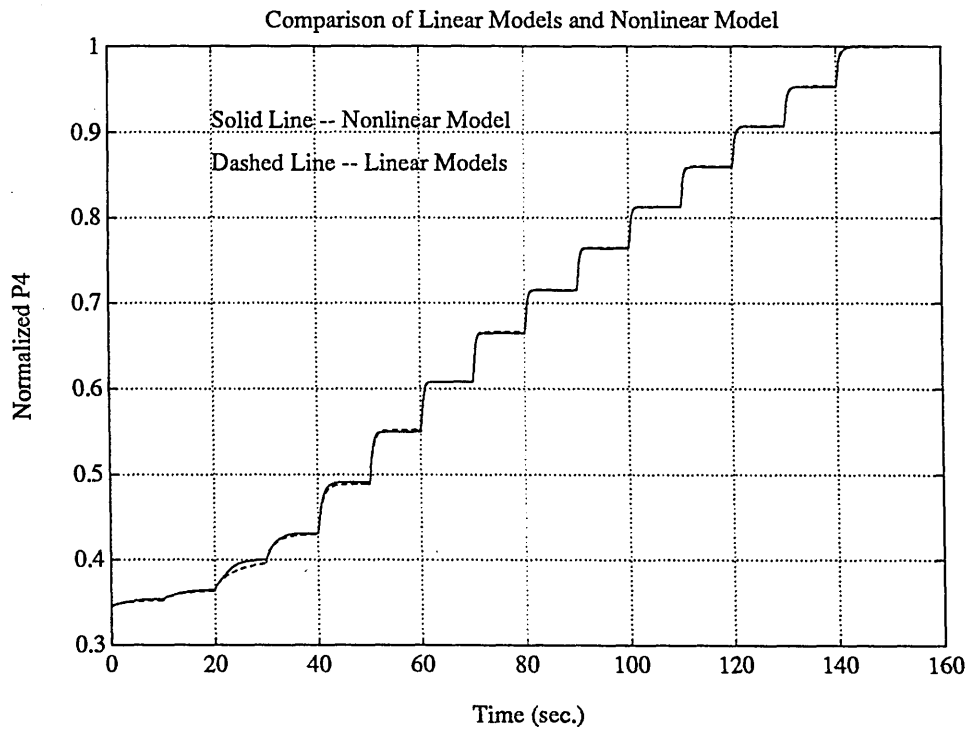


Figure 4.40: Comparing Linear and Nonlinear Model: Single-Spool Engine

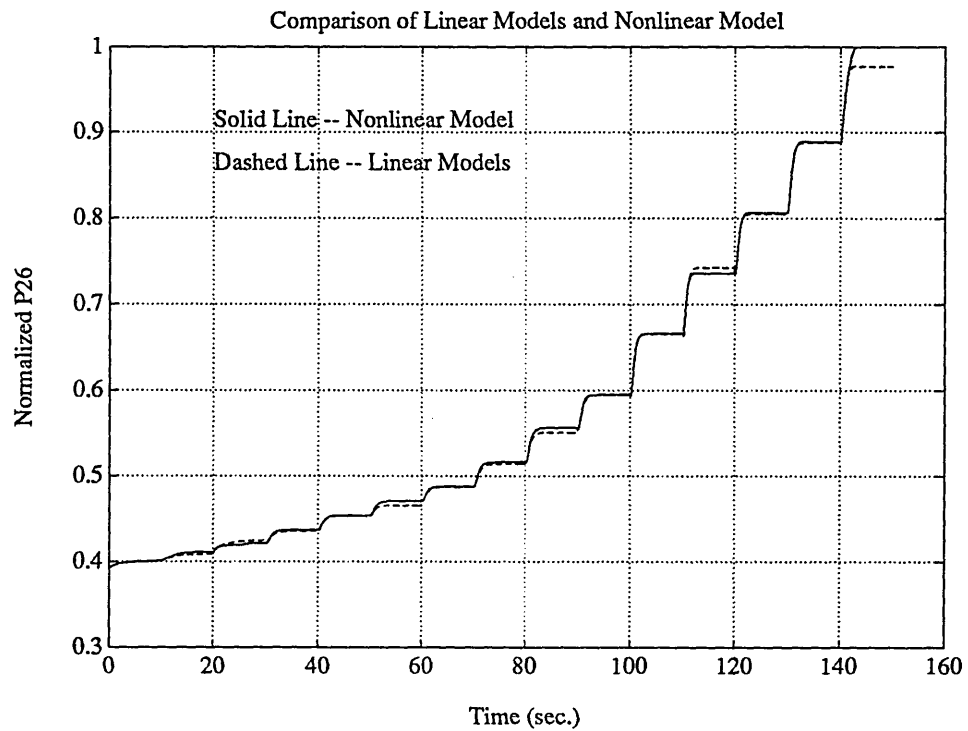
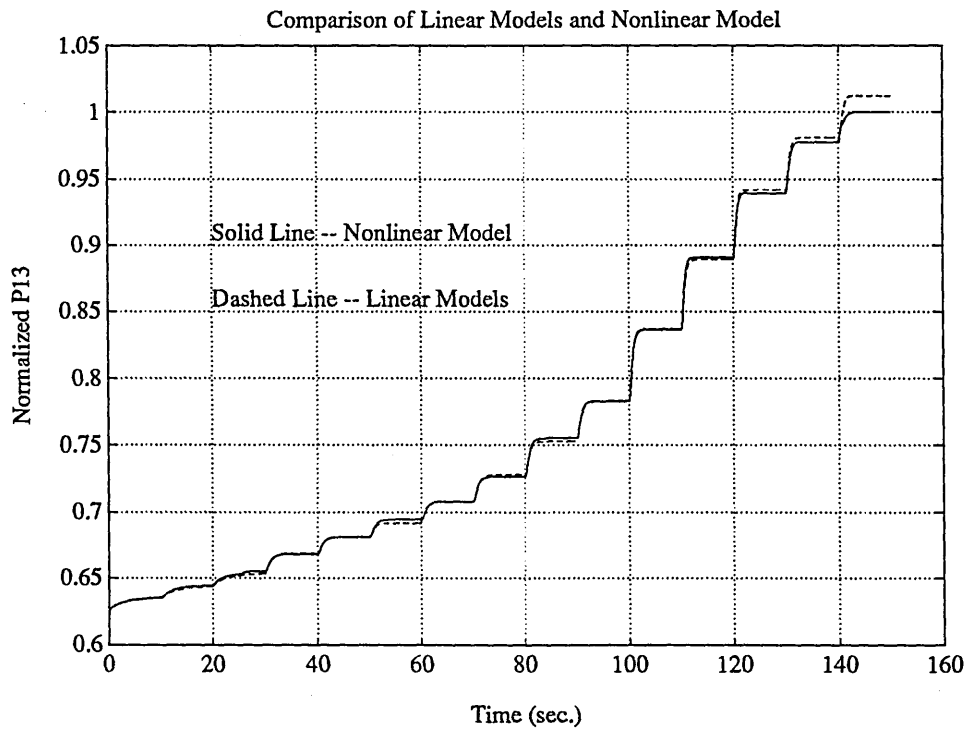


Figure 4.41: Comparing Linear and Nonlinear Model: Turbofan Engine

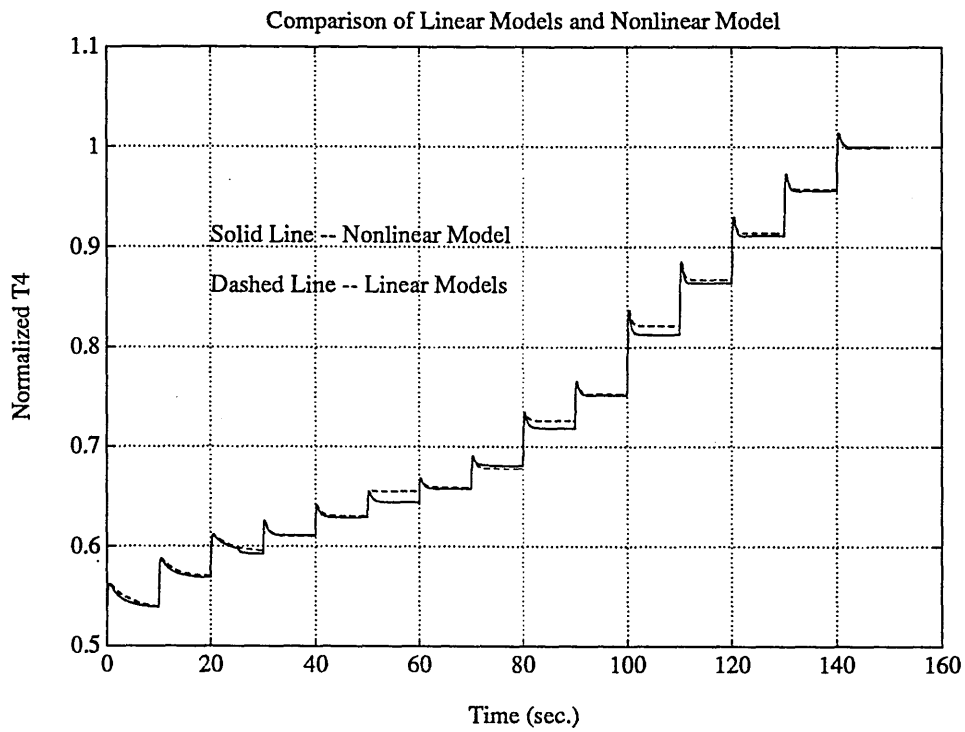
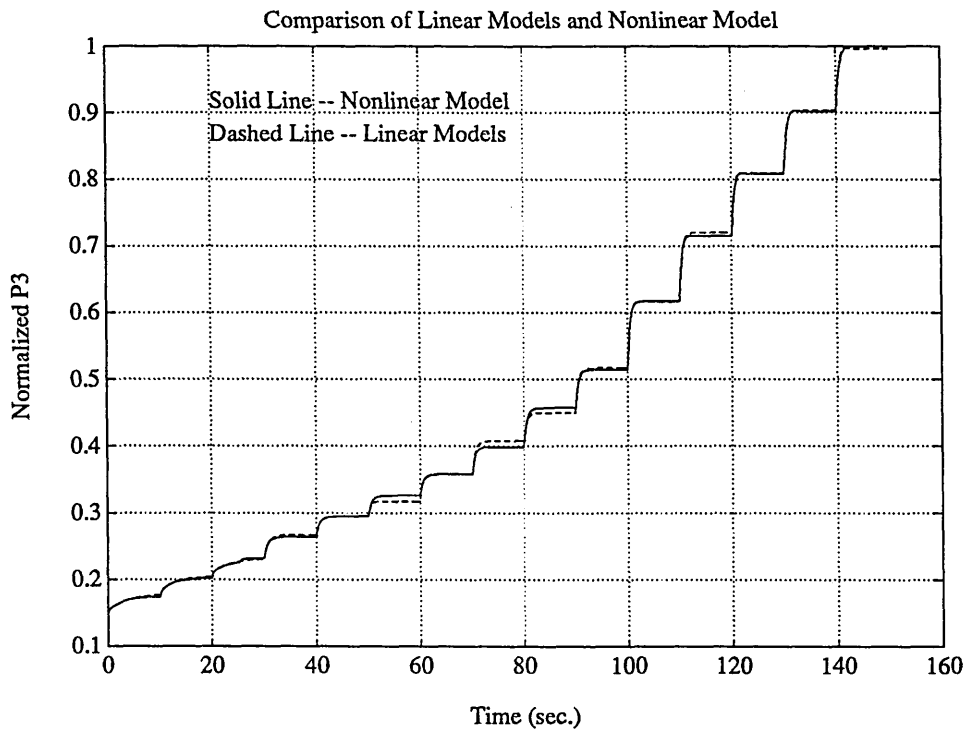


Figure 4.42: Comparing Linear and Nonlinear Model: Turbofan Engine

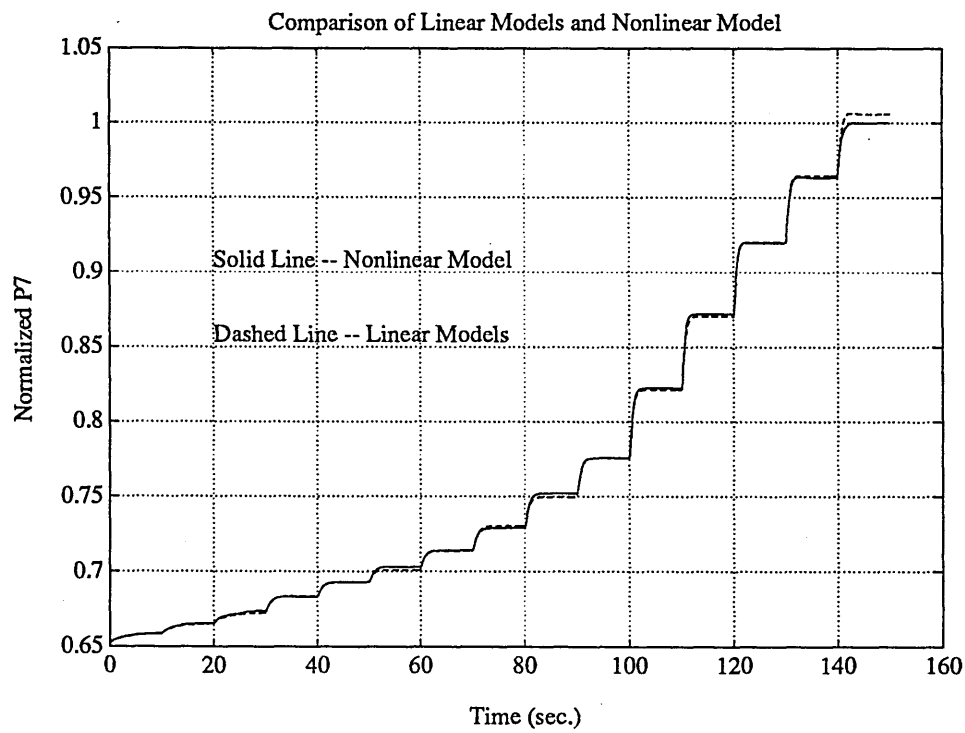
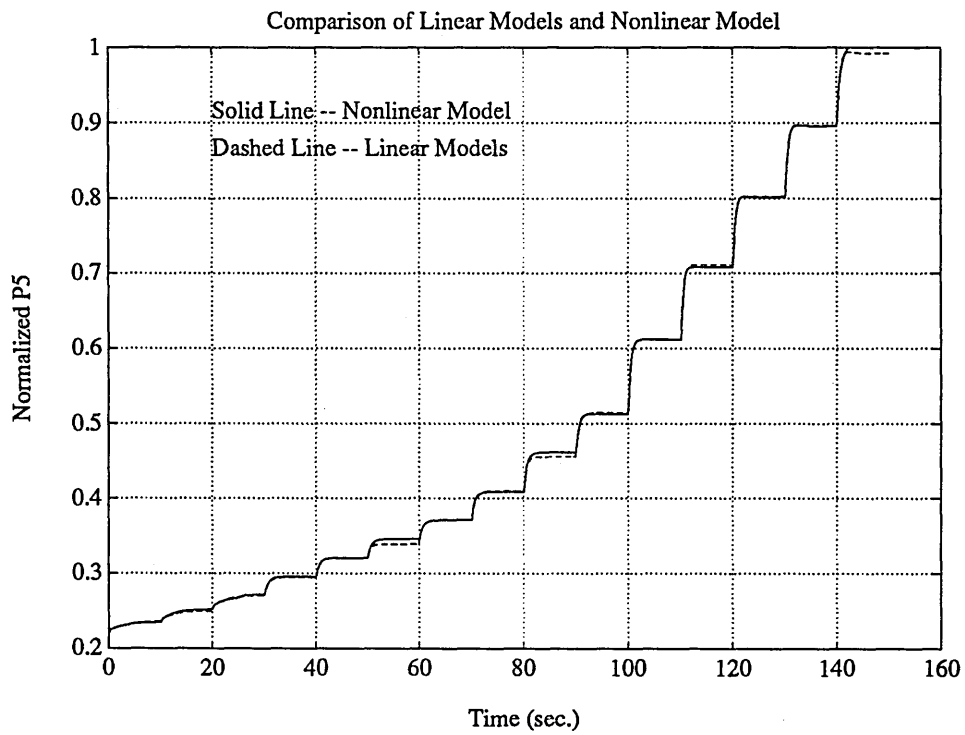


Figure 4.43: Comparing Linear and Nonlinear Model: Turbofan Engine

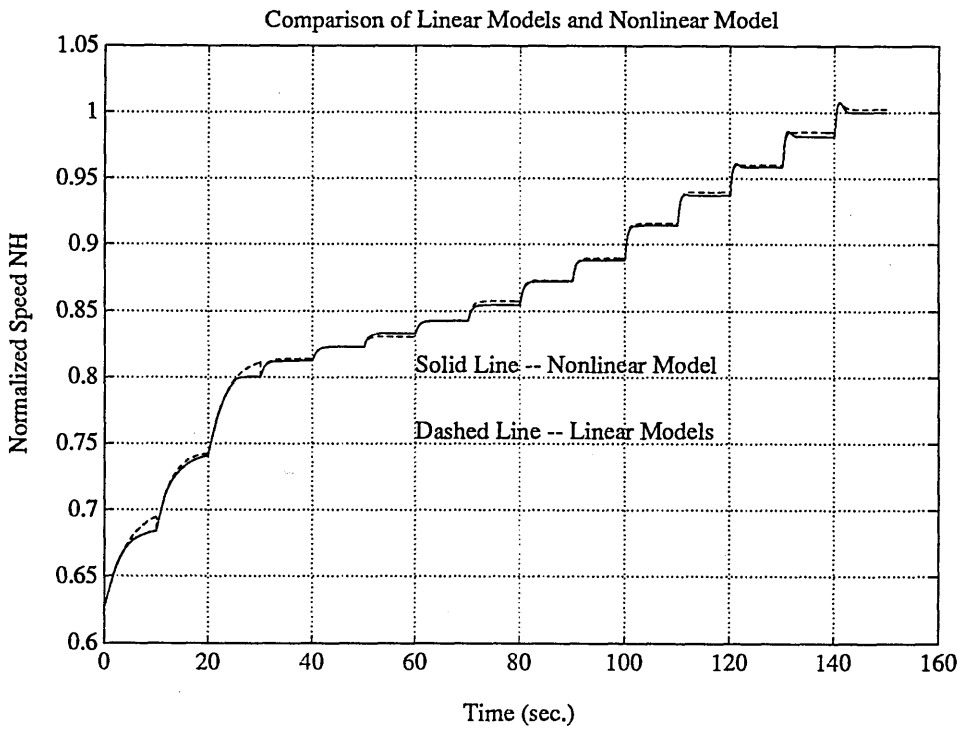
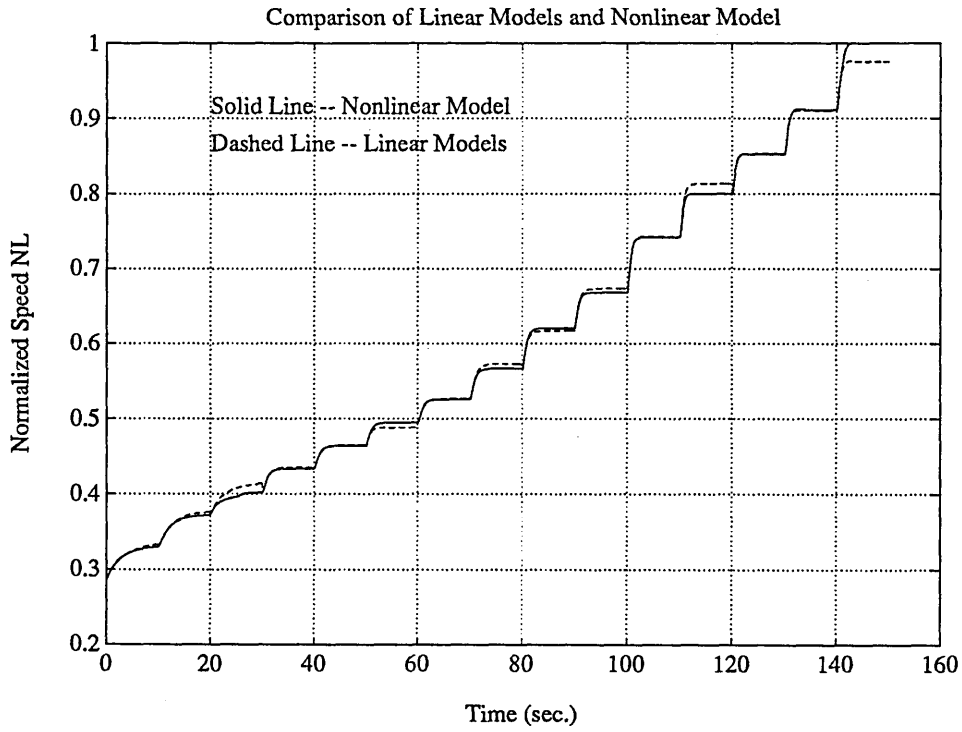


Figure 4.44: Comparing Linear and Nonlinear Model: Turbofan Engine

Chapter 5

Nonlinear Controller Designs for Gas Turbine Engines

SUMMARY

An approach to designing multivariable gain scheduled controllers for gas turbine engines is described in this chapter. The synthesis procedure is based on linearising a nonlinear engine model about a set of closely-spaced steady-state operating points and applying the linear synthesis methods. In this way, the nonlinear control problem is reduced to a series of linear control problems. Nonlinear feedback controllers whose feedback gains vary with engine non-dimensional shaft speed are then constructed. The objective of improving engine performance while ensuring engine safety has been translated into performance requirements on the compressor characteristics, through which the performance of the controllers are evaluated.

5.1 Introduction

In the present study, the performance requirements for the gas turbine engines can be summarised as:

- Rapid achievement of the required thrust changes.
- Avoiding compressor surge and turbine over-temperature.

The open-loop fuel controllers used in the previous chapter have achieved a satisfactory degree of performance. However, they are conservative in terms of usage of the available compressor surge margins during accelerations, and also no clues can be given as to how to improve the performance by manipulating a single fuel input. Furthermore, since only the open-loop controls are used, the achieved performance will deteriorate in the face of disturbances, measurement noises and engine parameter variations.

The use of modern control design techniques has been increasingly studied for a potential replacement to the conventional open-loop fuel controller. This is also encouraged by the recent developments in engine manufacturing technology which have made it possible for elements in engine components variable geometry to be used as potential control inputs. The multivariable controller will greatly improve engine performance if the variable geometries are appropriately controlled in co-ordination with fuel flow.

Since engine dynamics vary significantly over the entire operating range, linear multivariable controllers can perform well only around the steady-state points at which the linear design models are generated. To provide an adequate performance for a gas turbine engine over the entire operating range, a nonlinear multivariable feedback controller is required.

Unfortunately, systematic nonlinear design techniques are not available, especially for a nonlinear system such as a gas turbine engine. However, since there is a rich collection of linear design techniques, and some insights have been gained into engine operating characteristics from simulation study when using open-loop fuel controller, it is worthwhile to combine both, as a direct extension of linear design techniques, to produce practical nonlinear controllers for gas turbine engines. One approach, known as gain scheduling, has been used to design several gain

scheduled controllers for gas turbine engines. Sain [131] proposed a total synthesis method, which consists of designing a set of linear controllers and scheduling the gains against non-dimensional speed. Polley [61] used Edmunds' closed-loop synthesis methods to design a nonlinear controller for improved performance over the entire operating range [132]. From these previous works, it seems that gain scheduling is the only practical and pragmatic methodology for controlling a nonlinear engine system.

In this chapter, nonlinear controllers which could provide acceptable performance are designed. The performances of these controllers are validated based on the practical performance requirements interpreted on the compressor characteristics. A single parameter, non-dimensional shaft speed, has been used to schedule the gains of linear compensators. This selection is based on the author's understanding about dynamics of the engines used in the present work, and also reference to the previous works.

5.2 Gain Scheduling Approach

Gain scheduling has been considered as an alternative to adaptive control by Åström and Wittenmark [133]. The main idea of designing a gain scheduled controller is to break the control design process into two steps. First, one designs local linear controllers based on the linear design models of the nonlinear system at different operating conditions. Second, a global nonlinear controller is obtained by interpolating or scheduling the gains of the local linear controllers. An illustrative diagram for the gain scheduling scheme is shown in Figure 5.1.

The requirements for using this approach to a successful design depend on the selection of auxiliary measurements to characterise the variations of system dynamics and nonlinearities. Although this is an open-loop compensation, it has the advantage that the controller can quickly cope with the nonlinearities as the engine moves from one operating point to another.

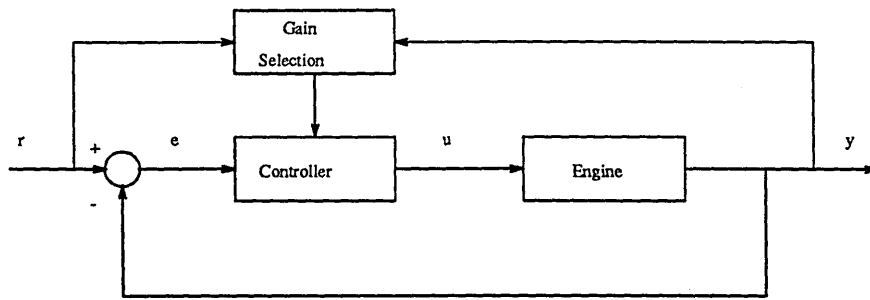


Figure 5.1: The Diagram Illustrating Gain Scheduling Scheme

However, gain scheduling remains an *ad hoc* methodology. Because the control algorithms are designed off-line with a priori information [134], the main burden of gain scheduling is identifying the proper control design to be used and effecting a smooth transfer from one design to another during system operations. Furthermore there is no precise analytical relationships between the compensator gains of neighbouring operating points. Also the robustness, performance and even nominal stability properties of the resultant nonlinear controllers are not addressed explicitly in the design process. Such properties are inferred from extensive computer simulations after designs are completed. One advantage of the gain scheduling approach is its potential to incorporate linear robust control methodologies into nonlinear controller designs.

Based on the previous works, the success of designing a good nonlinear controller depends upon the following:

- Having a smoothly and gradually changing nonlinear dynamic system.
- Using a simple, fixed controller dynamic structure.
- Selecting appropriate parameters, which reflect the system dynamics, to schedule against.
- Using a sufficient number of operating points to cover the operating range.

5.2.1 Selection of Scheduling Variable

Since gain scheduled controller design is based on linearisations, the limitation of capturing the nonlinearities can be addressed in the appropriate selection of the scheduling variables. Two prominent guidelines for selection are:

- The scheduling variable should capture the plant's nonlinearities.
- The scheduling variable should vary slowly.

These guidelines have been justified through simulation and implementation reported in the recent works by Rugh [135], Shamma and Athans[136] who also attempted to give them a theoretical foundation.

The limitations of gain scheduling can be deduced from these two guidelines. More explicitly, the guidelines of capturing the plant's "nonlinearities" and "varying slowly" in fact place fundamental limitations on the achievable performance of current gain scheduling practice.

A gain scheduled controller is based on a collection of linear time-invariant approximations to a nonlinear system at fixed operating points. In this sense, the guideline of capturing the nonlinearities is simply a reminder that the design models are only linearised approximations to the nonlinear system. Similarly, the slow variations guideline is a reminder that design models explicitly assume a fixed operating condition. If these design models are not an accurate reflection of the actual system, then one cannot demand guaranteed performance of the overall design [137].

The case of the restriction to slow variations on the scheduling variable most likely is due to the nature of scheduling algorithms. More precisely, the scheduling of controller gains is such that good performance may be expected for any fixed interpolated operating condition. However, performance may deteriorate rapidly as one experiences rapid changes over the range of operating conditions.

5.2.2 Controller Structure

The judicious selection of controller structure can lighten the burden in the process of designing gain scheduled controllers. This also serves as an important connection between the linear compensators and the nonlinear controllers. Two forms of controller structure have been considered to be appropriate:

- Simple Proportional and Integral (PI) or Proportional, Integral and Derivative (PID) structure.
- Observer-based structure which consists of the nominal design model plus observer and regulator gains.

In the first case, Nett [138] has pointed out that using the PI or PID control structure is equivalent to scheduling the residues of the controllers which makes them attractive for practical implementations. On the other hand, the observer structure of a controller mainly resulted from design techniques such as Linear Quadratic Gaussian with Loop Transfer Recovery (LQG/LTR) or H_∞ . Hyde [139] has successfully designed a gain scheduled controller based on H_∞ design technique using a generic VSTOL aircraft model and also given justifications for using observer-based control structure for scheduling.

5.2.3 Scheduling Functions

The selection of scheduling functions is crucial in the process of designing a gain scheduled controller. The point is if the gains of the resulting linear compensators vary monotonically, polynomial functions of appropriate degree can be found to achieve the required accuracy. To reduce the burdens of the gain scheduled controller design, it is necessary to examine the variations of the linear controller gains, and make decisions of how many gains are selected when scheduling for an adequate performance. Some of the gains may not vary significantly and can be replaced by their average values.

In the present work, the controller gains do not vary monotonically, therefore only linear interpolations on compensator gains are used. The scheduling functions can be written as:

$$F\left(\frac{N}{\sqrt{T_{in}}}\right) = \left(1 - \frac{N}{\sqrt{T_{in}}}\right)F_X + \frac{N}{\sqrt{T_{in}}}F_Y \quad (5.1)$$

The F matrix represents the gains between adjacent design points X and Y . $N/\sqrt{T_{in}}$ is the engine non-dimensional shaft speed, with $N/\sqrt{T_{in}} = 0$ corresponding to the operating point X , $N/\sqrt{T_{in}} = 1$ corresponding to the operating point Y , and $N/\sqrt{T_{in}}$ varying linearly between them.

5.3 Performance Requirements for Control

Two basic performance requirements for engine control are:

- Steady-state performance.
- Transient response.

The latter area is typically what one thinks of when discussing multivariable control design techniques, but meeting steady-state performance requirements is of equal importance for a gas turbine engine. Steady-state performance requirements typically include such features as obtaining the correct thrust level at each flight condition.

The task of satisfying steady-state performance requirements involves generating reference schedules, defining control variables requiring integral trim, and defining sensor and actuator accuracy requirements. Each integrator requires the selection of an engine output variable to schedule and sense to create an error term for the integrator. The integrator then trims the control variable to cause the error term to go to zero, so that the correct steady-state performance can be obtained.

Designing to meet transient response requirements involves defining the control mode structure and accompanying gains such that the engine can be accelerated or

decelerated between steady-state operating points with the required response rate while not exceeding the limitations. The transient controller must also provide adequate regulation at each steady-state operating point [140].

In the present work, the schedule between engine shaft speed and thrust is defined based on the steady-running line data obtained from the previous chapter. The plots of the schedules are shown in Figure 5.2 and 5.3.

These schedules are used when a pilot manipulates the power level angle to achieve a required thrust change. Since the engine thrust cannot be directly measured, such a change could be equivalently translated into the desired change in engine shaft speed based on the schedules. The use of speed as a measure of

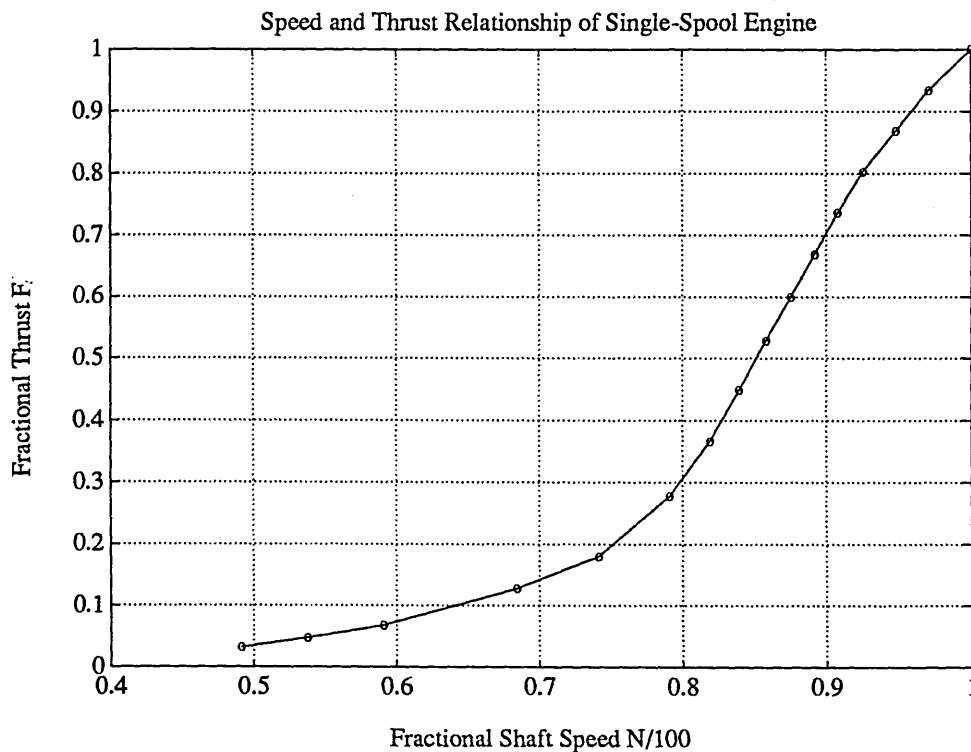


Figure 5.2: Shaft Speed and Thrust Relationship of Single-Spool Engine

thrust level is because the speed response rate dominates the mass flow change rate through an engine, therefore it can be considered as a main factor which effects the engine thrust changes. For the two-spool engine the LP shaft speed is used to indicate the thrust level. The qualitative justifications have been given by Sutton [12] and Maccallum. Typically, the desired thrust change can be selected

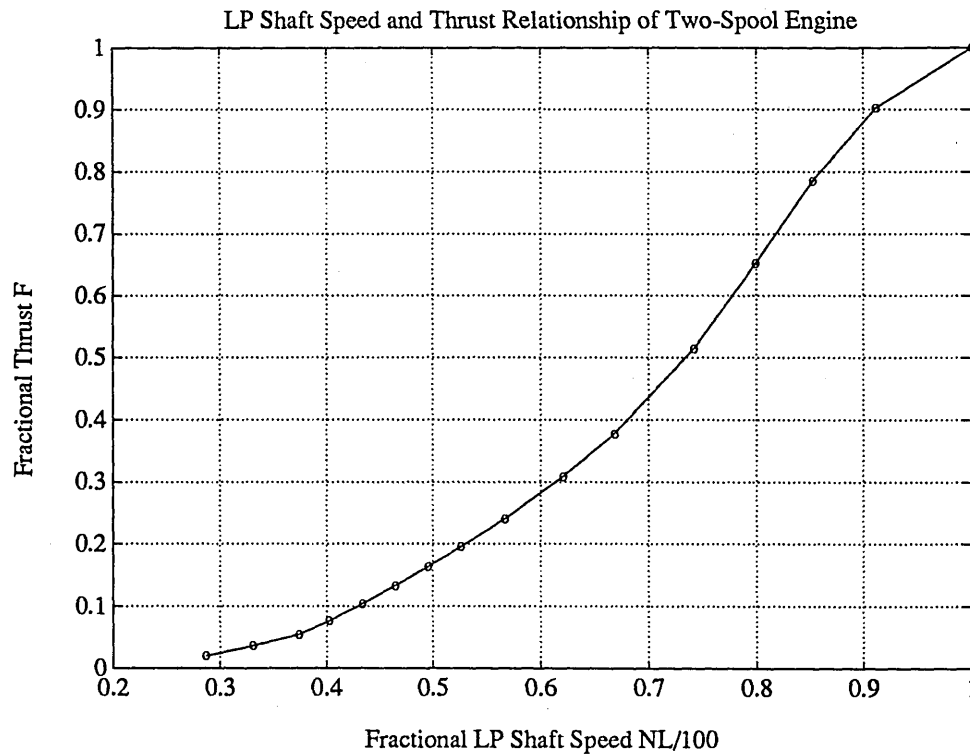


Figure 5.3: LP Shaft Speed and Thrust Relationship of Two-Spool Engine

as:

$$T_f(s) = \frac{1}{(\tau s + 1)^n} \quad (5.2)$$

A set of the curves resulted from function $T_f(s)$ is shown in Figure 5.4.

It should be noted that in the present work, the sensor and actuator dynamics have been neglected.

5.3.1 Surge Line Tracking

Since it is generally difficult to obtain on-line measurement of the non-dimensional mass flow through the compressor, the parameters used to define the compressor surge line are the compressor non-dimensional speed and pressure ratio. A trajectory defined in this way is applicable to all flight conditions.

Using these parameters and bearing in mind the performance and safety requirements of an engine, an ideal transient tracking trajectory can be defined on the compressor characteristics. This is formulated as follows: firstly a factor,

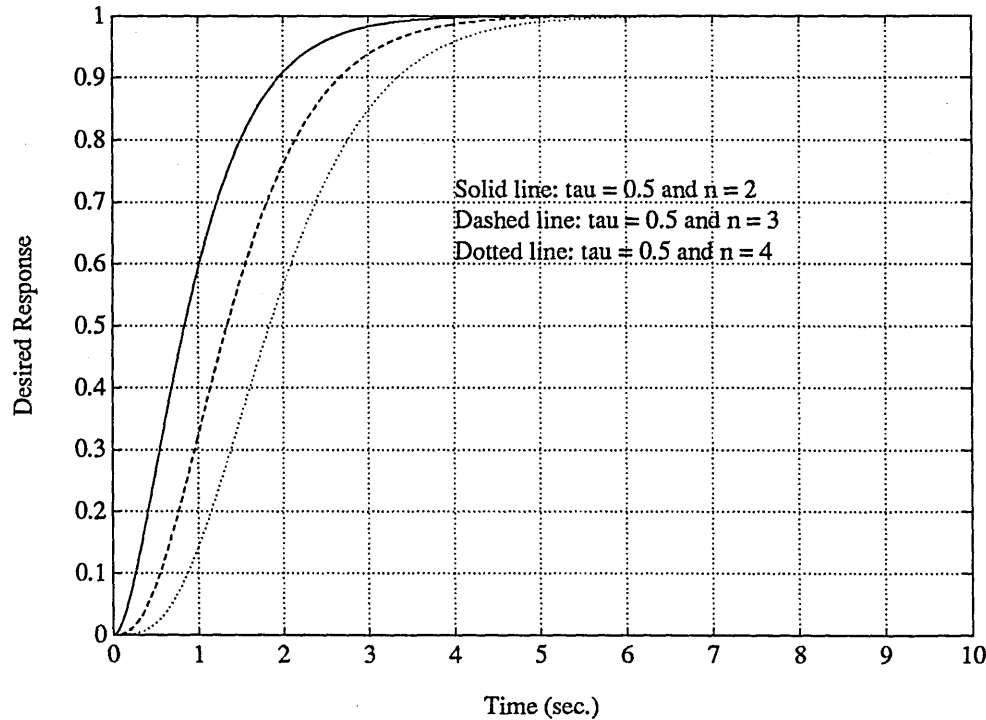


Figure 5.4: The Possible Selection of Desired Responses

typically 0.95, is used to lower the actual surge line to allow for the possible deterioration of the surge line during transients, secondly selecting a point (e.g. point 1 on Figure 5.5 to 5.8) on the lowered surge line for the switching towards the steady-running line leading to the desired steady-state take-off condition. The switching point 1 on the ideal transient tracking schedule is approximately selected. A helpful guideline is to use the plot of turbine inlet temperature against non-dimensional shaft speed. This selected point is also to keep the turbine inlet temperature below the safety limit. Thus, by measuring the non-dimensional shaft speed, the demanded pressure ratio can be “looked up”, as a result, the maximum compressor delivery pressure can be determined at any instant during accelerations. This pressure will serve as a limit for the actual pressure measured from the compressor, and the error between them is used to generate the control signal.

The tracking lines used in the present study are shown in Figure 5.5 and 5.6. It is noted in Figure 5.6 that a discontinuity (at $N_H/\sqrt{T_{26}} = 550$) is obvious for

the two-spool engine. This is due to the closing of bleed valve at that constant speed which increases the HP compressor delivery pressure [141]. For comparison, the formulated tracking lines are also plotted on the compressor characteristics as shown in Figure 5.7 and 5.8. The control strategy to achieve these performance

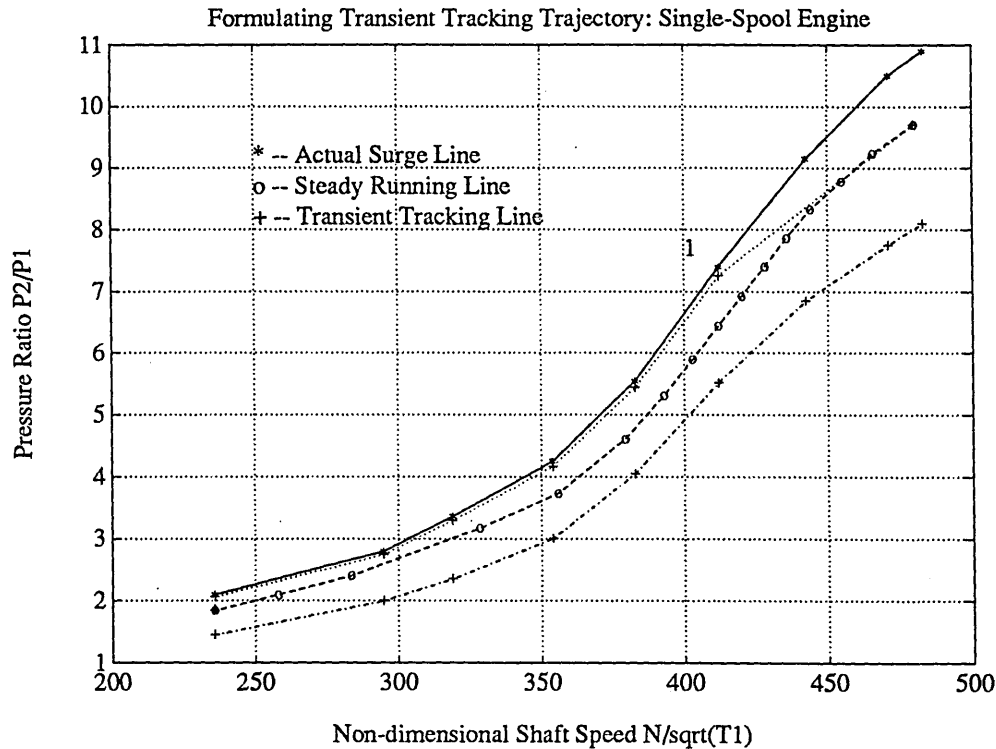


Figure 5.5: The Transient Tracking Trajectory of Single-Spool Engine

requirements and constraints is illustrated in Figure 5.9.

5.4 Linear Controller Designs

As the first step to design a gain scheduled controller, a set of linear controllers has firstly to be designed. The present section illustrates such a design sequence for one selected linear model for both engines. Similarly controllers can be designed for all other operating points, with small differences in the design parameters to vary the crossover frequencies and consequently the bandwidth of the closed-loop system. The design specifications will be presented according to the performance requirements, modelling uncertainties and noise and disturbance rejection expected from

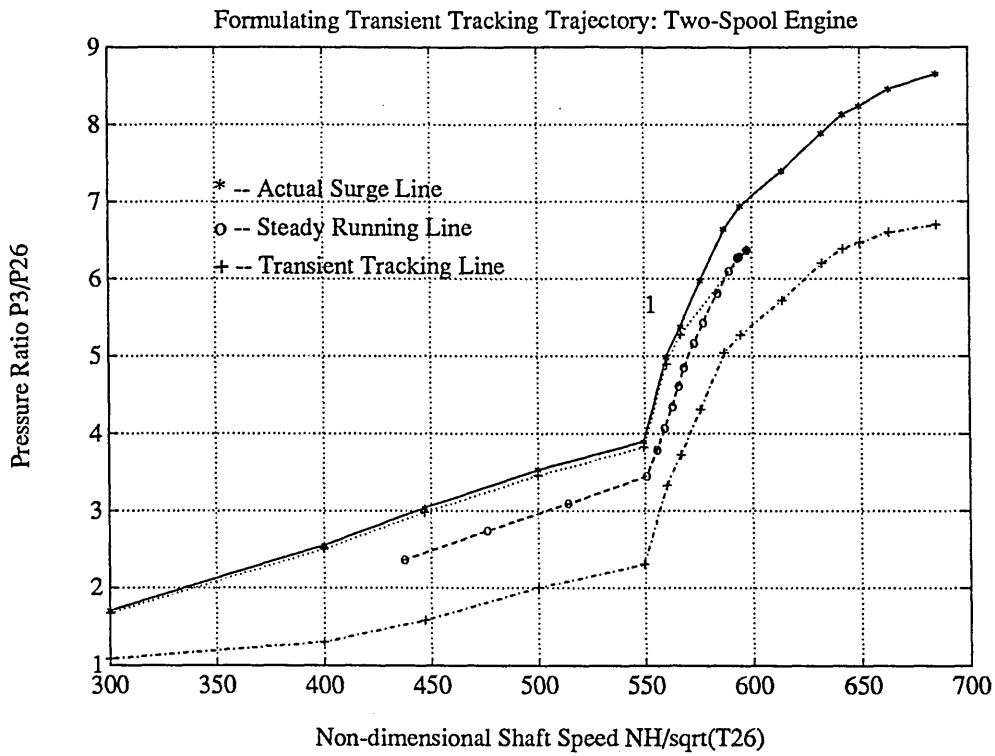


Figure 5.6: The Transient Tracking Trajectory of Two-Spool Engine

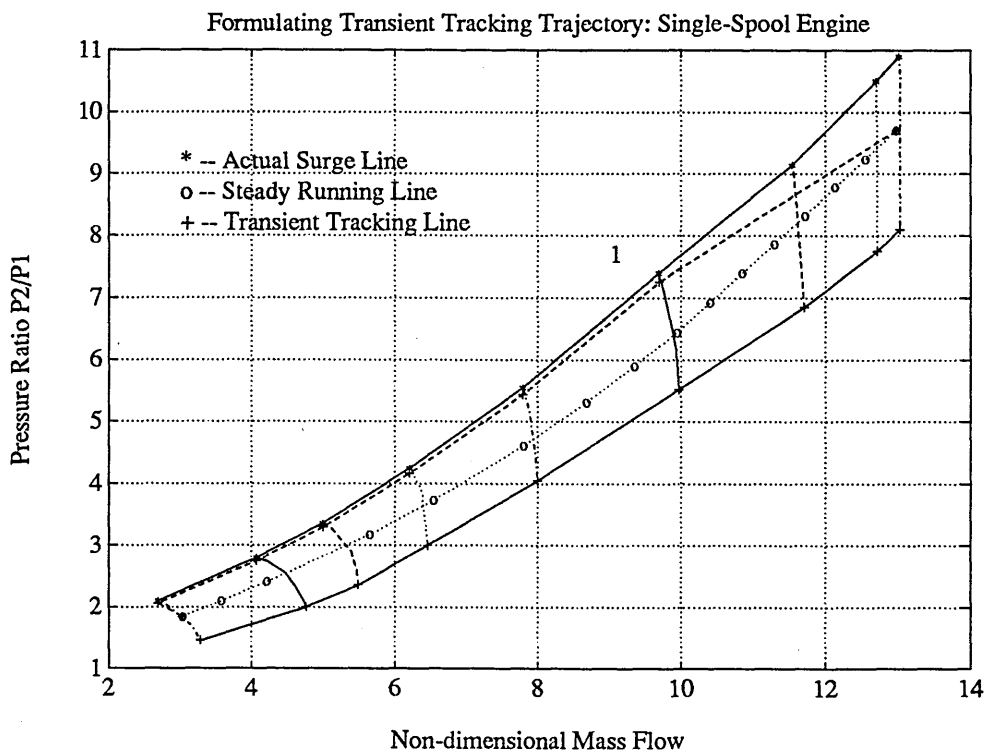


Figure 5.7: The Transient Tracking Trajectory of Single-Spool Engine

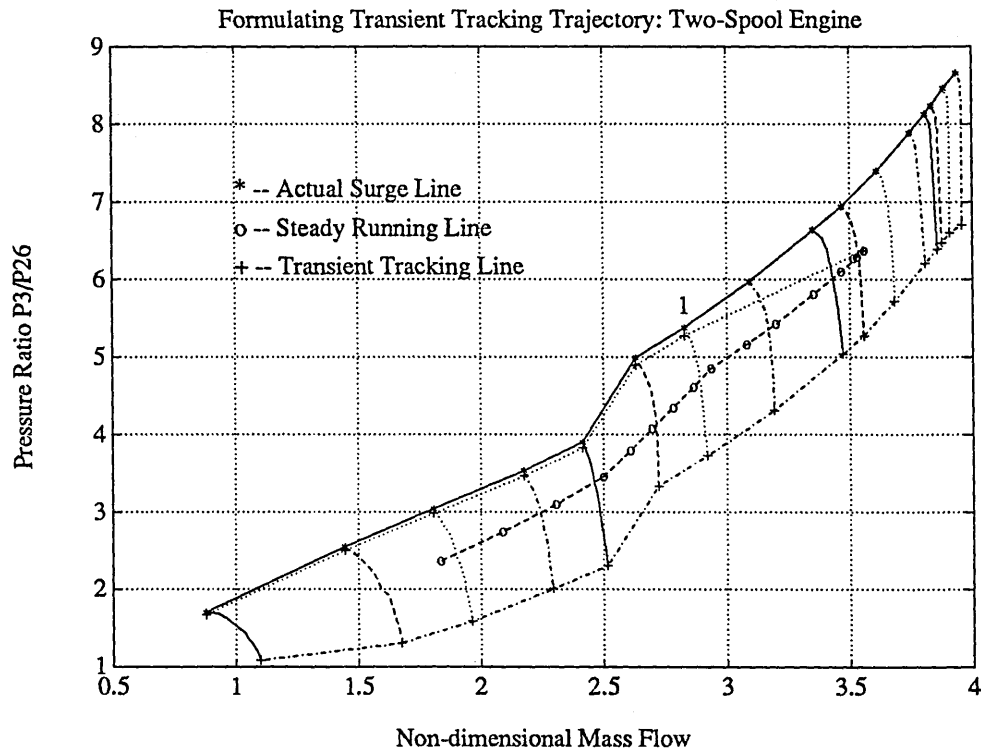


Figure 5.8: The Transient Tracking Trajectory of Two-Spool Engine

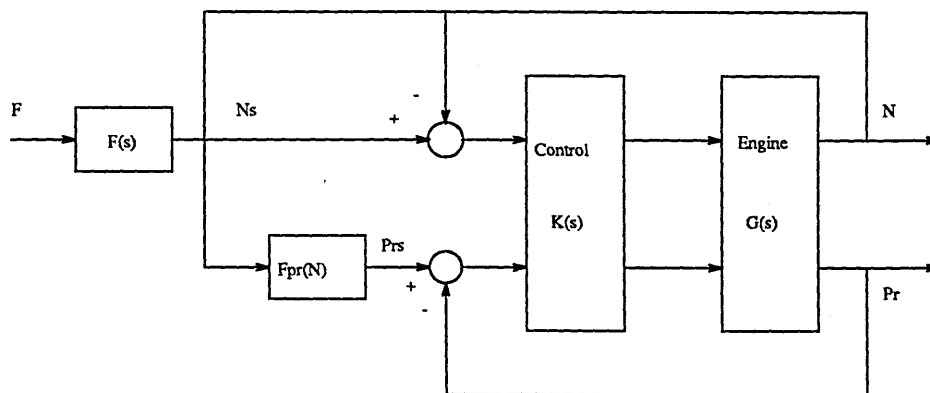


Figure 5.9: Tracking the Pressure Ratio on the Surge Line

an engine from the control point of view. A desired crossover frequency for this system is about 10 rad/sec . This is because in this range, the linear design models are asserted to be valid.

5.4.1 Design Specifications

Figure 5.10 shows the closed-loop configuration of a linear model, $G(s)$, of an engine, with the linear compensator, $K(s)$, to be designed.

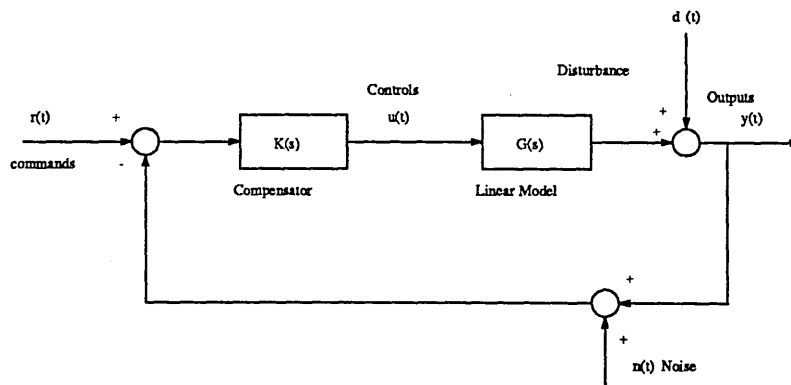


Figure 5.10: The Closed-Loop System

From Figure 5.10 the following equation can be derived:

$$y = GK(I + GK)^{-1}r + (I + GK)^{-1}d + GK(I + GK)^{-1}n \quad (5.3)$$

Equation 5.3 suggests that in order to have good command following and good disturbance rejection, GK has to be large and consequently the minimum singular value $\underline{\sigma}(GK)$ should be large in the command and disturbance's frequency regions. For good noise rejection GK has to be small and consequently the maximum singular value $\bar{\sigma}(GK)$ should be small in the frequency regions containing noise. Furthermore, according to Lehtomaki [142], to have a robust design, GK has to be small at the frequencies where modelling is uncertain, which implies that $\bar{\sigma}(GK)$ has to be small at these frequencies.

The nonlinear models of the engines are valid for frequencies up to approximately 50 rad/sec (as shown in the section of linear model validation in chapter 4), which indicates that the linear design models are good up to the same frequencies.

Measurement noise $n(t)$ generally occurs at high frequencies ($\omega \geq 20 \text{ rad/sec}$) and disturbances $d(t)$ generally occurs at low frequencies ($\omega \leq 0.2 \text{ rad/sec}$). To provide maximum command following and disturbance rejection, it is desired that:

$$\underline{\sigma}(GK(j\omega)) \geq 20\text{dB}, \omega \leq 0.2 \text{ rad/sec} \quad (5.4)$$

To cope with high frequency modelling errors and stability:

$$\overline{\sigma}(GK(j\omega)) \leq -20\text{dB}, \omega \geq 20 \text{ rad/sec} \quad (5.5)$$

Figure 5.11 summarises the frequency-domain performance specifications. Performance and robustness will be achieved by designing the compensator to ensure that the singular value plots satisfy the required frequency domain constraints.

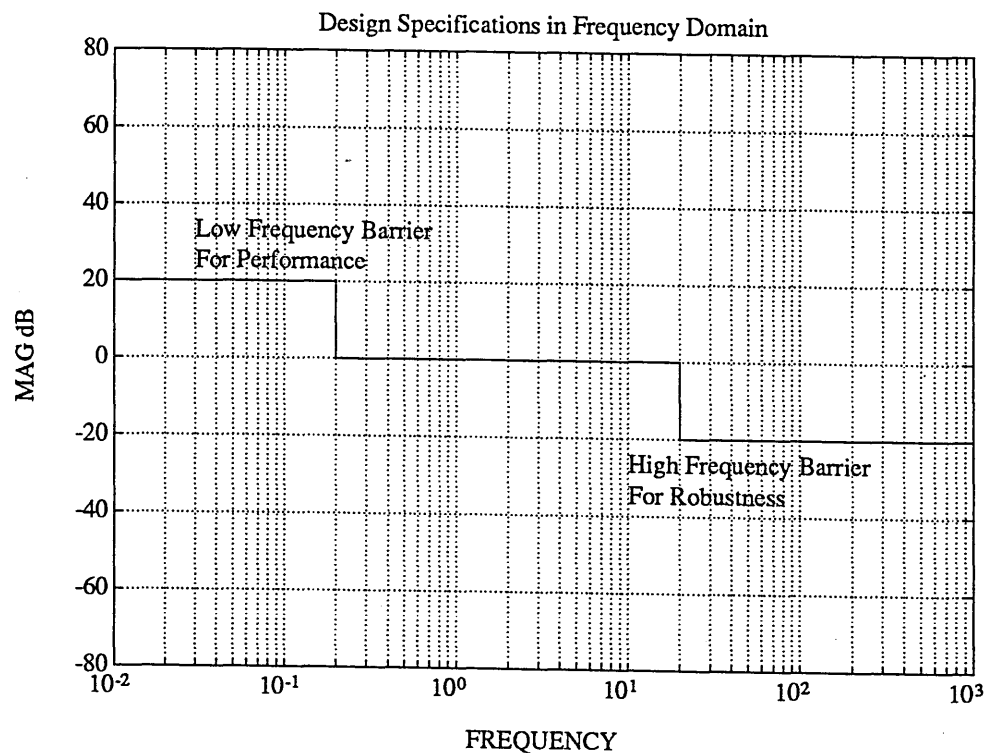


Figure 5.11: Frequency Domain Design Specifications

Control of the gas turbine engine specifically requires:

- Fast thrust response without overshoot,
- Zero steady-state error.

The fast thrust response requirement is fulfilled by designing to achieve a large bandwidth of the closed-loop system. The zero steady-state error requirement is met by using the integrators to ensure zero steady-state error.

Because of the presence of nonlinearities and control saturations, it is decided, in the present work, that the crossover frequency of all singular values should be around 5 rad/sec at the low speed operating points and around 10 rad/sec at the high speed operating points.

These performance requirements may be summarised up in terms of requirements for good feedback control:

- Low-frequency command following.
- Low-frequency disturbance rejection.
- Insensitivity to sensor error.
- Robustness to unmodelled high-frequency dynamics.
- Insensitivity to low-frequency modelling errors.

5.4.2 Selecting Design Model

The linear design models used to illustrate the design technique are selected at the middle of the engine operating range for both engines. This is corresponding to 85% of engine maximum speed and represents the nominal engine operating condition. The open-loop singular value plots of these linear design models are shown in Figure 5.12 and 5.13.

5.4.3 Design Using Closed-loop Synthesis

Closed-loop synthesis is a frequency domain design technique which uses the closed-loop Nyquist and Bode plots. This method was first proposed by Edmunds [48] and further refined by Nett. The detailed procedure of algorithm development

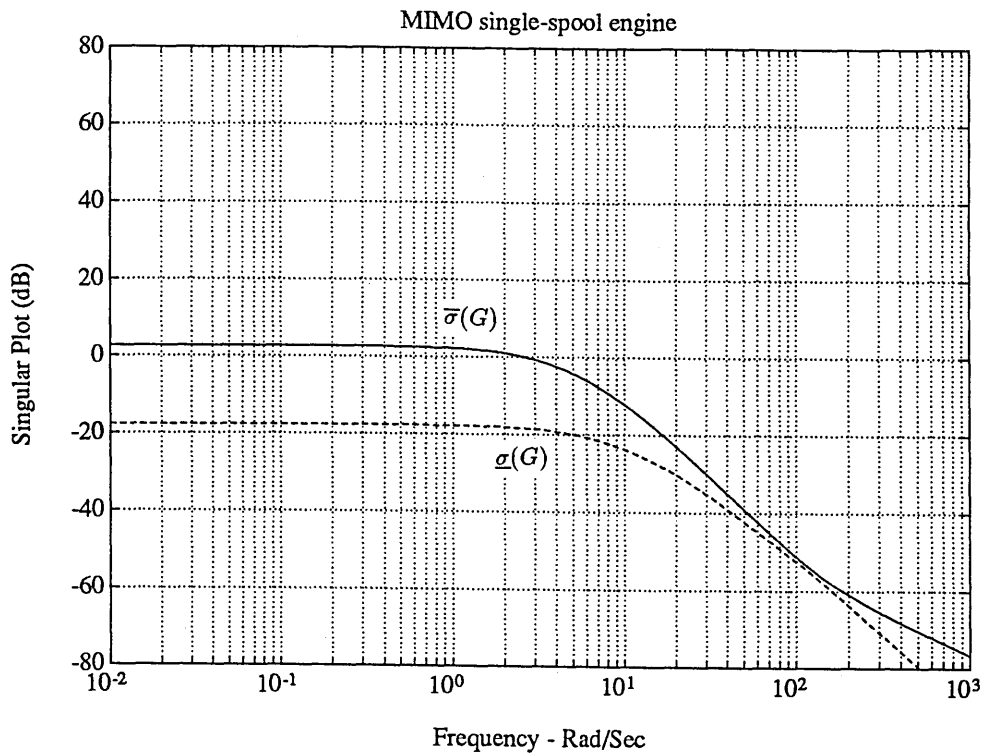


Figure 5.12: The Singular Value Plot for Single-Spool Engine

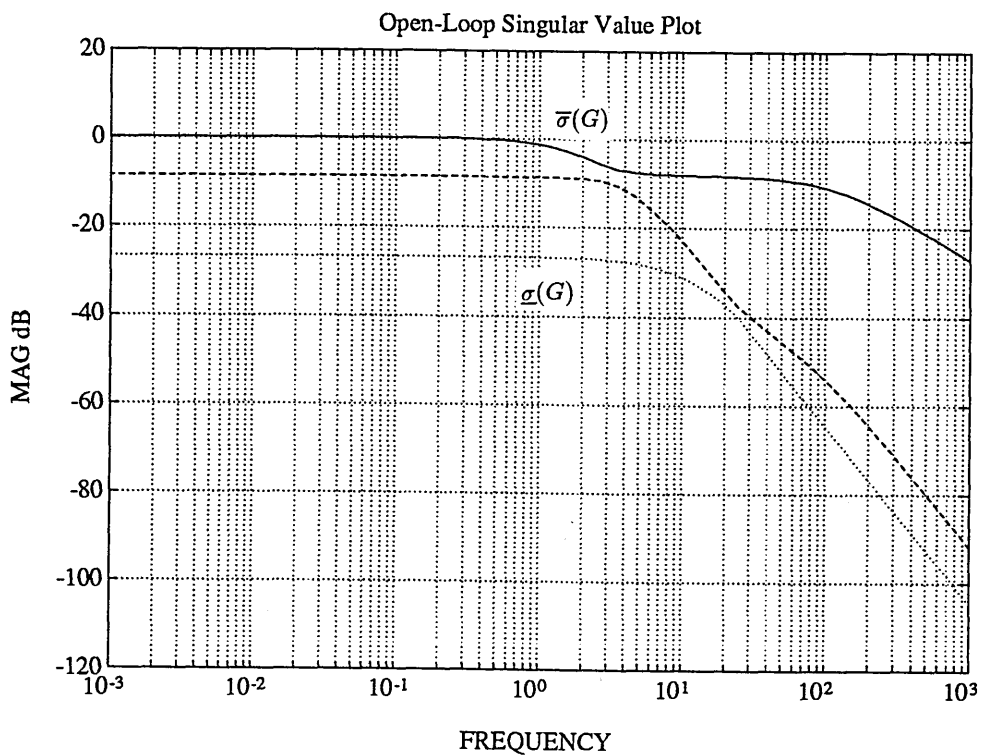


Figure 5.13: The Singular Value Plot for Two-Spool Engine

and the underlying design philosophy have been given by Maciejowski [143]. The advantage of using this method is that based on the performance requirements on the closed-loop system, an optimal PI controller can be synthesised.

By specifying the dynamic controller $K(s)$ shown in Figure 5.10 to have PI structure, the parameters of the PI controller are estimated by minimising the mean square error between the desired closed-loop response and the actual closed-loop response. This design method consists of the following four main steps [131]:

- Specification of desired closed-loop transfer function matrix.
- Selection of multivariable compensator structure (proportional or proportional/integral, etc.).
- Computation of compensator gains.
- Closed-loop performance evaluation.

In the present work, for the single-spool engine, the design of a 2-input and 2-output controller is demonstrated. The fuel flow is used to control the engine thrust, and the final nozzle area is used to control the compressor pressure ratio (or compressor delivery pressure). The desired closed-loop response is therefore selected as:

$$T_d(s) = \begin{bmatrix} a_1/(s + a_1) & 0 \\ 0 & a_2/(s + a_2) \end{bmatrix} \quad (5.6)$$

where $a_1 = 10$ and $a_2 = 10$.

Corresponding to this desired response, the controller $K(s)$ is:

$$K(s) = \begin{bmatrix} kp_{11} + ki_{11}/s & kp_{12} + ki_{12}/s \\ kp_{21} + ki_{21}/s & kp_{22} + ki_{22}/s \end{bmatrix} \quad (5.7)$$

Using the Multivariable Frequency Tool Box in Matlab, the achieved closed-loop frequency response and desired response are shown in Figure 5.14. It can be seen that within the system bandwidth, the desired response and achieved response are in good agreement.

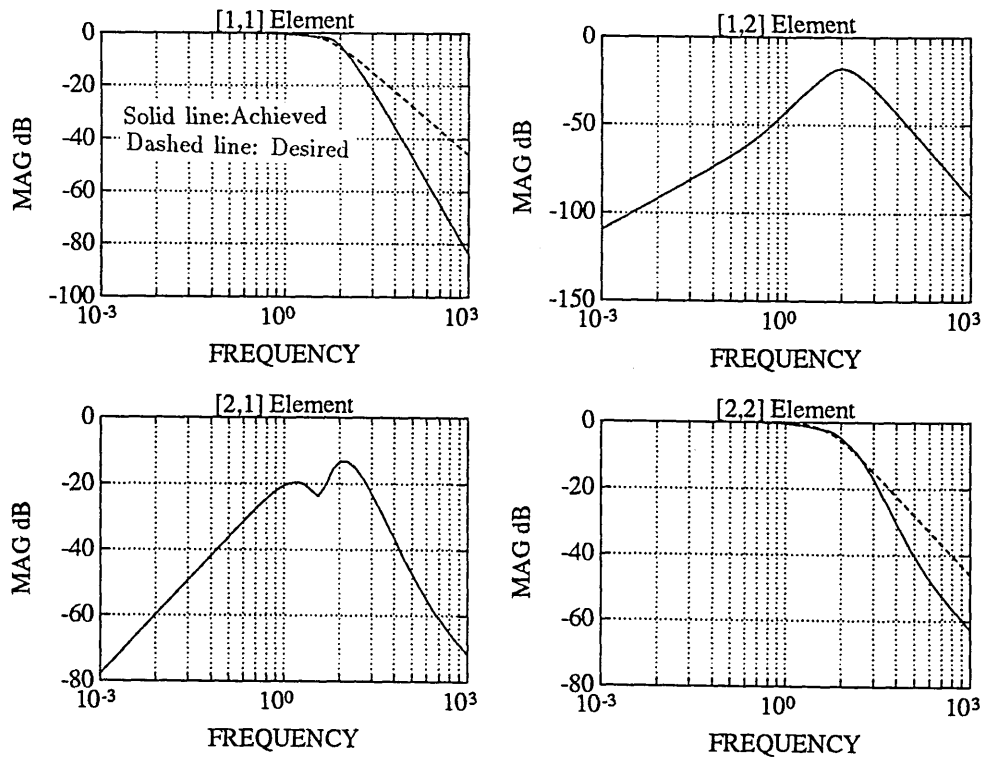


Figure 5.14: Closed-Loop Frequency Response

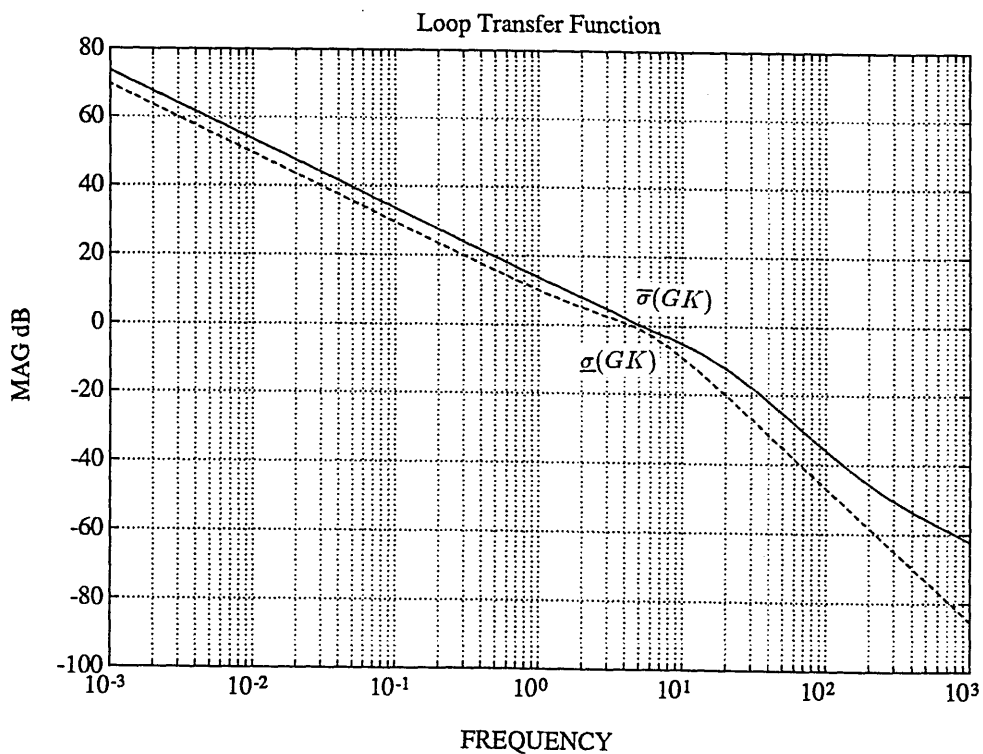


Figure 5.15: Singular Value Plot of Loop Transfer Function

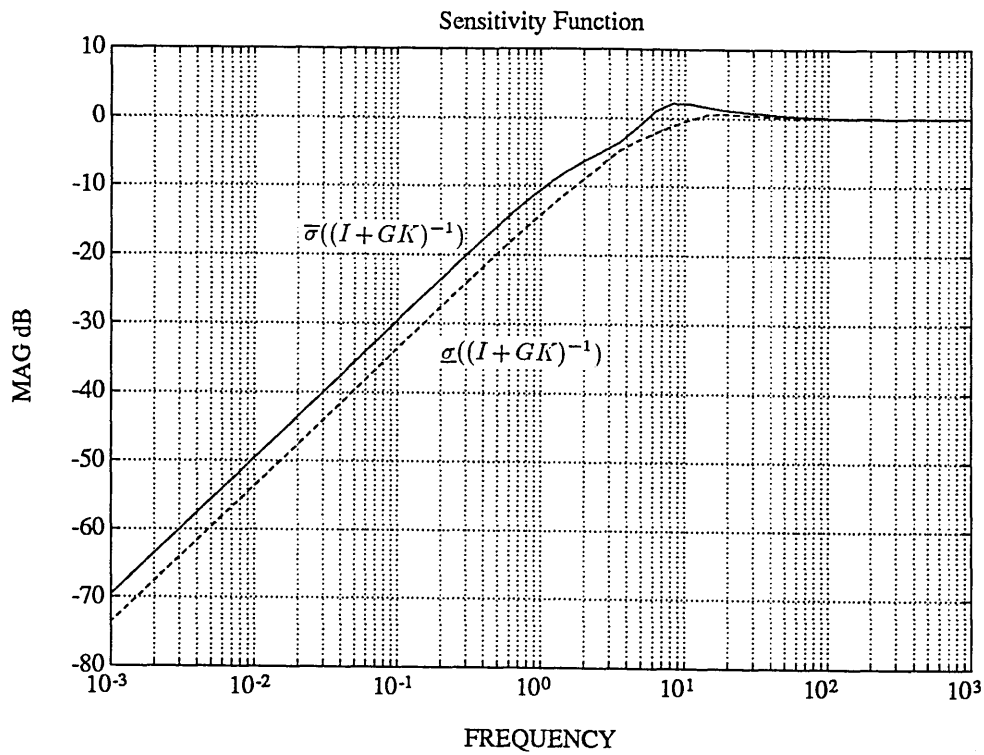


Figure 5.16: Singular Value Plot of Sensitivity Transfer Function

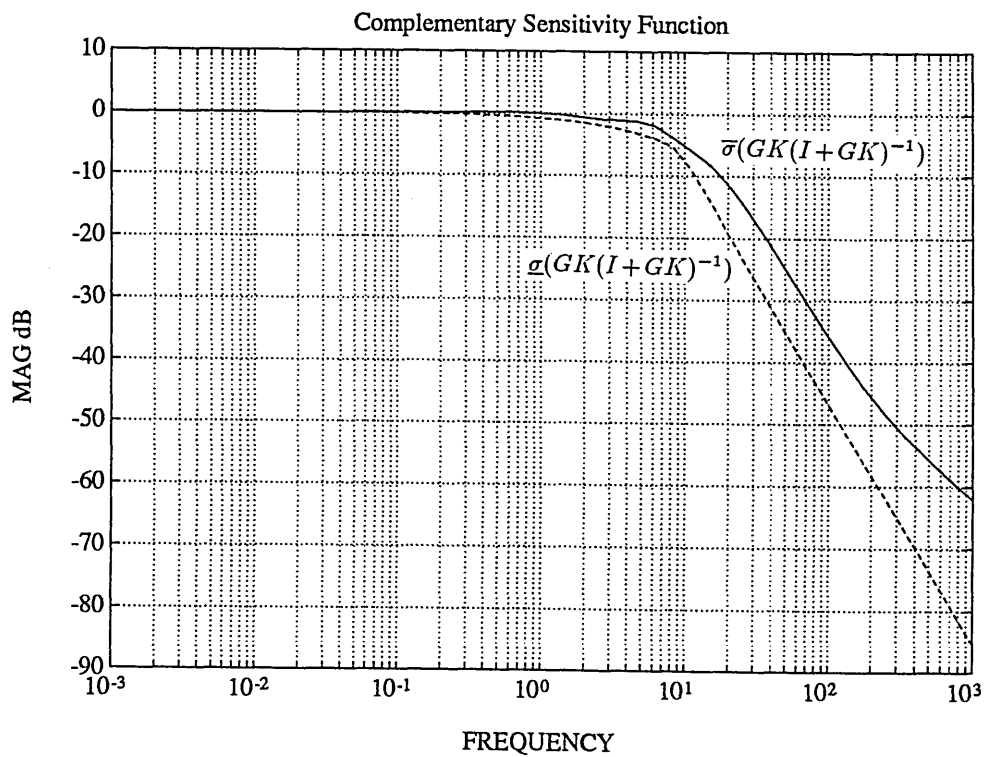


Figure 5.17: Singular Value Plot of Closed-Loop Transfer Function

Figures 5.14 to 5.16 show the characteristics of three singular value function. The singular value plot of the loop transfer functions (Figure 5.14) demonstrates satisfactory command following and disturbance rejection characteristics since the minimum singular value $\underline{\sigma}(GK)$ is large with respect to unity (or 0 dB) at frequencies below the desired crossover. For frequencies above crossover, since the maximum singular value $\bar{\sigma}(GK)$ is small with respect to unity (or 0 dB), sensor noise can be satisfactorily rejected and the stability of the closed-loop system will be robust to unmodelled high-frequency dynamics. The closed-loop transfer function singular value $\sigma(GK(I+GK)^{-1})$ plot (Figure 5.15) shows similar robustness properties to unmodelled high-frequency dynamics. Figure 5.16 shows the singular values of the sensitivity transfer function $\sigma((I+GK)^{-1})$. The plot indicates that the closed-loop system will be insensitive to low-frequency engine modelling errors since the maximum singular value is small with respect to unity (or 0 dB) at frequencies below the desired crossover.

Figure 5.18 to 22 show the results of a similar controller for the two-spool engine. This controller has 3-input and 3-output the outputs being the fuel flow, final nozzle area and HP compressor inlet guide vane setting. The desired response $T_d(s)$ and controller $K(s)$ take the form:

$$T_d(s) = \begin{bmatrix} a_1/(s+a_1) & 0 & 0 \\ 0 & a_2/(s+a_2) & 0 \\ 0 & 0 & a_3/(s+a_3) \end{bmatrix} \quad (5.8)$$

where $a_1 = 10$, $a_2 = 10$ and $a_3 = 10$.

$$K(s) = \begin{bmatrix} kp_{11} + ki_{11}/s & kp_{12} + ki_{12}/s & kp_{13} + ki_{13}/s \\ kp_{21} + ki_{21}/s & kp_{22} + ki_{22}/s & kp_{23} + ki_{23}/s \\ kp_{31} + ki_{31}/s & kp_{32} + ki_{32}/s & kp_{33} + ki_{33}/s \end{bmatrix} \quad (5.9)$$

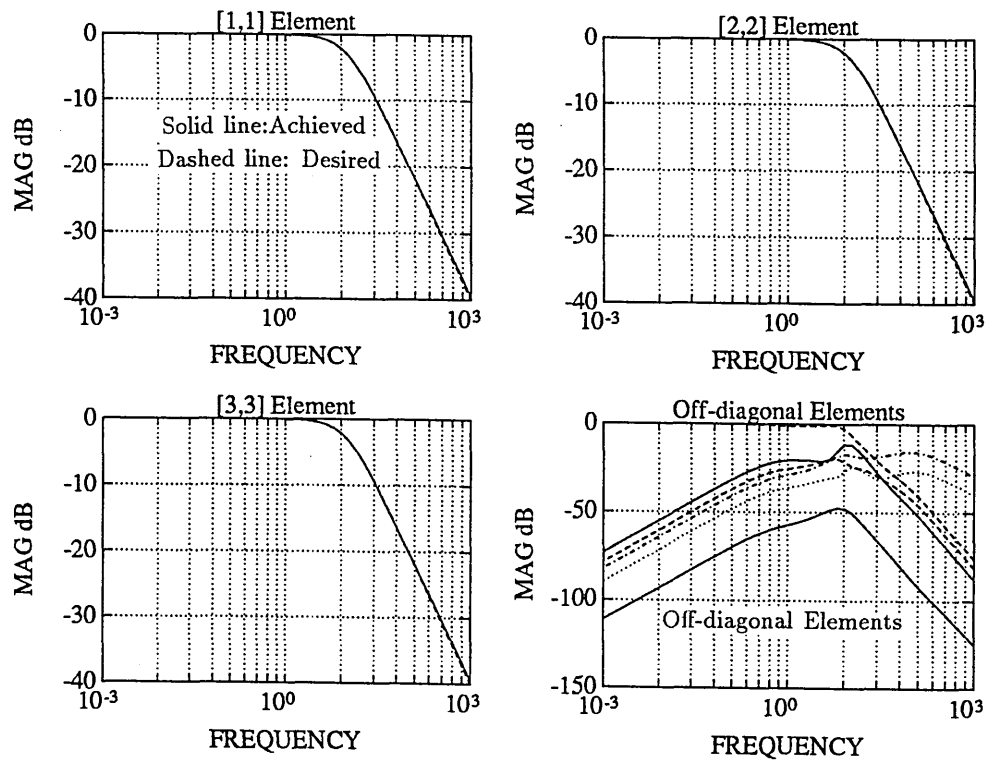


Figure 5.18: Closed-Loop Frequency Response

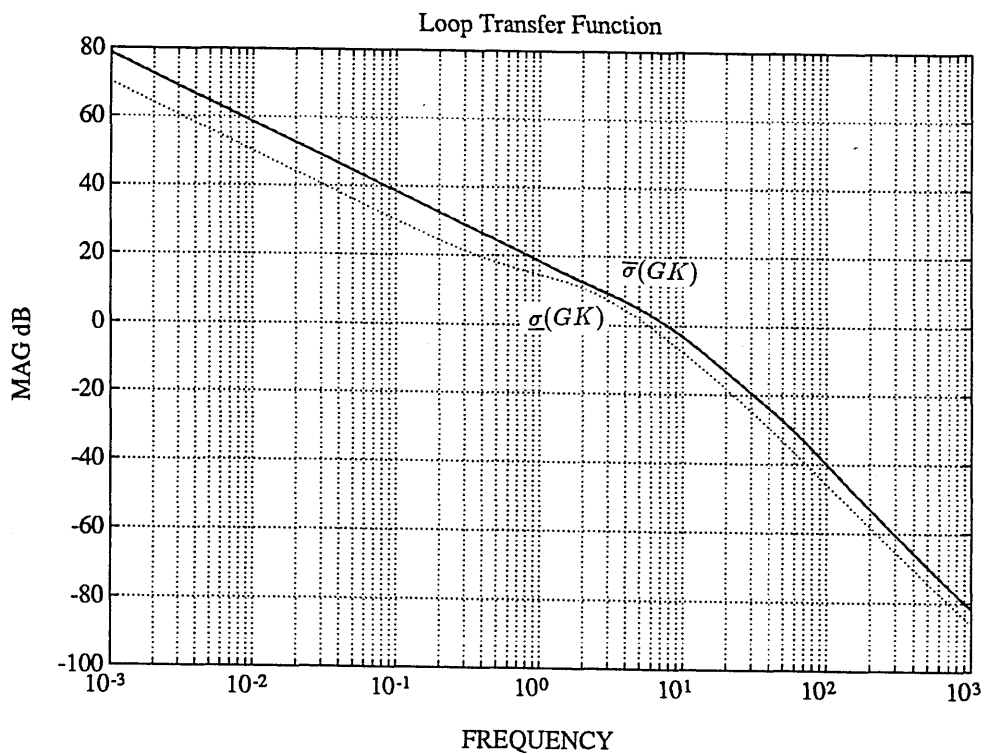


Figure 5.19: Singular Value Plot of Loop Transfer Function

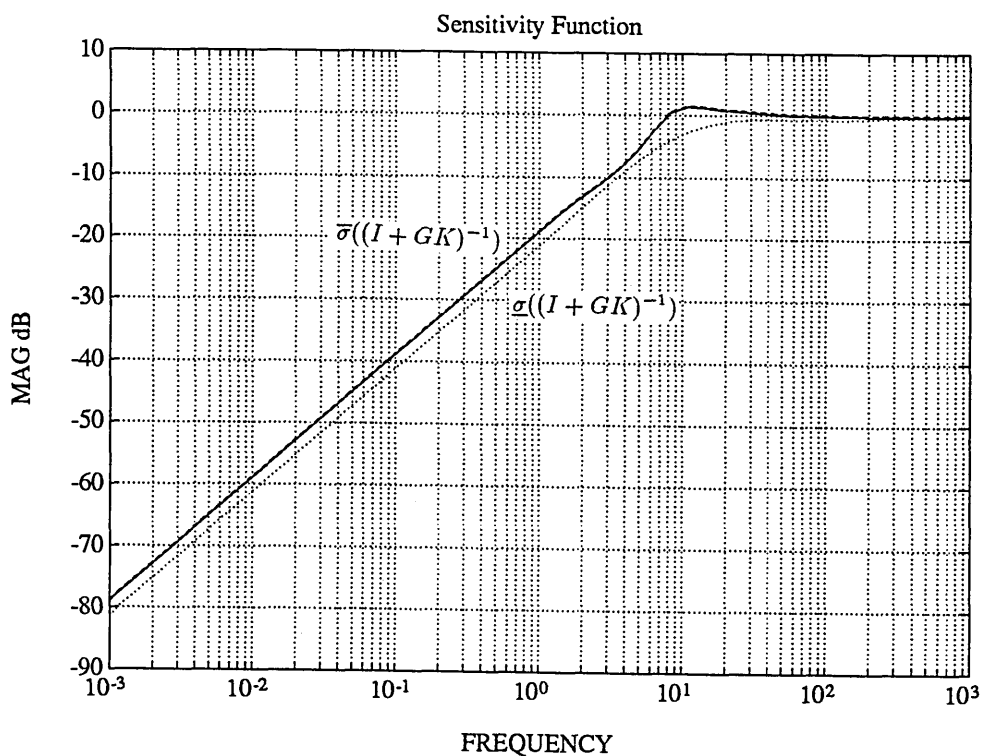


Figure 5.20: Singular Value Plot of Sensitivity Transfer Function

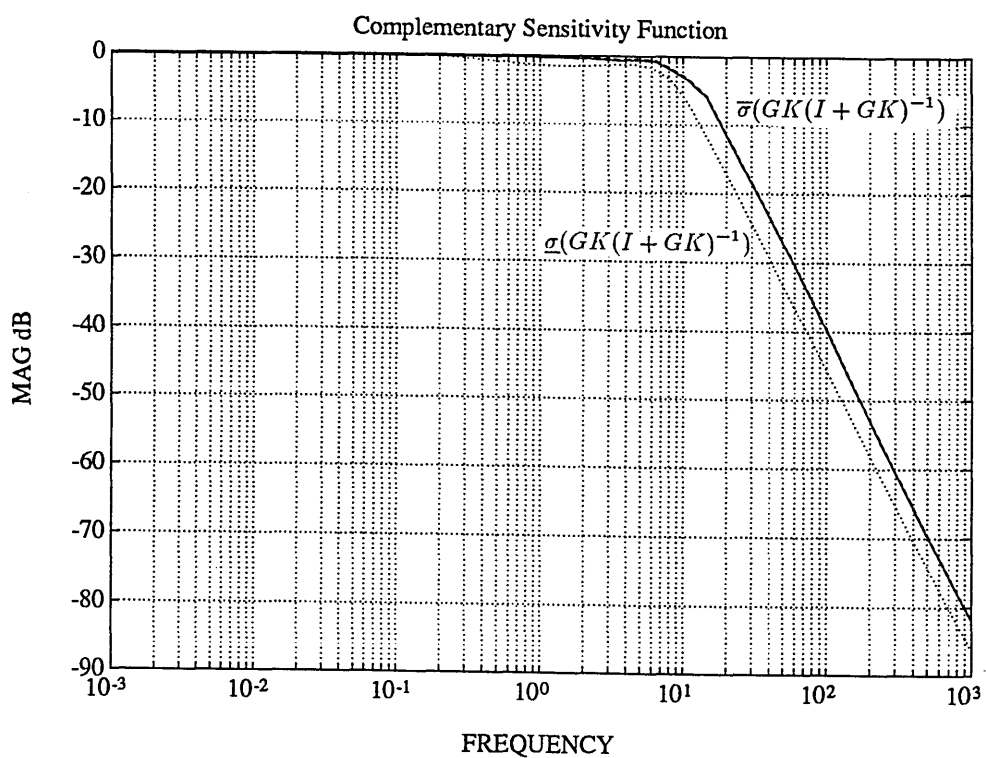


Figure 5.21: Singular Value Plot of Closed-Loop Transfer Function

5.5 Scheduled Nonlinear Controllers

In this section, two gain scheduled nonlinear controllers are constructed. In each case, sixteen local linear controllers are designed to cover the complete operating ranges of the engines. This is considered to be adequate and consistent with the first guideline for a successful design. The scheduling variable is the engine non-dimensional shaft speed (LP shaft for the two-spool engine). Equation 5.7 suggests that there are 4 proportional gains and 4 integral gains to be scheduled for the single-spool engine. Similarly, Equation 5.9 suggests there are 9 proportional gains and 9 integral gains to be scheduled.

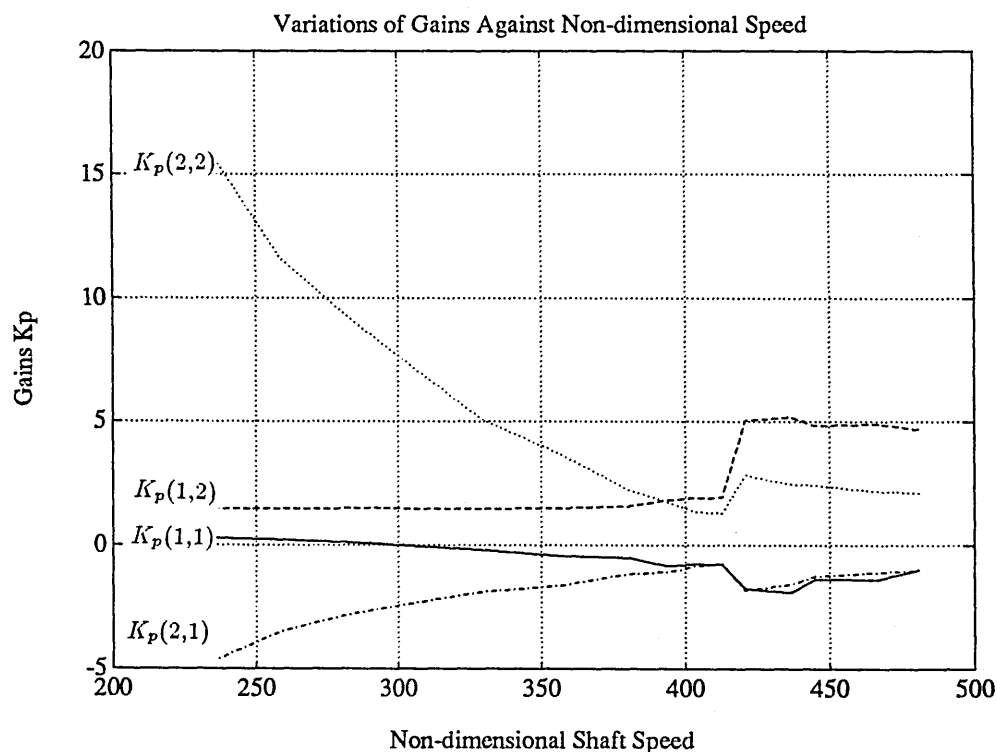


Figure 5.22: Variations of Proportional Gains K_p with Non-dimensional Speed

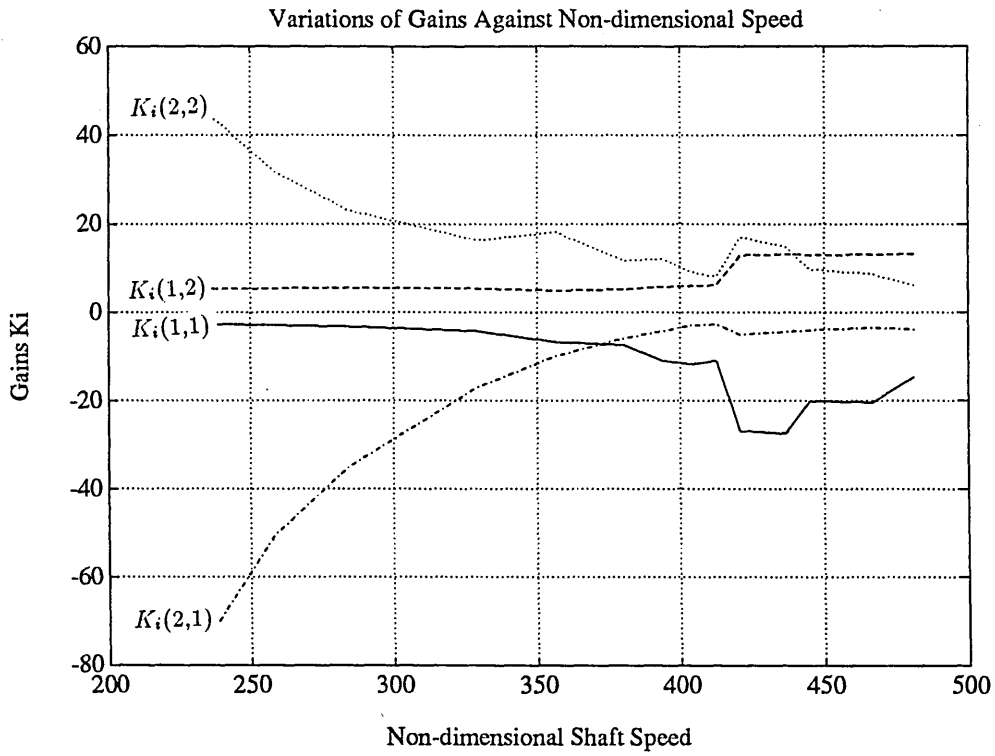


Figure 5.23: Variations of Integral Gains K_i with Non-dimensional Speed

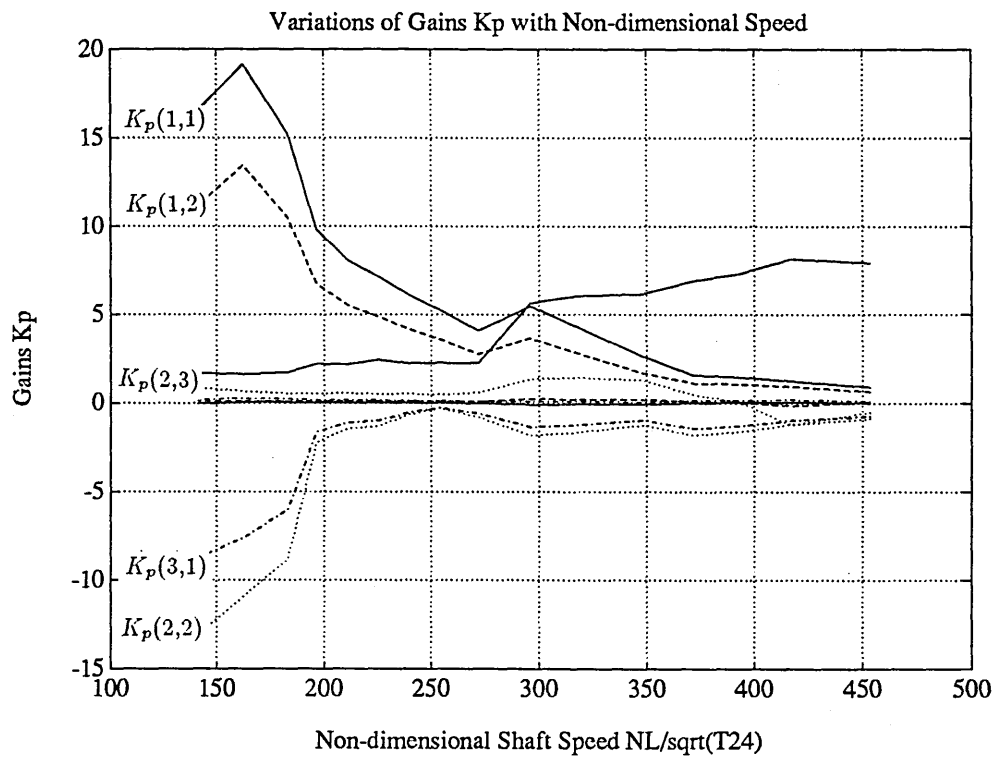


Figure 5.24: Variations of Proportional Gains K_p with Non-dimensional Speed

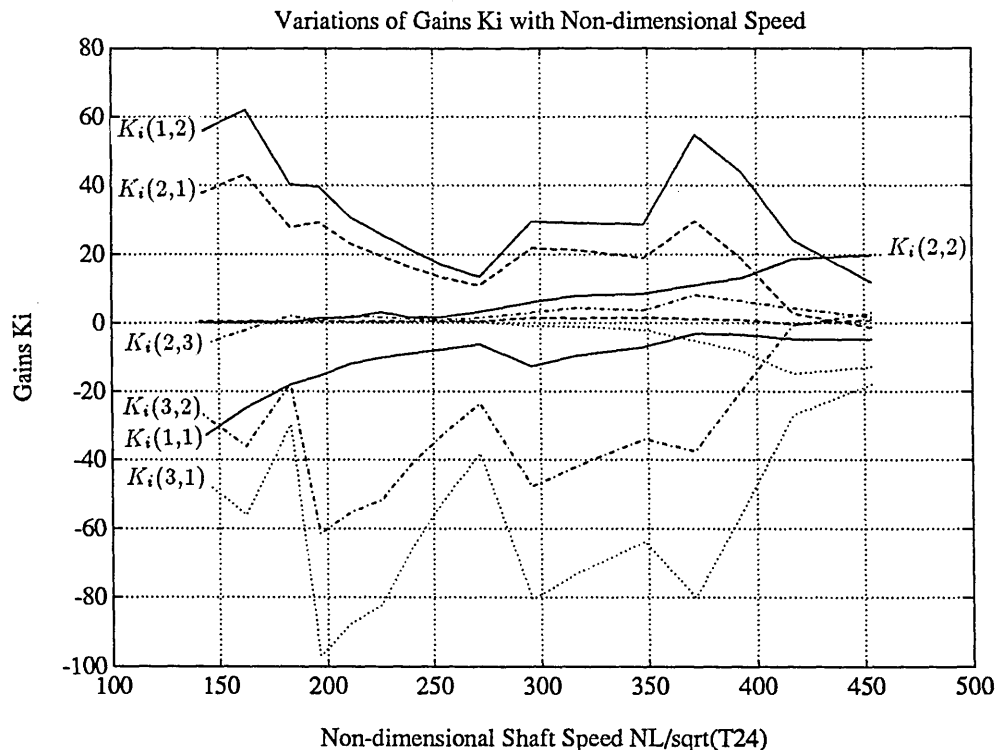


Figure 5.25: Variations of Integral Gains K_i with Non-dimensional Speed

5.6 Simulation and Comparisons

In this section, the designed nonlinear controllers are validated through simulations. To show the performance improvements, the simulation results are compared with those when using open-loop fuel controllers. [144].

5.6.1 The Single-Spool Engine

Figure 5.26 to 5.28 shows the comparisons of the simulations with these of using open-loop fuel controller (Chapter 4). It is seen that engine response rates have been significantly improved and the safety of the engine is guaranteed. From the compressor characteristics, it is seen that performance improvements are due to the fact that over the larger parts of the low speed ranges, more of the available surge margin has been used.

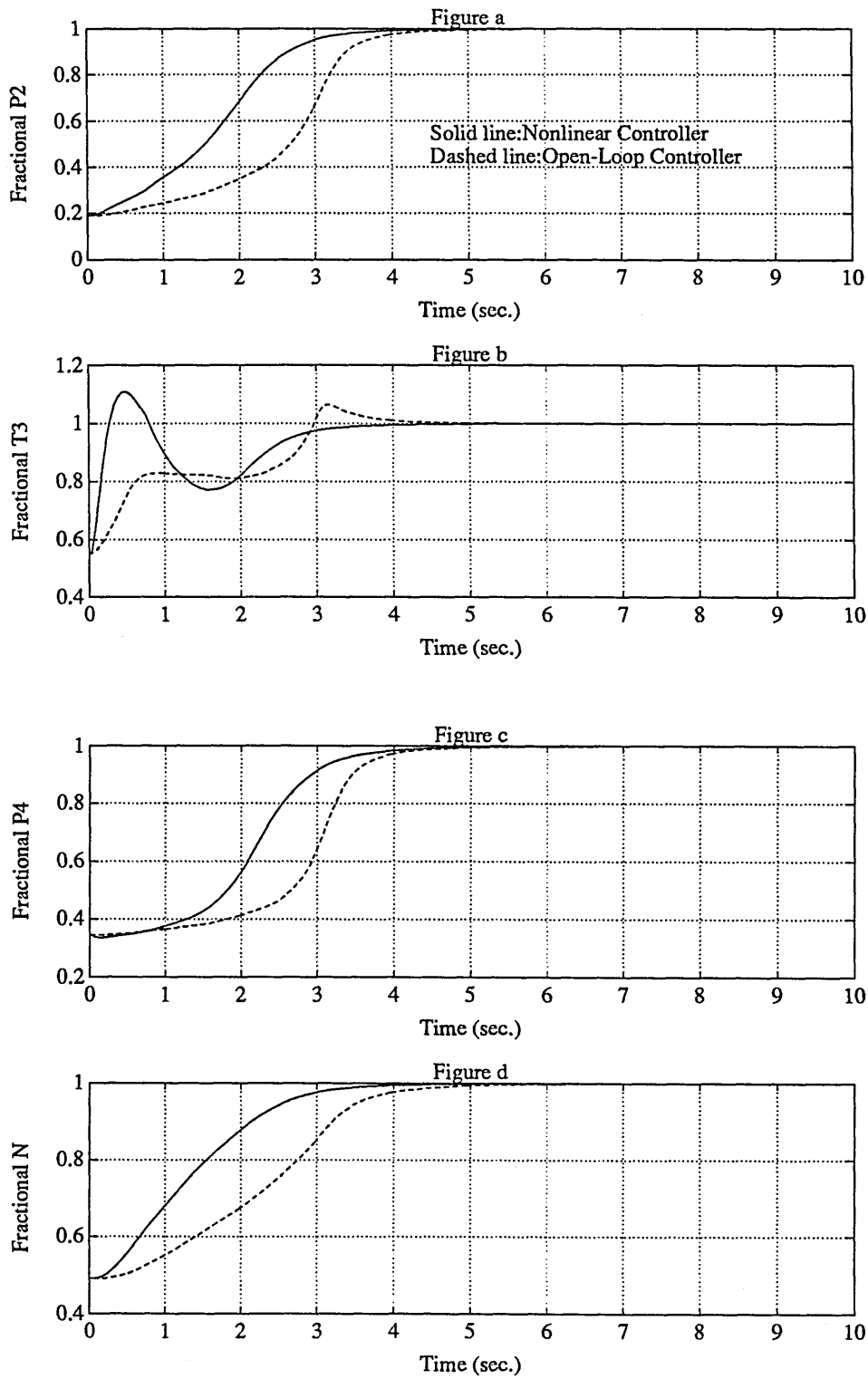


Figure 5.26: Comparison of Nonlinear Controller and Open-Loop Controller

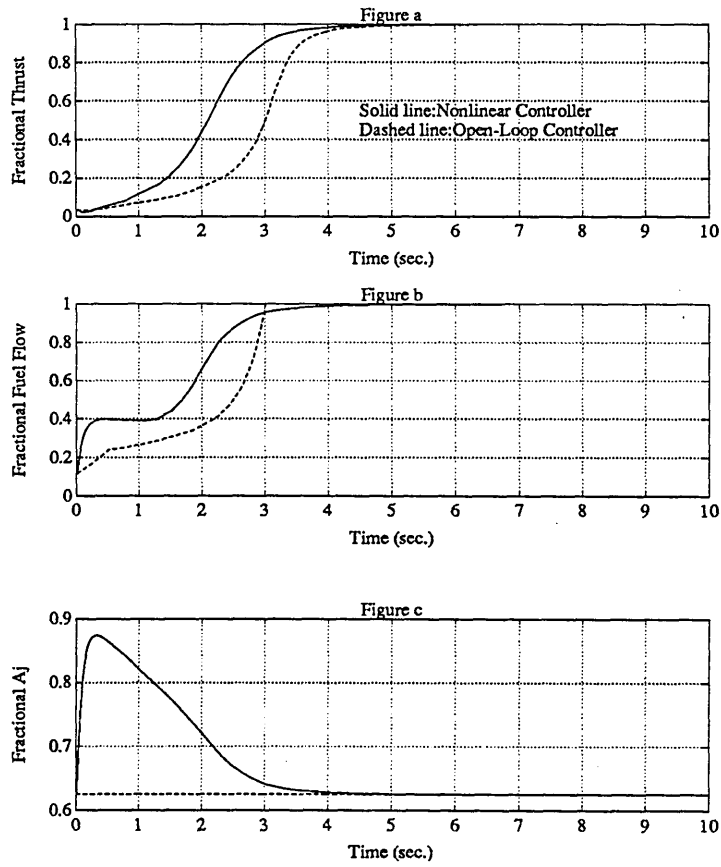


Figure 5.27: Comparison of Nonlinear Controller and Open-Loop Controller

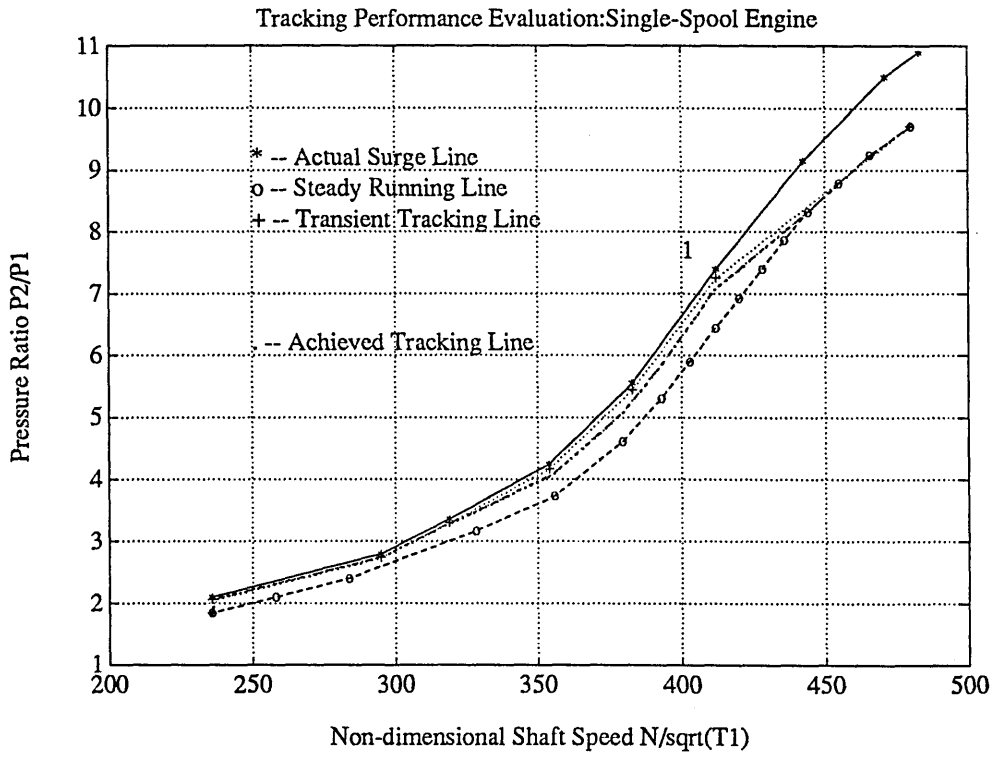


Figure 5.28: Tracking Performance Evaluation for the Single-Spool Engine

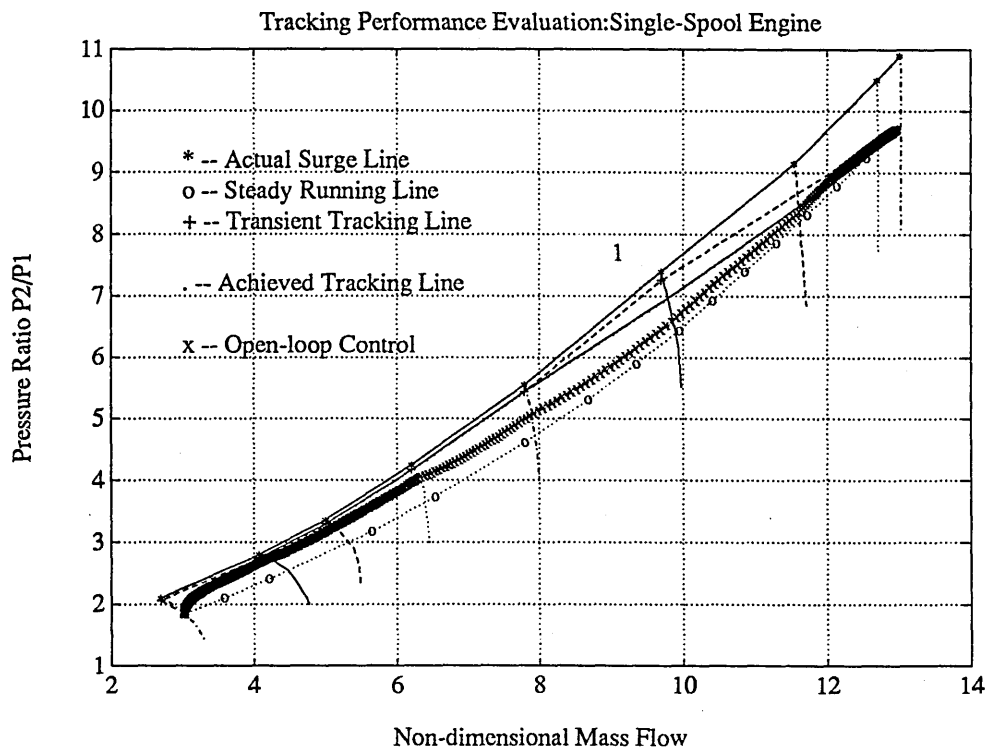


Figure 5.29: Tracking Performance Evaluation for the Single-Spool Engine

5.6.2 The Two-Spool Engine

The performance of nonlinear controller are shown from Figure 5.30 to 5.35 alongside with the results when using the open-loop fuel controller. Figures 5.30 and 5.31 show the responses of engine state variables. Figure 5.32 shows the thrust response and control inputs. It is seen that engine responses have been significantly improved compared with these due to the use of open-loop controller.

The transient tracking line in Figure 5.30 shows that more HP compressor surge margin over a wider low speed range has been used during the acceleration. In the high speed range, it seems that the transient tracking line is well below the predetermined tracking line. This is due to the fact that in this speed range, the bleed valve is scheduled to be closed, which has not explicitly accounted for in the linear design models. This introduces the nonlinearities. Through the thrust plot, it is seen that engine performance has been greatly improved. The control inputs are shown in Figure 3.34

5.7 Alternative Way to Control Surge

As an alternative, the control of compressor surge can be achieved by manipulating the compressor inlet guide vanes using the error between the transient pressure ratio and the corresponding surge pressure ratio. Figure 5.37 shows this scheme. The independent control of compressor pressure ratio by the inlet guide vane can be achieved using the closed-loop synthesis approach by restricting the controller to have specific structure, for example the $K(s)$ in Equation 5.7 has to be written as:

$$K(s) = \begin{bmatrix} kp_{11} + ki_{11}/s & kp_{12} + ki_{12}/s & 0 \\ kp_{21} + ki_{21}/s & kp_{22} + ki_{22}/s & 0 \\ 0 & 0 & kp_{33} + ki_{33}/s \end{bmatrix} \quad (5.10)$$

The error of pressure ratio is monitored at all instants of time, and control will not be active until this error becomes negative. This indicates that the transient

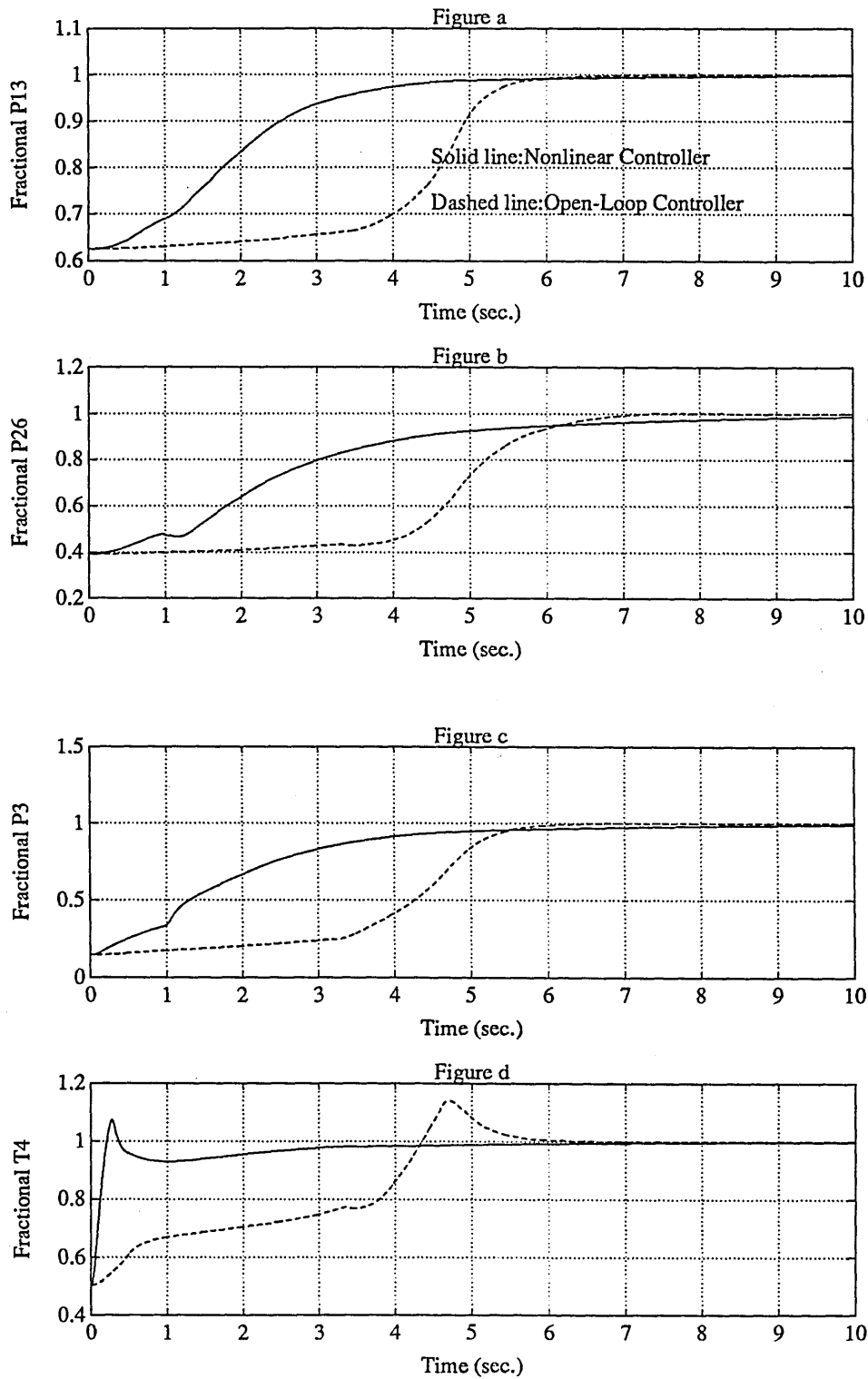


Figure 5.30: Comparison of Nonlinear Controller and Open-Loop Controller

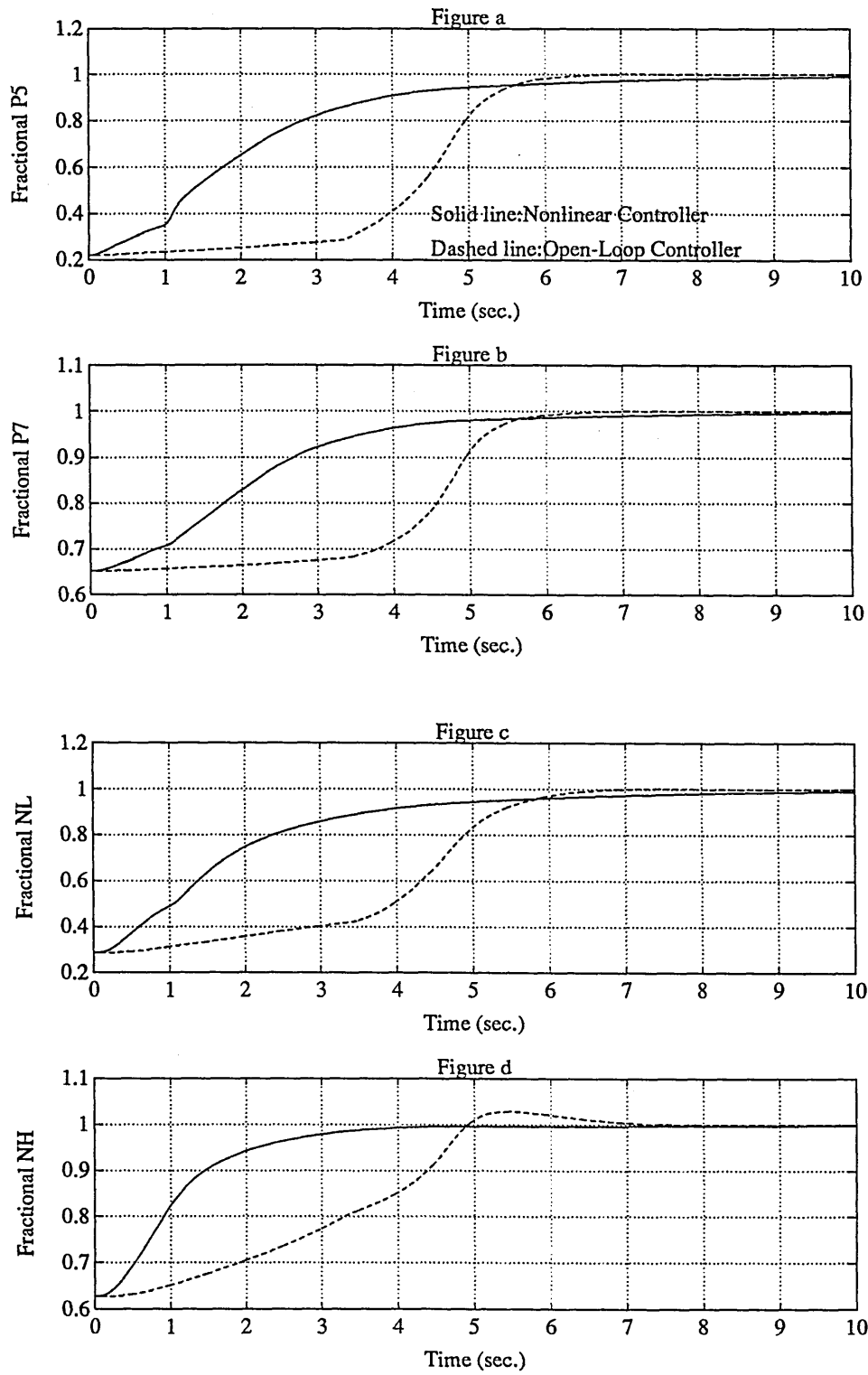


Figure 5.31: Comparison of Nonlinear Controller and Open-Loop Controller

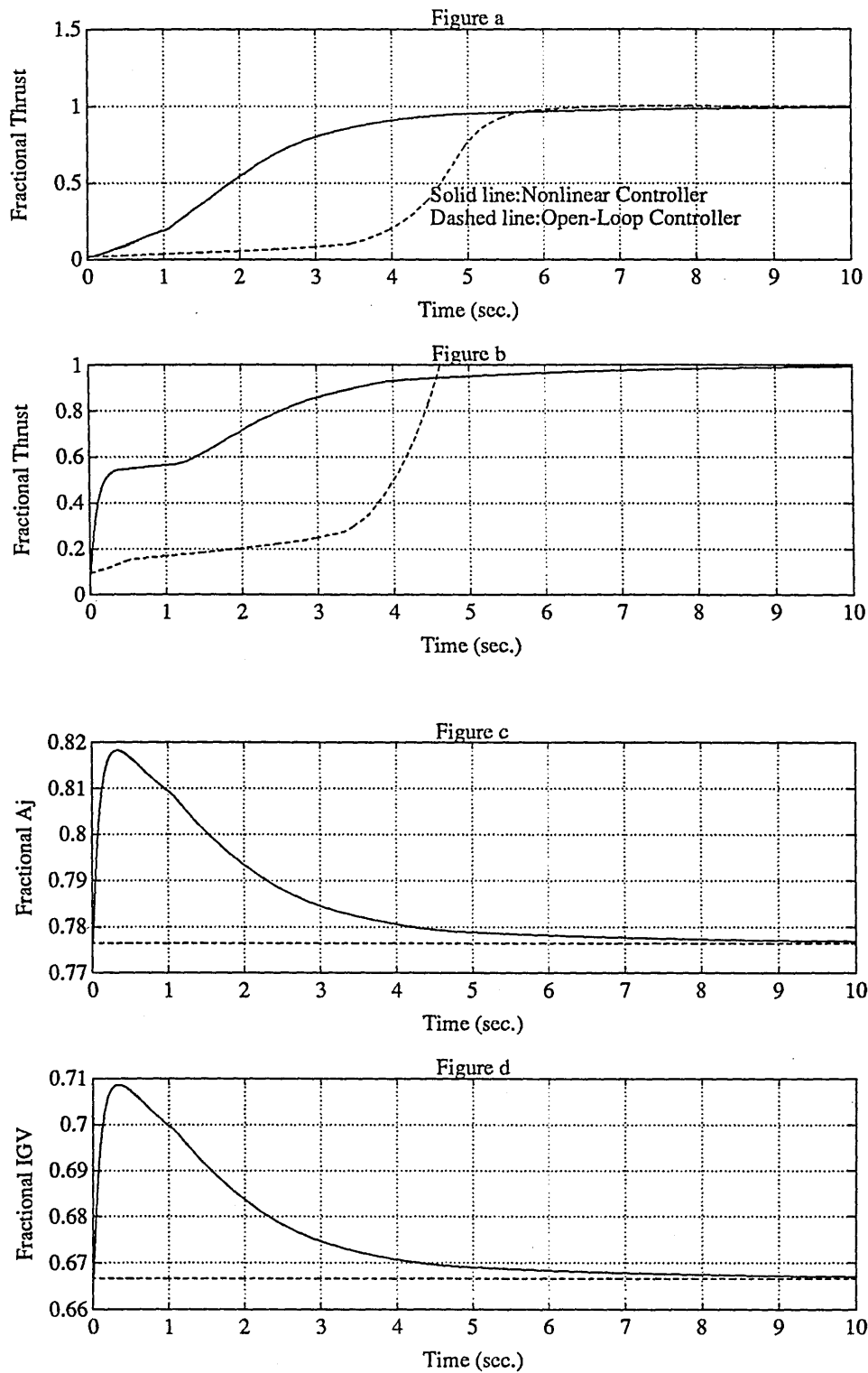


Figure 5.32: Comparison of Nonlinear Controller and Open-Loop Controller

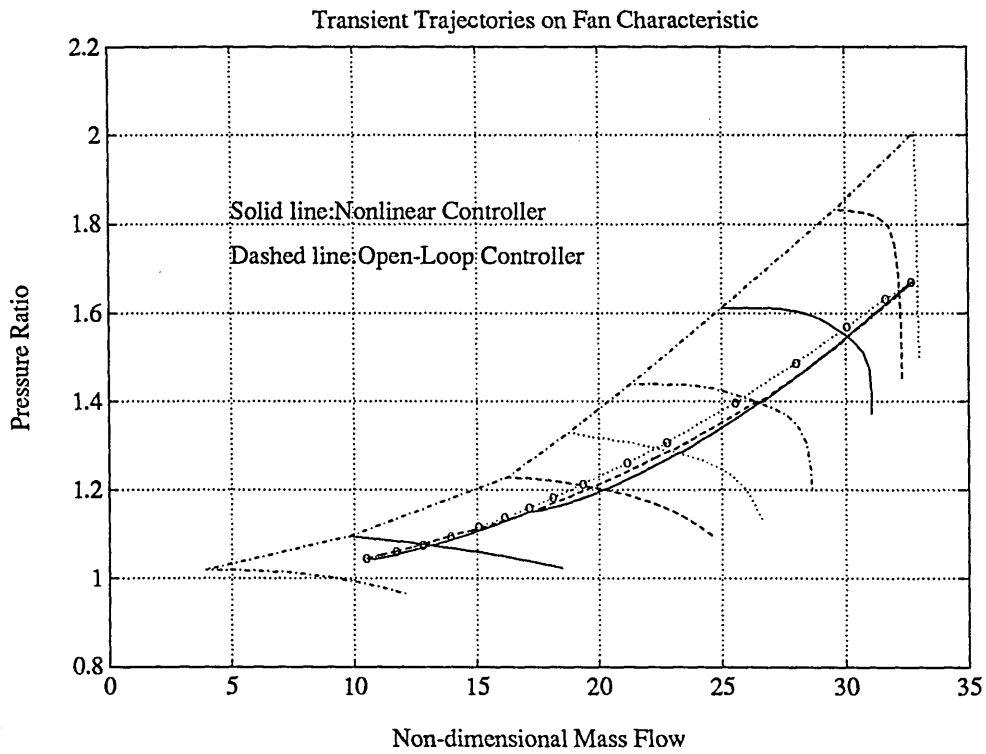


Figure 5.33: Comparison of Nonlinear Controller and Open-Loop Controller

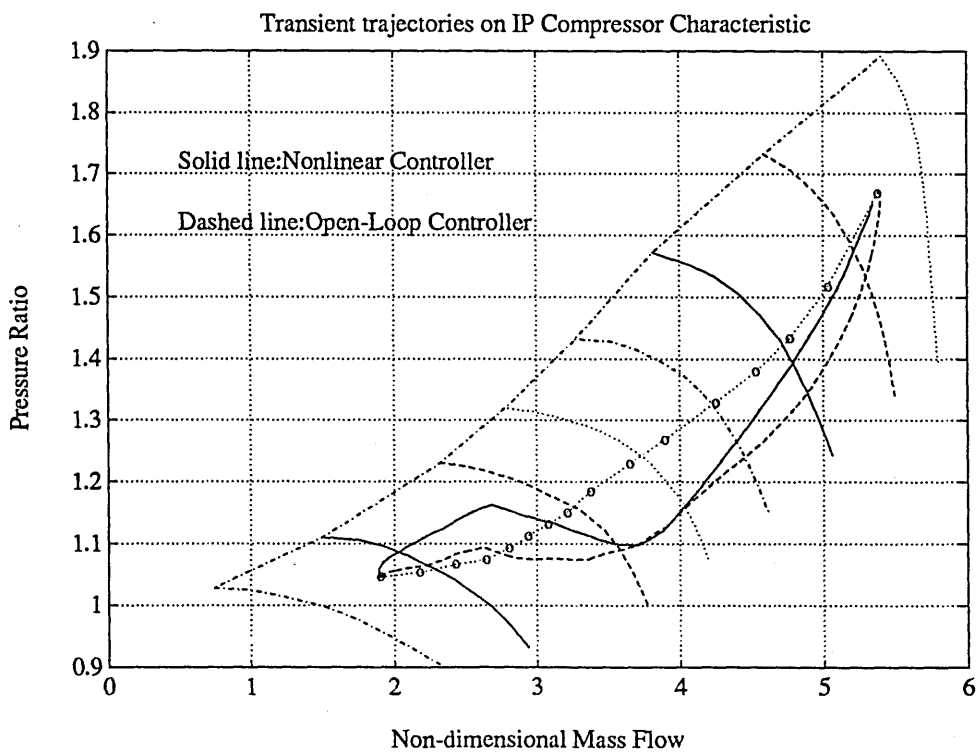


Figure 5.34: Comparison of Nonlinear Controller and Open-Loop Controller

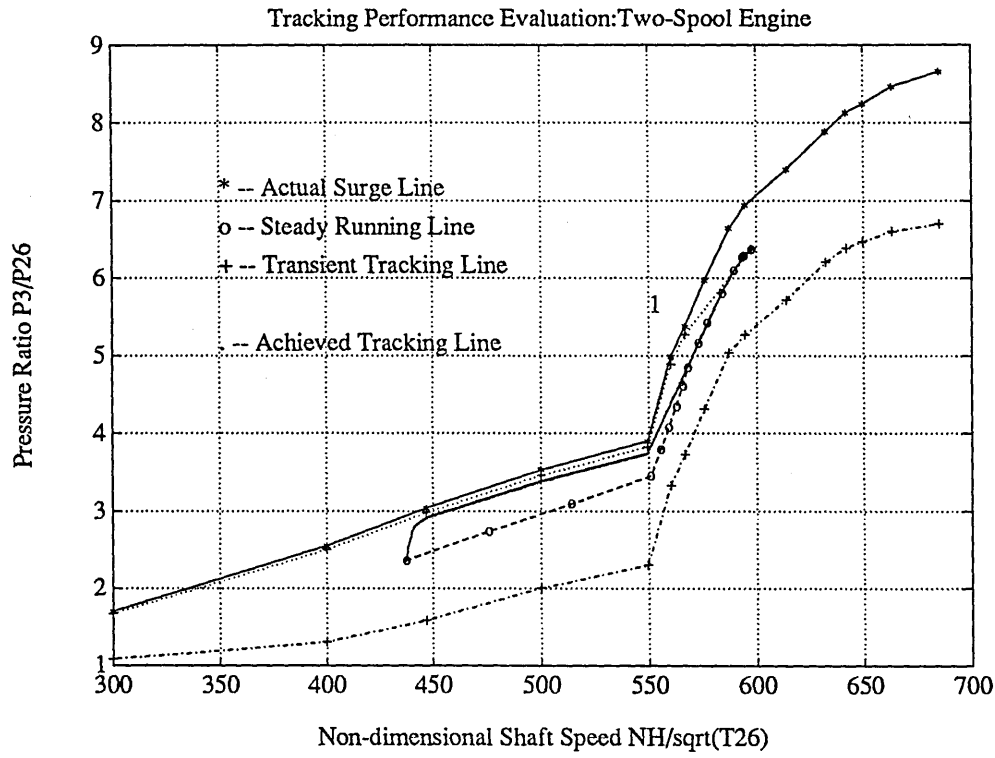


Figure 5.35: Comparison of Nonlinear Controller and Open-Loop Controller

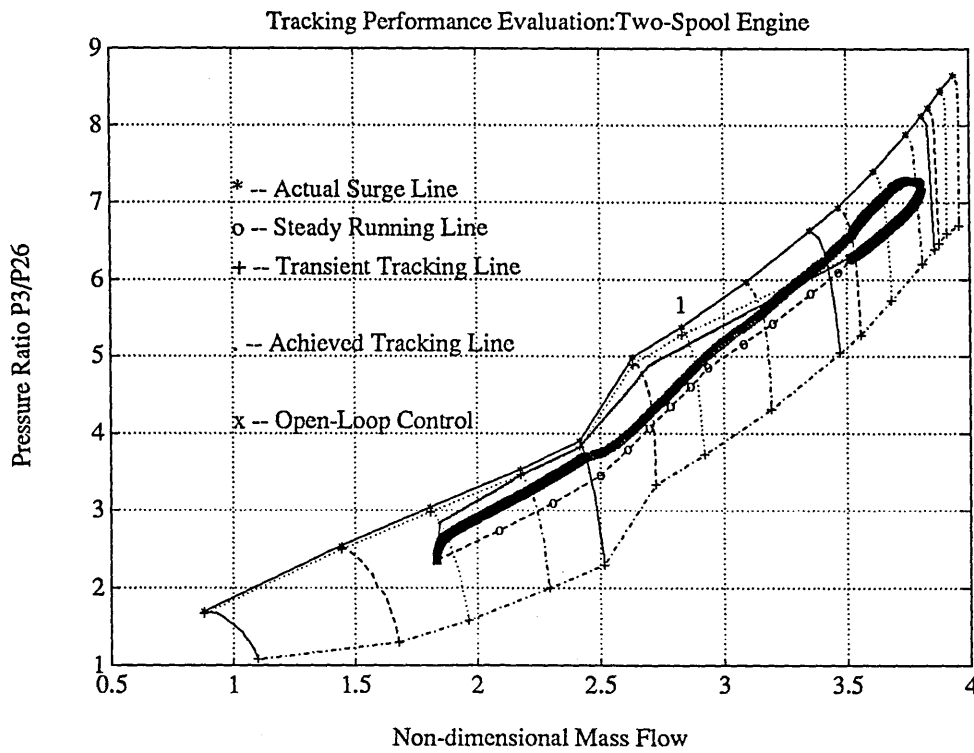


Figure 5.36: Comparison of Nonlinear Controller and Open-Loop Controller

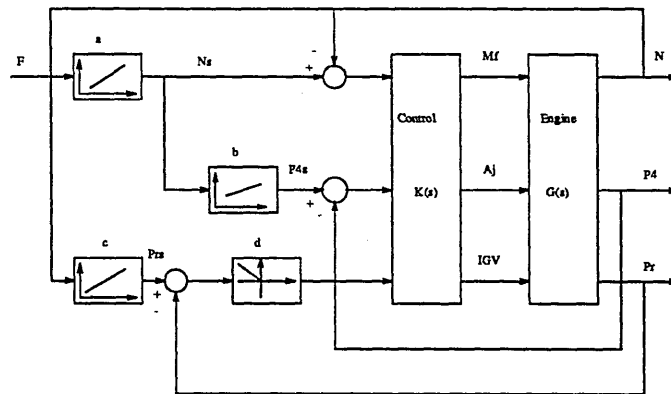


Figure 5.37: Alternative Way to Control Compressor Surge

trajectory has intersected the surge line.

This control scheme has the advantage that the controller will drive the engine in response to the demanded response as soon as it can, once the surge "warning" line has been reached. The trim control will attempt to control the trajectory by adjusting the compressor inlet guide vane setting.

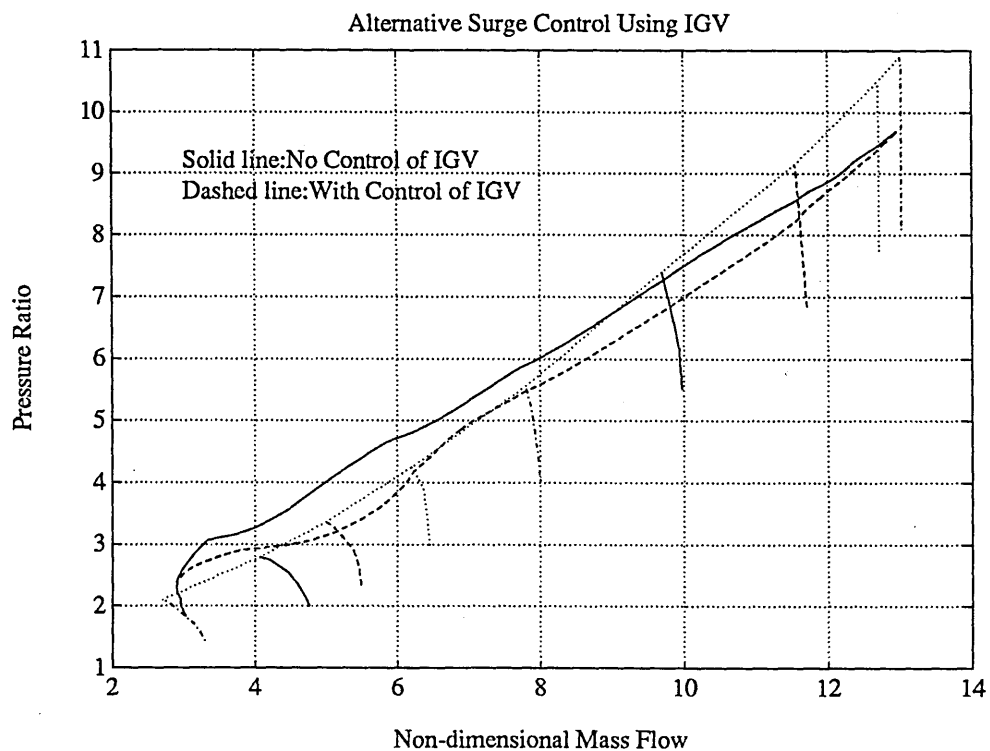


Figure 5.38: Comparisons of Transient Trajectory

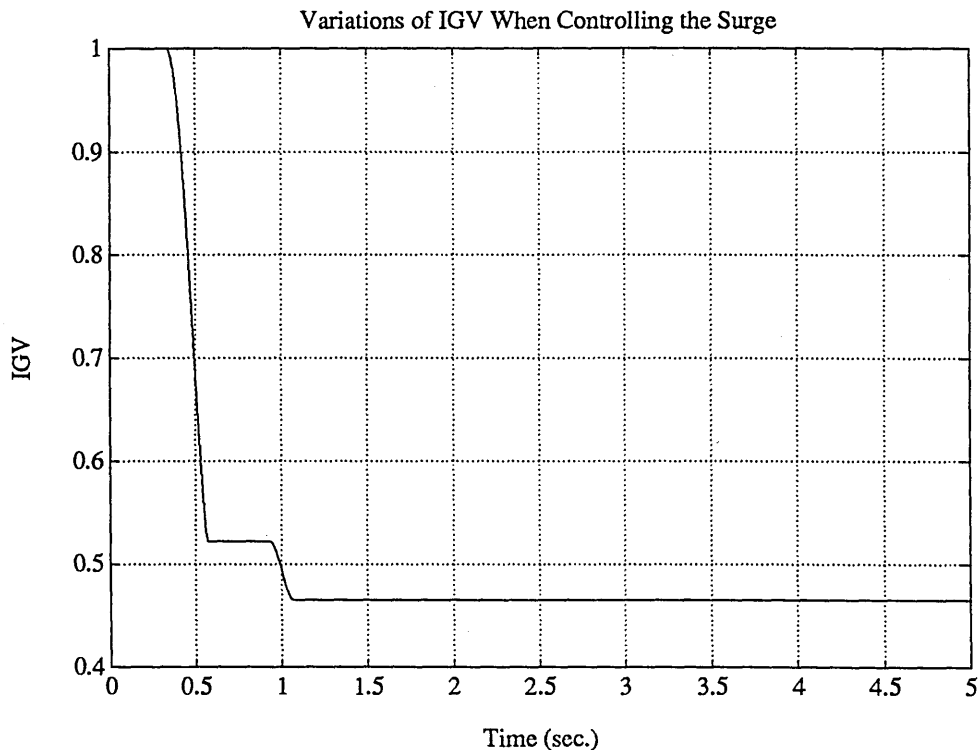


Figure 5.39: The Variation of Compressor Inlet Guide Vane

5.8 Conclusions

This chapter has demonstrated a practical approach used to design multivariable nonlinear feedback controllers for gas turbine engines. The choice of engine non-dimensional shaft speed (for the two-spool engine, LP non-dimensional speed is used) to schedule linear controller gains produces nonlinear controllers that adapt for the variations of engine dynamics over the entire operating range.

The use of the closed-loop synthesis method allows one to specify the simple PI structure for the linear controllers which makes the following scheduling procedure easier, and also offers very strong attractions for practical implementation.

Transient tracking lines are to ensure engine safety during transient operations. The contribution made by the author is the formulation of the practical performance requirements interpreted on the compressor characteristic. This pinpoints what control objectives should be targeted, and also makes it easier to be understood by both control engineers and gas turbine engine engineers.

The present work has shown that designs and the procedure of the applications are valid.

Chapter 6

Model-Based Control of Gas Turbine Engines

SUMMARY

A model-based control approach to synthesising nonlinear controllers for gas turbine engines is described in this chapter. In a gas turbine engine, since the main control variable, engine thrust, cannot be directly measured, a model-based observer is constructed using a nonlinear model of the engine in order to provide an on-line estimation of the thrust for use in feedback control. Both proportional and proportional-integral (PI) observers have been used in the design of the model-based observer. The latter is intended to provide a robust estimation in the event of modelling errors.

6.1 Introduction

One of the main control objectives for gas turbine engines is to achieve rapidly the required thrust change while ensuring stable operation of the compressors and keeping the turbine inlet temperature below the safety limit. To achieve this performance objective, it is necessary that the engine's thrust, compressor surge

margin and turbine inlet temperature be monitored at all instants of time. In practice, however, these performance variables can rarely be directly measured. In this situation, to control these variables, one solution is to use the available measurements from the engine in conjunction with a mathematical model to estimate these unmeasured variables [145]. In the present work, the thrust computed from the model is used for feedback control.

For linear systems, the observer theory has been well established and powerful design methods for observers are now widely available [146]. However, for nonlinear systems, due to their distinct behaviour, few methods are available with sufficient generality.

Suppose a nonlinear model of a system can be represented by:

$$\dot{x} = f(x, u) \quad (6.1)$$

$$y = h(x, u) \quad (6.2)$$

An open-loop observer computes state estimates $\hat{x}(t)$ by solving:

$$\dot{\hat{x}} = f(\hat{x}, u), \quad \hat{x}(0) = \hat{x}_0 \quad (6.3)$$

when given on-line measurements of u and estimates of the initial states \hat{x}_0 . For systems with asymptotically stable open-loop dynamics, the open-loop observer given above provides a simple method of reconstructing the system states. However, such an open-loop observer is potentially sensitive to disturbances and modelling errors.

Open-loop unstable systems or open-loop stable systems with slow dynamics are sensitive to errors in the initial state. To overcome this, a closed-loop observer can be constructed by feeding back the difference between the actual system outputs and the estimated outputs as follows:

$$\dot{\hat{x}} = f(\hat{x}, u) + K_p[y - h(\hat{x})] \quad (6.4)$$

where K_p is an observer gain vector. Determination of the observer gain that provides fast convergent estimates, in this nonlinear case, is a nontrivial task [147]. For systems that operate around a steady state, a popular approach consists of linearising the nonlinear model around the steady operating point and applying well-known linear observer design methods. Misawa and Hedrick [148] have given a very comprehensive overview of the different approaches to the nonlinear observer design problem.

6.2 Measurements and Disturbances

In a gas turbine engine, there are two important classes of outputs, e.g. those that are measurable and those that are not measurable. Measured outputs typically include shaft speeds, temperatures, and pressures throughout the engine gas path. These quantities are often used to model thermodynamic responses and are, therefore, generally state variables. Unmeasured outputs represent engine performance and limiting quantities such as thrust, surge margin, and turbine inlet temperature.

Disturbances may occur during engine operation. They are primarily caused by control actuator uncertainties or unsteady flow phenomena such as inlet flow distortion. Disturbances may be modelled explicitly for synthesis or, as is common, may be considered qualitatively during the design process in the selection of dynamic design criteria such as weightings and bandwidth. Validation of disturbance rejection and control performance is typically performed on detailed nonlinear simulations of the engine after a design has been completed [3].

6.3 The Algorithm of a Model-Based Observer

The idea of using the model-based observer to synthesise practical nonlinear controllers was first proposed by Gawthrop [149]. The basic philosophy is to run

a nonlinear model in parallel with the modelled system. In the present study, parametric uncertainty is assumed, but the model is assumed structurally correct as it is developed from basic thermodynamic principles.

The general scheme of a model-based observer is illustrated in Figure 6.1. The different aspects of the approach are listed below:

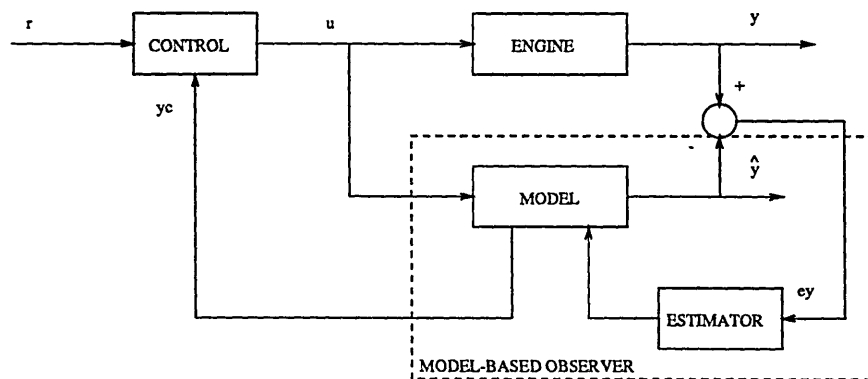


Figure 6.1: The structure of a model-based observer

- A dynamic simulation model is placed in parallel with the engine to be controlled. This model will usually be nonlinear.
- The measured outputs y of the engine are compared with the corresponding model outputs \hat{y} to create an error e_y .
- The model states have feedback applied to them in such a way as to drive the output error e_y to zero.
- The controller generates the control signal u in terms of any set of variables y_c generated within the model together with the setpoint r .
- If the model-based observer is working well, these variables y_c will be the same or close to the corresponding variables generated within the engine itself.

In Figure 6.1, the known control input which drive the engine is also fed to the mathematical model. The selected measurements from the engine are

compared with the corresponding quantities from the model. The differences between them are fed back to the appropriate parts of the model. In this way, the model states will be adjusted into alignment with the corresponding states of the engine. Therefore, the problem in using a model-based observer lies in designing the efficient algorithms for the feedback of e_y to the model such that the alignment of the states can be achieved in the shortest possible time while rejecting any possible disturbance and modelling error.

It should be noted that there are two differences between the engine and the model:

- Corresponding to each of the engine state variables, there is an element in u_r ; these are the additional inputs to the model and will be related to the error e_y . This provides a means of adjusting the model states towards the corresponding engine states.
- All the variables of the model are available for measurement, and the model could be implemented on an on-board computer.

The purpose of the model-based observer is to drive the model states towards the engine states. The purpose of the control is to drive appropriate model variables towards desired setpoints.

6.4 Proportional Observer

If we assume that the model is an exact representation of the engine, a proportional observer can be constructed as demonstrated in the present application.

Linearising the nonlinear model (equation 6.1 and 6.2) at the nominal operating point (x_o, u_o) , the linear observer design model is then given as:

$$\delta\dot{x} = A_o\delta x + B_o\delta u \quad (6.5)$$

$$\delta y = C_o\delta x \quad (6.6)$$

where A_o , B_o and C_o are matrices of appropriate dimensions. We drop the δ to simplify the exposition, which now follows.

The observer equation is:

$$\dot{\hat{x}} = A_o \hat{x} + B_o u + u_r \quad (6.7)$$

Here the inputs u_r have the same dimensions as the states. The idea is that if a difference exists between any of the engine outputs and model outputs, the corresponding element of u_r will be used to offset this error by compensating the model states using $K_p e_y$. The model-based observer can be created from the model together with the feedback:

$$u_r = K_p e_y \quad (6.8)$$

There are many possibilities for designing the observer feedback gains K_p , e.g. the Linear Quadratic (LQ) or the pole placement method. In the present work, the observer gain K_p is designed using LQ theory based on the linear model corresponding to the engine take-off condition.

Noted that the linear equation 6.5 and 6.6 are only used to design K_p (equation 6.8); the observer is implemented by equation 6.4. Hence although the feedback is linear, the observer itself is nonlinear.

6.4.1 Qualitative Deduction of Observer Gain

Before designing the observer gain vector K_p , let us make some qualitative deductions about how the observer gain K_p should be varied when both disturbance (d) and measurement noise (w) exist.

Assume there is no disturbance ($d = 0$) and no measurement noise ($w = 0$), and assume further the model is an accurate representation of the engine. Suppose the initial states for the model have been incorrectly guessed. As a result, the states of the engine will differ from those of the model, and this will immediately show up in the differences between the measurements from the engine and the

model. In this case, it would be logical to expect the gain K_p to be made as high as stability considerations will permit in order to feed back the correcting signals to the model to offset the initial state errors as quickly as possible. Thereafter, the gains could fade to zero and the model states will keep in line with the engine states.

If disturbance $d \neq 0$ and measurement noise $w = 0$, then any difference between the model states and engine states is due to the perturbations on the engine states. Because we have complete confidence in the system measurements, the gains K_p should be as high as possible, and also would be preferred to maintain high gains throughout the period when the states are being aligned.

If disturbance $d = 0$, but measurement noise $w \neq 0$, then we again have complete confidence in the model, therefore the model states will completely keep in line with the engine states. Because the measurements are known to be inaccurate, hence, we could ignore the measurements by setting the gains to zeros.

6.4.2 Design of Observer Gain K_p

In practice, both disturbance and measurement noise exist during the operation of gas turbine engines. Therefore, the LQ method is preferred for the determination of the observer gain K_p due to the inherent robust properties as known in the linear case. To use this method, one has to choose the matrices Q and R . R is the covariance of the measurement noise and can be simply set to be an identity matrix. Q can be considered to be a measure of level confidence in the model, and in real terms Q arises from the state error covariance between the engine and the model. A relatively large Q will generate relatively large gain which effectively puts low emphasis on the model outputs and greater emphasis on the measurements. Conversely, a relatively low Q will put more emphasis on the model responses to the system input. Since it is difficult to determine the exact value for Q during engine operation, the following approach is proposed to select

Q .

Using the linear design model, Q can be calculated by minimising the error norm of the measurements and the model outputs as:

$$\text{Min}_Q \|y - \hat{y}\|_2 \quad (6.9)$$

This minimisation is easily done using the available function *fmins* in Matlab, which implements the simplex search method. The observer gain K_p is then calculated using the resulting Q .

6.5 Proportional and Integral(PI) Observer

If modelling errors exist, or the engine is subjected to unknown disturbances, the engine states and model states will be different in the steady-state. This will show up as errors between the measurements and model outputs in steady-state. In this circumstance, the PI observer is considered to be appropriate [150].

Using the equation 6.5 and 6.6, a PI observer has been defined as [151]:

$$\begin{aligned} \dot{\hat{x}} &= (A_o - LC_o)\hat{x} + B_o u + Ly + Kv \\ \dot{v} &= y - C_o \hat{x} \end{aligned} \quad (6.10)$$

The system defined by equation 6.9 is said to be a full-order PI observer for the system if and only if:

$$\lim_{t \rightarrow \infty} e(t) = 0, \quad \lim_{t \rightarrow \infty} v(t) = 0 \quad (6.11)$$

and all the eigenvalues of the matrix

$$R = \begin{bmatrix} A_o - LC_o & K \\ -C_o & 0 \end{bmatrix} \quad (6.12)$$

have negative real parts. where $e(t) = \hat{x}(t) - x(t)$, For proof see [151].

The PI observer structure is shown in Figure 6.2, from which u_r is related to v as:

$$u_r = Lv + \int Kvd t \quad (6.13)$$

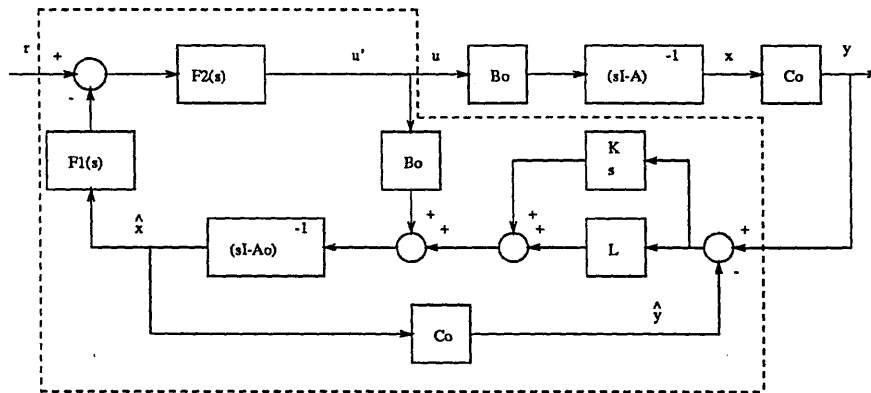


Figure 6.2: The Structure of a PI Observer

6.5.1 Robust Properties of PI Observer

In this section, the robust property of the PI observer is analysed when implemented in a state feedback scheme. Although the analysis is based on the linear model, the intention is that the robust properties will be preserved, to a certain degree, in the nonlinear observer.

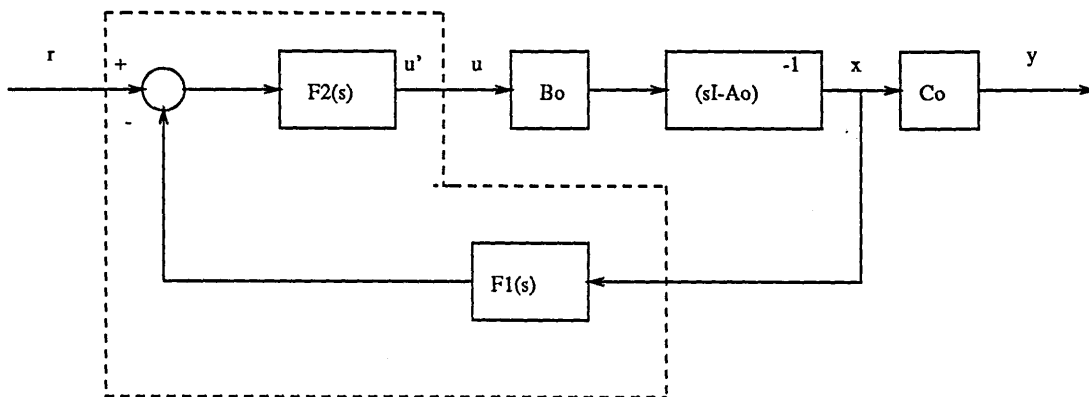


Figure 6.3: The Structure of a Linear Quadratic Regulator

Consider Figure 6.3, which is a general structure of a linear quadratic regulator. The loop transfer functions at the points of u and u' are essentially the same, and the robust properties are well recognised. When the system states are not available and an observer has to be used to estimate the states, the robust properties of the linear quadratic regulator are no longer guaranteed; that is the loop transfer functions at the points of u and u' are different. To overcome this problem, Doyle and Stein [152] have derived a necessary condition, and proposed an approach to

asymptotically recover the robust properties of the linear quadratic regulator, i.e., by adjusting the observer gain to force the loop transfer function at point u' to approach closely to the loop transfer function at point u . The condition is (refer to Figure 6.2, and assume $K = 0$):

$$L[I + C_o(sI - A_o)^{-1}L]^{-1} = B_o[B_o(sI - A_o)^{-1}B_o]^{-1} \quad (6.14)$$

for all values of s .

To satisfy equation 6.14, the following recovery procedure is proposed. The observer gain L is parameterised as a function of a scalar variable q . This function $L(q)$ is selected such that as $q \rightarrow \infty$, and the following result is achieved:

$$\frac{L(q)}{q} \rightarrow B_o W \quad (6.15)$$

where W is a non-singular matrix. Equation 6.14 is satisfied asymptotically. Adjustment of parameter q thus changes asymptotically the initial normal observer gains, $L(0)$, with poor robust properties into these of a linear quadratic regulator. One important assumption made in deriving the equations 6.14 and 6.15 is that there are no system transmission zeros in the right hand-plane. This is necessary because as $q \rightarrow \infty$, the poles of the resulting observer error dynamics will tend towards the finite transmission zeros of the system.

Following Doyle and Stein's analysis procedure, a similar condition is derived when using PI observer as:

$$(sL + K)[sI + C_o(sI - A_o)^{-1}(sL + K)]^{-1} = B_o[B_o(sI - A_o)^{-1}B_o]^{-1} \quad (6.16)$$

This equation points out a unique way to recover the robust properties when a PI observer is being used. If the integral gain K is set equal to B_o , then equation 6.14 is satisfied in the steady-state ($s \rightarrow 0$). Thus the robust properties of the linear quadratic regulator are recovered asymptotically in the steady-state.

This discovery points out some benefits in using a PI observer. The assumption of no transmission zeros in the right hand plane can be dropped as we are

not adjusting the poles of the observer. Robust properties are guaranteed to be recovered in the steady-state although this may not be true in the transient response.

Finally, it is noted that in Doyle and Stein's procedure, as $q \rightarrow \infty$, the observer gain L may become very large, therefore the degree of recovery may be limited.

6.5.2 Robust Design of PI Observer

In this section, a method for the robust design of the PI observer is suggested. Because our design is based on the linear model and implemented on a nonlinear system, some trial and error is involved to reach a successful design.

We assume the dynamic matrix A_o is subjected to perturbations, while B_o and C_o remain constants. In this case, the engine can be modeled as:

$$A = A_o + \Delta A \quad (6.17)$$

which falls into the category of structured perturbations. The $n \times n$ matrix ΔA defines the prescribed ranges of variation for the nominal set of plant parameter A_o .

A simple method has been used to determine the PI observer gains following Beale and Shafai [153]. Referring to Figure 6.3, assume $F_1(s) = I$, which is an identity matrix of appropriate dimension, and $F_2(s) = F$ is a constant state feedback matrix. In ideal case (no observer loop) the transfer function from r to x are given as:

$$x(s) = (sI - (A - B_o F))^{-1} B_o r(s) \quad (6.18)$$

Hence, the final state is:

$$x(\infty) = -(A - B_o F)^{-1} B_o r(\infty) \quad (6.19)$$

where $x(\infty) = \lim_{t \rightarrow \infty} x(t)$, $r(\infty) = \lim_{t \rightarrow \infty} r(t)$. Here A is the true plant matrix as given above.

In practice, the transfer functions from r and v to x and \hat{x} are given by:

$$\begin{bmatrix} x(s) \\ \hat{x}(s) \end{bmatrix} = (sI - \Sigma)^{-1} \left\{ \begin{bmatrix} B_o \\ B_o \end{bmatrix} r(s) + \begin{bmatrix} 0 \\ K \end{bmatrix} v(s) \right\} \quad (6.20)$$

where

$$\Sigma = \begin{bmatrix} A & -B_o F \\ LC_o & A_o - LC_o - B_o F \end{bmatrix} \quad (6.21)$$

For loop transfer characteristics of the full-state feedback implementation to be recovered at the steady-state in the PI observer-based implementation, it is necessary for $\hat{x}(s)$ and $x(s)$ to be identical at the steady-state. Equating the two, the following condition is given:

$$Kv(\infty) = \phi r(\infty) \quad (6.22)$$

where

$$\phi = [(A_o - B_o F)(A - B_o F)^{-1} - I] B_o \quad (6.23)$$

or

$$\phi = -\Delta A(A - B_o F)^{-1} B_o \quad (6.24)$$

The equation 6.27 provides a guideline to choose and tune the PI observer gains K and L . The procedure can be summarised as:

- Set $L = K_p$ (proportional observer) and $K = 0$, find the maximum possible magnitude of $v(\infty)$ by simulations.
- Optimise $J = \|Kv(\infty) - \phi r(\infty)\|_2$ in the least-square sense to find gain K .
- Further tuning the L and K using the nonlinear simulation.

6.5.3 Augmenting Integrators

If the steady-state errors between the engine and model are the only concerns, we can, as an alternative, force integration into the observer loop to eliminate these errors as we have done before. The procedure is as follows:

Using equation 6.5, 6.6 and 6.7, we define the new state variables as:

$$\dot{x}_r = y - \hat{y} \quad (6.25)$$

Appending the Equation 6.25 to the linear models (Equation 6.5), the following equations are obtained

$$\begin{bmatrix} \dot{\hat{x}} \\ \dot{x}_r \end{bmatrix} = \begin{bmatrix} A_o & 0 \\ -C_o & 0 \end{bmatrix} \begin{bmatrix} \hat{x} \\ x_r \end{bmatrix} + \begin{bmatrix} B_o \\ 0 \end{bmatrix} u + \begin{bmatrix} E_r \\ 0 \end{bmatrix} u_r + \begin{bmatrix} 0 \\ I \end{bmatrix} \hat{y} \quad (6.26)$$

$$\begin{bmatrix} \hat{y} \\ x_r \end{bmatrix} = \begin{bmatrix} C_o & 0 \\ 0 & I \end{bmatrix} \begin{bmatrix} \hat{x} \\ x_r \end{bmatrix} \quad (6.27)$$

Using the LQ or pole placement method to determine the output feedback gain:

$$u_r = -K_{11}\hat{y} - K_{12}x_r \quad (6.28)$$

This scheme is capable of eliminating the steady-state errors, but is not as good as the PI observer in terms of robustness when the engine is subjected to disturbances. This is because robustness is not explicitly considered in the design.

6.6 Control Strategy

Control strategy previously discussed in Chapter 5 is used in conjunction with the model-based observer. A brief outline is repeated here.

The performance requirements are met by using the closed-loop synthesis technique (described in Chapter 5) to design the controller and ensuring that the singular value plots satisfy the required frequency domain constraints. Control of the gas turbine engine specifically requires:

- Fast thrust response without overshoot
- Zero steady-state error.

The fast thrust response requirement is fulfilled by designing to achieve maximum crossover frequencies for the output variables while producing a thrust transient response with no overshoot. The zero steady-state error requirement is met by using a multivariable proportional plus integral (PI) controller (the integrators are added to ensure zero steady-state error). In the present work, the desired closed-loop response is selected as:

$$Q = \text{diag}\left[\frac{a_i}{s + a_i}\right], \quad i = 1, 2 \quad (6.29)$$

6.7 Single-Spool Turbojet Engine

In this section, the simulation results for the single-spool engine are presented. The nonlinear thermodynamic model developed in Chapter 2 is used as a basis for constructing a model-based observer. The measurements selected from the engine are shaft speed N and jet pipe temperature T_4 . The solid lines are the engine responses and the dashed lines are model responses.

6.7.1 Open-Loop Observer Without Control

The simulations shown in Figure 6.4 and 6.5 are based on the assumptions that the model is an exact representation of the engine, i.e. parametrically and structurally correct, but the initial states of the model have been incorrectly guessed, that is the model states are set to values different from the engine states. By subjecting the engine and the model to the same ramp fuel input, from idling to take-off condition in 4 seconds, the performance of the open-loop model-based observer is examined by setting $K_p = 0$. It is seen from the Figures that the open-loop dynamics dominate the observer performance. It is also seen that although the engine and model have converged to the same steady-state condition, The rates of convergence (3 seconds) are slow and are considered unsatisfactory in gas turbine application.

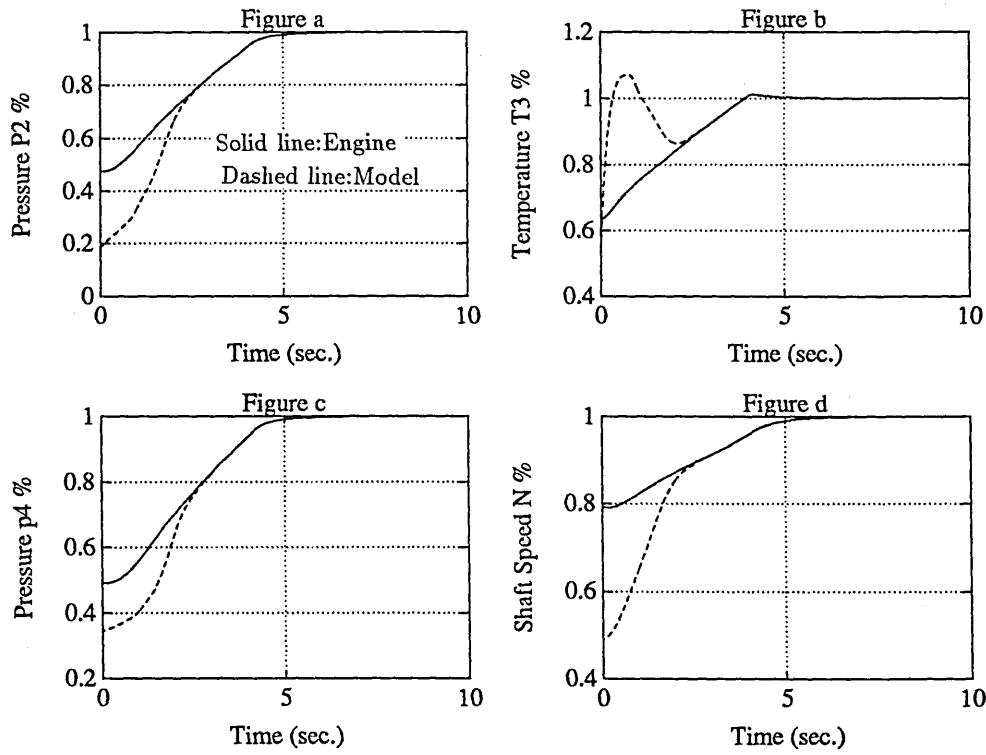


Figure 6.4: Responses of Open-Loop Observer Without Control

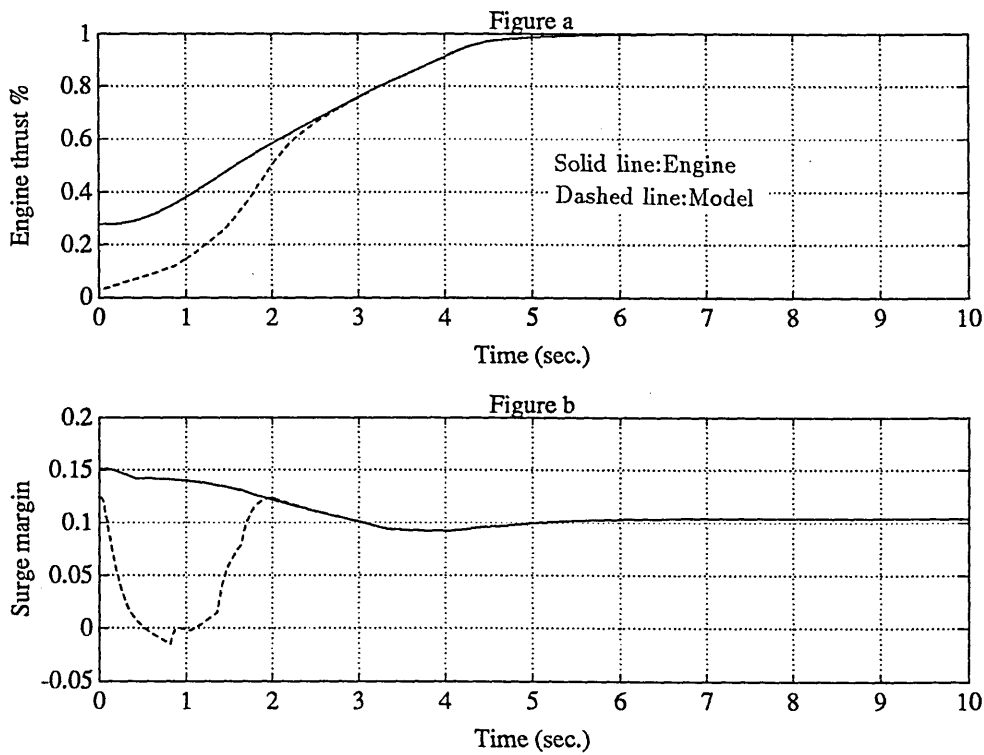


Figure 6.5: Responses of Open-Loop Observer Without Control

6.7.2 Closed-Loop Observer Without Control

Figure 6.6 and 6.7 show the simulation results when the observer loop is closed using the gain K_p . Comparing with the case of $K_p = 0$, it is seen that due to the feedback action, the errors between the engine and the model have been eliminated quickly, with the result that the closed-loop performance can be guaranteed. It is noted that in Figure 6.7b, when closing observer loop, the surge of the compressor (dashed line below 0 value in Figure 6.5b) in open loop case ($K_p = 0$) has been avoided.

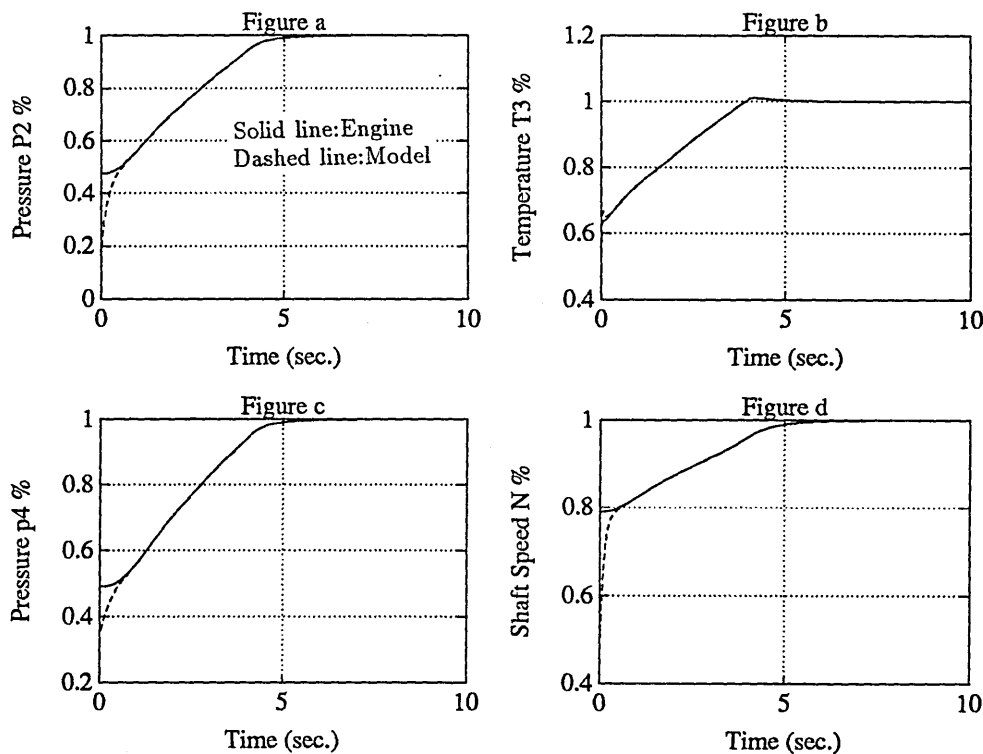


Figure 6.6: Responses of Closed-Loop Observer Without Control

6.7.3 Modelling Error and Use of PI Observer

A convenient way of modelling the turbine in a single-spool gas turbine engine is to use single characteristics as shown by Szuch [102]. These characteristics relate pressure ratio to non-dimensional mass flow and isentropic efficiency in simple manners, which are independent of non-dimensional shaft speed. Mathematically,

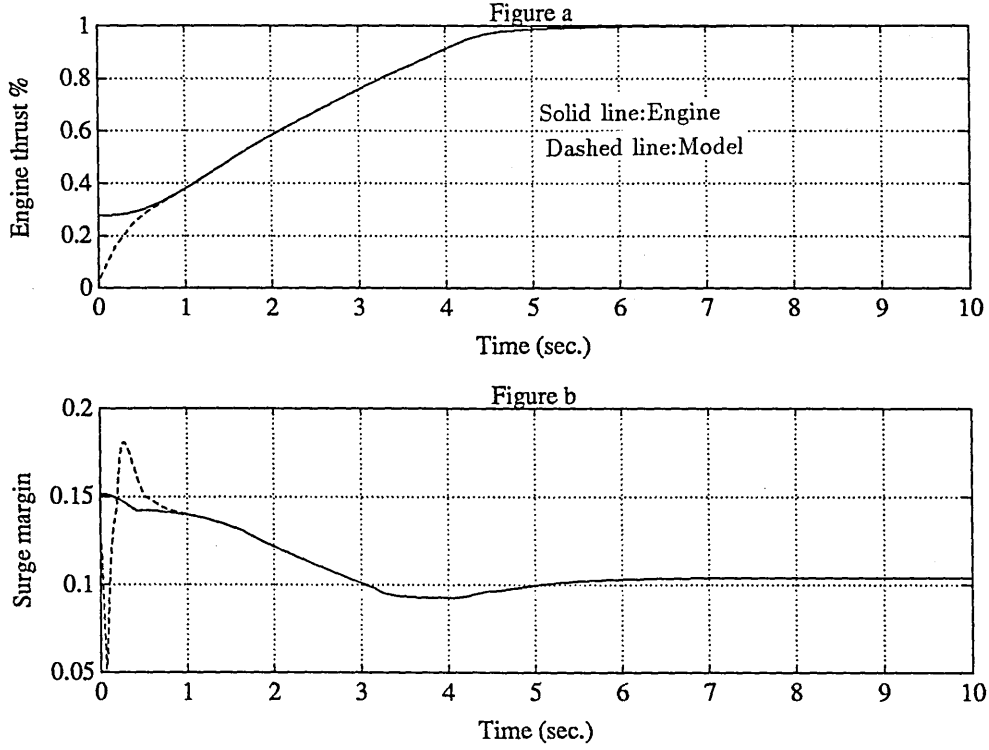


Figure 6.7: Responses of Closed-Loop Observer Without Control

they can be expressed as:

$$\begin{aligned}
 \frac{\dot{m}\sqrt{T_{in}}}{P_{in}} &= f_m\left(\frac{P_{in}}{P_{out}}\right) & \frac{P_{in}}{P_{out}} &\leq \left(\frac{P_{in}}{P_{out}}\right)_{max} \\
 &= \left(\frac{\dot{m}\sqrt{T_{in}}}{P_{in}}\right)_{max} & \frac{P_{in}}{P_{out}} &\geq \left(\frac{P_{in}}{P_{out}}\right)_{max}
 \end{aligned} \tag{6.30}$$

$$\begin{aligned}
 \eta_{is} &= f_e\left(\frac{P_{in}}{P_{out}}\right) & \frac{P_{in}}{P_{out}} &\leq \left(\frac{P_{in}}{P_{out}}\right)_{max} \\
 &= (\eta_{is})_{max} & \frac{P_{in}}{P_{out}} &\geq \left(\frac{P_{in}}{P_{out}}\right)_{max}
 \end{aligned} \tag{6.31}$$

If such a simplification is used in the observer, the resultant model will be different from the one used in the present study (using the speed-dependent characteristics), therefore the modelling errors will show up in e_y in steady-state. In this case, the PI observer is used to provide the robust estimations of the steady-state. The simulations are shown in Figure 6.8 and 6.9. The dotted line is due to the use of the PI observer. It is seen that robust steady-state estimations have been achieved.

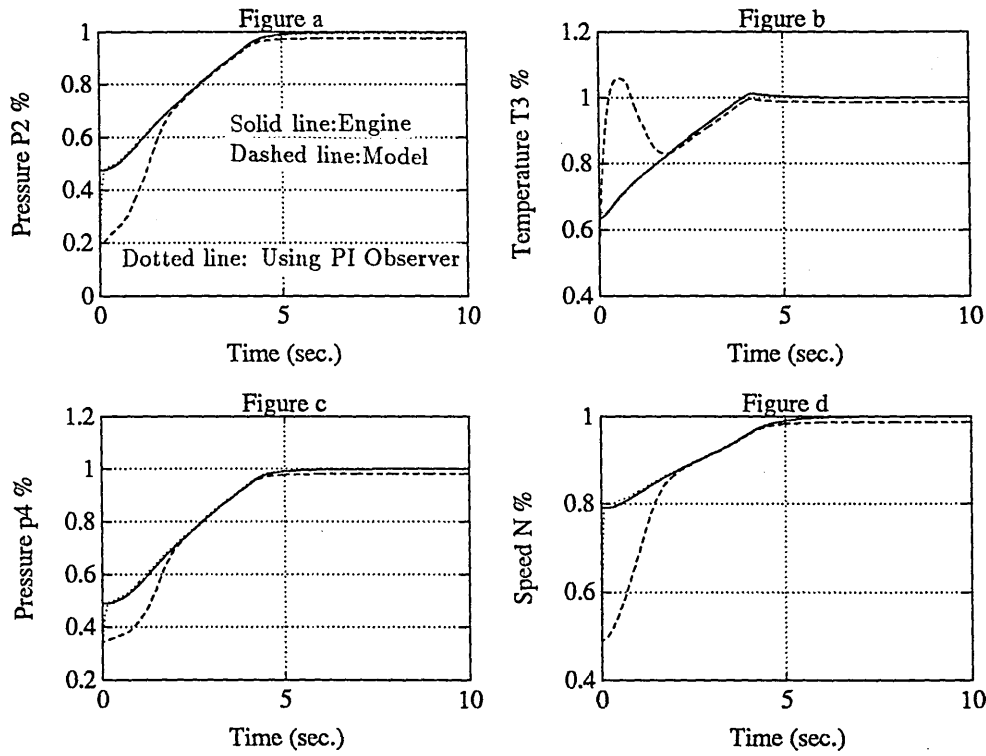


Figure 6.8: Responses Due to the Use of PI Observer

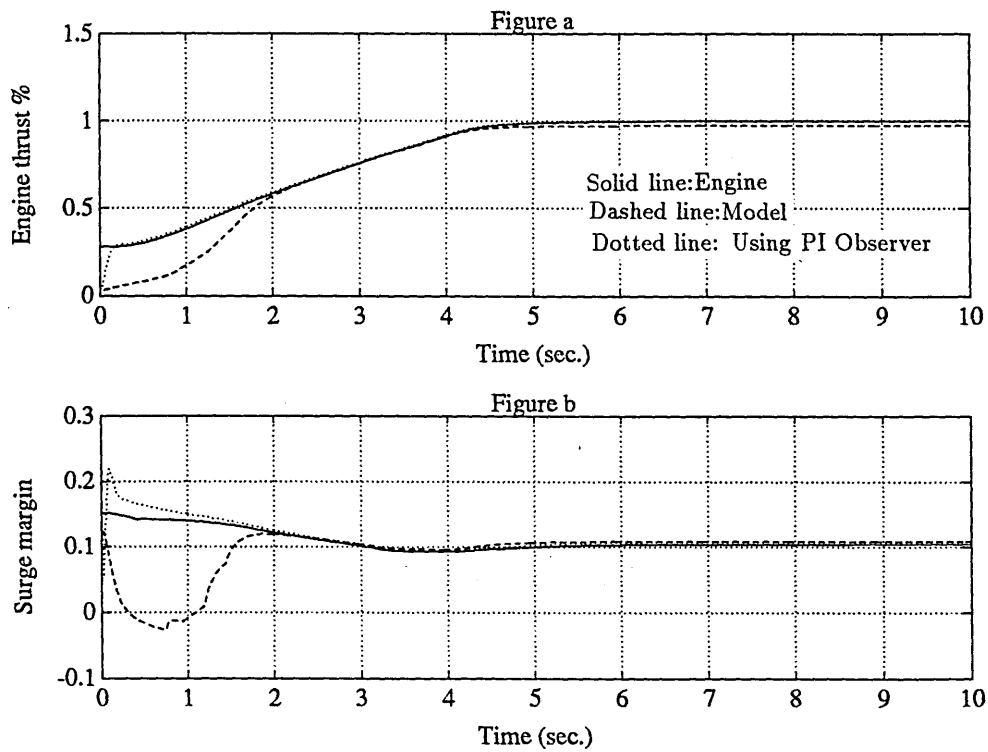


Figure 6.9: Responses Due to the Use of PI Observer

6.7.4 Closed-loop Control

The simulations of the closed-loop performance are shown in Figure 6.10 and 6.11. The linear controller is determined by selecting the desired closed-loop response as shown in equation 6.29 with $a_i = 4$, $i = 1, 2$. The computed thrust and shaft speed from the model are used for feedback control. It is seen that the thrust has been driven to the take-off value in about 4 seconds (Figure 6.10a). Closed-loop control demonstrate good thrust response and adequate surge margin (Figure 6.10b).

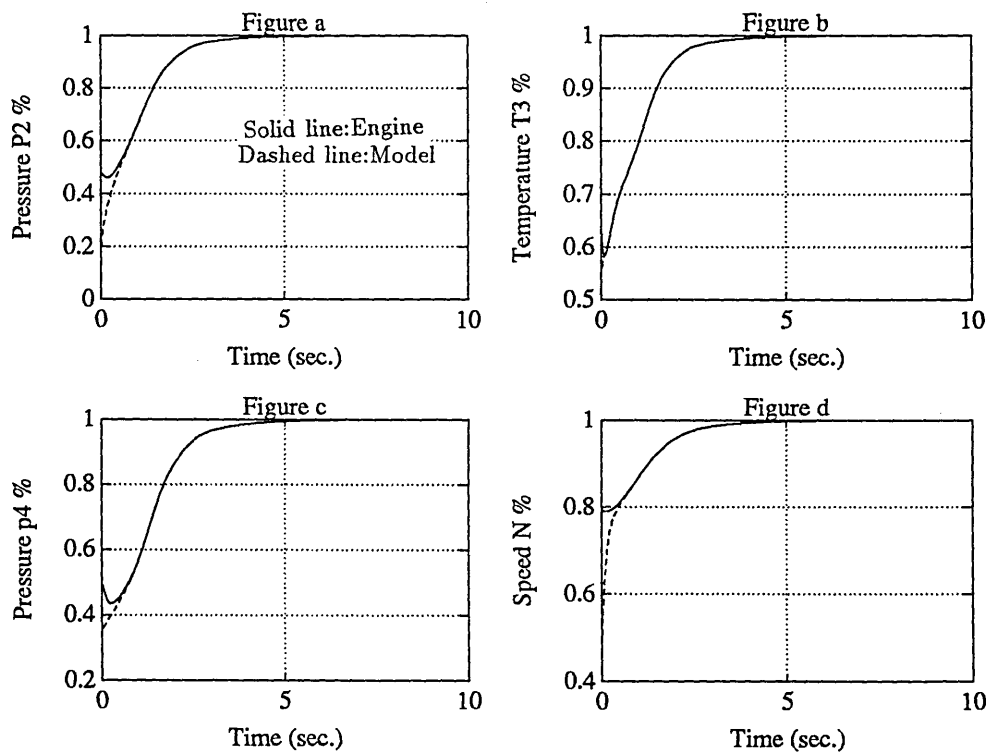


Figure 6.10: Responses of Closed-Loop Control and Observer

6.7.5 Inlet Flow Disturbance

Inlet flow distortion can cause the engine inlet pressure and temperature to fluctuate [154], and these may be treated as disturbances, which tend to cause the compressor to surge.

To simulate the effects of disturbances on the current control scheme, the

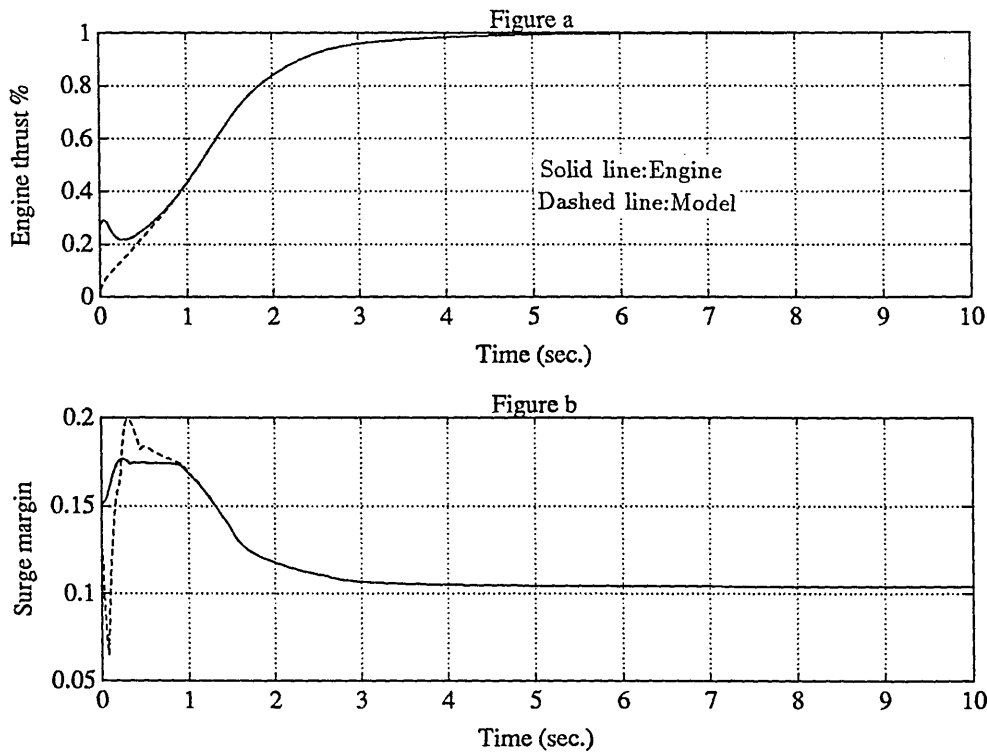


Figure 6.11: Responses of Closed-Loop Control and Observer

following simple model has been used. Moore [155] has suggested that the model of this type might be helpful.

$$P_1 = P_1 + A_d P_1 \sin(\omega_d t) \quad (6.32)$$

where $A_d = 0.1$ and $\omega_d = 10$ in the simulation study.

It is noted that this is equivalent to disturbing all the states along the engine gas path as well as shaft speed. The simulations are shown in Figure 6.12 and 6.13. It is seen that the model follows the engine very well after the disturbance occurred (at $t = 6$ second). It is noted that when disturbances occur, the compressor surge margin is greatly reduced. It is seen the model-based scheme has the ability to reduce the magnitude deviation of the surge margin.

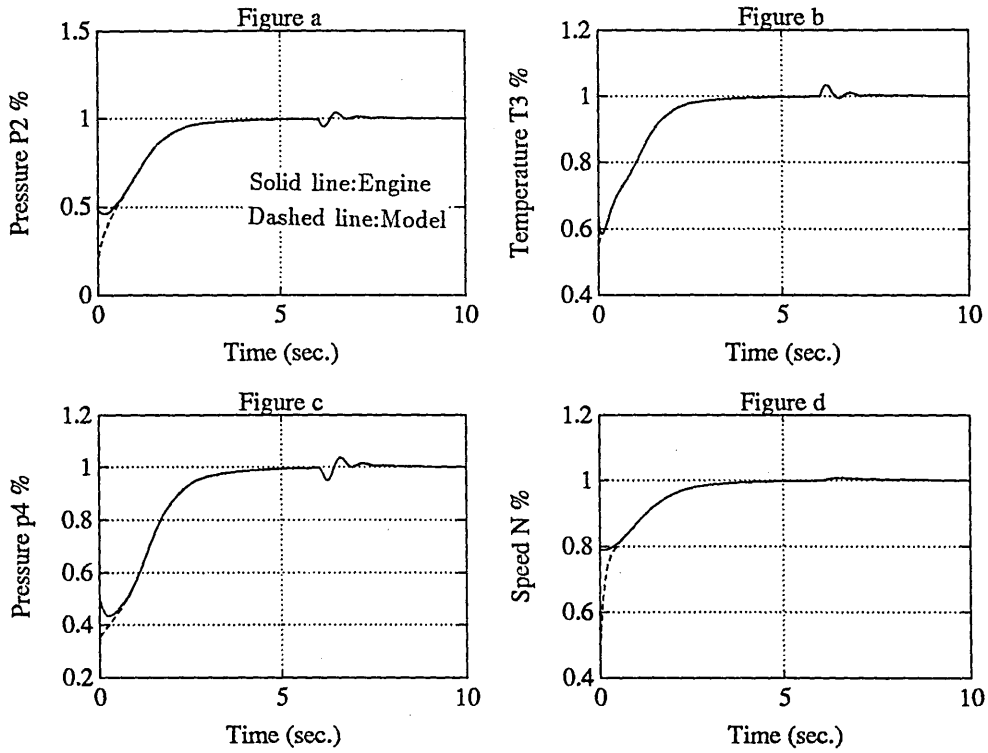


Figure 6.12: Closed-Loop Responses to Inlet Flow Disturbance

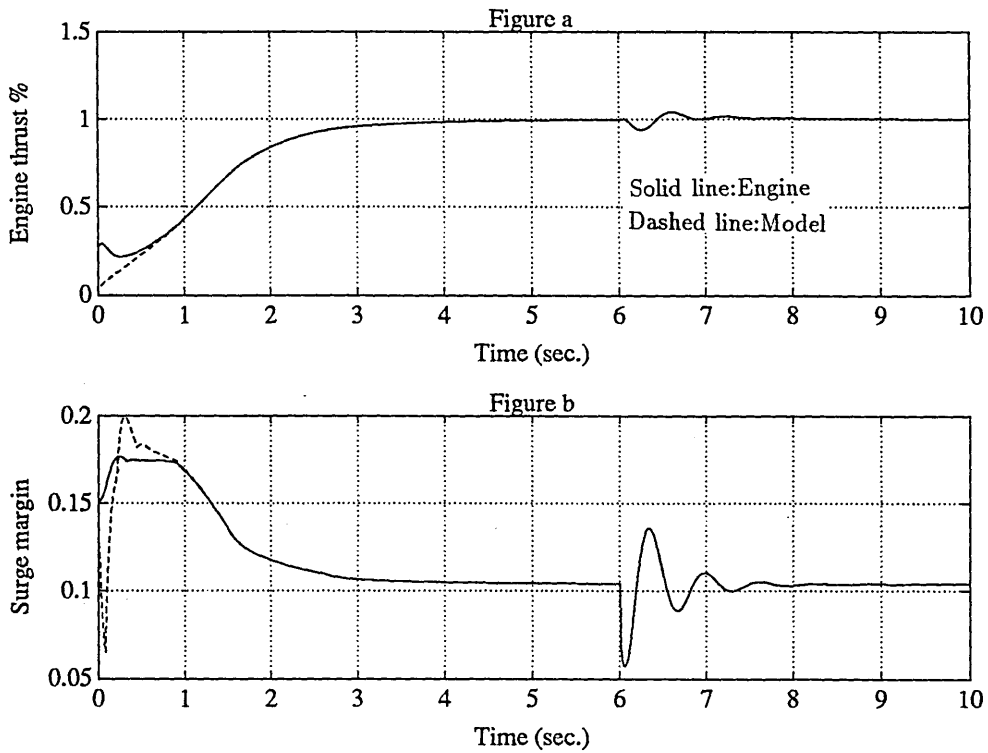


Figure 6.13: Closed-Loop Responses to Inlet Flow Disturbance

6.8 Two-spool Turbofan Engine

The simulation results for the two-spool turbofan engine are presented in this section. The procedure is same as in the case of single-spool engine. The measurements taken for this engine are the HP shaft speed N_H , LP shaft speed N_L , inter-turbine temperature T_5 and jet pipe temperature T_7 .

From Figure 6.14 to 6.15, we have plotted the responses of open-loop observer (dashed lines) and the closed-loop observers (dotted lines) together. The responses of the closed-loop observer clearly show that fast states alignment which are achieved in about 0.5 seconds.

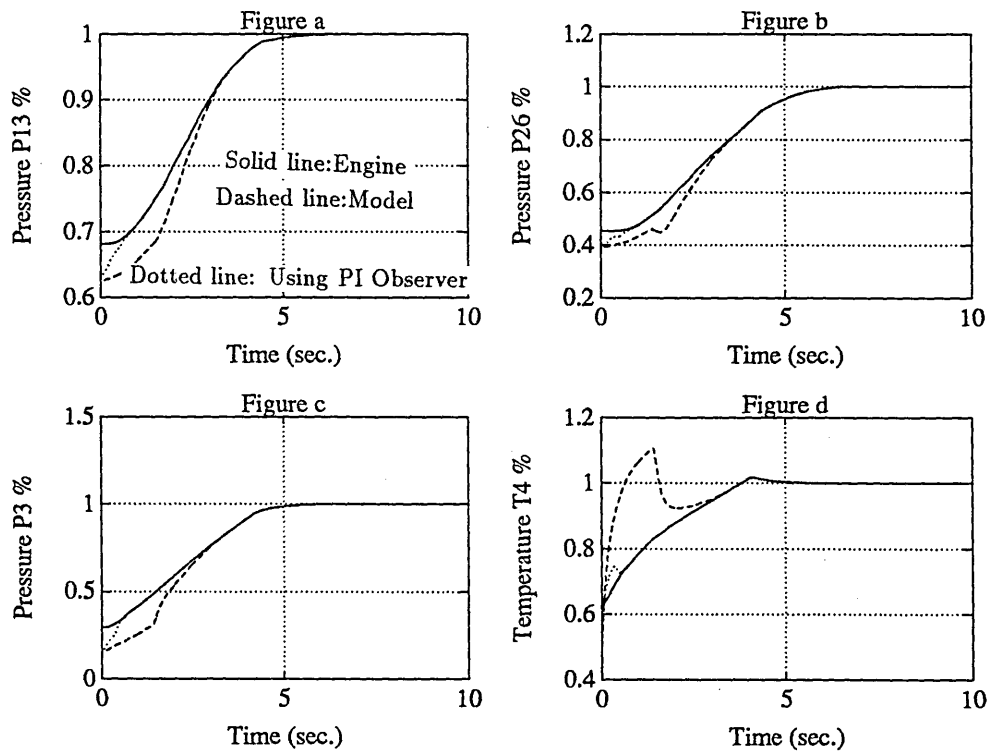


Figure 6.14: Closed-Loop Responses to Inlet Flow Disturbance

Three control inputs, fuel flow, final nozzle area and by-pass area are used to control thrust, LP shaft speed and inter-turbine temperature. To demonstrate the benefits of using the model-based observer, the responses of closed-loop control, while observer loop kept open ($K_p = 0$), are shown from Figure 6.16 to 6.21. It is seen that the responses are relatively slow and the desired responses are

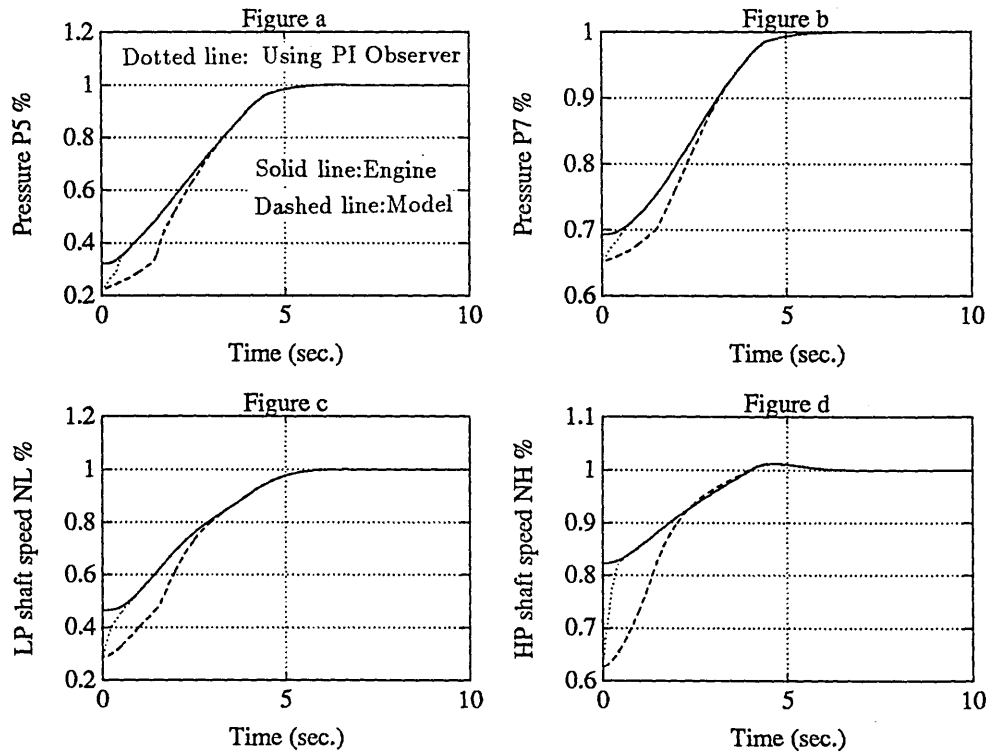


Figure 6.15: Closed-Loop Responses to Inlet Flow Disturbance

not achieved when using the linear controller. To make things worse, the linear controller has caused the HP compressor to surge as shown in Figure 6.21. This is because there are very strong nonlinearities of the engine dynamics over the operating range.

For comparison, the responses of the closed-loop observer and control are shown from Figure 6.22 to 6.27. It is seen that using the closed-loop observer has enable linear controller to work well to drive the engine from the idle to take off condition. The surge of the HP compressor, as shown previously, has been corrected. However, this is at the expense of large excursion of the transient running line of the IP compressor (compare Figure 6.20 and Figure 6.26).

The responses of the closed-loop system to the inlet flow disturbance are shown from Figure 6.28 to 6.30. It is seen the combination of linear controller and the model-based observer has the ability to eliminate the disturbance quickly.

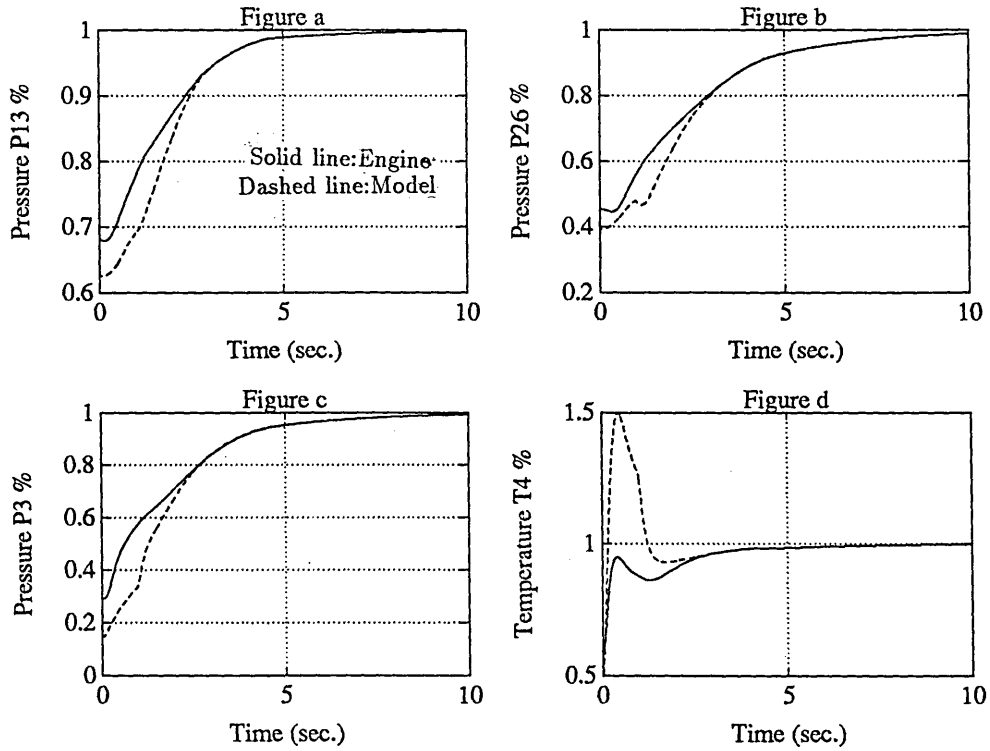


Figure 6.16: Open-Loop Observer and Closed-Loop Control

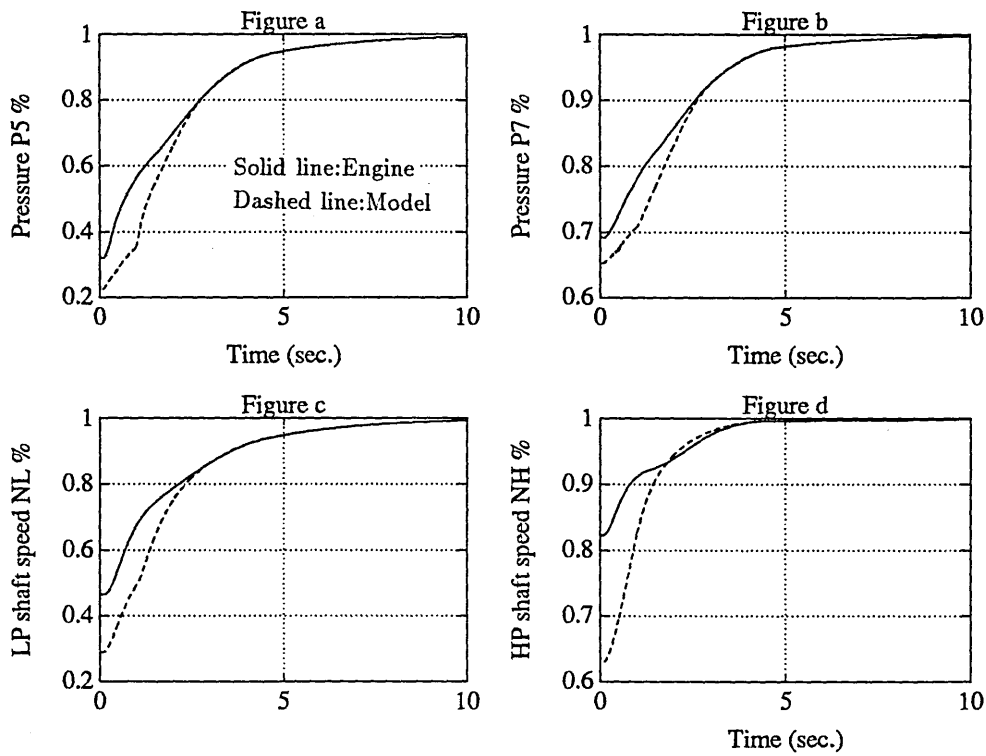


Figure 6.17: Open-Loop Observer and Closed-Loop Control

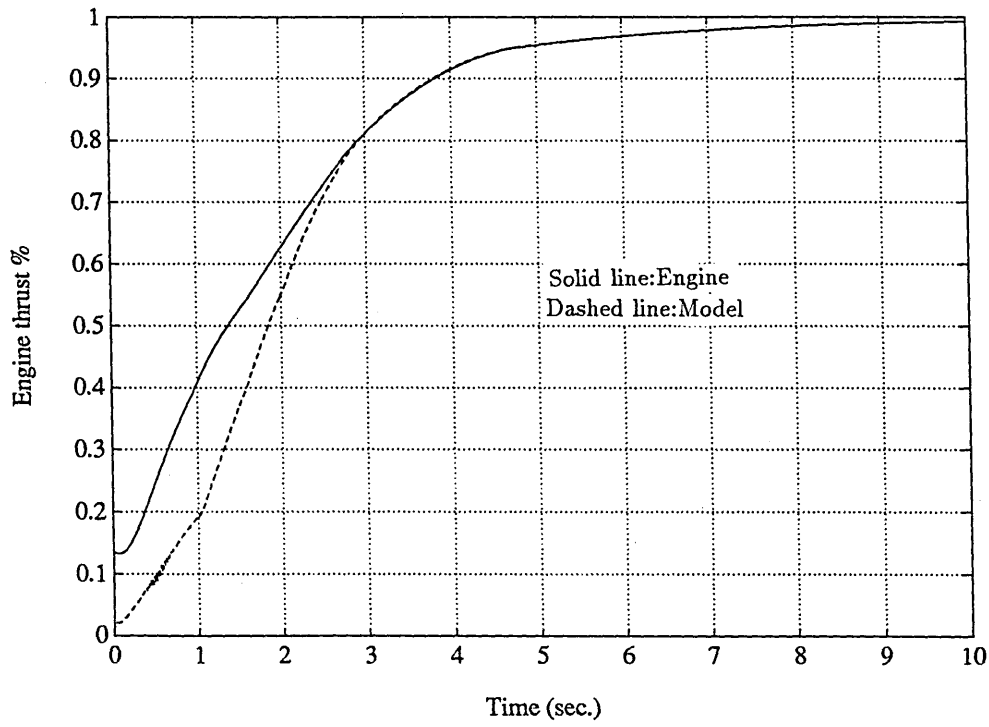


Figure 6.18: Open-Loop Observer and Closed-Loop Control

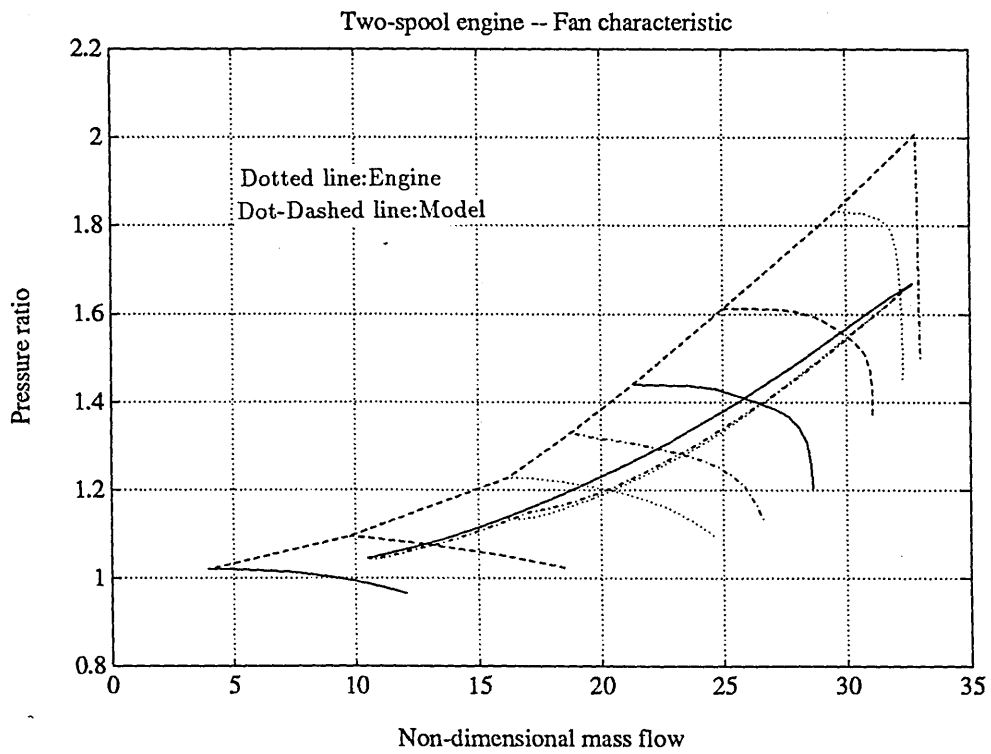


Figure 6.19: Open-Loop Observer and Closed-Loop Control

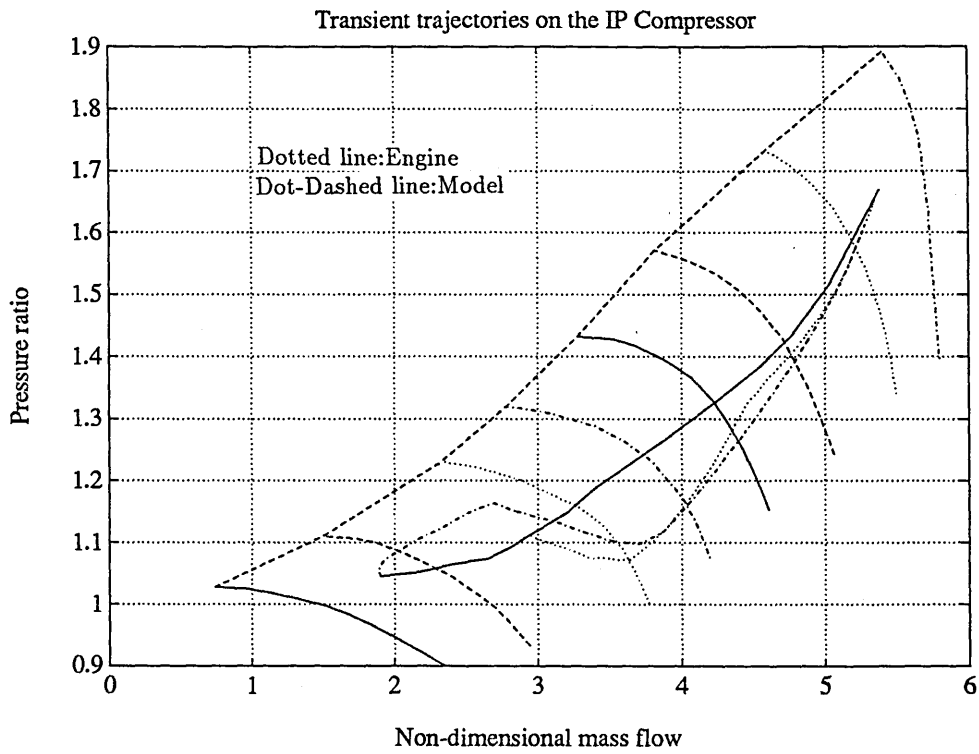


Figure 6.20: Open-Loop Observer and Closed-Loop Control

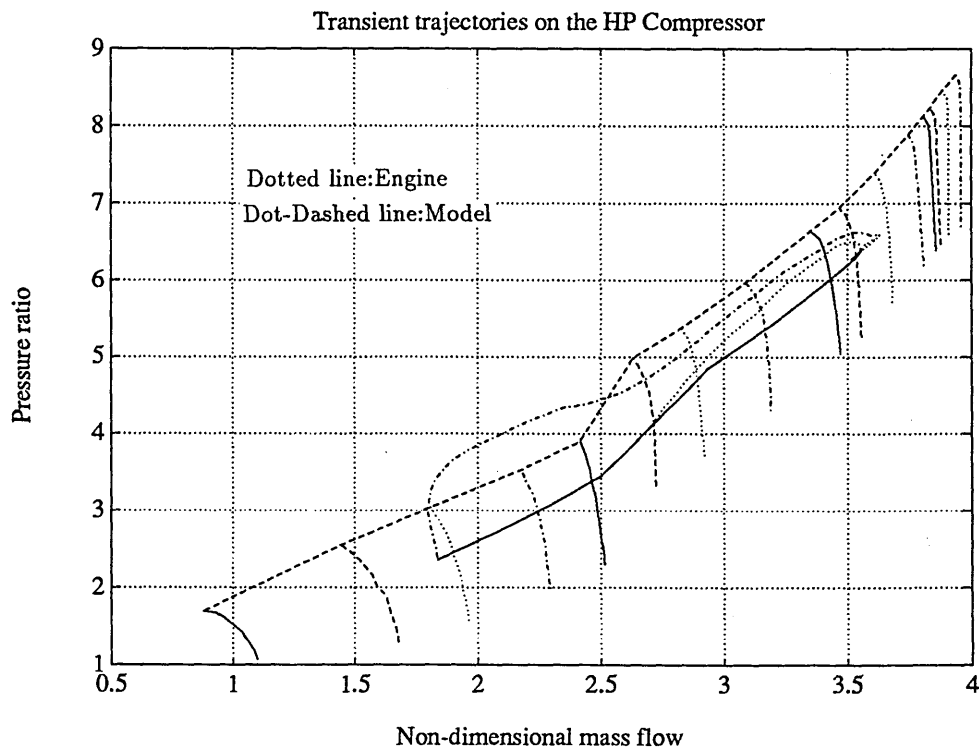


Figure 6.21: Open-Loop Observer and Closed-Loop Control

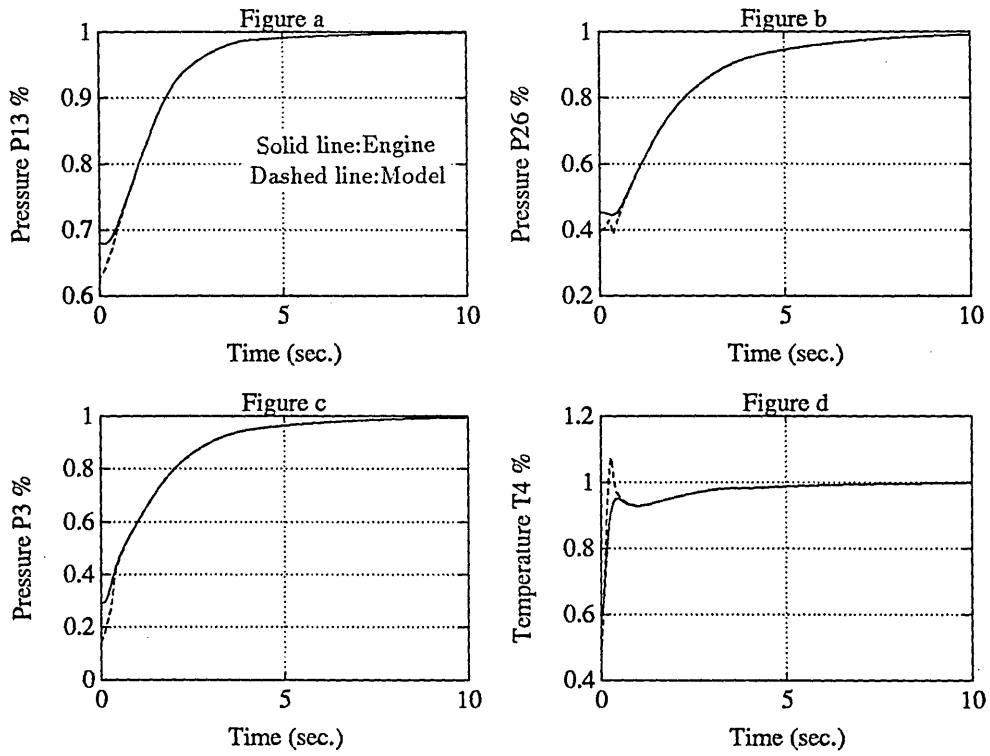


Figure 6.22: Closed-Loop Observer and Closed-Loop Control

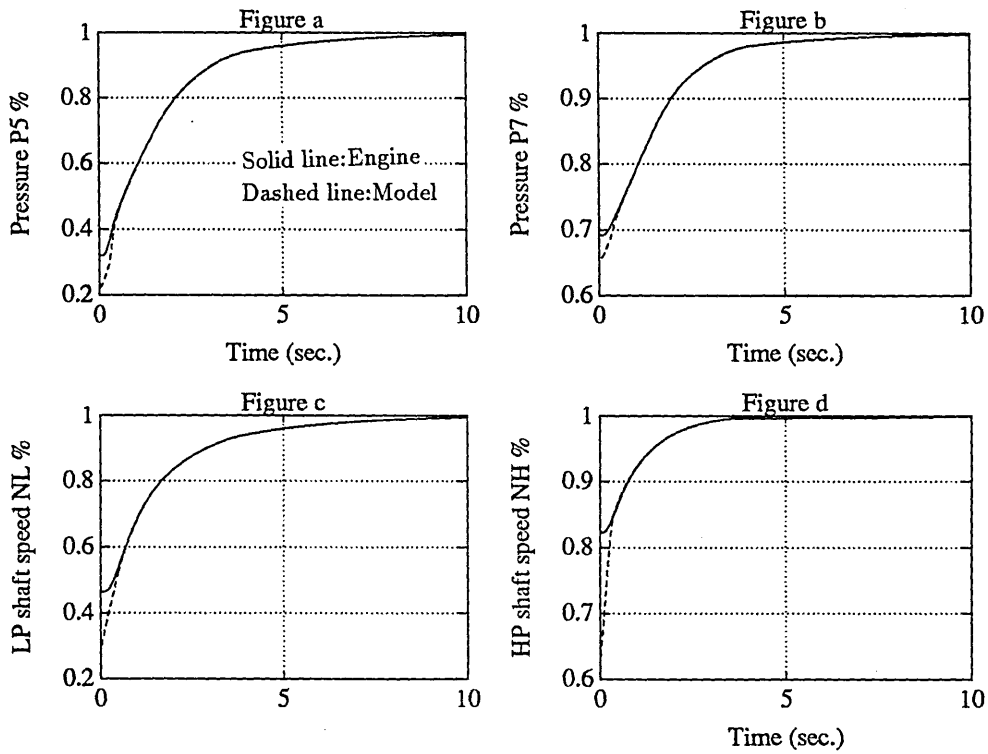


Figure 6.23: Closed-Loop Observer and Closed-Loop Control

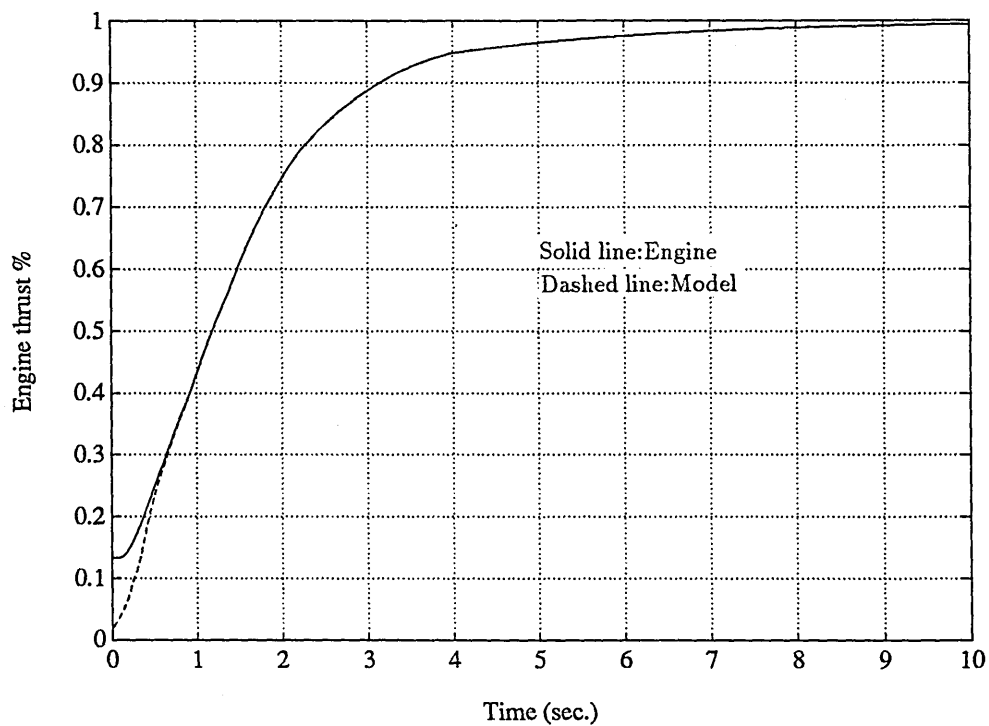


Figure 6.24: Closed-Loop Observer and Closed-Loop Control

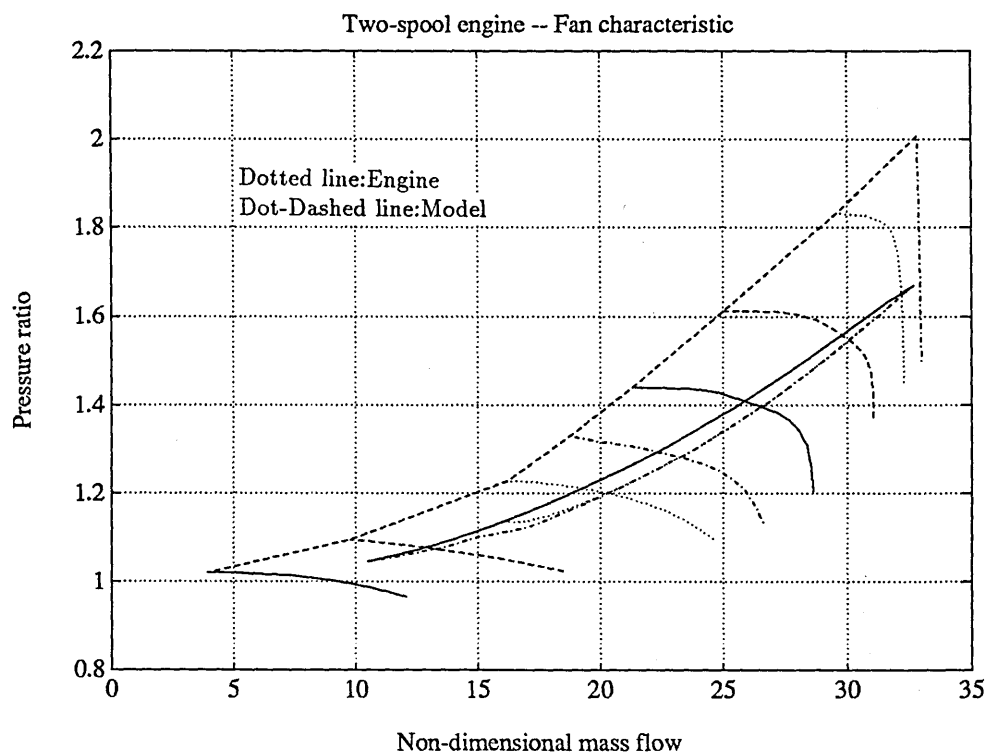


Figure 6.25: Closed-Loop Observer and Closed-Loop Control

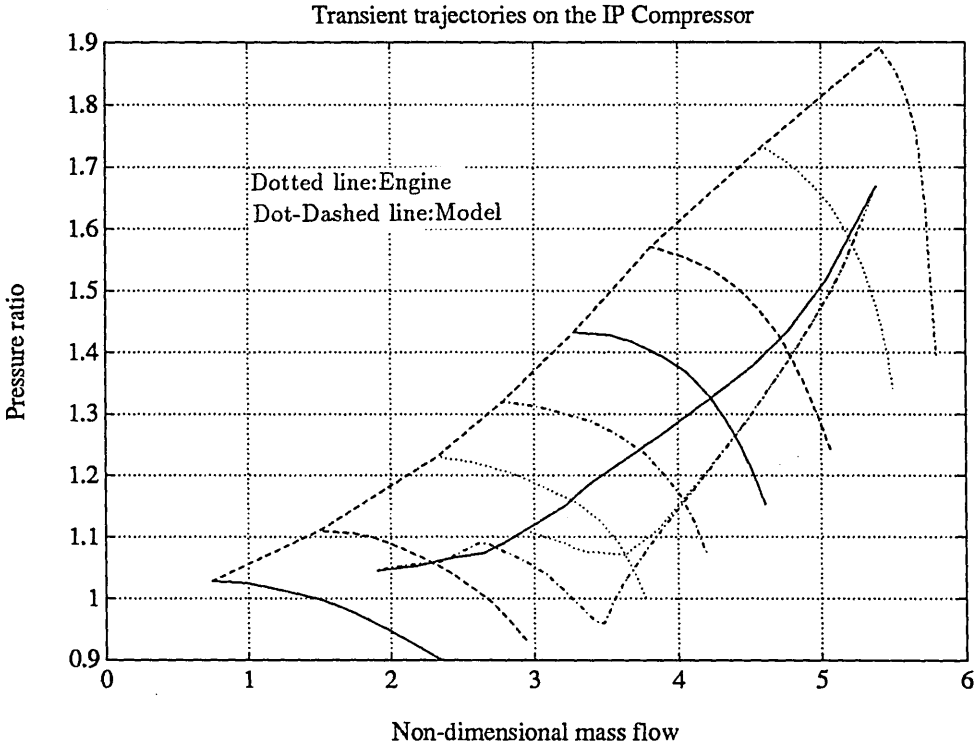


Figure 6.26: Closed-Loop Observer and Closed-Loop Control

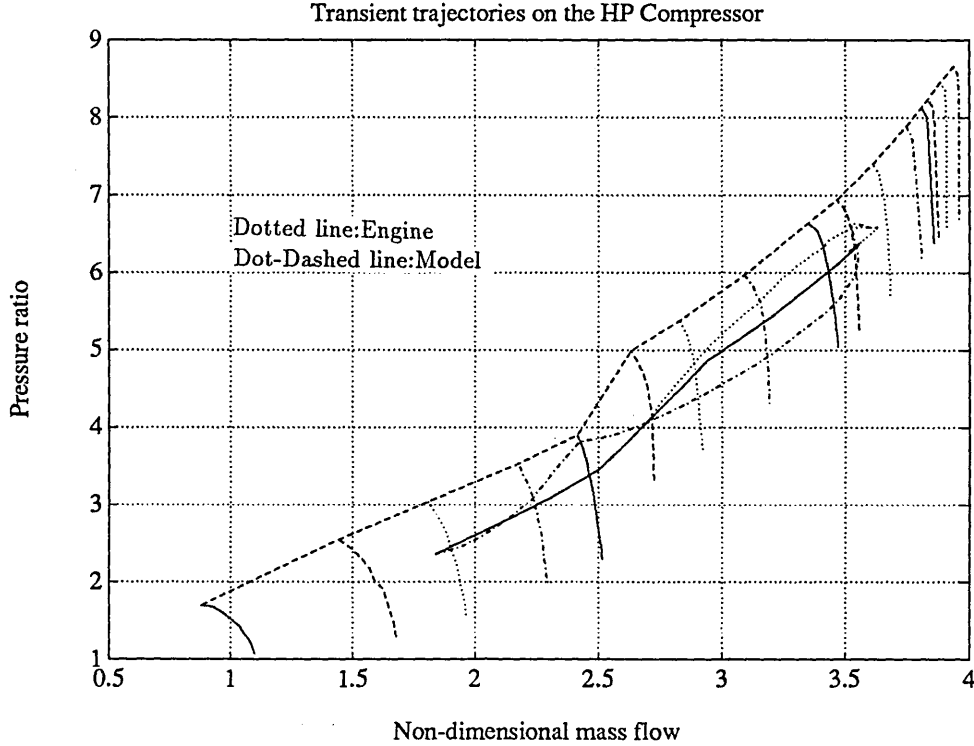


Figure 6.27: Closed-Loop Observer and Closed-Loop Control

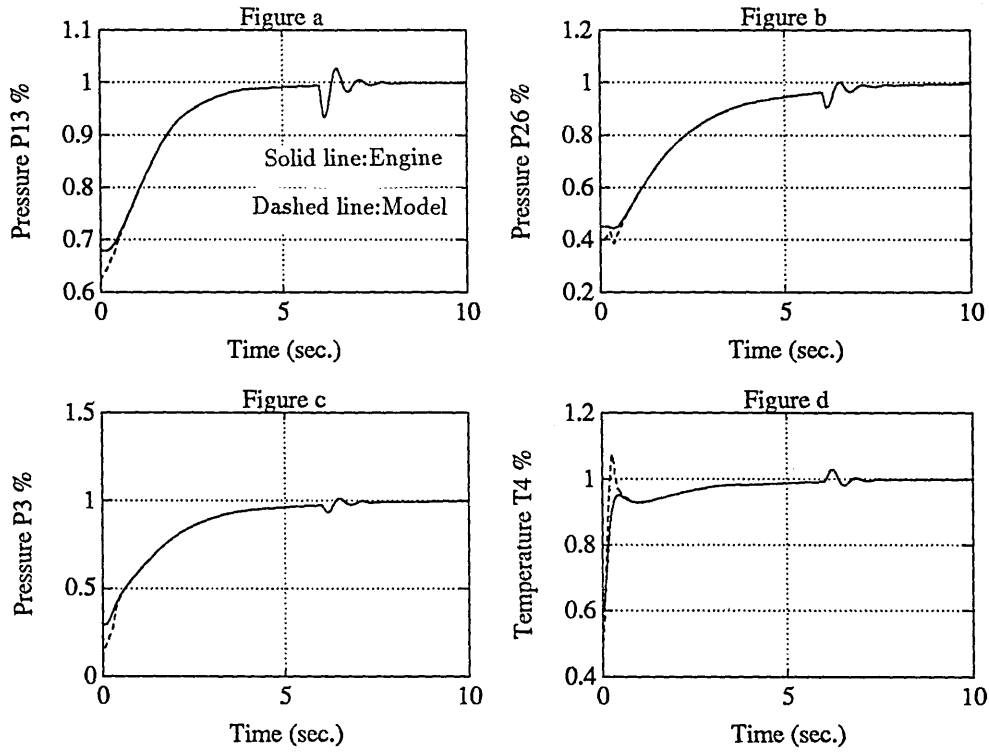


Figure 6.28: Closed-Loop Observer, Closed-Loop Control and Disturbance

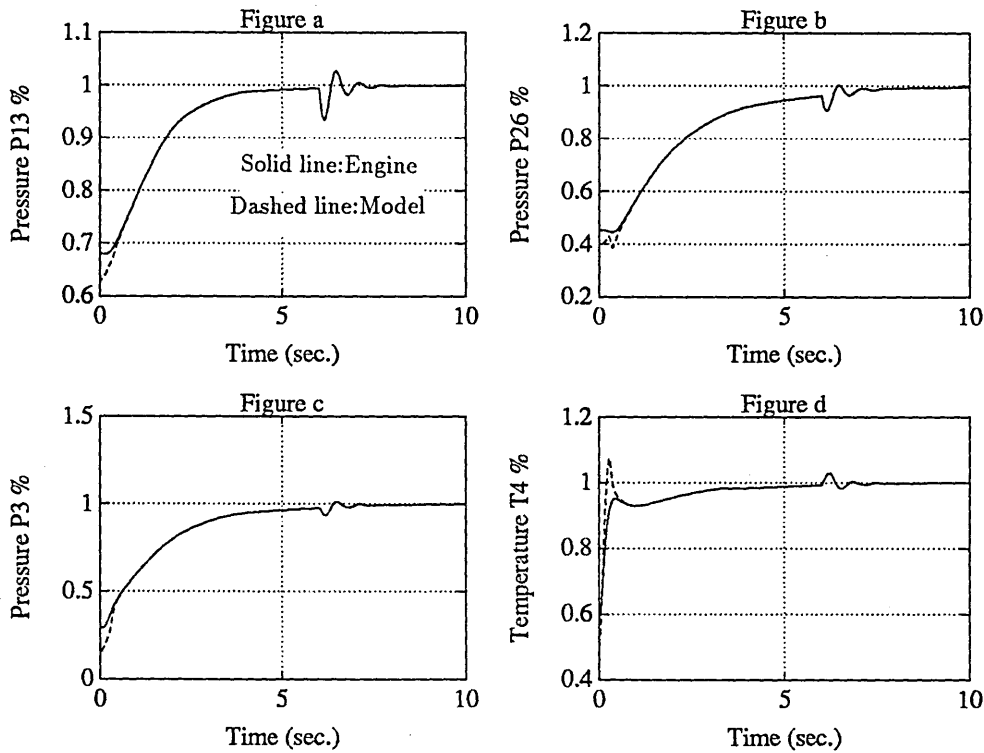


Figure 6.29: Closed-Loop Observer, Closed-Loop Control and Disturbance

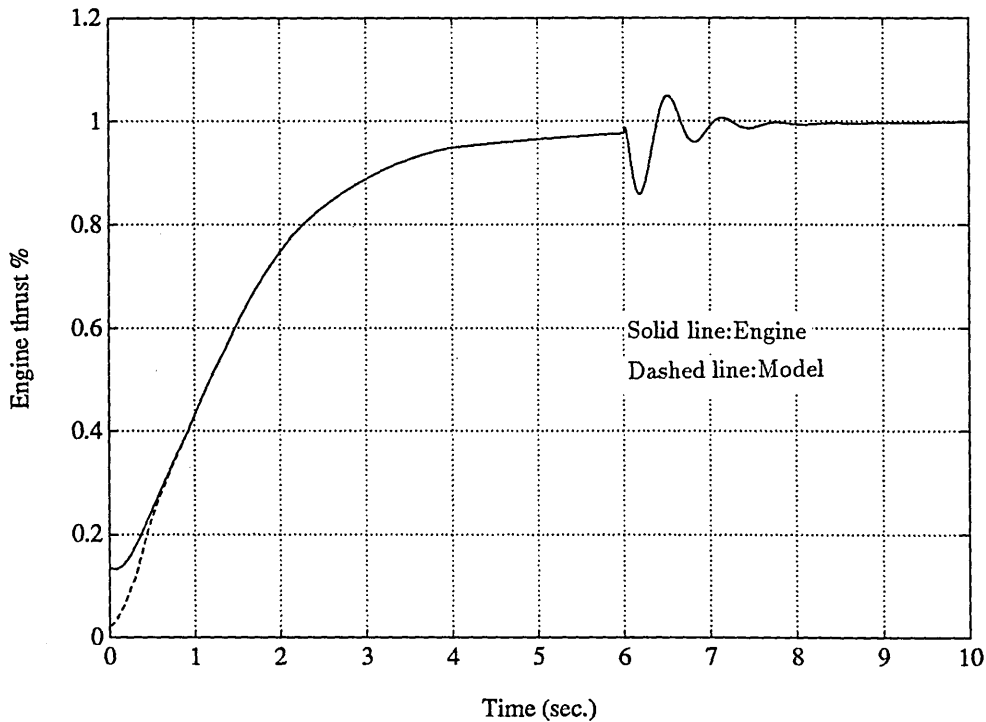


Figure 6.30: Closed-Loop Observer, Closed-Loop Control and Disturbance

6.9 Conclusions

Direct control of the engine thrust, as computed from the model, avoids the control mode analysis, which otherwise has to be used in engine control design. The latter process requires selection of the mode which best reflects the change of engine thrust. This process can be very time consuming, but is of critical importance to engine control design as shown in the previous work by Brown and Elgin [36].

It is shown that direct control of engine thrust is possible by using the proposed model-based observer control scheme. The time taken for the model states to converge to the engine states is all less than 0.5 second.

A procedure has been given for use of the model-based observer approach to synthesise the nonlinear controllers. The effectiveness of the control has been demonstrated by application to the engine control problems.

It can be seen that the focus has been on the observer rather than the controller, as control becomes relatively simple when all measurements are available.

Chapter 7

Conclusions and Further Work

SUMMARY

To complete this thesis, some general conclusions are drawn based on the research carried out in the present study. Further works as an extension of this study, and more generally towards modelling and control of gas turbine engines are suggested.

During the course of this research, the existing approaches to modelling and control of aircraft gas turbine engines and the relevant concepts regarding their integration have been brought under scrutiny. Resulting from this, it is considered that the following objective of the research has been achieved: the improvement of the performance of gas turbine engines by applying modern techniques to the design of the control system.

7.1 On Engine Modelling

In deriving the engine thermodynamic models for control, we considered:

- The use of Intercomponent Volumes (ICV) modelling approach and the selection of state variables.

- The potential performance improvements if variable geometry features are introduced.
- The approach of deriving analytical models for the engine components and the way of assessing the qualities of the resulting models.
- Efficiency of the simulation.
- The use of optimisation techniques in designing open-loop fuel schedule.
- The conservative aspects of using open-loop fuel schedule in achieving the potential performance improvements.
- Model validation.

This study has established the necessity and correctness of using the Intercomponent Volumes (ICV) models as appropriate models for engine control system designs. Based upon our early experience with the Continuity of Mass Flow (CMF) models, we agree with Munro and Winterbone's [156] conclusion that the iteration features of the CMF models are the inherent deficiencies when used for control. In CMF model, some dynamics have to be neglected to keep in line with the assumption made in the modelling phase that mass flow through an engine is constant at any instant of time. This can be considered as the step of model order reduction due to the necessity of modelling rather than for control. Such a procedure can be logically carried out in the ICV models according to the frequency range over which engine control systems function. However, when using ICV models, intercomponent volume sizes must be carefully chosen to avoid potential program instability.

The way of introducing variable geometry features such as variable inlet guide vanes, or bleeds on the compressors is relatively simple. Such treatments are equivalent to scaling the compressor characteristics. It is shown in the present study that the effectiveness of using these features on engine performance have

been correctly predicted as long as the effective ranges of the coefficients are constrained to avoid large variations due to the control requirements.

The use of the defined performance indices (as defined in Chapter 3) provides a framework for designers to evaluate three aspects of the resultant component models: *accuracy*, *complexity* and *predictability*. However, the disadvantage of the present approach is that there is no systematic procedure leading from the defined performance indices to the desired coordinate transformations. The selection of the appropriate transformation leading to a set of linear transformed curves depends on the designer's experience and insight with compressor characteristics.

The degree of agreement between the present simulation results as shown in Chapter 4 and data from base models developed by Pilidis and Maccallum [157] depends mainly upon the validity of the characteristics used in the models to represent the engine components. It should be noted that the deviations shown are likely due to the simplified treatment of some component characteristics, which are summarised as follows:

- The use of single characteristics for fan is not strictly accurate in the circumstances when turbofan operates at the high speeds since the "inner" and "outer" parts of fan will probably have different behaviour aerodynamically due to the shape of the fan blade. However, Petrides [99] has demonstrated that as long as the scaling factor for the "outer" part has been appropriately chosen, the loss of accuracy is always acceptable. The present results have confirmed this conclusion. Another interesting discovery is that the deviations are more obvious in the IP compressor predictions; that is this immediate component is more likely to be affected. When the accuracy of performance predictions is emphasised, the separate representations for fan are recommended. The calculated values of the performance indices presented in Chapter 3 have also confirmed above conclusions from another point of view.

- Turbine characteristics are also changed to the form of using pressure ratio as the independent variable. This is to be consistent with our intention of using most pressures as state variables.

The simulation technique is particularly useful in the studies of the modelling and control. It enables the developed models to be validated and deep understanding about the engine's steady-state and transient operating characteristics to be gained. Furthermore simulation could provide the valuable information as to unmeasured quantities such as surge margin for control study.

The purpose of using optimisation techniques to design an open-loop fuel schedule is to find the theoretical basis for the traditional designs which are based on the steady-state information. This technique has removed the ambiguity of selecting the coefficients for the controller, and provide a systematic approach to the open-loop fuel schedule design.

7.2 On Engine Control

In designing multivariable engine control systems, we considered:

- The algorithm to obtain good linear design models and the validation of the models.
- The procedure which may be followed and the precautions to be taken in nonlinear controller synthesis using the gain scheduling approach.
- The application of a model-based control approach and the advantages it brings about.
- Robust properties and design of model-based observers.

Chapter 5 has demonstrated the specific steps that may be followed so as to apply the gain scheduling approach to designing a nonlinear controller for gas turbine engines. The robust properties and the effectiveness of designs are demonstrated

and inferred from simulations. Furthermore it is seen that controller structure is playing a very important role in easing the scheduling procedure. In the present study the controller structure used is PI structure and the scheduling variable is non-dimensional shaft speed (LP speed for the turbofan). No quantitative justifications are given as to the selection of the scheduling variables. The disadvantage of designing a gain scheduled controller is that this is a very time-consuming process involving interactions between specifications and designs.

One benefit of using a model-based observer is that the task of synthesising a nonlinear controller is reduced to the synthesis of two parts: model-based observer and control. Although only the linear design techniques are used to design the observer gain and controller, application of this technique has given very promising results. The procedure of design and tuning of Proportional and Proportional and Integral observers is successful as shown in the present work. It could be equally used, as the author believes, as the guidelines for other applications. The significance here is it removes the need to carry out the complex control structure design as shown by Brown and Elgin [36].

7.3 Direct Extension of the Present Work

It would be useful to pursue the following subject as an extension to the work presented here:

- Implementing the model-based control to examining practical benefits when using this approach. For example, the investigation of an engine's operating characteristics under the conditions when sensors fail.
- Use of a symbolic modelling language such as REDUCE to develop the generic model for an engine. Such a model could consequently be used for any purposes (e.g. performance prediction or control).

- Introducing afterburning fuel control. This will require the interaction of control between the final nozzle area and afterburning fuel flow. This is important for military applications.
- Developing the adaptive engine control systems.

7.4 Further Works in Modelling and Control

The primary value of the present work is that it demonstrates the possibility of performance improvements and the credibility of using a multivariable controller to control gas turbine engines. This work could also be regarded as one step among others towards using an advanced control system as a potential replacement to the traditional control. For the final implementation and success of advanced control systems, the following perceived requirements in general have to be further elaborated.

7.4.1 Real Time Identification

It is generally agreed that the most significant gains in engine control will be achieved if the engine modelling process can be improved. One important aspect of the modelling process is the identification of dynamic models from the engine test data. Of particular interest is the real time identification with time-varying parameters using closed-loop test data. This would allow an engine model updated in real time as the engine moves from one flight condition to another. This kind of research could eventually lead to a self-tuning or adaptive engine control system.

7.4.2 Nonlinear Modelling

It is very important to develop analytically tractable nonlinear models. This may consist of two steps: firstly developing appropriate nonlinear engine model structure, and secondly identifying the parameters within this structure. Nonlinear

models will be required both for the successful application of nonlinear control design techniques and for the study of nonlinear engine phenomena such as compressor surge.

7.4.3 Engine Control System Design

New nonlinear control design techniques are needed to be developed to allow for direct design using the developed nonlinear model. These nonlinear techniques should include adaptive control, nonlinear feedback control and performance-seeking control. Many of these techniques, however, require improvements in nonlinear engine modelling before nonlinear engine control designs can be achieved. In addition, work needs to be done in the areas of microprocessor implementation of modern control algorithms, the effect of sample-rate and multiple sampling rate on system performance, and the direct design of controls in the discrete-time domain rather than digitising continuous-time domain designs.

7.4.4 Engine Control Reliability

Research towards improving the engine control system reliability is another very important aspect. In particular, techniques that incorporate analytical redundancy need to be pursued. The evaluation and demonstration of detection, isolation, and accommodation of sensor failures on a full-scale engine are needed. The robust properties of analytically redundant algorithms need to be more completely understood to predict maximum achievable performance, and also a better procedure of modelling system reliability performance is required.

Appendix A

This appendix presents the definitions of symbols used in Chapter 3, and numerical values for the compressor of the single-spool engine.

Nomenclature

a_i, b_i	=	coefficients for the polynomials.
x	=	compressor non-dimensional mass flow group
y	=	compressor pressure ratio
z	=	compressor isentropic efficiency
X	=	the new non-dimensional group ($X = x/y$)
Y	=	the new non-dimensional group ($Y = y$)
Z	=	the new non-dimensional group ($Z = z/y^2$)

A.1 Selecting Appropriate Transformations

Directly fitting polynomials to the given characteristics does not produce good results as shown in section 3.3.1 of Chapter 3. An improvement can be obtained by regrouping the non-dimensional parameters to give a set of monotonic curves. Numerically such regrouping can be considered as weighting on each characteristic to “straighten” each non-dimensional speed curve. The following features should be targeted in search of appropriate transformations.

- The set of transformed characteristics should ideally be linear.

- Fitted polynomials should be explicit; that is the non-dimensional mass flow should be expressed as a function of non-dimensional shaft speed and pressure ratio.

The search strategy adopted was to intelligently apply each of the possible transformations suggested in Table 3.2 to the characteristics, one at a time. The resulting transformed characteristics were firstly be plotted, and assessed qualitatively. As an example, choose the following as new grouped variables $X = x^2 * y$, $Y = y$ and $Z = x * y$. The resultant transformed characteristics are shown in Figure A1 and A2. Compared with those obtained for $X = x/y$, $Y = y$ and $Z = z/y^2$ (Figure 3.9 and 3.10), it is seen that the relationships between X and Y , and X and Z are not linear, and as a result second order polynomials will be required to fit the coefficients a_i and b_i , this will increase the complexity of the equations (e.g. Equation 3.22). This is therefore rejected.

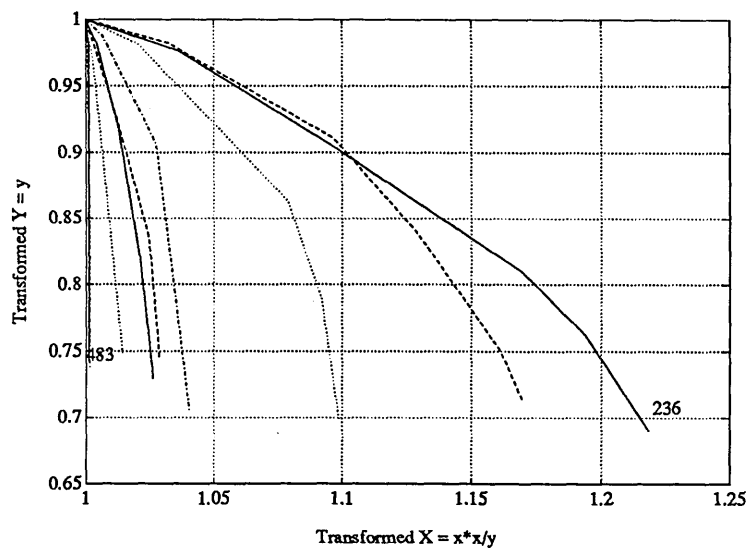


Figure A.1: Transformed Curves Using $X = x^2 * y$ and $Y = y$

If favourable, the various quantitative criteria were then calculated (i.e. the monotonic index, error index and predictability index). At the end of the search those transforms providing the most favourable values (i.e. the monotonic index and error index were small, and predictability index was close to one) were

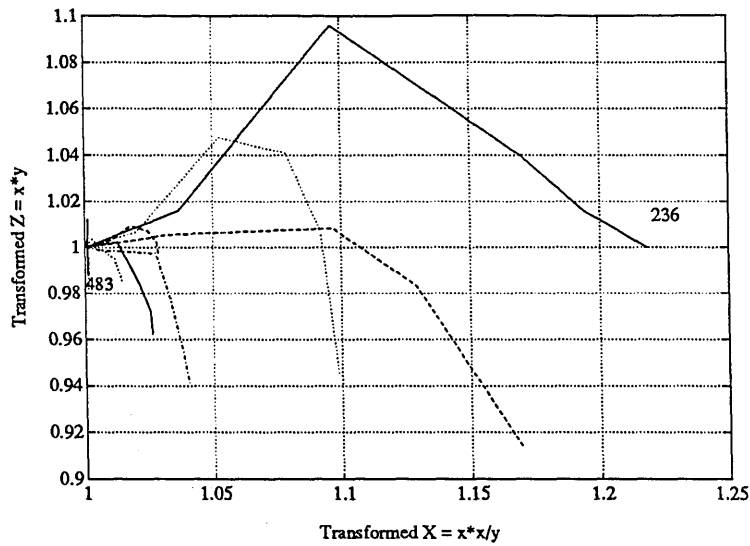


Figure A.2: Transformed Curves Using $X = x^2 * y$ and $Z = x * y$

selected. Table 3.3 gives the final selection for turbofan engine.

A.2 Numerical Values for a Compressor

In this section, numerical values are given when applying the proposed technique to the compressor of the single-spool engine. Original compressor characteristics are represented by x , y and z , which are defined as: $x = \dot{m}\sqrt{T_{in}}/P_{in}$, $y = P_{out}/P_{in}$ and $z = \eta_{is}$.

$x = [$
 2.69990 2.79860 2.96040 3.15780 3.22360 3.28930
 4.07880 4.21040 4.47350 4.60510 4.73670 4.76960
 5.00000 5.10000 5.26300 5.39450 5.46030 5.49320
 6.21030 6.24980 6.38130 6.41420 6.44710 6.46030
 7.79580 7.82870 7.89440 7.96020 7.99310 7.99970
 9.69540 9.80230 9.86810 9.93380 9.96670 9.97330
 11.5456 11.5785 11.6114 11.6443 11.6772 11.7101
 12.6969 12.7035 12.7100 12.7133 12.7133 12.7133
 13.0127 13.0258 13.0258 13.0258 13.0258 13.0258];

$y = [$
 2.10000 2.05000 1.90000 1.70000 1.60000 1.45000
 2.80000 2.75000 2.55000 2.35000 2.10000 2.00000
 3.36000 3.30000 3.08000 2.90000 2.65000 2.35000
 4.25000 4.20000 3.85000 3.50000 3.15000 3.00000
 5.55000 5.45000 5.10000 4.55000 4.15000 4.05000
 7.40000 6.90000 6.55000 6.18000 5.65000 5.52000
 9.15000 8.85000 8.35000 7.85000 7.35000 6.85000
 10.5000 10.3500 9.65000 9.00000 8.35000 7.75000
 10.9000 10.7000 9.90000 9.20000 8.60000 8.10000];

$z = [$
 0.62500 0.63500 0.68500 0.65000 0.63500 0.62500
 0.72200 0.72600 0.72800 0.71000 0.67000 0.66000
 0.73500 0.74000 0.77000 0.76500 0.74000 0.69500
 0.80200 0.80100 0.80000 0.78500 0.76500 0.75500
 0.82800 0.82900 0.83000 0.81500 0.80500 0.79700
 0.84200 0.84500 0.85000 0.84800 0.84400 0.84000
 0.84200 0.84500 0.84200 0.84000 0.83800 0.83000
 0.83500 0.83600 0.83500 0.83200 0.83000 0.82000
 0.82500 0.82800 0.83500 0.82600 0.82000 0.81500];

The transformed characteristics are represented by X , Y and Z . where $X = x/y$, $Y = y$ and $Z = z/y^2$. This is plotted in Figure 3.9 and 3.10.

$X = [$
 1.00000 1.06180 1.21190 1.44480 1.56710 1.76440
 1.00000 1.05100 1.20430 1.34520 1.54840 1.63710
 1.00000 1.03850 1.14830 1.25000 1.38460 1.57080
 1.00000 1.01830 1.13430 1.25420 1.40070 1.47370
 1.00000 1.02260 1.10200 1.24550 1.37120 1.40620

1.00000 1.08430 1.14990 1.22690 1.34640 1.37900
 1.00000 1.03680 1.10210 1.17560 1.25910 1.35480
 1.00000 1.01500 1.08920 1.16820 1.25910 1.35660
 1.00000 1.01970 1.10210 1.18600 1.26870 1.34700];

$Y = [$

2.10000 2.05000 1.90000 1.70000 1.60000 1.45000
 2.80000 2.75000 2.55000 2.35000 2.10000 2.00000
 3.36000 3.30000 3.08000 2.90000 2.65000 2.35000
 4.25000 4.20000 3.85000 3.50000 3.15000 3.00000
 5.55000 5.45000 5.10000 4.55000 4.15000 4.05000
 7.40000 6.90000 6.55000 6.18000 5.65000 5.52000
 9.15000 8.85000 8.35000 7.85000 7.35000 6.85000
 10.5000 10.3500 9.65000 9.00000 8.35000 7.75000
 10.9000 10.7000 9.90000 9.20000 8.60000 8.10000];

$Z = [$

1.00000 1.06620 1.33890 1.58700 1.75020 2.09750
 1.00000 1.04240 1.21570 1.39610 1.64970 1.79170
 1.00000 1.04370 1.24680 1.39720 1.61860 1.93300
 1.00000 1.02270 1.21550 1.44320 1.73640 1.88930
 1.00000 1.03830 1.18710 1.46450 1.73880 1.80760
 1.00000 1.15430 1.28850 1.44400 1.71950 1.79290
 1.00000 1.07280 1.20080 1.35540 1.54240 1.75880
 1.00000 1.03040 1.18390 1.35620 1.57180 1.80260
 1.00000 1.04150 1.22690 1.40540 1.59670 1.78890];

The a_1 and b_1 shown in Equation 3.23-24 and 3.27-28 are given as follows.
 They are also plotted in Figure 3.11 and 3.12.

$a_1 = [$

-0.4095 -0.4566 -0.5328 -0.6297 -0.6665 -0.6618 -0.7102 -0.7411 -0.7468

1.4066 1.4586 1.5314 1.6250 1.6604 1.6531 1.7017 1.7333 1.7395];

$b_1 = [$

1.2403 1.3961 1.6413 1.8818 1.9972 2.1106 2.1387 2.2480 2.2579

-0.2603 -0.3998 -0.6490 -0.8991 -1.0065 -1.1281 -1.1479 -1.2566 -1.2623];

The reconstructed characteristics are as follows:

$x_{new} = [$

2.69990 2.79860 2.96040 3.15780 3.22360 3.28930

4.07880 4.21040 4.47350 4.60510 4.73670 4.76960

5.00000 5.10000 5.26300 5.39450 5.46030 5.49320

6.21030 6.24980 6.38130 6.41420 6.44710 6.46030

7.79580 7.82870 7.89440 7.96020 7.99310 7.99970

9.69540 9.80230 9.86810 9.93380 9.96670 9.97330

11.5456 11.5785 11.6114 11.6443 11.6772 11.7101

12.6969 12.7035 12.7100 12.7133 12.7133 12.7133

13.0127 13.0258 13.0258 13.0258 13.0258 13.0258];

$y_{new} = [$

2.09390 2.04070 1.91160 1.71130 1.60610 1.43640

2.80560 2.74030 2.54440 2.36420 2.10450 1.99100

3.35540 3.28640 3.09000 2.90780 2.66680 2.33360

4.22980 4.18070 3.87040 3.54960 3.15750 2.96200

5.51590 5.43210 5.13850 4.60770 4.14270 4.01320

7.33510 6.92230 6.60100 6.22410 5.63860 5.47890

9.07210 8.83270 8.40890 7.93120 7.38850 6.76650

10.4184 10.3015 9.72430 9.10980 8.40220 7.64370

10.8197 10.6592 9.98840 9.30580 8.63220 7.99470];

$z_{new} = [$

0.62270 0.64480 0.66110 0.66240 0.64870 0.61490

0.70760 0.72660 0.73860 0.71620 0.67430 0.65210

0.72940 0.74840 0.76320 0.76800 0.74230 0.69360

0.78810 0.79670 0.81310 0.79470 0.76510 0.74890
0.82030 0.82710 0.83510 0.82420 0.80190 0.79450
0.82730 0.84950 0.85680 0.85820 0.84110 0.83510
0.83420 0.84250 0.84780 0.84670 0.83940 0.82560
0.82780 0.83170 0.84070 0.84010 0.83110 0.81560
0.82140 0.82700 0.83450 0.83200 0.82300 0.81060];

This is plotted in Figure 3.17 and 3.18, together with original data for comparisons.

Bibliography

- [1] G.F.C. rogers and Y.R. Mayhew. Engineering thermodynamics work and heat transfer. In *Longman Group Limited. Second Edition*, 1967.
- [2] D.J. Nuske and P.E. Wellstead. Identification of an automotive gas turbine part2. parameter fitting. *Int. J. Control*, 24(3):311–324, 1975.
- [3] R.L. DeHoff and JR W.Earl.Hall. Optimal control of turbine engines. *Journal of Dynamic Systems, Measurement, and Control*, 101:117–126, 1979.
- [4] E.W. Otto and B.L. Taylor. Dynamics of a turbojet engine considered as a quasi-static system. In *NACA Technical Note 2091*, 1950.
- [5] D. Novik. Some linear dynamics of two-spool turbojet engines. In *NACA Technical Note 3274*, 1956.
- [6] M.R. Maltby. Acceleration performance of holicopter engines. *J. of Engineering for Gas Turbines and Power*, 109:127–131, 1987.
- [7] J.R. Ketchum and R.T. Craig. Simulation of linearized dynamics of gas turbine engines. In *NACA Technical Note 2826*, 1952.
- [8] R.W. Pack and A.J. Philips. Linear dynamics of a gas turbine engine. In *NACA Technical Note 2849*, 1952.
- [9] H. Gold and S. Rosenzweig. A method for estimating speed response of gas turbine engines. In *NACA RM E51*, 1952.

- [10] P.V. Crooks and D.W. Willshire. The theoretical estimation of engine speed response data for a turbojet engine. In *NGTE M268, 1956*, 1956.
- [11] V.L. Larrowe and M.M. Spencer. Analog computer simulation of gas turbine engines for control study. In *SAE Progress in Technology, Vol. 9: Gas Turbine Fuel Controls. Analysis and Design, New York*, 1965.
- [12] A.E. Sutton. Application of multivariable control to a turbofan engine. In *Proceedings of IEE Control 91, Edinburgh, UK. Mar.*, 1991.
- [13] etc al H.A. Barker, P.H. Hammond. A model library for the control engineering community. In *Proceedings of IEE Control 91, Edinburgh, UK. Mar.*, 1991.
- [14] R. Shoureshi and K. McLaughlin. Application of bond graphs to thermofluid process and systems. *J. of dynamic System, Measurement, and Control*, 107:241-245, 1985.
- [15] G.J. Michael and F.A. Farrar. Identification of multivariable gas turbine dynamics from stochastic input-output data. In *United Aircraft Research Laboratories, East Hartford, Conn., Rept. R-941620-3. Mar.*, 1975.
- [16] R.L. DeHoff. Identification of a stol propulsion plant model from flight data. *Journal of Guidance and Control*, 2:235-240, 1979.
- [17] W. Merrill. Identification of multivariable high performances turbofan engine dynamics from closed-loop data. In *NASA TM-82785*, 1981.
- [18] F.A. Farrar and G.J. Michael. Estimation and control of critical gas turbine variables. In *ASME Paper76-WA/AUT-12*, 1976.
- [19] R.L. DeHoff and W.E. Hall. JR. System identification principles applied to multivariable control synthesis of the f100 turbofan engine. In *Proceedings of Joint Automatic Control Conference, San Francisco, June 1977 Vol.2 pp.1007-1012*, 1977.

- [20] W. Merrill. Multivariable identification using centralized fixed modes. In *Propulsion Controls*, pp. 3-10, 1980.
- [21] W. Merrill and G. Leininger. Identification and dual adaptive control of a turbojet engine. *International Journal of Control*, 34:529-546, 1981.
- [22] D.E. Warner and E.D. Ward. Filtered sequential regression parameter identification applied to a gas turbine engine model. *J. of dynamic System, Measurement, and Control*, pages 253-258, 1977.
- [23] T. Schobeiri and H. Haselbacher. Transient analysis of gas turbine power plants, using the huntorf compressed air storage plant as an example. In *Gas turbine Conference and Exhibit, Houston, Texas-March 18-21, 1985*, pages 1-8, 1985.
- [24] T. Schobeiri. Transient analysis of gas turbine power plants, using the huntorf compressed air storage plant as an example. In *Gas turbine Conference and Exhibit, Dusseldorf, West West Germany-June 8-12, 1986*, pages 1-8, 1986.
- [25] J.F. Dugan and R.E. Filippi. Effect of design overall compressor pressure ratio division on acceleration characteristics of three hypothetical two-spool turbojet engines. In *NACA RM E56 D13*, 1956.
- [26] R.A. Onions and A.M. Foss. Improvements in the dynamic simulation of gas turbines. In *Proceedings of AGARD Conference on Engine Handling. No. 324*, 1982.
- [27] N.J. Krikelis and F. Papadakis. Gas turbine modelling using pseudo-bond graphs. *Int.J. System Sci*, 19(4):537-550, 1988.
- [28] N.R.L. Maccallum. Axial compressor characteristics during transients. In *Proceedings of AGARD Conference on Engine Handling. No. 324*, 1982.

- [29] R.L. DeHOFF and JR W.E. Hall. Jet engine systems models: Part ii state space techniques and modelling for control. In *Control and Dynamic Systems, Vol.14 pp. 259-298*, 1978.
- [30] R.L. DeHoff B. Lehtinen and R.D. Hackney. Multivariable control altitude demonstration on the f-100 turbofan engine. *Journal of Guidance and Control*, 4:50-58, 1981.
- [31] B. Lehtinen W. Merrill and J. Zeller. The role of modern control theory in the design of controls for aircraft turbine engines. *Journal of Guidance*, 7, 1984.
- [32] R.L. DeHoff and W.E.JR. Hall. F-100 multivariable control synthesis program. In *AFAPL-TR-77-35. Vol. I and II*, 1977.
- [33] R.L. DeHoff and W.E.JR. Hall. Multivariable quadratic synthesis of an advanced turbofan engine controller. *Journal of Guidance and Control*, 1:136-142, 1978.
- [34] C.A. Skira and R.L. DeHoff. A practical approach to linear modal analysis for multivariable turbine engine control design. In *Alternative for Linear Multivariable Control, edited by J.L. Peczkowski and J.L. Melsz, National Engineering Consortium, Chicago, pp. 71-87*, 1978.
- [35] M. Athans and P. Kapsouris. Model reduction for the multivariable engine control design. *IEEE Journal of Guidance and Control*, 6, 1983.
- [36] H. Brown and J.A. Elgin. Aircraft engine control mode analysis. *J. of Engineering for Gas Turbines and Power*, 107:838-844, 1985.
- [37] T.J. McAvoy. Interaction analysis. In *Instrument Society of America Monograph Series*, 1983.
- [38] P. Grosdidier and M. Morari. Closed-loop properties from steady-state gain information. *Ind. Eng. Chem. Fund. K24, pp. 221-235*, 1985.

- [39] P. Kapanouris and M. Athans. Gain scheduled multivariable control for the ge-21 turbofan engine. In *Proceedings of American Control Conference*, June, 1985.
- [40] C.N. Nett. A quantitative theory for control structure design: The role and use of block relative gains. In *Proceedings of American Control Conference*, June, 1987.
- [41] C.N. Nett and H.A. Spang. Control structure analysis and synthesis: A missing link in the evolution of modern control theories. In *Proceedings of American Control Conference*, June, 1987.
- [42] L.E. Rosenblad. Evaluation of control techniques for aircraft propulsion systems. *Journal of Engineering for Gas Turbines and Power*, 112:229-232, 1990.
- [43] P.D. McMorran. Design of gas turbine controller using the inverse nyquist method. In *Proceedings of IEEE, Vol. 117 No. 10*, 1970.
- [44] H.H. Rosenbrock and N. Munro. The inverse nyquist array method. In *Alternative for Linear Multivariable Control*, edited by J.L. Peczkowski and J.L. Melsz, National Engineering Consortium, Chicago, pp. 71-87, 1978.
- [45] S. Engell and N. Munro. Regulator design for the f-100 turbofan engine. In *Proceedings of IEEE, Vol. 117 No. 10*, 1978.
- [46] H.A. Spang. Insight into the application of the inverse nyquist array method to turbofan engine control. In *Alternative for Linear Multivariable Control*, edited by J.L. Peczkowski and J.L. Melsz, National Engineering Consortium, Chicago, pp. 138-155, 1978.
- [47] B.A. Dixon A.G.J. MarFarlane, P.D. McMorran and S.S. Hodge. Applications of multivariable control techniques to aircraft gas turbine engines. In

Multivariable Control Systems Design and Applications, Manchester, England, sept. 1-3, 1971, pp. 1-7, 1971.

- [48] J.M. Edmunds. Control system design and analysis using closed-loop nyquist and bode array. *Int.J.Control*, 30(5):773–802, 1979.
- [49] G.L. Teper L.G. Hofmann and R.F. Whitbeck. Application of frequency domain multivariable synthesis techniques to an illustrative problem in jet engine control. In *Alternative for Linear Multivariable Control*, edited by J.L. Peczkowski and J.L. Melsz, National Engineering Consortium, Chicago, pp. 71-87, 1978.
- [50] B. Kouvaritakis and J.M. Edmunds. The characteristic frequency and characteristic gain design method for multivariable feedback systems. In *Alternative for Linear Multivariable Control*, edited by J.L. Peczkowski and J.L. Melsz, National Engineering Consortium, Chicago, pp. 229-246, 1978.
- [51] G.G. Leininger. Application of the mna design method to a nonlinear turbofan engine - multivariable nyquist array method. In *NASA CR-163855*, 1981.
- [52] G.G. Leininger. New dominance characteristics for the multivariable nyquist array method. *International Journal of Control*, 30:459–475, 1979.
- [53] R.M. Schafer and M.K. Sain. Input compensation for dominance of turbofan models. In *Alternative for Linear Multivariable Control*, edited by J.L. Peczkowski and J.L. Melsz, National Engineering Consortium, Chicago, pp. 156-169, 1978.
- [54] H. Brown. V/stol propulsion control analysis. In *NASA CR-163855*, 1981.
- [55] A.G.J. MacFarlane and B. Kouvaritakis. A design technique for linear multivariable feedback systems. *Int. J. Control*, 25(6):837–874, 1977.

- [56] R. Perez and O. NwoKah. Full envelope multivariable control of a gas turbine engine. In *Proceedings of American Control Conference, Boston, Massachusetts. June 26-28, 1991.*
- [57] D.A. Baker and C.J. Maday. Design of noninteracting multivariable feedback control nyquist and bode array. *J. of Engineering for Gas Turbines and Power*, 107:845–850, 1985.
- [58] R. Basso M.K. Sain, R.J. Leake and R. Gejji. Alternative methods for the design of jet engine control systems. In *Proceedings of the Joint Automatic Control Conference, West Lafayette, Ind. July, 1976.*
- [59] R.R. Gejji and M.K. Sain. Application of polynomial techniques to multivariable control of jet engine. In *Proceedings of the 4th International Symposium on Multivariable Technological Systems, Preprints, Frederiction, New Brunswick, Canada, pp. 421-429. July, 1976.*
- [60] S. Adibhatla J.A. Polley and K.S. Baheti. Design of jet engine control system by multivariable frequency-domain method. In *Proceedings of American Control Conference, June, 1986.*
- [61] P.J. Hoffman J.A. Polley, S. Adibhatla. Multivariable turbofan engine control for full flight envelope. *J. of Engineering for Gas Turbines and Power*, 111:130–137, 1989.
- [62] G.J. Michael and F.A. Farrar. Stochastic regulation of nonlinear multivariable dynamic systems. In *Final Report for Period 1 Feb. 1973 through Jan. 1976. Report ONR-CR-215-219/4F, 1976.*
- [63] E. Beattie and W. Spock. Application of multivariable optimal control techniques to a variable area turbine engine. In *JACC Paper, Purdue University, Lafayette, Ind., July, 1976.*

- [64] M.D. Ward C.R. Stone, N.E. Miller and R.D. Schmidt. Turbine engine control synthesis. In *Technical Report AFAPL-TR-75, Mar., 1975.*
- [65] R.J. Bowles. Sub-optimal control of a gas turbine engine. In *Ad-777852, Master of Science Thesis, AF Institute of Technology, Wright Patterson AFB, Ohi. USA, 1973.*
- [66] J.G. Elliott and W.R. Seitz. Application of modern control theory to the design of integrated airframe/engine control systems. In *The Bendix Corporation, Technical Report. BRL/TR-75-7669, 1975.*
- [67] M.S. Weinberg. A multivariable control for the f-100 engine operating at sea level static. In *ASD-TR-75-28, Nov, 1975.*
- [68] W.C. Merril. An application of modern control theory to jet propulsion systems. In *NASA TM X-71726, May,, 1975.*
- [69] C.A. Harvey and G. Stein. Quadratic weights for asymptotic regulator properties. *IEEE Transactions on Automatic Control*, 23:378-387, 1978.
- [70] P. Kapasouris M. Athans. Linear-quadratic gaussian with loop-transfer recovery methodology for the f-100 engine. *J. of Guidance*, 9(1):45-52, 1986.
- [71] et al M. Athans. Linear-quadratic gaussian with loop transfer recovery methodology for the f-100 engine. *IEEE Journal of Guidance and Control*, 9:66-72, 1985.
- [72] R.V. Monopoli. Model following control of gas turbine engines. *J. of Dynamic Systems, Measurement, and Control*, 103:285-289, 1981.
- [73] O. Taiwo. Design of multivariable controllers for an advanced turbofan engine by zakian's method of inequalities. *J. of Dynamics and Control*, 101:299-307, 1979.

- [74] S. V. Rao D.E. Moellenhoff and C.A. Skaravan. Design of robust controller for gas turbine engines. In *Gas Turbine and Aeroengine Congress and Exposition, June 11-14 1990. Brussels, Belgium, 1990.*
- [75] S.D. Hancock and P.J. Fleming. Gas turbine engine controller design using multi-objective optimization techniques. In *Proceedings of the First European Control Conference Grenoble, France. July 2-5, 1991.*
- [76] S.G. Hiesener. Design of a nonlinear precompensator for a turbofan engine. In *Proceedings of the First European Control Conference Grenoble, France. July 2-5, 1991.*
- [77] J. Larjola. Simulation of surge margin changes due to heat transfer in gas turbine transients. In *Gas Turbine and Aeroengine Conference and Exposition. Paper No. 84-GT-129, 1984.*
- [78] P.J. Ashmole. Introducing the rolls-royce tay. In *AIAA/SAE/ASME 19th Joint Propulsion Conference. Seattle, Washington. June 27-29, 1983.*
- [79] K. Bammert and G. Krey. The use of a hybrid computer in the optimization of gas turbine control parameters. *J. of Engineering for GPower*, pages 257–264, 1973.
- [80] I.H. Ismail and F.S. Bhinder. Simulation of aircraft gas turbine engines. *Journal of Engineering for Gas Turbines and Power*, 113:95–99, 1991.
- [81] N.R.L. Maccallum. Thermal influences in gas turbine transients- effects of changes in compressor characteristics. In *ASME Paper 79-GT-143, 1979.*
- [82] N.R.L. Maccallum. Models for the representation of turbomachine blades during temperature transients. In *ASME Paper 76-GT-23, 1976.*
- [83] J.R. Szuch. Models for jet engine systems: Part i techniques for jet engine systems modelling. In *Control and Dynamic Systems, Vol.14 pp. 213-256, 1981.*

- [84] J.R. Szuch. Hydes - a generalized hybrid computer program for studying turbojet or turbofan engine dynamics. In *NASA TM X-3014*, 1975.
- [85] R.K. Agrawal and M. Yunis. A generalized mathematical model to estimate gas turbine starting characteristics. *J. of Engineering for Power*, 104:194-201, 1982.
- [86] A.H. Lefebvre and E.R. Norster. The design of tubular gas turbine combustion chambers for optimum mixing performance. In *Proceedings of Instn. Mech. Engrs. Vol. 183. pp. 150-155*, 1969.
- [87] G.F.C. Rogers H. Cohen and H.I.H. Saravanamuttoo. Gas turbine theory. In *Longman, Second Edition*, 1987.
- [88] T.R. Harman. Gas turbine engineering. In *The Macmillan Press*, 1981.
- [89] M. Alves. The influence of the combustion chamber during gas turbine during transients. In *M.Sc. Thesis. School of Mechanical Engineering, Cranfield Institute of Technology*, 1989.
- [90] K. Seldner and H. Gold. Computer and engine performance study of a generalized parameter fuel control for jet engines. In *NASA TN D-5871*, 1970.
- [91] J. Odgers and C. Carrier. Modelling of gas turbine combustors: Considerations of combustion efficiency and stability. *J. of Engineering for Power*, pages 105-112, 1973.
- [92] G.F. Aker and H.I.H. Saravanamuttoo. Predicting gas turbine performance degradation due to compressor fouling using computer simulation techniques. *Journal of Engineering for Gas Turbines and Power*, 111:343-350, 1989.

- [93] H.I.H. Saravanamutoo and B.D. MacIsaac. Thermodynamic models for pipeline gas turbine diagnostics. *J. of Engineering for Power*, 105:875–884, 1983.
- [94] H.I.H. Saravanamutoo D.E. Muir and D.J. Marshall. Health monitoring of variable geometry gas turbines for canadian navy. *Journal of Engineering for Gas Turbines and Power*, 111:244–250, 1989.
- [95] J.E.A. Roy-Aikins. Considerations for the use of variable geometry in gas turbines. In *Gas Turbine and Aeroengine Conference and Exposition. Brussels, Belgium. June 11-14, Paper No. 90-GT-271*, 1986.
- [96] N.R.L. Maccallum. Further studies of the influence of thermal effects on the predicted acceleration of gas turbines. In *Gas Turbine Conference and Products Show. March 9-12, Houston, Texas, Paper No. 81-GT-21*, 1981.
- [97] N.R.L. Maccallum and P. Pilidis. Gas turbine transient fuel scheduling with compensation for thermal effects. In *Gas Turbine Conference and Exhibit. Dusseldorf, West Germany. June 8-12, Paper No. 86-GT-208*, 1986.
- [98] P. Pilidis and N.R.L. Maccallum. The effect of heat transfer on gas turbine transients. In *Proceedings of Gas Turbine Conference and Exhibit, Dusseldorf, West Germany. 8-12 June*, 1986.
- [99] P. Petrides. Different computer models for the simulation of a typical turbofan engine originating from different fan treatment and air flow distribution. In *Ph.D. Thesis. Department of Mechanical Engineering, University of Glasgow*, 1988.
- [100] N.R.L. Maccallum. Computational models for the transient performance of rb183-02 (spey) and rb183-03 (tay) engines. In *Research Report RR/1, 13th Aug.*, 1984.

- [101] F. Nawrocki. Ensuring surge-free engine operation on today's turbofan powered business jets. In *AIAA/ASME/SAE/ASEE 25th Joint Propulsion Conference Monterey, CA / July 10-12, 1989*, pages 230–232, 1989.
- [102] Szuch et al. F-100 multivariable control synthesis: Program-evaluation of a multivaribel control using a real-time engine simulation. *NASA TP 1056*, 1977.
- [103] A.M. El-Gammal. An algorithm and criteria for compressor characteristics real time modeling and approximation. *J. of Engineering for Gas Turbines and Power*, 113:112–118, 1991.
- [104] N.R.L. Maccallum and P. Pilidis. The prediction of surge margins during gas turbine transients. In *Gas Turbine Conference and Exhibit. Houston, Texas. March 18-21, Paper No. 85-GT-208*, 1985.
- [105] E.P. Cockshutt. Equilibrium performance analysis of gas turbine engines using influence coefficient techniques. In *AGARD Conference Proceedings No. 151*, 1974.
- [106] B. Thomson. Basic transient effects of aero-gas turbines. In *AGARD Conference Proceedings No. 151*, 1974.
- [107] D.L. Smith. Linear modelling of a marine gas turbine power plant. In *Proceedings of ASME Gas Turbine and Aeroengine Congress, Amsterdam, The Netherlands. 6-9 June*, 1988.
- [108] J.H. Horlock. Axial flow compressor. In *Robert E. Krieger Publishing, Malabar, FL*, 1982.
- [109] G.I. Converse and R.G. Griffin. Extended parametric representation of compressor fans and turbine. In *NASA CR-174645*, 1984.

- [110] G.C. Oates. Engine off-design performance. In *Aerothermodynamics of Gas Turbine and Rocket Propulsion*, J.S. Przemieniecki, ed. AIAA Education Series, Washington, DC, 1988.
- [111] P. Eykhoff. System identification. In *Wiley, London*, 1974.
- [112] D.M. Trujillo and H.R. Busby. Investigation of a technique for the differentiation of empirical data. *J. of Dynamic Systems, Measurement, and Control*, 105:200–202, 1983.
- [113] N.R.L. Maccallum. Personal communication. 1990.
- [114] D.L. Smith and V.A. Stammetti. Sequential linearization as an approach to real-time marine gas turbine simulation. *Journal of Engineering for Gas Turbines and Power*, 112:187–191, 1990.
- [115] J.Q. Howell. A least-square-distance curve-fitting techniques. In *NASA TN D-6374*, 1971.
- [116] M.J. Maron. Curve fitting and function approximation. In *Numerical Analysis: a Practical Approach, 2nd ed.*, Macmillan Publishing Company, New York, 1987.
- [117] J.R. Leigh. Digital control algorithms. In *Applied Digital Control*, Prentice-Hall International, UK, Ltd, 1985.
- [118] S.H. Rock R.I. DeHoff and M.M Akhter. Development of multivariable controllers for aircraft turbine engines. In *Theory and Application of Optimal Control in Aerospace Systems*, 1981.
- [119] J.R. Mihalow K. Selder and R.J. Blaha. Generalized simulation techniques for turbojet engines. In *NASA TM-7610*, 1982.
- [120] P. Pilidis. Digital simulation of gas turbine performance. In *Ph.D. Thesis. Department of Mechanical Engineering, University of Glasgow*, 1983.

- [121] L. Merahi. Gas turbine models for compensation of transient fuel flow schedules. In *M.Sc. Thesis. Department of Mechanical Engineering, University of Glasgow*, 1988.
- [122] L.M. Darbouche. Predicted transient performance of a derivative two-spool turbofan engine with a 4-stage ip compressor. In *M.Sc. Thesis. Department of Mechanical Engineering, University of Glasgow*, 1991.
- [123] H.I.H. Saravanamuttoo and B.D. MacIsaac. The use of a hybrid computer in the optimization of gas turbine control parameters. *J. of Engineering for Gas Turbines and Power*, pages 257-264, 1973.
- [124] B. D. macisaac and H. I. H. Saravanamuttoo. Aerothermodynamic factors governing the response rate of gas turbine engines. In *AGARD Conference Proceedings No. 151*, 1974.
- [125] G.E. Davies. Fluidics in aircraft engine controls. *J. of Engineering for Gas Turbines and Power*, 103:324-329, 1981.
- [126] E.H. Warne. Gas turbine fuel and control system. In *Proceedings Technical Advances in Gas Turbine Design April 9-11th, Warwick, U.K.*, 1969.
- [127] A.J. Fawke and H.I.H. Saravanamuttoo. Digital computer simulation of the dynamic response of a twin-spool turbofan with mixed exhausts. In *Aeronautical Journal, Sept. pp. 471-478*, 1973.
- [128] A.J. Fawke and H.I.H. Saravanamuttoo. Experimental investigation of methods for improving the dynamic response of a twin-spool turbojet engine. In *Gas Turbine Conference and Products Show. March 28-April 1, Houston, Texas, Paper No. 72-GT-14*, 1972.
- [129] C. Reboulet and C. Champetier. A new method for linearizing nonlinear systems: the pseudolinearization. *Int. J. of Control*, 40:631-638, 1983.

- [130] W.T. Baumann and W.J. Rugh. Feedback control of nonlinear systems by extended linearization. *IEEE Transactions on Automatic Control*, 31:40–46, 1986.
- [131] J.L. Peczkowski and M.K. Sain. Design of nonlinear multivariable feedback controls by total synthesis. In *Proceedings of 1984 American Control Conference*. pp. 688-697, 1984.
- [132] J.D. Powell G.F. Franklin and M.L. Workman. Digital control of dynamic systems. In *Addison-Wesley Publishing Company*, 1990.
- [133] K.J. Astrom and B. Wittenmark. Adaptive control. In *Addison-Wesley Publishing Company*, 1989.
- [134] K.J. Astrom and B. Wittenmark. Computer controlled systems: Theory and design. In *Prentice-Hall Information and System Sciences Series. Edited by T. Kailath*, 1984.
- [135] W.J. Rugh. Analytical framework for gain scheduling. In *IEEE Control Systems Magazine*, 11, 1991.
- [136] J.S. Shamma and M. Athans. Analysis of gain scheduled control. *IEEE Transactions on Automatic Control*, 35:898–907, 1990.
- [137] M. Fliess. Some remarks on gain schedulling. In *Proceedings of the First European Control Conference Grenoble, France. July 2-5, 1991*.
- [138] C.N. Nett and J.A. Polley. Integrated design/implementation of nonlinear digital controllers. In *Proceedings of American Control Conference*, 1988.
- [139] R.A. Hyde and K. Glover. Meeting vstol aircraft performance requirements using scheduled h_∞ controllers. In *Proceedings of 1991 American Control Conference, Boston, Massachusetts. June 26-28, 1991*.

- [140] J. Ackerman. Robustness against sensor failures. *Automatica*, 20:211–215, 1984.
- [141] J.E. Moller M.G. Dunn, C. Padova and R.M. Adams. Performance deterioration of a turbofan and a turbojet engine upon exposure to a dust environment. *J. of Engineering for Gas Turbines and Power*, 109:336–343, 1987.
- [142] A.J. Laub A.G. Safonov and G.L. Hartmann. Feedback properties of multivariable systems: The role and use of the return difference matrix. *IEEE Transactions on Automatic Control*, 26:47–65, 1982.
- [143] J.M. Maciejowski. Multivariable feedback design. In *Addison-Wesley Publishing Company*, 1989.
- [144] J.C. Doyle and G. Stein. Multivariable feedback design: Concepts for a classical/modern synthesis. *IEEE Transactions on Automatic Control*, 26:4–16, 1981.
- [145] R. Weber and C. Brosilow. The use of secondary measurements to improve control. *AIChE Journal*, 18, 1985.
- [146] J. O'Reilly. Observers for linear systems. In *Mathematics in Science and Engineering*, 1983.
- [147] T. Ohtani and M. Masubuchi. Design methods of nonlinear dynamic compensator based upon canonical forms. In *Proceedings of First IFAC Symposium on Design Methods of Control Systems. ETH Zurich, Switzerland. 4-6 Sept., 1991.*
- [148] E.A. Misawa and J.K. Hedrick. Nonlinear observers - a state-of-the-art survey. *J. of Dynamic Systems, Measurement, and Control*, 111:344–352, 1989.

- [149] P.J. Gawthrop. Model-based observer control: An introduction. In *Control Group Research Report R-91/9*, Department of Mechanical Engineering, University of Glasgow, 1991.
- [150] R.W. Jones. Nonlinear inferential control using model-based observer control. In *Control Group Research Report R-91/7*, Department of Mechanical Engineering, University of Glasgow, 1991.
- [151] W. Mielczarski. Observing the state of a synchronous generator: Part 1. theory. *Int. J. of Control*, 45:987–1000, 1987.
- [152] J.C. Doyle and G. Stein. Robustness with observer. *IEEE Transactions on Automatic Control*, 24:607–611, 1979.
- [153] S. Beale and B. Shafai. Robust control system design with a proportional integral observer. *Int. J. of Control*, 50:97–111, 1989.
- [154] B.H. Goethert and W.F. Kimzey. Effect of high-frequency fluctuations of inlet flow on compressor stall. In *Proceedings of the 32nd Meeting of the Propulsion and Energetics Panel of AGARD. Toulouse, France, 9-13 Sept.*, 1968.
- [155] F.K. Moore. Stall transients of axial compression systems with inlet distortion. *J. Propulsion*, 2:552–561, 1986.
- [156] N. Munro D.E. Winterbone and P.M.G. Lourtie. A preliminary study of the design of a controller for an automotive gas turbine. *J. of Engineering for Power*, pages 244–250, 1973.
- [157] P. Pilidis and N.R.L. Maccallum. A general programme for the prediction of the transient performance of gas turbines. In *ASME paper 85-GT-209*, 1985.